N° d'ordre:

Archive CNRS.

THESE

Présentée à

l'Université Louis Pasteur de Strasbourg

pour obtenir le grade de

DOCTEUR

de l'Université Louis Pasteur

Par

Aldjia CHOUALEB

Fonctionnalisation de clusters de cobalt et de cobalt-ruthénium par les alcynes. Application à la formation de nouveaux matériaux magnétiques.

Soutenue le 13 Septembre 2003 devant la commission d'examen:

Dr. P. BRAUNSTEIN	Directeur de recherche CNRS à l'ULP, Strasbourg *Directeur de thèse*
Dr. J. ROSÉ	Chargé de recherche CNRS à l'ULP, Strasbourg *Co-directeur de thèse*
Pr. M. CHETCUTI	Professeur à l'ECPM, Strasbourg *Rapporteur interne*
Pr. M. VEITH	Professeur à l'Universität des Saarlandes, Sarrebruck, Allemagne. *Rapporteur externe*
Pr. M. I. BRUCE	Professeur à l'University of Adelaide, South Australia. *Rapporteur externe*
Pr. A. TIRIPICCHIO	Professeur à l'Università di Parma, Parme, Italie *Examinateur*
Dr. C. ESTOURNES	Maître de Conférence à l' IPCMS, Strasbourg *Membre invité*
Pr. R. WELTER	Professeur à l'Université Louis Pasteur, Strasbourg. *Membre invité*

A mes parents

A mes frères et sœurs

et à tous ceux que j'aime et estime

Ce travail a été réalisé au laboratoire de chimie de coordination de l'Université Louis Pasteur, Strasbourg, associé au C.N.R.S (UMR 7513). Qu'il me soit permis d'exprimer ma profonde gratitude à Monsieur le Dr. Pierre Braunstein, directeur de recherche au CNRS, pour m'avoir accueillie dans son laboratoire et pour la formation que j'ai pu y acquérir. J'ai appris grâce à lui à travailler avec rigueur.

Je remercie le Dr. Jacky Rosé pour le suivi de ce travail, pour ses conseils judicieux et aussi pour m'avoir supportée durant les moments difficiles.

Je tiens à adresser mes plus vifs remerciements à Messieurs les Professeurs M. I. Bruce, A. Tiripicchio, M. Veith et M. Chetcuti pour avoir accepté de juger ce travail.

Mes remerciements vont également à nos collaborateurs de l'IPCMS et plus particulièrement le Dr. Claude Estournès pour toutes les mesures physiques qu'il a réalisées, pour m'avoir aidée pour les interprétations des résultats et pour toutes les discussions enrichissantes que nous avons eues.

Je tiens à remercier le Pr. Richard Welter du laboratoire DECMET (cristallographie) pour avoir collaboré à ce travail et **pour sa sympathie.**

Je remercie également le Pr. Salah Eddine Bouaoud de l'Université des Frères Mentouri-Constantine (Algérie), qui a guidé mes premiers pas dans la recherche, de m'avoir encouragée à rejoindre l'équipe du Dr. P. Braunstein pour effectuer cette thèse après avoir y réaliser des stages dans le cadre de collaboration entre l'Université des Frères Mentouri et l'Université Louis Pasteur

Je tiens à remercier également Anne pour le travail synthétique et pour sa patience avec nous; Soumia pour le travail administratif; Marc pour le travail technique rapide et efficace et les chercheurs du laboratoire, Roby, Olivier et Xavier pour leur sympathie.

Je remercie mes collègues du laboratoire notamment Nicola, la reine de la RMN, pour tous les "petits-grands" services qu'elle m'a rendu et pour avoir partagé mes angoisses de fin de parcours ; Mireia pour sa gentillesse et sa chaleur méditerranéenne; Jean-philippe, le roi de la chimie organique, avec qui j'ai eu beaucoup de discussion sur la chimie et la vie professionnelle; Aude la plus gentille des françaises que j'ai connu, Adel et ses blagues sans fin; Luc avec sa gentillesse et son humour et avec qui j'ai eu beaucoup de discussions sur mes coutumes et traditions qu'il connaît presque par cœur, Coco avec qui les discussions sont très compliquées; Pierre pour sa modestie et sa gentillesse, Abdellatif et Nicolas sans oublier mes anciens collègues Guislaine, Walter, Djing, Fanny, Fredy, Andreas et aussi tous les stagiaires et étudiants Erasmus qui m'ont croisée pendant mes trois années de thèse; Je pense plus particulièrement à Vito, Roberto, Magno, Bénédikt et Marion.

Enfin, je tiens à remercier tous mes amis, en particulier, Fatima, Yazid, Fadéla, Münever, Soraya, Fatima, Ismahanne, Dany, Hatiss, Catherine, Patricia et aussi mon cousin Hichem, qui m'ont encouragée par leur réconfort dans mes moments les plus difficiles.

SOMMAIRE

LISTE DES FIGURES

CHAPITRE 1

CHAPITRE 2

CHAPITRE 3

Introduction générale

Les clusters sont des complexes moléculaires constitués d'au moins trois atomes métalliques entre lesquels les interactions métal-métal jouent un rôle important. Ces métaux sont entourés de ligands qui assurent la stabilité du cluster moléculaire en permettant de répartir la densité électronique sur l'ensemble de l'édifice et d'en renforcer ainsi sa cohésion. Les complexes dinucléaires contenant une liaison métal-métal directe sont souvent inclus dans la chimie des clusters car ils nous renseignent utilement sur les approches synthétiques et certaines propriétés (structurales, électroniques, de réactivité).

L'idée que plusieurs centres métalliques à proximité les uns des autres dans une même molécule, peuvent donner lieu à des phénomènes de synergie et de coopérativité est inhérente à la catalyse.[1,2] En effet, un centre métallique ayant au moins deux voisins métalliques à proximité aura sûrement une réactivité très différente de celle qu'il aurait en leur absence. Ces effet de coopérativité ont fait l'objet de nombreuses études.

Deux grandes classes de clusters ont été envisagées dans le cas des métaux de transition:

- les clusters à haut degré d'oxydation qui sont formés par les éléments de transitions de la gauche du tableau périodique dans des degrés d'oxydation +II et +III associés à des ligands π–donneurs tels que les halogénures, RO^-, O^{2-} ou S^{2-}.

- les clusters à bas degré d'oxydation qui comportent les éléments de transition à droite du tableau périodique, dans des degrés d'oxydation zéro ou négatif, associés à des ligands π–accepteurs, tels que CO, CNR, NO, PR_3 qui peuvent stabiliser les bas degrés d'oxydation.[3] On s'intéresse plus particulièrement à cette seconde classe de clusters avec d'autres ligands π–accepteurs qui sont les hydrocarbures insaturés tels que **les alcynes**.

Les alcynes sont des réactifs très étudiés en raison de l'importance que revêt leur activation et leur intérêt en tant que matière première en chimie fine. L'étude de la sélectivité de leurs interactions *multisites* avec les clusters ainsi que l'orientation et la mobilité de l'alcyne par rapport au coeur métallique ont fait l'objet de recherches actives.[4,5]

La modification de la réactivité d'un alcyne coordiné à plusieurs centres métalliques peut être l'occasion de nouvelles réactions stoechiométriques ou catalytiques. Cette activation de l'alcyne dépendra de son mode de coordination, de la nature des métaux et de leurs autres ligands.

La richesse de la chimie des clusters-alcynes tient essentiellement à la grande variété d'arrangements structuraux qu'on peut obtenir du fait des divers modes de coordination des alcynes (Figure 1) et au rôle des effets électroniques sur la modification de la réactivité de ces clusters.

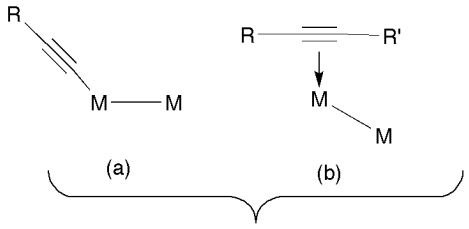

interaction avec un seul atome métallique

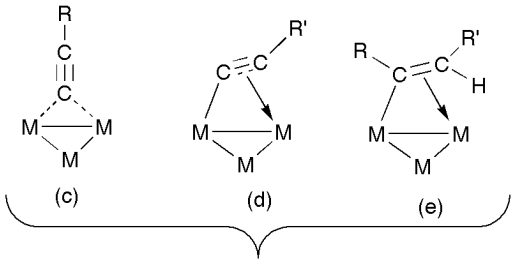

interaction avec deux atomes métalliques

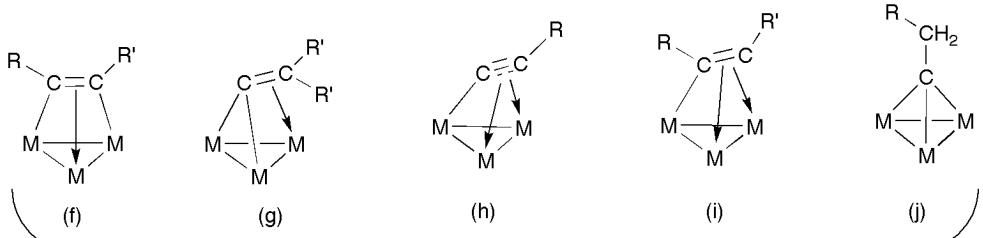

interaction avec trois atomes métalliques

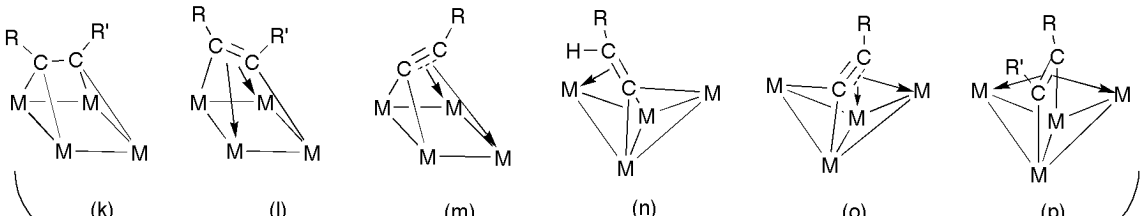

interaction avec quatre atomes métalliques

Figure 1: Diverses représentations de structures de molécules issues de réactions entre clusters et alcynes.

Un alcyne peut interagir avec un, deux, trois ou quatre atomes métalliques. L'interaction avec un seul atome peut être sous forme d'acétylure [mode de coordination (*a*)] ou d'une interaction

π simple [mode de coordination (*b*)]. Ces deux modes de coordination sont rarement rencontrés dans les clusters, cela est dû au fait que la liaison C≡C interagit avec les autres atomes métalliques dans le cluster.

En interagissant avec trois atomes métalliques l'alcyne peut être lié d'une façon μ_3-η^2 qui peut être 2σ+1π [modes (*f*) et (*g*)][6,7] ou 2π+1σ [modes (*h*) et (*i*)].[8] Le mode de coordination μ_3–alkylidyne [mode (*j*)], où le cluster contient un coeur pseudotétraédrique M_3C, est fréquement rencontré avec les clusters de cobalt.[9]

Dans les clusters tétranucléaires les modes de coordination (*k*), (*l*) et (*m*) sont possibles avec les clusters plan qui sont rares. Cependant, le mode le plus courant dans ces clusters est celui (*p*) où l'alcyne est en interaction μ_4-η^2 avec le cœur métallique qui possède une structure dite *papillon*. En effet, si l'on considère la grande famille des clusters tétraédriques, la coordination de l'alcyne au cluster s'accompagne, en général, de la rupture d'une liaison métal-métal pour donner le cluster *papillon*. Ainsi, la réaction du cluster $[Co_3Mo(CO)_{11}(\eta^5\text{-}C_5H_4Me)]$ avec PhC≡CH conduit à la perte de deux ligands CO avec une rupture sélective de la liaison Mo-Co pour conduire au cluster *papillon* $[Co_3Mo(CO)_9(\mu_4\text{-}\eta^2\text{-}PC_2H)(\eta^5\text{-}C_5H_4Me)]$ **(1)**[10] qui est un exemple d'un octaèdre *closo* Co_3MoC_2 à 7 paires électroniques (eq 1).

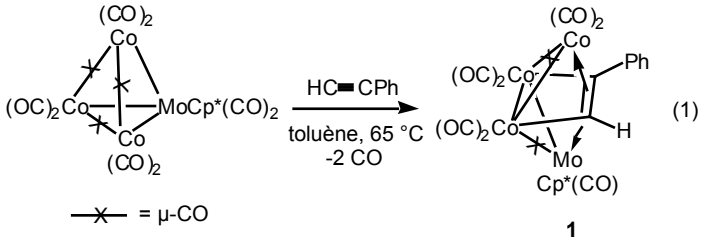

(1)

1

La coordination des alcynes aux quatre métaux provoque un allongement de la liaison triple par rapport à celle observée pour le ligand libre. Cette activation résulte à la fois d'un dépeuplement des orbitales liantes de l'alcyne (en direction des atomes métalliques situés aux extrémités des ailes du *papillon*) et d'une rétrocordination de caractère antiliant (en provenance des atomes de l'arête) (Figure 2c). Une véritable circulation des électrons semble donc s'instaurer, qui pourrait également avoir un parallèle dans les répartitions de densité électronique sur une surface métallique fixant de tels ligands.

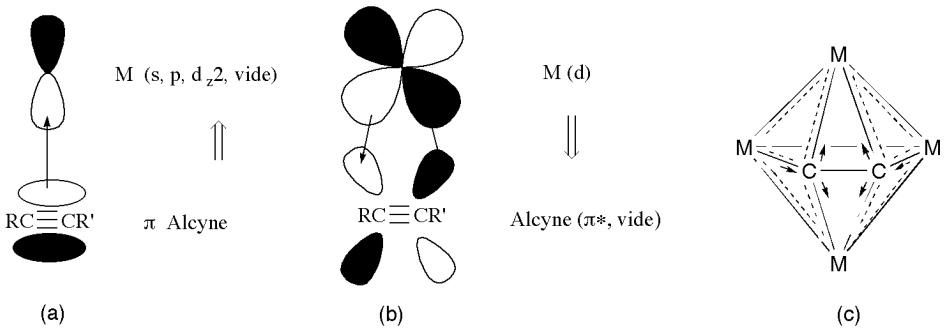

Figure 2: Les deux composantes de la liaison alycne-métal -"**push-pull** bonding"- (a): la **π-donation** des orbitales π remplies de l'alcyne aux orbitales s, p ou d_{z2} vides du métal (b): la **rétrodonation** des orbitales d remplies du métal vers l'orbitale π* vide de l'alcyne.
(c): Exemple de "circulation" électronique dans un cluster M_4C_2.

Si la rupture d'une liaison métal-métal est le comportement classique des clusters tétraédriques en présence d'alcynes, la molécule $[WOs_3(\mu\text{-H})Cp(CO)_{12}]$[11] se comporte différement, en effet, l'alcyne se coordine sans rupture d'une liaison métal-métal, ceci de façon μ_3-η^2 sur la face Os_3 pour conduire au cluster $[WOs_3(\mu\text{-H})Cp(CO)_{10}(\mu_3\text{-}\eta^2\text{-}HC_2H)]$ **(2)**.

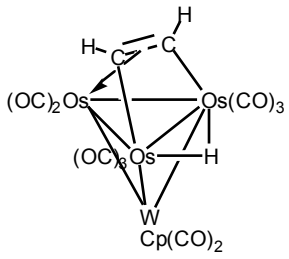

2

Dans d'autres cas, on peut obtenir des clusters de structures inattendues. Ainsi, la réaction de $[WIr_3Cp(CO)_{11}]$ avec PhC≡CPh conduit à la formation de $[WIr_3Cp(CO)_7(\mu_3\text{-}\eta^2\text{-}PhC_2Ph)_2]$ **(3)** où les deux ligands alcynes se lient au cluster d'une façon μ_3-η^2, ainsi que $[WIr_3Cp(CO)_5(\mu_3\text{-CPh})(\mu\text{-CPh})\{\mu\text{-}\eta^4\text{-C(Ph)C(Ph)C(Ph)C(Ph)}\}]$ **(4)** (eq 2).[12]

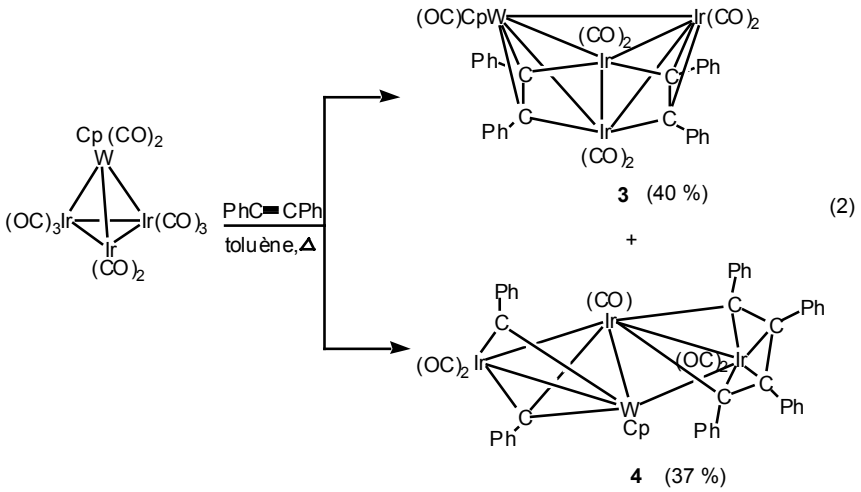

(2)

Historiquement, l'intérêt suscité par les interactions cluster-alcyne reposait sur le désir général de mieux connaître les interactions entre molécules organiques et clusters, en particulier dans le cadre de la recherche d'analogies entre clusters moléculaires et surfaces métalliques[13] et de l'importance de l'acétylène comme matière première en chimie organique industrielle. Or, quelque soit la façon dont l'alcyne se coordine au cluster, on a observé la formation de liaisons métal-carbone; les clusters résultants sont donc de ce fait plus stables. En effet, l'activation de l'alcyne et la stabilité des composés qui en résultent, permettent d'envisager des réactions de couplage et de fonctionnalisation de cet alcyne.

Couplage des clusters et systèmes π-conjugués.

Les systèmes π-conjugués possèdent des propriétés originales dues à la répartition électronique associée à la délocalisation des électrons. Il y a eu un intérêt, rapidement croissant, pour les propriétés chimiques et physiques uniques des matériaux contenant de longues chaînes de carbone sp en pont, spécialement pour leurs applications potentielles en tant que matériaux pour l'optique non-linéaire, ou de fils moléculaires,... . Les polyynes organiques, dont certains sont naturellement fluorescents, sont connus pour montrer un comportement émissif.[14] L'incorporation de centres métalliques dans de tels systèmes peut leur conférer des propriétés plus importantes, par exemple, les rendre phosphorescents ou augmenter la durée de vie de la photoluminescence résultant d'un plus grand couplage spin-orbite.

Par ailleurs, des études électrochimiques de clusters de métaux de transition ont montré qu'ils sont des réservoirs d'électrons potentiels avec des propriétés rédox qui dépendent de la sphère de coordination du coeur métallique.[15] Ce n'est donc pas surprenant que l'interconnection de ces clusters moléculaires par des chaînes carbonées insaturées et conjuguées fasse l'objet de

nombreuses études.[16-18] Ainsi, Bruce et *al.* ont obtenu le cluster, illustré dans la Figure 3a, par élimination de AuBr[P(tol)$_3$] dans la réaction entre {Au[P(tol)$_3$]}$_2${μ-(C≡C)$_n$} (n = 2–4) et le cluster alkylidyne [Co$_3$(μ_3-CBr)(μ-dppm)(CO)$_7$].[17] De même Humphrey et *al*. ont pu obtenir des diclusters du type [M$_2$Ir$_2$(μ-CO)$_4$(CO)$_4$(η^5-C$_5$H$_4$R)$_2$]$_2$(μ_8-η^4-R$_1$C$_2$BC$_2$R$_1$) (Figure 3b) par la réaction du cluster tétraédrique [M$_2$Ir$_2$(CO)$_{10}$(η^5-C$_5$H$_4$R$_2$)] avec les diynes du type R$_1$- C≡C - B - C≡C - R$_1$ (B = Espaceur).[18]

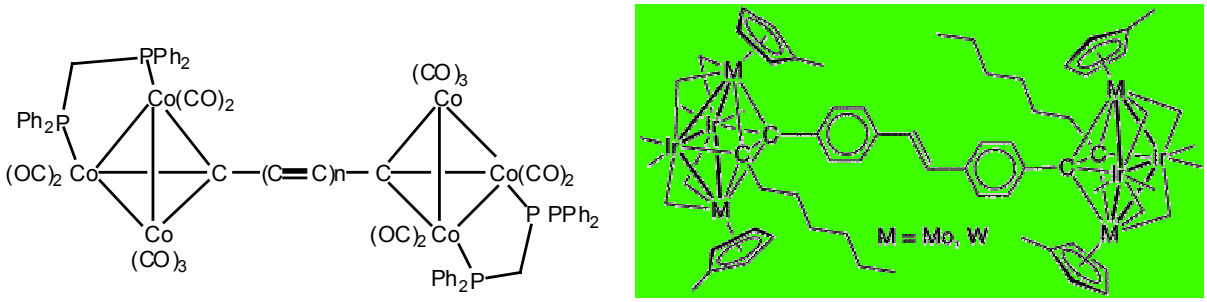

(a) (b)

Figure 3. Exemples de deux clusters couplés par des chaînes carbonées, insaturées et conjuguées.

Pour notre part, nous allons privilégier la réaction de couplage de deux unités acétyléniques, préalablement incorporées dans des clusters moléculaires.

Clusters et nanoparticules.

Un des défis actuel concerne l'utilisation de clusters moléculaires comme précurseurs de particules qui ne pourraient être obtenues par d'autres approches plus conventionelles et qui présenteraient des propriétés intrinsèques originales dans le domaine des matériaux hybrides organiques-inorganiques ainsi dans le domaine des nanoparticules confinées dans un espace inorganique. Ainsi, des particules métalliques supportées sur SiO_2 ou sur AlO_2, présentant des propriétés catalytiques originales ont été obtenues à partir de clusters Fe/Pd[19] et Pd/Mo,[20] respectivement.

Les nanoparticules sont des objets se situant par leurs dimensions entre l'état moléculaire et l'état massif. Le développement des recherches dans ce domaine est justifié par les propriétés singulières de ces objets, propriétés qui se révèlent très différentes de celle du même matériau massif.

Les deux aspects qui sont particulièrement intéressants dans le domaine des nanoparticules sont l'effet de surface et l'effet de taille quantique. Contrairement aux matériaux massifs où le nombre d'atomes de surface est négligeable par rapport au nombre d'atomes de cœur, dans le

cas des nanoparticules, il y a énormément de surface de contact avec les molécules du voisinage, ce qui est particulièrement intéressant dans le domaine de la catalyse. Dans les nanoparticules, les atomes sont regroupés en très petites entités, et non plus en structures de taille infinie par rapport à la taille des atomes. Dans ce cas, le gap entre la bande de conduction et de valence augmente sensiblement. Si la taille diminue encore, les électrons ne sont plus contenus dans la bande de conduction, mais sur des niveaux quantiques. Les propriétés électroniques, magnétiques ou optiques sont alors complètement modifiées par rapport au matériau massif.

Les nanoparticules peuvent être élaborées selon des méthodes physiques ou chimiques. Ces dernières semblent être mieux adaptées pour obtenir de petites nanoparticules uniformes, et peuvent aboutir à deux types de nanoparticules: soit supportées dans une **matrice** solide, soit libres, sous forme de poudre ou dispersées dans un liquide et qui peuvent être obtenues par réduction de sels métalliques,[21] par réduction électrochimique[22] ou par décomposition de précurseurs organométalliques par traitement thermique.[23] Dans ce dernier cas, les composés utilisés de préférence ont leur(s) centre(s) métallique(s) à bas degré d'oxydation (proche de zéro), et les clusters à bas degré d'oxydation sont donc des candidats particulièrement adaptés. Cela permet d'éviter l'utilisation de réducteurs chimiques qui peuvent engendrer des impuretés qui s'adsorbent à la surface des particules et sont difficiles à éliminer; cependant, la taille des particules est incontrôlable. En fait, à mesure que la taille des particules diminue, le rapport entre le nombre d'atomes de surfaces et d'atomes total augmente. Donc, les propriétés physiques et chimiques des matériaux peuvent être facilement modifiées en contrôlant simplement la taille des particules. Ainsi, la dispersion des particules dans **des matrices poreuses** s'avère bien adaptée pour un contrôle de la taille par celle des pores. Il existe trois grands types de matrices poreuses: les zéolithes dont les pores sont formés par le squelette cristallin d'alumino-silicate, les matrices poreuses organisées de type MCM-41 et les xérogels obtenus par séchage lent de silice ou d'alumine. Une méthode qui permet l'élaboration de ce dernier type de matrice est le procédé **sol-gel**.

Braunstein et *al*. s'intéressent à l'élaboration de nouveaux matériaux catalytiques ou magnétiques par ancrage de clusters moléculaires dans des matrices inorganiques. Ainsi, des matrices xérogel et des matrices organisées de type MCM-41 ont été utilisées pour l'ancrage de clusters bimétalliques, dans le but de former des nanoparticules magnétiques (Figure 4).[24] En effet, les progrès actuels de la synthèse conduisent à une meilleure compréhension des

propriétés des matériaux magnétiques nanoscopiques (diamètre < 100 nm) qui offrent des perspectives attrayantes dans le domaine des aimants permanents et de l'enregistrement magnétique. L'étude de ces matériaux est liée à une démarche corrélant les propriétés structurales et magnétiques au mode d'élaboration.

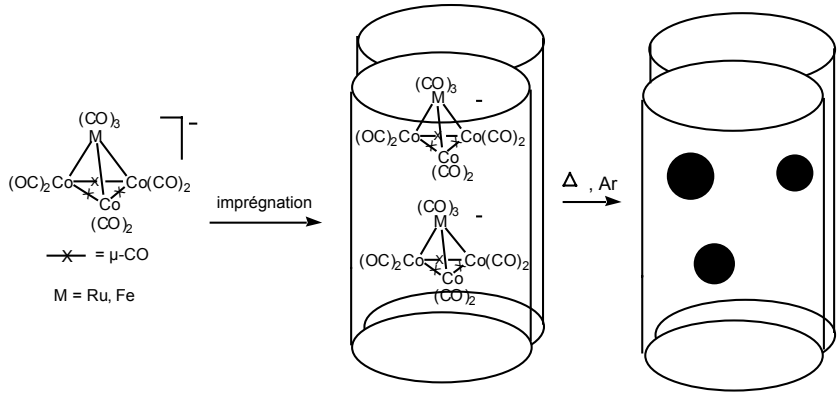

Figure 4. Schéma de principe de synthèse de nanoparticules par imprégnation de clusters bimétalliques dans des pores de matrices organisées.

Par ailleurs, l'ancrage covalent des clusters moléculaires dans les matrices inorganiques permet d'éviter les problèmes de migration non controlée lors de la conversion en nanoparticules métalliques. Ainsi, des nanoparticules de platine, de cobalt ou d'or confinées et hautement monodispersées ont été obtenues par ancrage puis traitement thermique de clusters de cobalt et ou de platine ainsi que de colloïdes d'or à l'intérieur de membranes d'alumine ou de matrices de silice poreuses (Figure 5).[25,26]

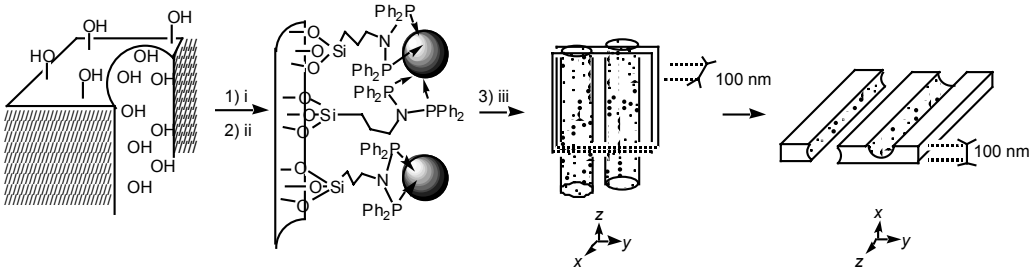

Figure 5. (i) Fonctionnalisation des matrices par des ligands contenant la fonction alcoxysilyle, (ii) coordination de clusters/colloïdes à l'intérieur de matrices fonctionnalisées, (iii) traitement thermique: vue des particules de métal à l'intérieur des pores puis vue d'une coupe de pore.

Clusters et surfaces d'or.

Un autre sujet en plein essor où les clusters sont récemment impliqués est la formation de monocouches auto-assemblées (SAMs: Self Assembled Monolayers).

Les monocouches auto-assemblées suscitent un très grand enthousiasme dans la communauté scientifique. En effet, dans des domaines divers avec des implications interdisciplinaires importantes, l'étude de ces monocouches débouche sur des résultats remarquables.[27,28]

L'auto-assemblage, au sens général du terme, peut être défini comme la formation spontanée de structures hiérarchiques complexes à partir de "briques" simples.[29] L'auto-assemblage implique par définition de multiples niveaux d'énergie et de multiples degrés de libertés. C'est au début des années 1980,[29] avec l'apparition de techniques nouvelles comme la microscopie à effet tunnel (STM), que l'étude des monocouches auto-assemblées a pris son essor. Bien que les unités moléculaires organométalliques soient utilisées depuis longtemps dans la construction de systèmes de plus en plus complexes en chimie supramoléculaire, les études physiques des surfaces sur ces systèmes sont récentes et peu développées. Il n'y a guère que des systèmes organiques qui ont fait l'objet d'études détaillées.

Dans ce cadre, les thiols (RSH) furent pris comme modèle de base. Actuellement, les SAMs constituent la base de nombreuses recherches de modèles biologiques. Le but est de comprendre les propriétés de la surface d'un point de vue physique et chimique.

Les chaînes alcane-thiols[29] (association d'un alcane et d'un groupement fonctionnel thiol SH) imitent les molécules biologiques, qui s'auto-assemblent, en formant une monocouche organisée sur des surfaces métalliques. Les alcane-thiols s'adsorbent spontanément sur une surface d'or, d'argent, de platine ou de cuivre à partir d'une solution. L'or est le métal le plus fréquemment utilisé car il ne s'oxyde pas dans les conditions ambiantes (Figure 6).

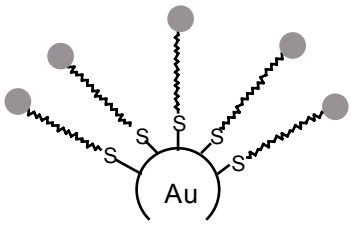

Figures 6. Description schématique de couches auto-organisées sur une surface d'or

Le groupement thiol (S-H) de la molécule se lie à la surface d'or par la formation d'une liaison covalente thiolate (S-Au) : il y a chimisorption. Les forces attractives de van der Waals entre les chaînes voisines augmentent la stabilité et l'ordre des SAMs.

L'organisation de clusters sur une surface doit conduire à l'émergence de nouvelles propriétés telles que la modification du comportement redox de l'ensemble par rapport à celui d'un cluster moléculaire isolé.[30]

On voit que la chimie des clusters jouent un rôle majeur dans des domaines importants et très divers. Il importe donc de savoir d'abord synthétiser de manière rationnelle et systématique des clusters fonctionnalisés ou fonctionnalisables de nucléarité et composition données avec de bon rendements.

Dans le présent travail nous exposerons la préparation de nouveaux alcynes et de nouveaux clusters alcynes fonctionnalisés ainsi que leur caractérisation, essentiellement par RMN, IR et RX et l'étude des propriétés magnétiques de certains de ces clusters.

Notre étude a été focalisée au début sur le cluster tétraédrique homométallique $[Co_4(CO)_{12}]$. Ce cluster, qui se fragmente en présence des alcynes, a dû être préalablement stabilisé par des phosphines bidentates. La fonction $-Si(OR)_3$ a été incorporée par la suite dans ces clusters stabilisés par de nouveaux alcynes en vu d'une condensation ultérieure de ces espèces avec des matrices minérales par des méthodes sol-gel. Nous nous sommes également intéressés à la réactivité de ces clusters stabilisés avec les diynes. Ce travail a fait l'objet du premier chapitre.

Nous avons par la suite étendu notre étude au cluster hétéropolymétallique ionique, $[NEt_4][RuCo_3(CO)_{12}]$, qui est isoélectronique de $[Co_4(CO)_{12}]$. Un aspect particulier de ce travail a concerné l'optimisation de la synthèse de ce cluster mixte. Ainsi, il peut être obtenu avec un rendement de 73% par déhalogénation carbonylante du complexe $[NEt_4][RuCl_4(CH_3CN)_2]$ en présence de $[Co_2(CO)_8]$, dans le THF selon le Schéma réactionnel suivant:[31]

$$RuCl_3, x\,H_2O + [Et_4N]Cl \xrightarrow{HCl,\ Hg} 1/2\ [Et_4N]_2[Ru_2Cl_7(OH)_3].\ HCl$$

$$1/2\ [Et_4N]_2[Ru_2Cl_7(OH)_3].\ HCl \xrightarrow{CH_3CN} [Et_4N][RuCl_4(CH_3CN)_2] + x\,H_2O$$

$$[Et_4N][RuCl_4(CH_3CN)_2] + 5/2\ Co_2(CO)_8 \xrightarrow{THF} [Et_4N][RuCo_3(CO)_{12}].\ 1/3\ THF + 2CoCl_2$$

L'accès simple à ce composé et sa stabilité ont permis d'effectuer de nombreuses études sur le comportement réactionnel de l'entité $RuCo_3$.[5a,b, 32-41]

Le second chapitre a donc fait l'objet de la synthèse de clusters alcynes mixtes Ru/Co, contenant la fonction $-Si(OR)_3$ ou –SR par deux approches complémentaires. L'incorporation de la fonction SR a été réalisée afin de permettre ultérieurement la fixation de ces clusters sur une surface d'or, ceci par une liaison S-Au dative ou covalente. On peut noter aussi que le composé $[Co_2(CO)_8]$ est un produit commercial qui réagit rapidement avec les alcynes à

température ambiante pour donner des complexes de types $[Co_2(CO)_6(\mu\text{-}\eta^2\text{-alcyne})]$. Ainsi, pour bien caractériser les nouveaux ligands et leur complexes, nous avons exploité sa réactivité.

Le troisième chapitre a été consacré à la synthèse de clusters-alcynes mixtes Ru/Co (ou Fe/Co) fonctionnalisables au travers de fonctions pendantes tels que des liaisons multiples. Ces clusters ont également été étudiés pour des réactions de couplage entre deux unités clusters-alcynes.

Enfin, la synthèse de nanoparticules magnétiques, dispersées dans des matrices de silice mésoporeuse, par greffage de nos alcynes et clusters-alcynes contenant la fonction alcoxysilyle sera exposée dans le quatrième chapitre. Cette étude fut réalisée en collaboration avec l'Institut de Physique et Chimie des Matériaux de Strasbourg (IPCMS) .

Références:

(1) Braunstein, P.; Rosé, J. *Catalysis by Di- and Polynuclear Metal Clusters,* Adams, R. D.; Cotton, F. A., Eds,; John Wiley, NewYork, **1998**, 443.

(2) Braunstein, P.; Rosé, J. *Heterometallic Clusters in Catalysis*, in *Metal Clusters in Chemistry,* Braunstein, P.; Oro, L. A.; Raithby, P. R., Eds.; Wiley-VCH, Weinheim (Germany), **1999**, Vol. 2, pp. 616-677.

(3) Braunstein, P. *L'Actualié. Chimique*. **1996**, *7*, 75-85.

(4) (a) Sappa, E.; Tiripicchio, A.; Braunstein, P. *Chem. Rev.* **1983**, *83*, 203-239; (b) Raithby, P.; Rosales, M. J. *Adv. Inorg. Chem. Radiochem.* **1985**, *29*, 169-247.

(5) (a) Braunstein, P.; Rosé, J.; Bars, O. *J. Organomet. Chem.* **1983**, *252*, C101-C105; (b) Braunstein, P.; Jiao, F. Y.; Rosé, J.; Granger, P.; Balegroune, F.; Bars, O. Grandjean, D. *J. Chem. Soc., Dalton Trans.* **1992**, 2543-2550; (c) Waterman, S. M.; Humphrey, M. G.; Tolhurst, V.-A.; Bruce, M. I.; Low, P. J.; Hockless, D. C. R. *Organometallics* **1998**, *17*, 5789-5795; (d) Ferrand, V.; Süss-Fink, G.; Neels, A.; Stoeckli-Evans, H. *Eur. J. Inorg. Chem.* **1999**, 853-862; (e) Zhu, B.-H.; Zhang, W.-Q.; Zhao, Q.-Y.; Bian, Z.-G.; Hu, B.; Zhang, Y.-H.; Yin, Y.-Q.; Sun, J. *J. Organomet. Chem.* **2002**, *650*, 181-187.

(6) (a) Bruce, M. I.; Low, P. J.; Werth, A.; Skelton, B. W.; White, A. H. *J. Chem. Soc., Dalton Trans.* **1996**, 1551-1566.

(7) Albiez, T.; Bernhardt, W.; Schnerning, C. v.; Roland, E.; Bantel, H.; Vahrenkamp, H. *Chem. Ber*. **1987**, *120*, 141-151.

(8) (a)Mathur, P.; Srinivasu, C.; Ahmed, M. O.; Puranik, V. G.; Umbarkar, S. B. *J. Organomet Chem*. **2002,** 659, 196-201; (b) Fischer, K.; Müller, M.; Vahrenkamp, H. *Angew. Chem. Int. Ed. Engl*. **1984**, *23*, 140-142.

(9) (a) Went, M. J. *Adv. Organomet. Chem.* **1997**, *41*, 69-125; (b) Braunstein, P.; Graiff, C.; Morise, X.; Tiripicchio, A. *J. Organomet Chem*. **1997,** *541*, 417-422; (c) Bruce, M. I.; Halet, J. F.; Kahlal, S.; Low, P. J.; Skelton, B. W.; White, A. H. *J. Organomet Chem*. **1999,** *578*, 155-168.

(10) Chetcuti, M. J.; Fanwick, P. E.; Gordon, J. C. *Inorg. Chem.* **1991**, *30*, 4710-4717.

(11) Churchill, M. R.; Bueno, C.; Park, J. T.; Shapley, J. R. *Inorg. Chem.* **1984**, *23*, 1017-1021.

(12) Shapley, J. R.; Humphrey, M. G.; McAteer, C. H. *In Selectivity in catalysis*; ACS Symposium Series; Davis, M., Suib, S., Eds; American Chemical Society: Washington, DC, 1993; Vol. 517, Chapter 9.

(13) (a) Muetterties, E. L. *Chem. Soc. Rev*., **1982**, *11*, 283, (b) Mutterties, E. L.; Rhodin, T. N.; Band, E.; Brucker, C. F.; Pretzer, W. R., *Chem. Rev*. **1979**, *79*, 91.

(14) Yam, V. W. W.; Chong, S. H. F.; Ko, C. C.; Cheung, K. K. *Organometallics* **2000,** *19*, 5092-5097.

(15) Zanello, P.; de Biani, F. F. *In Metal Clusters in Chemistry*; Braunstein, P., Oro, L. A., Raithby, P. R., Eds.; Wiley-VCH: Weinheim,Germany, 1999; Vol. 2, p 1104.

(16) Diederich, F. *Nature* **1994**, *369*, 199-207.

(17) Bruce, M. I.; Smith, M. E. Zaitseva, N. N.; Skelton, B. W.; White, A. H. *J.Organomet. Chem.* **2003**, *670*, 170-177.

(18) Lucas, N. T.; Notaras, E. G. A.; Cifuentes, P. P.; Humphrey, M. G. *Organometallics* **2003**, *22*, 284-301 et références citées.

(19) Braunstein, P.; Devenish, R.; Gallezot, P.; Heaton, B. T.; Humphreys, C. J.; Kervennal, J.; Mulley, S.; Ries, M, *Angew.Chem. Int. Ed. Engl.,* **1988**, 27, 927-929.

(20) Braunstein, P.; Bender, R.; Kervennal, J, *Organometallics*, **1982**, *22*, 1236-1238.

(21) Faraday, M. *Philos. Trans. R. Soc. London,* **1875***, 147,* 145.

(22) Reetz, M. T.; Helbig, W. *J. Am. Chem. Soc.,* **1994,** *116*, 7401.

(23) Voir par exemple: (a) Hess, H. P.; Parker H. P. *J. Appl. Sci.,* **1966,** *10,* 1915; (b) Suslick, K. S.; Fang, M.; Hyeon, T. *J. Am. Chem. Soc.,* **1996,** *118*, 11960-11961s; (c) Gonsalves, K. E.; Rangarajan, S. E. Garcia-Ruiz, A.; Law, C. C. *J. Mater. Sci. Lett.,* **1996,** *15,* 1264. (d) Zhao, X. Q.; Zheng, F.; Liang, Y.; Hu, Z. Q.; Xu, Y. B. *J. Mater. Lett.,* **1994,** *21,* 285.

(24) Schweyer, F.; Braunstein, P.; Estournès, C.; Guille, J.; Kessler, H.; Paillaud, J.-L.; Rosé, J. *Chem. Commun.* **2000**, 1271-1272.

(25) Braunstein, P.; Kormann, H. -P.; Meyer-Zaika, W.; Pugin, R.; Schmid, G. *Chem. Eur. J*. **2000**, *6*, 4637-4646.

(26) Schweyer-Tihay, F.; Braunstein, P.; Estournès, C.; Guille, J. L.; Lebeau, B.; Paillaud, J.–L.; Richard-Plouet, M.; Rosé, J. *Chem. Mater***. 2003**, *15*, 57-62.

(27) Dhirani, A.; Zehner, R. W.; Hsung, R. P.; Guyot-Sionnest, P.; Sita, L. R. *J. Am. Chem. Soc.* **1996**, *118*, 3319-3320.

(28) Hasan, M.; Bethell, D.; Brust, M. *J. Am. Chem. Soc*. **2002**, *124*, 1132-1133 et références cités

(29) Schreiber, F. *Prog. Surf. Sci.* **2000**, *65*, 151-256.

(30) Prokopuk, N.; Shriver, D. F. *Chem. Mater*. **1998,** *10*, 10.

(31) Braunstein, P.; Rosé, J, *Inorg. Synth.,* **1989**, *26,* 356-360.

(32) Braunstein, P.; Rosé, J. *J. Organomet Chem*. **1984,** *262*, 223-226.

(33) Braunstein, P.; Rosé, J.; Tiripicchio- Camellini, M. *Angew. Chem. Int. Ed. Engl.* **1985**, *24*, 767-768.

(34) P. Braunstein, P.; Rosé, J.; Dedieu, A.; Dusausoy, Y.; Mangeot, J. P.; Tripicchio, A.; . Tripicchio- Camellini, M. *J. Chem. Soc. Ddalton Trans*. **1986**, 225-234.

(35) Braunstein, P.; Rosé, J.; Granger, P.; Raya, J.; Bouaoud, S.-E.; Grandjean, D. *Organometallics* **1991,** *10*, 3686.

(36) Hirschinger, J.; Granger, P.; Rosé, J. *J. Phys. Chem*. **1992**, *96*, 4815-4820.

(37) Braunstein, P.; Rosé, J.; Tiripicchio, A.; Tiripicchio- Camellini, M. *J. Chem. Soc. Ddalton Trans*. **1992**, 911-920.

(38) Braunstein, P.; Mourey, L.; Rosé, J.; Granger, P.; Richert, T.; Balegroune, F.; Grandjean, D. *Organometallics* **1992,** *11*, 2628.

(39) Braunstein, P.; Rosé, J.; Toussaint, D.; Jääskeläinen, S.; Ahlgrèn, M.; Pakkanen, T. A.; Pursiainen, J.; Toupet, L. *Organometallics* **1994,** *13*, 2472.

(40) Bouherour, S.; Braunstein, P.; Rosé, J.; Toupet, L. *Organometallics* **1999,** *18,* 4908.

(41) Braunstein, P.; Graiff, C.; Massera, C.; Predieri, G.; Rosé, J.; Tiripicchio, A. . *Inorg. Chem.* **2002,** *41*, 1372-1382.

Chapitre 1

Les réactions des clusters tétranucléaires de cobalt stabilisés par des diphosphines avec des alcynes contenant la fonction -Si(OR)$_3$.

Ce chapitre est présenté sous la forme d'une publication en cours d'impression dans *Organometallics*.

Reactions of Diphosphine-Stabilized Tetracobalt Carbonyl Clusters with –Si(OR)$_3$ Functionalized Alkynes

Aldjia Choualeb,[a] Pierre Braunstein,*[a] Jacky Rosé,[a] Salah-Eddine Bouaoud[b] and Richard Welter[c]

[a] *Laboratoire de Chimie de Coordination (UMR 7513 CNRS), Université Louis Pasteur, 4 rue Blaise Pascal, F-67070 Strasbourg Cedex, France*

[b] *Département de chimie-Faculté des Sciences-Université des Frères Mentouri-Constantine, Route de Ain el Bey, Algeria*

[c] *Laboratoire DECMET (UMR 7513 CNRS), Université Louis Pasteur, 4 rue Blaise Pascal, F-67070 Strasbourg Cedex, France*

Short-bite ligand cluster stabilization is achieved in the tetrahedral clusters $[Co_4(\mu\text{-}CO)_3(CO)_7(\mu\text{-}dppy)]$ (**1a-c**), obtained in high yields by reactions of $[Co_4(CO)_{12}]$ with one equiv. of the diphosphine ligands dppy, $Ph_2PCH_2PPh_2$ (dppm), $Ph_2PNHPPh_2$ (dppa) or $(Ph_2P)_2N(CH_2)_3Si(OEt)_3$ (dppaSi), respectively. The structure of **1a** has been determined by X-ray diffraction and the P atoms occupy axial positions on the basal face, transoid to a Co-Co bond. Clusters **1a-c** were reacted with phenylacetylene to afford the corresponding butterfly clusters $[Co_4(\mu\text{-}CO)_2(CO)_6(\mu\text{-}dppy)(\mu_4\text{-}\eta^2\text{-}PhC_2H)]$ (**2a-c**) by insertion of the alkyne into a Co-Co bond of the precursor. This was established by an X-ray diffraction study of $[Co_4(\mu\text{-}CO)_2(CO)_6(\mu\text{-}dppm)(\mu_4\text{-}\eta^2\text{-}PhC_2H)]$ (**2a**). In an alternative synthetic procedure, the alkyne cluster $[Co_4(CO)_{10}(\mu_4\text{-}\eta^2\text{-}PhC_2H)]$ (**3**), prepared from $[Co_4(CO)_{12}]$ and phenylacetylene, was reacted with the diphosphines dppy. This led in good yields to butterfly

clusters, isomeric of **2a-c** in term of the position of the bridging carbonyls, as revealed by an X-ray diffraction study of the dppa derivative **2'b•**$0.5CH_2Cl_2$. In order to obtain suitable cluster precursors to sol-gel materials, we have reacted **1a,b** with the new trialkoxysilyl alkyne $PhC{\equiv}CC(O)NH(CH_2)_3Si(OMe)_3$ (**L^1**) and isolated the corresponding butterfly, functionalized clusters $[Co_4(\mu\text{-}CO)_2(CO)_6(\mu\text{-}dppy)\{\mu_4\text{-}\eta^2\text{-}PhC_2C(O)NH(CH_2)_3Si(OMe)_3\}]$ (**4a,b**), respectively. Similar reactions between **1a,b** and the alkyne $HC{\equiv}CCH_2NHC(O)NH(CH_2)_3Si(OEt)_3$ (**L^2**) afforded the related clusters $[Co_4(\mu\text{-}CO)_2(CO)_6(\mu\text{-}dppy)\{\mu_4\text{-}\eta^2\text{-}HC_2CH_2NHC(O)NH(CH_2)_3Si(OEt)_3\}]$ (**5a,b**). The cluster $[Co_4(\mu\text{-}CO)_2(CO)_6(\mu\text{-}dppm)\{\mu_4\text{-}\eta^2\text{-}HC_2(CH_2)_2OC(O)NH(CH_2)_3Si(OEt)_3\}]$ (**6a**) was obtained by reaction of **1a** with $HC{\equiv}C(CH_2)_2OC(O)NH(CH_2)_3Si(OEt)_3$ (**L^3**). Reaction of $[Co_4(CO)_{12}]$ with **L^1** led to the formation of the dinuclear complex $[Co_2(CO)_6\{\mu\text{-}\eta^2\text{-}PhC_2C(O)NH(CH_2)_3\ Si(OMe)_3\}]$ (**7**), which was also prepared by reaction of $[Co_2(CO)_8]$ with **L^1**. Reaction of **1a** with dppaSi afforded the mixed-diphosphine cluster $[Co_4(\mu\text{-}CO)_3(CO)_5(\mu\text{-}dppm)(\mu\text{-}dppaSi)]$ (**8**), which was characterized by X-ray diffraction. In the course of attempts at linking two molecules of **2a** with 1,4 diodobenzene under Sonogashira conditions, the dinuclear complex $[Co_2(CO)_4(\mu\text{-}dppm)\{\mu\text{-}\eta^2\text{-}PhC_2H\}]$ (**9**) was isolated instead. Reaction of 1,4-bis(trimethylsilyl)butadiyne (**L^4**) with $[Co_4(CO)_{12}]$ afforded the known complex $[\{Co_2(CO)_6(\mu_2\text{-}\eta^2\text{-}Me_3SiC_2\text{-})\}_2]$ (**10**) and with **1a** yielded the desired product $[Co_4(CO)_8(\mu\text{-}dppm)(\mu_4\text{-}\eta^2\text{-}Me_3SiC_2C{\equiv}CSiMe_3)]$ (**12**), in addition to the known complex $[Co_2(CO)_4(\mu\text{-}dppm)(\mu\text{-}\eta^2\text{-}Me_3SiC_2C{\equiv}CSiMe_3)]$ (**13**). Desilylation of **12** using TBAF/THF-H_2O occurred unexpectedly at the cluster core-bound alkyne carbon to afford $[Co_4(\mu\text{-}CO)_2(CO)_6(\mu\text{-}dppm)\ (\mu_4\text{-}\eta^2\text{-}HC_2C{\equiv}CSiMe_3)]$ (**16**), instead of the anticipated cluster $[Co_4(\mu\text{-}CO)_2(CO)_6(\mu\text{-}dppm)\ (\mu_4\text{-}\eta^2\text{-}Me_3SiC_2C{\equiv}CH)]$. The crystal structure of **16** has been determined by X-ray diffraction.

Introduction

The confinement of molecular clusters in the cavities of meso- or nano-porous inorganic matrices, followed by thermal activation under inert atmosphere, has considerable potential for the stabilization of highly dispersed metal particles whose coalescence into larger, ill defined aggregates can thus be prevented. This approach has obvious relevance to the fabrication of microelectronic devices[1] and to the preparation of new catalyts whose selectivity will critically depend on the size and dispersion of the metal particles and also on the shape of the cavity in which they are embedded.[2,3] We have shown that impregnation of a mesoporous xerogel or of MCM-41 with an organic solution of the heterometallic cluster $[NEt_4][Co_3Ru(CO)_{12}]$, and subsequent thermal treatment lead to highly dispersed magnetic nanoparticles under milder conditions than when conventional metal salts are used as precursors.[4]

In addition to the impregnation method, and since the nature of the interactions between the metal cluster and the host matrix plays a very important role, in particular but not solely in controling the quantity of metal incorporated, it appears attractive to develop anchoring methods which consit in the grafting of molecular metal clusters into the pores of the matrix[5] by using a bifunctional ligand which would provide a stronger link between the molecular precursor and the host.[6] This ligand should also lead to a stable molecular species in order to minimize the risk of breaking the metal-ligand interaction, and thus avoid leaching of the metal complex. We have begun to explore general approaches to this aim, by attaching first one end of the ligand to the inorganic matrix and then react the other functional end with the molecular cluster, or first prepare the functionalized cluster and react it with the host matrix to generate the covalent linkage.[7] We have prepared the short-bite alkoxysilyl-functionalized diphosphine ligands $(Ph_2P)_2N(CH_2)_3Si(OMe)_3$ and $(Ph_2P)_2N(CH_2)_4SiMe_2(OMe)$ and $(Ph_2P)_2N(CH_2)_3Si(OEt)_3$ [7,8] and used them to derivatize

the pore walls of nanoporous alumina membranes.[7] The covalent attachment of the diphosphine ligands by Si-O bond formation provides a molecular anchor that allowed subsequent reaction with the derivative $[Co_4(CO)_{10}(\mu\text{-dppa})]$ (dppa = $Ph_2PNHPPh_2$) **1b**,[9] which has a more selective substitution chemistry than the parent $[Co_4(CO)_{12}]$ (Scheme 1).[7]

Scheme 1. Anchoring of a Co_4 Cluster into Functionalized Alumina Membranes.[7]

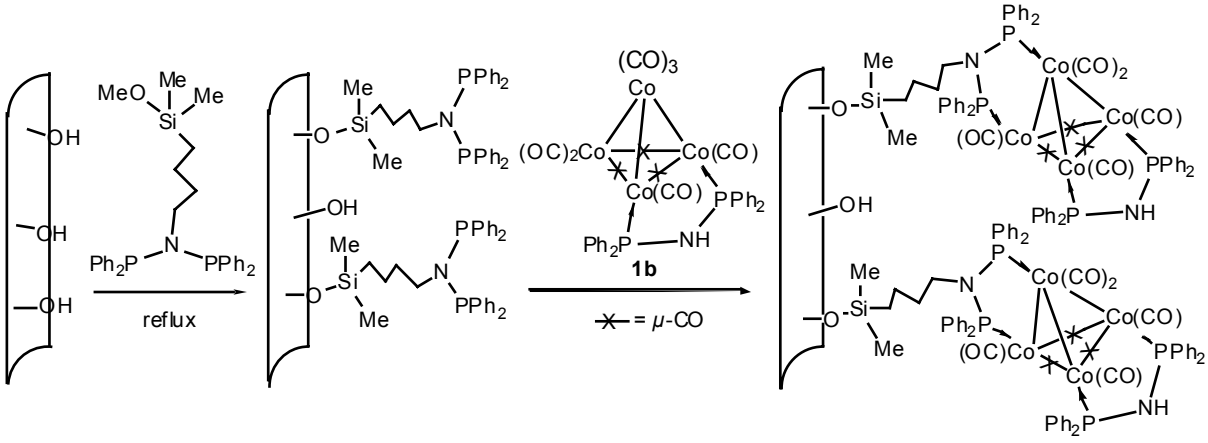

We have also used an ordered mesoporous silica of the type SBA-15 as matrix,[10] with $(Ph_2P)_2N(CH_2)_3Si(OMe)_3$ as anchoring ligand.[7] The molecular cluster to be tethered was again $[Co_4(CO)_{10}(\mu\text{-dppa})]$ and subsequent thermal treatment of the organometallic hybrid mesoporous silica led to pure nanocrystalline Co_2P particles that were more regular in spatial repartition, size and shape than when a silica xerogel, obtained by the sol-gel process, was used.[11]

In such systems, the dative bonding between the functional ligand and the cluster results from donation of the phosphorus lone pair to the metal, and the improved stability of the diphosphine system compared to a monophosphine linkage results from the formation of a stable $\overline{\text{MPNPM}}$' five-membered ring. Generating a *covalent* linkage between the metal complex and the host matrix represents an attractive extension and we have already applied the sol-gel process to incorporate mono- and bimetallic species into an inorganic matrix by condensation of alkoxysilyl-substituted metal alkyl complexes with TEOS.[12] We were interested in developing other ligand systems that would form strong, covalent bonds with the

metal cluster and could be amenable to condensation with an inorganic matrix or its precursor (e.g. TEOS). Functional alkynes appeared to us suitable candidates since interaction of their carbon-carbon triple bond with two or more metal centers can lead to the formation of strong, covalent metal-carbon σ bonds[13] and we have recently reported our first results in this direction.[14] In this context, we have focused the present work on the preparation and characterization of molecular precursors based on tetranuclear cobalt carbonyl clusters, which could give rise to interesting magnetic materials.[4] The cluster $[Co_4(CO)_{12}]$ has a rich substitution chemistry[15-18] and its reactions with suitably functionalized alkynes may afford suitable precursors for subsequent anchoring processes upon condensation reaction between this function and surface OH groups. However $[Co_4(CO)_{10}(\mu_4\text{-}\eta^2\text{-alkyne})]$ clusters, of which the first example reported in the literature was $[Co_4(CO)_{10}(\mu_4\text{-}\eta^2\text{-}EtC_2Et)]$,[19] are often prone to decomposition, giving $[Co_2(CO)_6(\mu\text{-}\eta^2\text{-alkyne})]$ complexes,[15b,20] which is consistent with the greater reactivity of $[Co_4(CO)_{10}(\mu_4\text{-}\eta^2\text{-alkyne})]$ clusters compared to the corresponding dicobalt complexes $[Co_2(CO)_6(\mu\text{-}\eta^2\text{-alkyne})]$.[21] Stabilization of these clusters against fragmentation with bi-or polydentate phosphines is therefore desirable.[22]

It was also hoped that this metal core stabilization would lead to improved yield and selectivity of reactions between the metal clusters and alkynes. We have focused on short-bite diphosphine ligands such as $Ph_2PCH_2PPh_2$ (dppm), $Ph_2PNHPPh_2$ (dppa) and the functionalized diphosphine $(Ph_2P)_2N(CH_2)_3Si(OEt)_3$ (dppaSi) known to be suitable for supporting a metal-metal bond and increasing cluster stability.[23] By combining the beneficial basicity of phosphine donors and the bridging ability of these diphosphine ligands which results in five-membered rings, we hoped to obtain functional alkyne-substituted clusters more stable than when starting from $[Co_4(CO)_{12}]$.

In this paper, we describe the synthesis and X-ray diffraction studies of diphosphine derivatives of $[Co_4(CO)_{12}]$, of two isomers of Co_4-alkyne diphosphine clusters and report an

investigation on the substitution reactions of diphosphine derivatives of $[Co_4(CO)_{12}]$ with new alkynes containing alkoxysilyl functions suitable to form sol-gel materials. We also undertook an investigation of the reactions of $[Co_4(CO)_{12}]$ and its diphosphine derivatives with the conjugated, protected diyne 1,4-bis(trimethylsilyl)butadiyne. Only a few reactions of $[Co_4(CO)_{12}]$ with diynes have been reported.[24] Subsequent functionalization of these clusters should be possible and studies with non-protected diynes have shown that they behave toward the cluster effectively as two separate alkyne units. Recently, the first example of tetracobalt metalloligated (or 'spiked') triangular cluster containing an acetylide ligand, $[Co_4(CO)_{10}(\mu\text{-}CO)\{H_2C{=}CC(Me)_2N(Me)C(Me)C(\mu_4\text{-}C)\}]$, was prepared by reaction of $[Co_4(CO)_{12}]$ with the diacetylenic amine $N(Me)(HC{\equiv}CCMe_2)_2$.[25]

Results and Discussion

Synthesis and Characterization of the Clusters $[Co_4(\mu\text{-}CO)_3(CO)_7(\mu\text{-}dppy)]$ (1a-c). Reaction of $[Co_4(CO)_{12}]$ with one equiv. of dppm, dppa or dppaSi in CH_2Cl_2 or in hexane at room temperature afforded rapidly the tetrahedral clusters **1a-c** in which the diphosphine ligand has substituted two carbonyl ligands and bridges two basal cobalt atoms (Scheme 2). This has been previously reported in the case of **1b**.[9] The structure of **1a** has now been determined by X-ray diffraction to provide more comparative data. A view of the structure is shown in Figure 1 and selected bond distances and angles are given in Table 1.

The molecular structure of **1a** contains a slightly distorted tetrahedral Co_4 cluster. There is almost a mirror plane passing through the cluster which contains the atoms Co(3), Co(4), C(6), C(7), C(10) and C(23). The basal face Co(1)-Co(3) has three edge-bridging carbonyl groups and the P substituents occupy axial positions at Co(1) and Co(2) with P(1)-Co(1)-Co(4) and P(2)-Co(2)-Co(4) angles of 159.56(4) and 157.70(4)°, respectively. The Co-Co edge bridged by the dppm ligand (Co(1)-Co(2) = 2.4268(8) Å), is shorter than the other

two (Co(1)-Co(3) = 2.4565(7) Å and Co(2)-Co(3) = 2.4540(8) Å). The remaining seven carbonyl ligands are essentially linear (Co-C-O = 177.0(4)-179.2(4)°). The Co-P bond lengths (Co(1)-P(1) = 2.190(1) Å and Co(2)-P(2) = 2.194(1) Å) are within the range of those observed in phosphine and phosphite derivatives of $[Co_4(CO)_{12}]$.[26,27] The five-membred ring Co_2P_2C adopts an envelope conformation with the CH_2 group at the flap. The P(1)-C(23)-P(2) angle of 114.5(2)° is larger than in $[Co_4(CO)_8\{\mu\text{-}Me_2PCH_2PMe_2\}_2]$ (107.5(4) and 110.7(4) °) taken for comparison in the absence of a dppm analog.[28a] The P-C-P angle in dppm complexes is generally smaller than the P-N-P angle in the corresponding dppa complexes, with typical values of *ca*. 107 and 119°, respectively.[23c,d] A notable exception was found in the rectangular cluster $[Pd_4(\mu\text{-}Cl)_2(\mu\text{-}dppm)_2(\mu\text{-}dppa)_2]^{2+}$ which displays P-C-P and P-N-P angles of 118.9(2) and 113.5(2), respectively.[23b] In the free ligands, the P-C-P and P-N-P angles in dppm and dppa are 106.2(3)[28b] and 118.9(2)°, respectively.[28c,d]

The structural similarity between clusters **1a-c** is supported by the pattern of the ν(CO) absorptions in the IR spectrum and the singlet in the $^{31}P\{^1H\}$ NMR spectrum for the two equivalent P nuclei. The broadening of the $^{31}P\{H\}$ NMR signals for all complexes is consistent with the rapid relaxation[29] induced by the quadrupolar Co nuclei (I = 7/2). Best yields of **1a** were obtained with very short reaction times since this molecule progressively transforms to give the green, tetrasubstituted cluster $[Co_4(CO)_8(\mu\text{-}dppm)_2]$. This latter cluster is also obtained by reaction of excess dppm with $[Co_4(CO)_{12}]$ or by thermal treatment of $[Co_2(CO)_6(\mu\text{-}dppm)]$.[30] Since it did not react with PhC≡CH, even when Me_3NO was used as CO activator, it was not further investigated.

Synthesis and Characterization of the Clusters $[Co_4(\mu\text{-}CO)_2(CO)_6(\mu\text{-}dppy)(\mu_4\text{-}\eta^2\text{-}PhC_2H)]$ (2a-c). Clusters **1a-c** were reacted with excess phenylacetylene to afford the green butterfly clusters **2a-c** in high yield (Scheme 2). This was established by an X-ray diffraction

study of **2a** and a view of the structure is shown in Figure 2. Selected bond distances and angles are given in Table 2 and discussed below. Insertion of the alkyne into a Co-Co bond of the precursor has occurred between one of the phosphine-substituted Co centers of **1a** and, most likely, the apical Co atom since it should be easier to break a Co-Co bond not supported by a bridging CO ligand. However, the related isoelectronic cluster $[RuCo_3(CO)_{12}]^-$, which has an apical $Ru(CO)_3$ fragment, also reacted with alkynes to afford butterfly clusters in which a Co-Ru bond forms the hinge of the butterfly,[31] implying that in this case a CO-bridged Co-Co bond was the site of alkyne insertion.

Scheme 2. Synthetic Routes to Butterfly Clusters 2a-c and Their Isomers 2'a-c

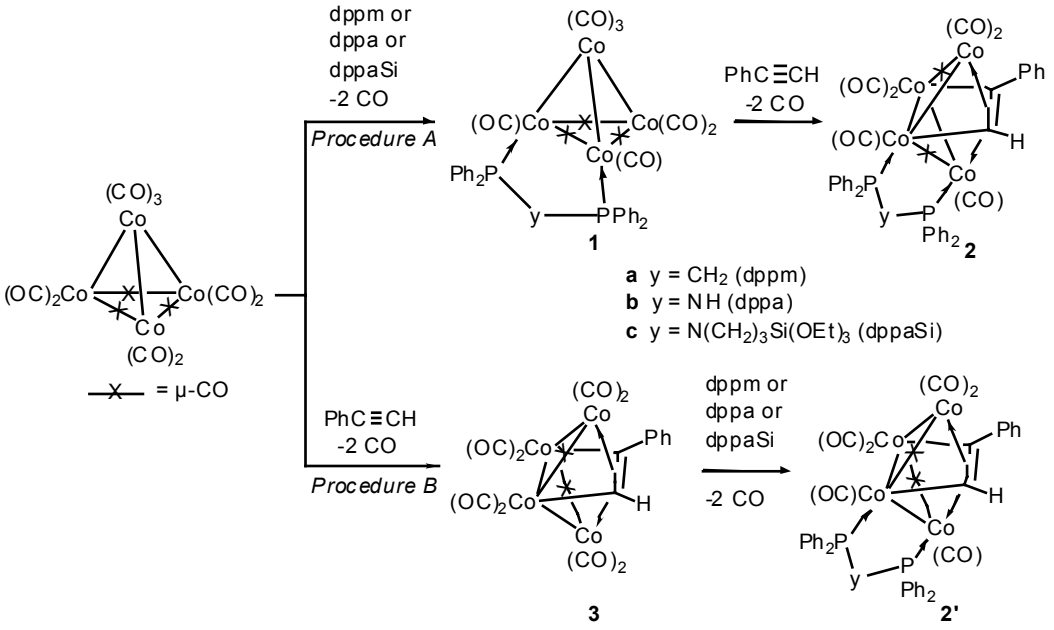

Whereas the ^1H NMR spectrum of **1a** in $CDCl_3$ showed a broad resonance at 2.85 ppm for the CH_2 protons, they appeared as an ABXY spin system ($CH^ACH^BP_2$) in **2a**, as expected from the loss of symmetry in **2**. At room temperature, the $^{31}P\{H\}$ NMR spectrum of **2b** contains two broad resonances at δ 81.2 and 87.4 ppm for the two chemically different P nuclei, in contrast to **2a** and **2c** for which only one broad resonance was observed, at 28.3 and 81.0 ppm, respectively. We verified for **2a** that at 0 °C this resonance splits into two broad signals with a 1:1 intensity. The *J*(PP) coupling could not be resolved owing to the broadness of the

signals. We assume that **2b,c** have a structure analogous to that of **2a**. We have no evidence for the formation of isomeric structures corresponding to an opposite orientation of the alkyne in the cluster; the latter would be disfavored for steric reasons, owing to repulsion between the phenyl groups.

Synthesis and Characterization of the Isomeric Clusters [$Co_4(\mu\text{-}CO)_2(CO)_6(\mu\text{-dppy})(\mu_4\text{-}\eta^2\text{-}PhC_2H)$] (2'a-c). In an alternative synthetic procedure, we reacted the alkyne-cluster **3**, derived from [$Co_4(CO)_{12}$] and phenylacetylene,[24] with the diphosphines dppy (Scheme 2, Procedure B). Although this led to the expected carbonyl substitution at the butterfly cluster in good yields, an X-ray diffraction study of the dppa derivative **2'b**•0.5CH_2Cl_2 revealed that an isomer of **2b** has formed. A view of the structure of **2'b** is shown in Figure 3 and selected bond distances and angles are given in Table 3. Like in **2b**, a Co-Co bond connecting a wing-tip and a hinge atom is supported by the diphosphine and the alkyne phenyl group is in a remote position with respect of the PPh_2 group. However, disubstitution of CO in **3** by dppa has occurred regiospecifically on an unbridged Co-Co edge, and the two bridging carbonyls do not span the same Co-Co bonds as established in **2a** and assumed in **2b**. Clusters **2b** and **2'b** are not mirror images of each other. Their IR spectra are however very similar. Disubstitution of CO in [$Co_4(CO)_{10}(\mu_4\text{-}\eta^2\text{-alkyne})$] clusters by monophosphines has been reported to occur regiospecifically on the wing-tip atoms,[32] which is of course impossible with diphosphines such as dppy. As was observed for **2b**, the $^{31}P\{H\}$ NMR spectrum of **2'b** shows two signals, at δ 79.7 and 87.6 ppm.

The alkyne C(9)-C(10) bond of 1.405(4) Å in **2a** and 1.409(4) Å in **2'b**•0.5CH_2Cl_2 are significantly elongated when compared to the free alkyne (1.19 Å), consistent with their 2σ, 2π bonding.[13a] The Co-Co distances range from 2.410(1) Å to 2.620(1) Å in **2a** and from 2.419(1) Å to 2.543(1) Å in **2'b**•0.5CH_2Cl_2, the shorter bonds being those supported by the

bridging ligands and the longer being the hinge of the butterfly Co(1)-Co(3). The differences in Co-C(9) and Co-C(10) distances reflect the presence of the phenyl group at C(10) and of the dppm ligand. The dihedral angles between the butterfly wings of 121.7° in **2a** and 117° in **2'b** lead to non-bonding Co(2)···Co(4) distances of 3.52 Å and 3.55 Å, respectively. The alkyne hydrogen at C(9) was not detected by ^{1}H NMR spectroscopy (masked by aryl protons), but it was located by X-ray diffraction in both structures. In the butterfly cluster $[Co_4(CO)_8(PPh_3)_2(\mu_4\text{-}\eta^2\text{-}HC_2H)]$, the C-H ^{1}H NMR resonance was observed as a triplet at 7.82 ppm.[33] We assume that clusters **2'a-c** have a similar structure, although spectroscopic data in solution would not allow the identification of minor structural changes.

Attempts to functionalize clusters **2b** and **2'b** by deprotonation of the NH group using DBU or KH as a base followed by addition of $Cl(CH_2)_3Si(OEt)_3$ or $O{=}C{=}N(CH_2)_3Si(OMe)_3$, failed. Other approaches were therefore attempted (see below).

Synthesis of Alkoxysilyl-Functionalized Alkyne Clusters. With the objective to incorporate in a Co_4 cluster a functional alkyne that could be subsequently condensed with a silica matrix via the sol-gel method, we decided to take advantage of the stabilizing effect of dppm or dppa on the Co_4 core to react **1a,b** with the new alkyne $PhC{\equiv}CC(O)NH(CH_2)_3Si(OMe)_3$ (**L^1**), and the recently reported alkynes $HC{\equiv}CCH_2NHC(O)NH(CH_2)_3Si(OEt)_3$ (**L^2**) and $HC{\equiv}C(CH_2)_2OC(O)NH(CH_2)_3Si(OEt)_3$ (**L^3**).[14] Alkyne **L^1** was prepared in two steps by the method outlined in eq 1 which involved treatment of 3-phenylpropiolic acid with thionyl chloride followed by addition of 3-aminopropyl trimethoxysilane. The ligand was characterized by ^{1}H, ^{13}C and ^{29}Si NMR and IR spectroscopy. The infrared spectrum in dichloromethane contains a strong absorption band at 2220 cm^{-1} for the C≡C triple bond.

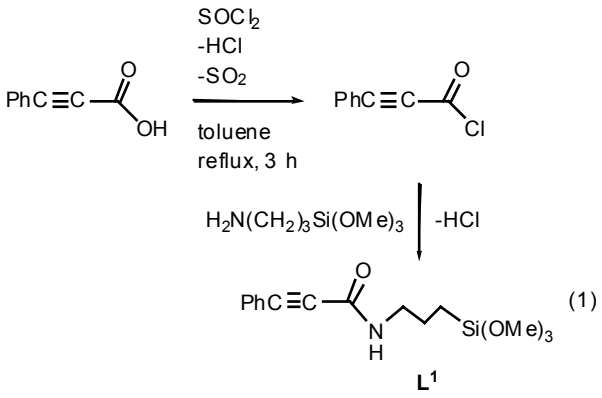

The reactions of **1a,b** with $\mathbf{L^1}$ and $\mathbf{L^2}$ afforded the clusters **4a,b** and **5a,b**, respectively, and **6a** was obtained by reaction of **1a** with $\mathbf{L^3}$. The analytical and spectroscopic data confirmed the presence of both the functional alkyne and the diphosphine in the clusters. The structures shown for these compounds were deduced from their spectroscopic properties and by analogy with those established by X-ray diffraction for **2a** and **2b**.

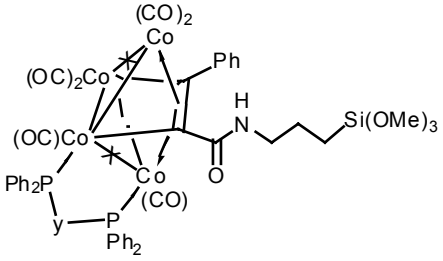

4a y = CH_2
4b y = NH

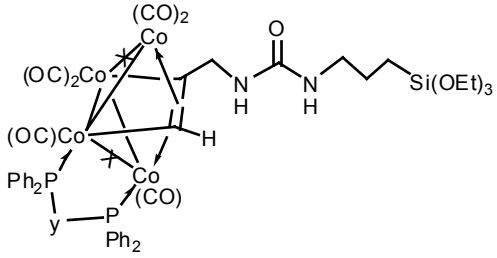

5a y = CH_2
5b y = NH

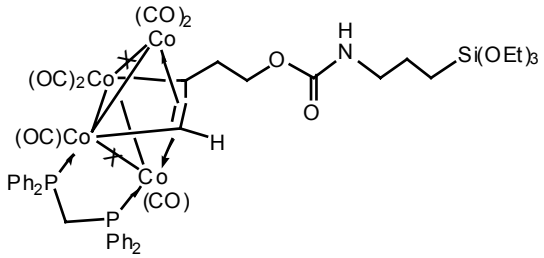

6a

Like in the case of **2b**, two broad $^{31}P\{^1H\}$ NMR resonances are observed for **4b** and **5b** at δ 91.1, 103.5 and 78.3, 89.0 ppm, respectively, but only one broad signal was observed for **4a**, **5a** and **6a**, like for **2a**. The IR spectrum of all clusters show a characteristic ν(C=O) band for the amide function in the region 1646-1720 cm^{-1} in addition to those for the Co-bound carbonyls. All these clusters were obtained in the form of a paste which is difficult to purify

since column chromatography cannot be applied (presence of the alkoxysilyl groups). Residual alkyne often contaminates the samples.

It was not possible to prepare the clusters **4a**,**b**, **5a,b** and **6a** by first reacting $[Co_4(CO)_{12}]$ with the corresponding alkynes followed by the addition of the diphosphines because the blue $[Co_4(CO)_{10}(\mu_4\text{-}\eta^2\text{-alkyne})]$ clusters rapidly fragment in solution to give i.a. the red $[Co_2(CO)_6(\mu\text{-}\eta^2\text{-alkyne})]$ complexes. The latter can be obtained directly by reaction of $[Co_2(CO)_8]$ with the corresponding alkyne (in the case of $\mathbf{L^1}$, see Scheme 3).[20] Complex **7** was characterized by IR and NMR ^{1}H spectroscopy and elemental analysis. These observations clearly illustrate the advantage of using a diphosphine-stabilized precursor cluster for subsequent reactions with functional alkynes.

Scheme 3

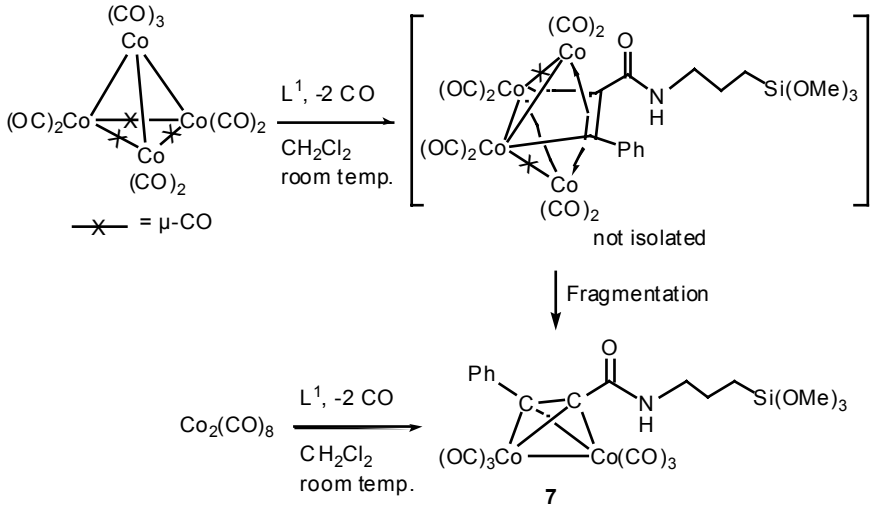

Nevertheless, complexes of the type $[Co_2(CO)_6(\mu\text{-}\eta^2\text{-alkyne})]$ may be useful synthons for the subsequent synthesis of tri and tetranuclear clusters.[34] We are currently evaluating complex **7** with its $Si(OMe)_3$ function as precursor to the synthesis of Co-containing materials by the sol-gel route.

Synthesis of $[Co_4(\mu\text{-}CO)_3(CO)_5(\mu\text{-}dppm)(\mu\text{-}dppaSi)]$ (8). In order to broaden the scope of possibilities of attachment of a functional Co_4 cluster to a silica matrix, we also examined the incorporation of dppaSi in **1a** (eq 2). This reaction afforded the mixed-diphosphine cluster **8** which was characterized by X-ray diffraction. A view of the structure is shown in Figure 4 and selected bond distances and angles are given in Table 4.

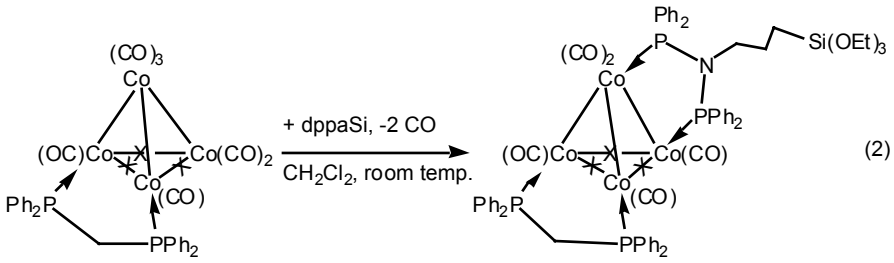

1a **8** (2)

The molecular structure of **8** can be derived from that of the parent cluster **1a** by substituting an apical and an equatorial carbonyl group on Co(3) and Co(4), respectively, with the dppaSi ligand. The two different diphosphine ligands bridge opposite edges of a distorted Co_4 tetrahedron and each Co is thus substituted by a P donor. The structure is similar to those of $[Co_4(CO)_8(\mu\text{-}dmpm)_2]$[28a] and $[Rh_4(CO)_8(\mu\text{-}dppm)_2]$.[35] The Co-Co bond lengths are in the range 2.434(1)-2.543(1) Å and are comparable with those found in the literature for similar structures.[27,28a,36] The five terminal carbonyls display Co-C-O angles between 177.1(4) and 178.9(4)°. The Co-C distances range from 1.757(5) to 1.793(5) Å and are substantially shorter than the Co-(μ-C) distances involving the bridging carbonyls C(2)O(2) and C(6)O(6) (1.920(4)-1.941(4) Å). The Co(2)-C(4) distance of 1.897(5) Å is considerably shorter than the Co(3)-C(4) distance of 1.981(4) Å, which suggests that C(4)O(4) occupies a bent semibridging position.[37] The refinement of the X-ray data shows that the $CSi(OEt)_3$ group is disordered over two positions with occupancy factors of 2/3 and 1/3. The Si-O, C-O and C-C distances have been fixed at values of 1.6, 1.45 and 1.55 Å, respectively.

At room temperature, the $^{31}P\{^{1}H\}$ NMR spectrum contains only two broad resonances at 28.1 and 100.5 ppm, corresponding to the dppm and dppaSi ligands, respectively, which is not surprising for such clusters.[28a]

Formation of $[Co_2(CO)_4(\mu\text{-dppm})\{\mu\text{-}\eta^2\text{-}PhC_2H\}]$ (9) from $[Co_4(\mu\text{-CO})_2(CO)_6(\mu\text{-dppm})(\mu_4\text{-}\eta^2\text{-}PhC_2H)]$ (2a). We attempted the linking of two molecules of **2a** with 1,4-diodobenzene under Sonogashira conditions.[38] Unfortunately, no coupling reaction was observed and instead, fragmentation of **2a** afforded the red dinuclear complex **9** (eq 3).[39] Cluster fragmentation was probably triggered by the base which is necessary for the reaction. Similar behavior was recently observed with other alkyne-substituted clusters.[14]

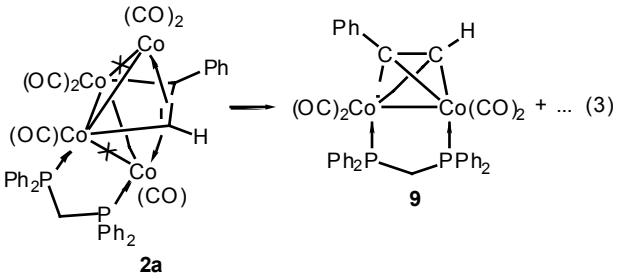

Compound **9** was identified by its ^{1}H NMR data and the Co_2C_2H proton was observed as a triplet at 5.79 ppm (^{3}J(PH) = 7.5 Hz) which is in agreement with literature values for related clusters.[40] Compounds of the type $[Co_2(CO)_4(\mu\text{-dppm})(\mu\text{-}\eta^2\text{-alkyne})]$ are generally prepared by reaction of the appropriate alkyne with $[Co_2(CO)_6(\mu\text{-dppm})]$[40] or by reaction of dppm with the dinuclear complexes $[Co_2(CO)_6(\mu\text{-}\eta^2\text{-alkyne})]$.[41]

Reaction of Co_4 Clusters with a Protected Diyne. With the objective of introducing protected functionalities in $[Co_4(CO)_{12}]$, we explored its reactivity with 1,4-bis(trimethylsilyl)butadiyne $Me_3SiC{\equiv}CC{\equiv}CSiMe_3$ (**L^4**), also because reactions of diynes with this cluster have been very little investigated.[24] The reaction was performed in hexane or in dichloromethane. TLC indicated the formation of a blue intermediate which rapidly

transforms in solution to give the known, green product [{$Co_2(CO)_6(\mu\text{-}\eta^2\text{-}Me_3SiC_2\text{-})\}_2$] (**10**) in 21% yield (Scheme 4). We assume that initial coordination of one of the triple bonds to [$Co_4(CO)_{12}$] yielded an intermediate of the type [$Co_4(CO)_{10}(\mu_4\text{-}\eta^2\text{-}Me_3SiC_2C{\equiv}CSiMe_3)$]. The presence of a second triple bond was suggested to facilitate further rearrangements and fragmentation into two Co_2 units.[24]

Scheme 4

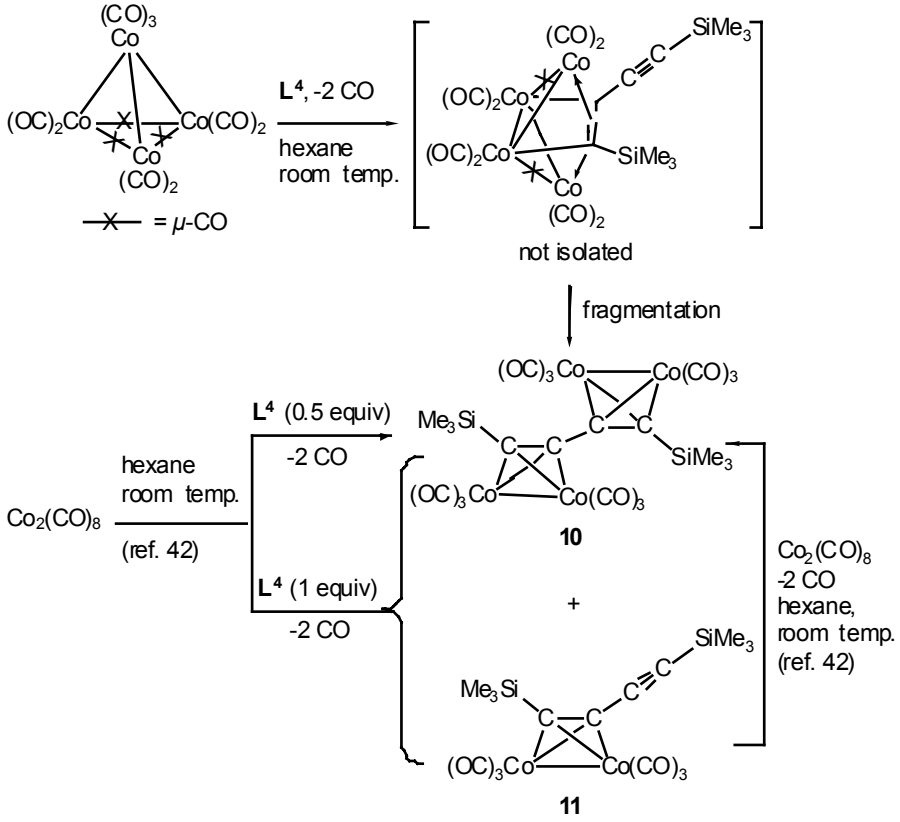

Complex **10** was also obtained directly by reaction of [$Co_2(CO)_8$] with $\mathbf{L^4}$, in addition to [$Co_2(CO)_6(\mu\text{-}\eta^2\text{-}Me_3SiC_2C{\equiv}CSiMe_3)$] (**11**),[42] or by reaction of this latter with [$Co_2(CO)_8$][42] (Scheme 4). Complexes **10** and **11** also form by deprotonation of [$Co_2(CO)_6(\mu\text{-}\eta^2\text{-}Me_3SiC_2H)$], itself prepared by reaction of [$Co_2(CO)_8$] with $Me_3SiC{\equiv}CH$, followed by intermolecular C-C coupling between two molecules of the resulting complex.[43] Complex **10** has recently been isolated (in 6% yield) from the reaction of [$Mo_2(\mu\text{-}\eta^2\text{-}Me_3SiC_2C{\equiv}CSiMe_3)(CO)_4Cp_2$] with [$Co_2(CO)_8$].[44] Preliminary experiments have indicated that **10** exhibits electrical conductivity.[43]

We then turned again to the diphosphine stabilized cluster **1a** and reacted it with $\mathbf{L^4}$. Heating the reaction mixture in dichloromethane for *ca*. 3 days afforded the desired product $[Co_4(CO)_8(\mu\text{-dppm})(\mu_4\text{-}\eta^2\text{-}Me_3SiC_2C{\equiv}CSiMe_3)]$ (**12**) in addition to the known, red complex $[Co_2(CO)_4(\mu\text{-dppm})(\mu\text{-}\eta^2\text{-}Me_3SiC_2C{\equiv}CSiMe_3)]$ (**13**) and other unidentified products (Scheme 5). No reaction was detected at room temperature. Complex **13**, which results from fragmentation of **12** during reaction, has also been obtained directly by reaction of $[Co_2(CO)_6(\mu\text{-}\eta^2\text{-}Me_3SiC_2C{\equiv}CSiMe_3)]$ with dppm.[45,46] In hexane at 80 °C, **1a** rapidly reacted with $\mathbf{L^4}$ but **12** was obtained in very low yield whereas **13** was the major product. Increasing the reaction temperature favours the transformation of **12** to **13**. When **12** was exposed to air, it also transformed to **13**.

Scheme 5

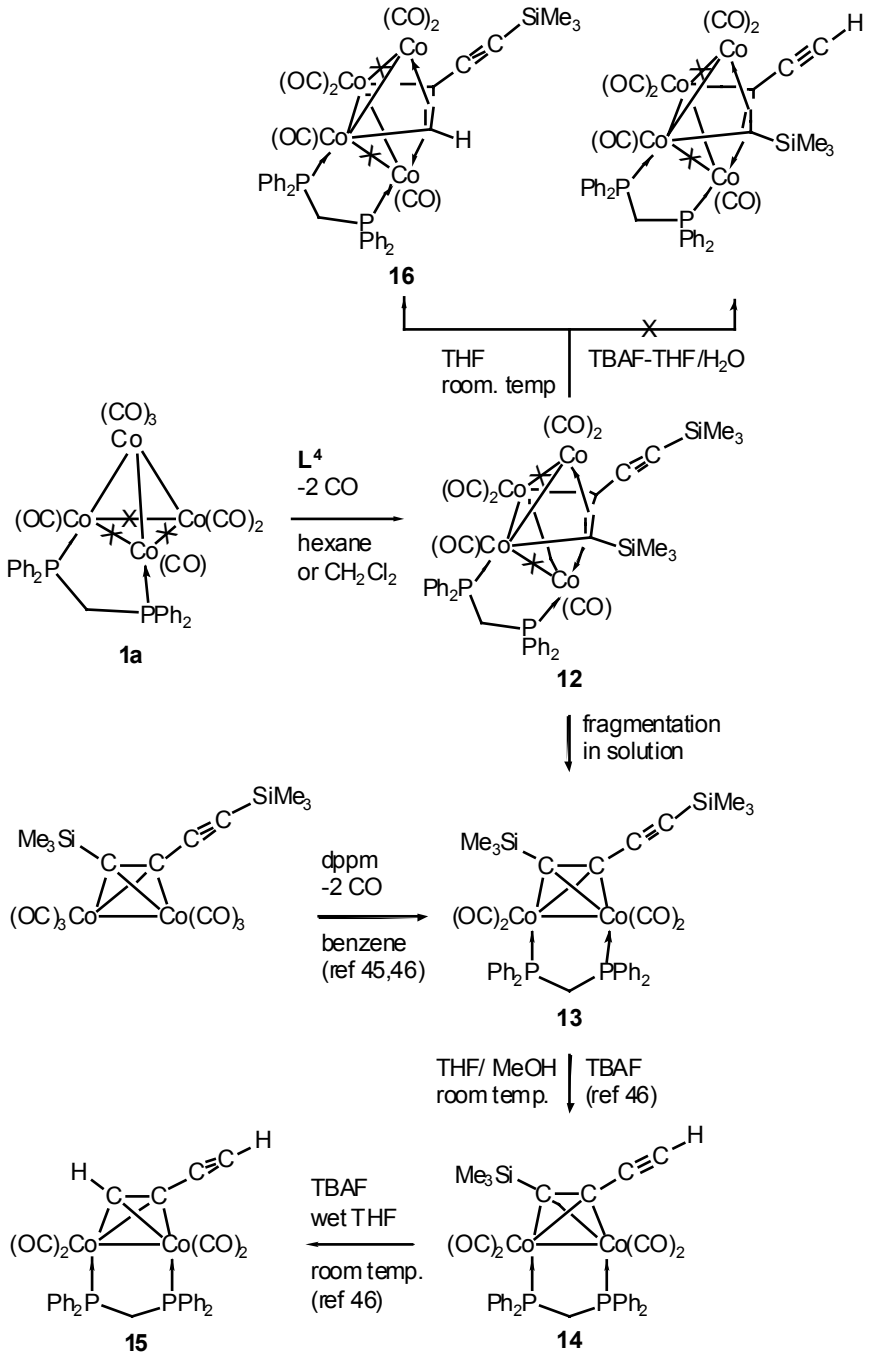

Both complexes **12** and **13** were identified by their IR, NMR spectra and elemental analyses. Their ^{1}H NMR spectra are very similar, with two different signals for the -$SiMe_3$ groups. Their PCH_2P protons appear as an ABXY or ABX_2 (X = Y = P) spin system, respectively. The identity of **12** was deduced by comparison with related $[Co_4(CO)_8(\mu\text{-dppm})(\mu_4\text{-}\eta^2\text{-alkyne})]$ clusters discussed above. The $\nu(C{\equiv}C)$ absorption was not observed for **12** whereas it appears at 2115 cm^{-1} for **13**.[46]

The complex **13** was deprotected at the alkynyl group using Bu_4NF to give **14** (Scheme 5). When stronger desilylation conditions were used (TBAF, moist THF, room temp.), complex **15** was obtained rapidly in high yield.[46] The desilylation of **12** using TBAF/THF-H_2O was monitored by TLC and necessitates a few hours to afford a green, air sensitive product. We did not observe by ^1H NMR the CH resonance of the expected product $[Co_4(\mu\text{-}CO)_2(CO)_6(\mu\text{-}dppm)(\mu_4\text{-}\eta^2\text{-}Me_3SiC_2C{\equiv}CH)]$. The product **16** was characterized by ^1H NMR and IR spectroscopy and its structure could be established by X-ray diffraction and shown to be, surprisingly, that of $[Co_4(\mu\text{-}CO)_2(CO)_6(\mu\text{-}dppm)(\mu_4\text{-}\eta^2\text{-}HC_2C{\equiv}CSiMe_3)]$. A view of the molecule is shown in Figure 5 and selected bond distances and angles are given in Table 5. Unexpectedly, desilylation occurred at the Co-C-$SiMe_3$ group and not at the alkynyl carbon. The reactivity of **12** thus contrasts with that of the mixed-metal cluster $[RuCo_3(CO)_{10}(\mu_4\text{-}\eta^2\text{-}Me_3SiC_2C{\equiv}CH)]^-$ which is obtained rapidly by desilylation of $[RuCo_3(CO)_{10}(\mu_4\text{-}\eta^2\text{-}Me_3SiC_2C{\equiv}CSiMe_3)]^-$.[47]

The molecular structure of **16** is thus similar to that of **2a**. The non-bonding Co(2)···Co(4) distance is 3.52 Å and the dihedral angle between the wings is 117.8°. The orientation of the C(9)-C(10) bond, which is parallel to the Co(1)-Co(3) hinge of the metal butterfly, is again consistent with a minimization of the steric repulsions with the dppm ligand. In order to achieve a C-C coupling analogous to the oxidative coupling of **14** or of $[Co_2(CO)_4(\mu\text{-}dppm)(HC{\equiv}CC_2C{\equiv}CH)]$ under standard Eglinton-Glaser conditions ($Cu(OAc)_2$, pyridine), which afforded the dimer $[Co_2(CO)_4(dppm)(Me_3SiC_2C{\equiv}C\text{-})]_2$,[45] and the trimer $[Co_2(CO)_4(\mu\text{-}dppm)(\text{-}C{\equiv}CC_2C{\equiv}C\text{-})]_3$,[46] respectively, and with the aim of forming clusters linked through π-delocalized backbones, the isolated cluster **16** was reacted with TBAF but deprotection at the alkynyl group was unsuccessful.

In conclusion, we have shown that prior stabilization of the Co_4 core of $[Co_4(CO)_{12}]$ by the short-bite disphosphine ligands $Ph_2PCH_2PPh_2$ (dppm), $Ph_2PNHPPh_2$ (dppa) or

$(Ph_2P)_2N(CH_2)_3Si(OEt)_3$ (dppaSi) is beneficial and the stabilized tetrahedral clusters **1a-c** have been fully characterized. The butterfly clusters $[Co_4(\mu\text{-}CO)_2(CO)_6(\mu\text{-dppy})(\mu_4\text{-}\eta^2\text{-}PhC_2H)]$ (**2a-c**) were isolated in excellent yield by insertion of the alkyne into a Co-Co bond of the diphosphine-stabilized precursor or by reaction of $[Co_4(CO)_{12}]$ with phenylacetylene followed by CO substitution with the diphosphines dppy. Isomers were obtained which differ by the position of the bridging carbonyls, as established by an X-ray diffraction study on **2a** and **2'b**. Reaction of the new alkyne $PhC{\equiv}CC(O)NH(CH_2)_3Si(OMe)_3$ ($\mathbf{L^1}$) with **1a,b** afforded the butterfly clusters $[Co_4(\mu\text{-}CO)_2(CO)_6(\mu\text{-dppy})\{\mu_4\text{-}\eta^2\text{-}PhC_2C(O)NH(CH_2)_3Si(OMe)_3\}]$ (**4a,b**), respectively. Similar reactions with the alkyne $HC{\equiv}CCH_2NHC(O)NH(CH_2)_3Si(OEt)_3$ ($\mathbf{L^2}$) led to $[Co_4(\mu\text{-}CO)_2(CO)_6(\mu\text{-dppy})\{\mu_4\text{-}\eta^2\text{-}HC_2CH_2NHC(O)NH(CH_2)_3Si(OEt)_3\}]$ (**5a,b**). Cluster $[Co_4(\mu\text{-}CO)_2(CO)_6(\mu\text{-dppm})\{\mu_4\text{-}\eta^2\text{-}HC_2(CH_2)_2OC(O)NH(CH_2)_3Si(OEt)_3\}]$ (**6a**) was obtained by reaction of **1a** with $HC{\equiv}C(CH_2)_2OC(O)NH(CH_2)_3Si(OEt)_3$ ($\mathbf{L^3}$). Reaction of $[Co_4(CO)_{12}]$ with $\mathbf{L^1}$ led to the formation of $[Co_2(CO)_6\{\mu\text{-}\eta^2\text{-}PhC_2C(O)NH(CH_2)_3\ Si(OMe)_3\}]$ (**7**), which was also prepared by reaction of $[Co_2(CO)_8]$ with $\mathbf{L^1}$. Reaction of **1a** with dppaSi afforded the mixed-diphosphine cluster $[Co_4(\mu\text{-}CO)_3(CO)_5(\mu\text{-dppm})(\mu\text{-dppaSi})]$ (**8**). The 1,4-bis(trimethylsilyl) butadiyne ($\mathbf{L^4}$) afforded with $[Co_4(CO)_{12}]$ the known complex $[\{Co_2(CO)_6(\mu\text{-}\eta^2\text{-}Me_3SiC_2\text{-})\}_2]$ (**10**) and with **1a** gave the desired product $[Co_4(CO)_8(\mu\text{-dppm})(\mu_4\text{-}\eta^2\text{-}Me_3SiC_2C{\equiv}CSiMe_3)]$ (**12**), in addition to the known complex $[Co_2(CO)_4(\mu\text{-dppm})(\mu_2\text{-}\eta^2\text{-}Me_3SiC_2C{\equiv}CSiMe_3)]$ (**13**). Desilylation of **12** using TBAF/THF-H_2O occurred unexpectedly at the cluster core-bound alkyne carbon to afford the structurally characterized $[Co_4(\mu\text{-}CO)_2(CO)_6(\mu\text{-dppm})(\mu_4\text{-}\eta^2\text{-}HC_2C{\equiv}CSiMe_3)]$ (**16**), instead of the expected cluster $[Co_4(\mu\text{-}CO)_2(CO)_6(\mu\text{-dppm})(\mu_4\text{-}\eta^2\text{-}Me_3SiC_2C{\equiv}CH)]$.

Experimental Section

All the reactions and manipulations were carried out under an inert atmosphere of purified nitrogen using standard Schlenk tube techniques. Solvents were dried and distilled under nitrogen before use: toluene over sodium, tetrahydrofuran, hexane and pentane over sodium-benzophenone, dichloromethane over phosphorus pentoxide. Nitrogen (Air liquide, R-grade) was passed through BASF R3-11 catalyst and molecular sieve columns to remove residual oxygen and water. The ligands $Ph_2PCH_2PPh_2$ (dppm)[48], $Ph_2PNHPPh_2$ (dppa)[49] and $(Ph_2P)_2N(CH_2)_3Si(OEt)_3$ (dppaSi)[8] and the clusters $[Co_4(CO)_{10}(\mu_4\text{-}\eta^2\text{-}PhC_2H)]$[20] and $[Co_4(CO)_{10}(\mu\text{-dppa})]$[9] were synthesized by literature methods. Elemental C, H and N analyses were performed by the Service de microanalyses du CNRS (ULP Strasbourg). Infrared spectra (cm^{-1}) were recorded on a IFS-66 FTIR Brucker or a Perkin Elmer 1600 series FTIR spectrometers. The ^1H NMR spectra were recorded at 200.13 or 300.13 MHz, $^{31}P\{^1H\}$ NMR spectra at 121.5, 161.97 or 202.46 MHz and $^{29}Si\{^1H\}$ NMR spectra at 79.48 on Bruker AC200, AC300, AVANCE 300, AVANCE 400 or AVANCE 500 instruments.

Synthesis of $[Co_4(\mu\text{-}CO)_3(CO)_7(\mu\text{-dppm})]$ (1a). To a solution of $[Co_4(CO)_{12}]$ (0.350 g, 0.612 mmol) in 50 mL of CH_2Cl_2 was added with stirring a solution of dppm (0.235 g, 0.612 mmol) in 10 mL of CH_2Cl_2 at room temperature. The color of the solution changed immediately from black to dark red. Analytical TLC (CH_2Cl_2/hexane 40/60) indicated the formation of two products. The solvent was immediately evaporated under reduced pressure and the residue was chromatographed on a SiO_2 column, with CH_2Cl_2/hexane (40/60) as eluent, yielding the green tetrasubstituted $[Co_4(CO)_8(\mu\text{-dppm})_2]$ (0.097 g, 0.079 mmol, 13%) and the dark red product **1a** (0.380 g, 0.422 mmol, 70%). Recrystallization from hexane afforded after one week single crystals suitable for X-ray diffraction. IR (hexane, ν_{CO}): 2068 (vs), 2027 (vs), 2019 (vs), 1996 (w), 1989 (m), 1979 (w), 1845 (m), 1830 (sh), 1802 (sh),

1795 (w). ^{1}H NMR (200.13 MHz, $CDCl_3$) δ: 2.85 (br, 2H, CH_2), 7.12-7.45 (m, 20H, Ph). $^{31}P\{^{1}H\}$ NMR (121.5 MHz, $CDCl_3$) δ: 27.8 (br, $w_{1/2}$ = 84 Hz). Anal. Calcd. for $C_{35}H_{22}Co_4O_{10}P_2$: C, 46.7; H, 2.46, Found: C, 46.99; H, 2.53.

Synthesis of [Co_4(μ-CO)$_3$(CO)$_7$(μ-dppaSi)] (1c). A solution of dppaSi (0.083 g, 0.140 mmol) in 10 mL of CH_2Cl_2 was added to a solution of [$Co_4(CO)_{12}$] (0.080 g, 0.140 mmol) in 20 ml of the same solvent. The color of the solution changed in a few minutes from black to dark red, and analytical TLC (hexane) indicated that all starting material was consumed. The solution was filtered and the solvent was evaporated under reduced pressure and extraction of the product with hexane followed by recrystallization from hexane afforded **1c** (0.097 g, 0.088 mmol, 63%). IR (hexane, ν_{CO}): 2068 (vs), 2024 (vs), 2018 (vs), 1999 (sh), 1994 (m), 1980 (sh), 1839 (m), 1793 (m), 1782 (m). ^{1}H NMR (300.13 MHz, $CDCl_3$) δ: -0.45 (m, 2H, $SiCH_2$), 0.12 (m, 2H, $CH_2CH_2CH_2$), 0.98 (t, ^{3}J(HH) = 7.14 Hz, 9H, CH_3), 2.54 (m, 2H, NCH_2), 3.38 (q, ^{3}J(HH) = 7.14 Hz, 6H, OCH_2), 7.48-7.81 (m, 20H, Ph). $^{31}P\{^{1}H\}$ NMR (121.5 MHz, $CDCl_3$) δ: 92.8 (br, $w_{1/2}$ = 166 Hz). Anal. Calcd. for $C_{43}H_{41}Co_4NO_{13}P_2Si$: C, 46.72; H, 3.74; N, 1.27. Found: C, 46.05; H, 3.68; N, 1.23.

Synthesis of [Co_4(μ-CO)$_2$(CO)$_6$(μ-dppm)(μ$_4$-η^2-PhC$_2$H)] (2a/2'a)

Reaction of [Co_4(μ-CO)$_3$(CO)$_7$(μ-dppm)] (1a) with PhC≡CH. A solution of phenylacetylene (1.11 mL, 10.11 mmol) was added to a solution of **1a** (0.471 g, 0.523 mmol) in 80 ml of hexane. The mixture was stirred at room temperature for 10 days (or 3 h at 80 °C). The reaction was monitored by TLC (CH_2Cl_2/hexane, 50/50) which indicated the progressive formation of a green compound. The solution was filtered, and the solid was collected, washed with hexane and recrystallized from CH_2Cl_2/hexane at –30 °C to give green, single crystals of **2a** (0.410 g, 0.433 mmol, 83%). IR (CH_2Cl_2, ν_{CO}): 2049 (s), 2007 (vs), 1977 (sh),

1839 (mw), 1785 (sh). IR (KBr, ν_{CO}): 2042 (s), 1999 (vs), 1979 (vs), 1847 (m), 1785 (m). ^{1}H NMR (200.13 MHz, $CDCl_3$) δ: 3.32 (m, 1H, C*H*^{A}CH^{B}P$_2$, part of an ABXY spin system), 3.93 (m, 1H, CH^{A}C*H*^{B}P$_2$, part of an ABXY spin system), 6.96-7.55 (m, 25H, Ph), HC_2 masked by aryl protons. ^{31}P{^{1}H} NMR (202.46 MHz, $CDCl_3$) δ: (25 °C) 28.3 (br, $w_{1/2}$ = 422 Hz); (0 °C) 27.9 (br, 29.0, br). Anal. Calcd. for $C_{41}H_{28}Co_4O_8P_2$: C, 52.04; H, 2.98. Found: C, 51.81; H, 3.01.

Reaction of [Co$_4$(CO)$_{10}$(μ$_4$-η^2-PhC$_2$H)] (3) with dppm. A solution of dppm (0.093 g, 0.243 mmol) in 25 mL of CH_2Cl_2 was added to a solution of **3** (0.150 g, 0.243 mmol) in 25 mL of CH_2Cl_2. The mixture was stirred at room temperature and the color of the solution changed instantaneously from blue to green. TLC with CH_2Cl_2/hexane (50/50) as eluent indicated the formation of only one product and some decomposition. The residue was chromatographed on a SiO_2 column with CH_2Cl_2/hexane (50/50) as eluent. Recrystallization of the product from CH_2Cl_2/hexane at –30 °C afforded a green powder of **2'a** (0.168 g, 0.177 mmol, 73%). IR (CH_2Cl_2, ν_{CO}): 2049 (vs), 2007 (vs), 1983 (vs), 1836 (mw), 1784 (w). IR (KBr, ν_{CO}): 2045 (s), 1998 (vs, br), 1828 (m), 1737 (w). Anal. Calcd. for $C_{41}H_{28}Co_4O_8P_2$: C, 52.04; H, 2.98. Found: C, 51.91; H, 3.11. The ^{1}H and ^{31}P NMR data are the same as for **2a**.

Synthesis of [Co$_4$(μ-CO)$_2$(CO)$_6$(μ-dppa)(μ$_4$-η^2-PhC$_2$H)] (2b/2'b)

Reaction of [Co$_4$(μ-CO)$_3$(CO)$_7$(μ-dppa)] (1b) with PhC≡CH. A solution of phenylacetylene (0.37 mL, 3.37 mmol) was added to a solution of **1b** (0.224 g, 0.248 mmol) in 60 ml of hexane. The mixture was heated to 80 °C for 3 h and the reaction was monitored by TLC (CH_2Cl_2/hexane, 40/60) which indicated the progressive formation of a green compound. This latter was treated like **2a** and green crystals of **2b** were obtained after recrystallization for ten days (0.220 g, 0.232 mmol, 94%). IR (CH_2Cl_2, ν_{CO}): 2050 (vs), 2005 (vs), 1971 (sh), 1832 (m). IR (KBr, ν_{CO}): 2041 (vs), 2005 (s), 1990 (vs), 1972 (vs), 1947 (m),

1840 (m), 1810 (m). ^{1}H NMR (300.13 MHz, $CDCl_3$) δ: 4.11 (br, NH), 6.40-7.68 (m, 25 H, Ph), HC_2 masked by aryl protons. $^{31}P\{^{1}H\}$ NMR (121.5 MHz, $CDCl_3$) δ: 81.2 br, 87.4 br. Anal. Calcd. for $C_{40}H_{27}Co_4NO_8P_2 \cdot 1/3C_6H_{14}$: C, 51.68; H, 3.27; N, 1.44. Found: C, 51.67; H, 3.36; N, 1.57.

Reaction of $[Co_4(CO)_{10}(\mu_4\text{-}\eta^2\text{-}PhC_2H)]$ (3) with dppa. Similarly to the synthesis of **2'a**, reaction of **3** (0.250 g, 0.405 mmol) with dppa (0.156 g, 0.405 mmol) was monitored by TLC which indicated the formation of the desired product and some decomposition. Recrystallization of the product gave green single crystals of **2'b** (0.360 g, 0.379 mmol, 94%), suitable for X-ray diffraction (see text). IR (CH_2Cl_2, ν_{CO}): 2048 (vs), 2003 (vs), 1987 (sh), 1827 (m). IR (KBr, ν_{CO}): 2046 (vs), 2005 (s), 1993 (sh), 1985 (vs), 1922 (m), 1841 (mw), 1819 (m). $^{31}P\{^{1}H\}$ NMR (121.5 MHz, $CDCl_3$) δ: 79.7 br, 87.6 br. Anal. Calcd. for $C_{40}H_{27}Co_4NO_8P_2 \cdot 1/2CH_2Cl_2$: C, 50.04; H, 2.90; N, 1.44. Found: C, 50.42; H, 3.12; N, 1.58. The ^{1}H NMR spectra is the same as that for **2b** (see above).

Synthesis of $[Co_4(\mu\text{-}CO)_2(CO)_6(\mu\text{-}dppaSi)(\mu_4\text{-}\eta^2\text{-}PhC_2H)]$ (2c/2'c)

Reaction of $[Co_4(\mu\text{-}CO)_3(CO)_7(\mu\text{-}dppaSi)]$ (1c) with PhC≡CH. Cluster **1c** (0.100 g, 0.090 mmol) and phenylacetylene (0.098 mL, 0.892 mmol) were refluxed in 20 ml of CH_2Cl_2 for 3 h. The color of the solution changed from dark red to green. The solution was filtered, the solvent was evaporated and the residue recrystallized from CH_2Cl_2/hexane to give a green powder of **2c** (0.091 g, 0.079 mmol, 88%). IR (CH_2Cl_2, ν_{CO}): 2048 (s), 2000 (vs), 1971 (vs), 1831 (m), 1789 (w). IR (KBr, ν_{CO}): 2041 (s), 1997 (vs), 1969 (vs), 1830 (m). ^{1}H NMR (300.13 MHz, $CDCl_3$) δ: -0.045 (m, 2H, $SiCH_2$), 0.94 (m, 11H, $CH_2CH_2CH_2$ and CH_3), 3.35 (m, 2H, NCH_2), 3.47 (m, 6H, OCH_2), 6.81-7.71 (m, 25H, Ph), HC_2 masked by aryl protons. $^{31}P\{^{1}H\}$ NMR (121.5 MHz, $CDCl_3$) δ: 81.0 (br, $w_{1/2}$ = 337 Hz). Anal. Calcd. for $C_{49}H_{47}Co_4NO_{11}P_2Si \cdot 1/3C_6H_{14}$: C, 51.89; H, 4.41; N, 1.19. Found: C, 51.71; H, 4.77; N, 1.43.

Reaction of $[Co_4(CO)_{10}(\mu_4\text{-}\eta^2\text{-}PhC_2H)]$ (3) with dppaSi. By a similar procedure to that detailed for **2'b**, the product **2'c** was synthesized by reaction of **3** (0.252 g, 0.408 mmol) with dppaSi (0.242 g, 0.408 mmol) in CH_2Cl_2. TLC indicated that the reaction was instantaneous. Yield of **2'c**: 0.422 g, 0.367 mmol, 90%. IR (CH_2Cl_2, ν_{CO}): 2050 (vs), 2001 (vs), 1970 (s), 1834 (m), 1783 (w); IR (KBr, ν_{CO}): 2045 (vs), 1995 (vs), 1962 (s), 1839 (m), 1823 (m). Anal. Calcd. for $C_{49}H_{47}Co_4NO_{11}P_2Si\cdot 1/3C_6H_{14}$: C, 51.89; H, 4.41; N, 1.19. Found: C, 51.93; H, 5.07; N, 1.64. The ^1H and $^{31}P\{^1H\}$ NMR data are the same as for **2c**.

Synthesis of $PhC{\equiv}CC(O)NH(CH_2)_3Si(OMe)_3$ (L^1) . A mixture of 3-phenylpropiolic acid (2.00 g, 13.70 mmol) and thionyl chloride (1.95 g, 1.20 ml, 16.44 mmol) in 50 mL toluene was stirred and heated to reflux for 3 h. The orange reaction mixture was allowed to cool to room temperature and the solvent was evaporated to dryness. It was dissolved in 25 mL of freshly distilled toluene and the mixture was cooled in an ice bath. A solution of 3-aminopropyltrimethoxysilane (4.82 mL, 27.40 mmol) in 25 mL of toluene was then added dropwise. After the addition was complete, the ice bath was removed and the mixture stirred at room temperature for 1 h and then poured into 100 mL of cold water. The mixture was filtered and the solid was discarded. The aqueous phase was separated, extracted with 50 ml of ethyl acetate and this extract was combined with the organic phase. The organic fraction was dried over $MgSO_4$ and evaporation of the solvent afforded a viscous yellow liquid of $\mathbf{L^1}$ (1.84 g, 5.97 mmol, 44% (based on acid)). IR (CH_2Cl_2): 2220 (s, $\nu_{C\equiv C}$), 1654 (s, $\nu_{C=O}$), 1514 (vs, δ_{NH}). ^1H NMR (300.13 MHz, $CDCl_3$) δ: 0.69 (m, 2H, $SiCH_2$), 1.70 (m, 2H, $CH_2CH_2CH_2$), 3.34 (m, 2H, NCH_2), 3.51 (s, 9H, CH_3), 6.26 (br, NH), 7.31-7.56 (m, 5H, Ph). $^{13}C\{^1H\}$ NMR (100.62 MHz, $CDCl_3$) δ: 6.18 (s, $SiCH_2$), 22.06 (s, $CH_2CH_2CH_2$), 42.13 (s, NCH_2), 50.28 (s, CH_3), 83.18 and 84.22 (2s, C≡C), 120.28 (s, C_{ipso} of C_6H_5), 128.46, 129.44 and 132.33 (3s, CH of C_6H_5), 153.40 (s, C=O). $^{29}Si\{^1H\}$ NMR (79.48 MHz, $CDCl_3$) δ: - 42.7.

Synthesis of $[Co_4(\mu\text{-}CO)_2(CO)_6(\mu\text{-}dppm)\{\mu_4\text{-}\eta^2\text{-}PhC_2C(O)NH(CH_2)_3Si(OMe)_3\}]$ (4a). A solution of $PhC{\equiv}CC(O)NH(CH_2)_3Si(OMe)_3$ (1.256 g, 4.080 mmol) in 5 ml of CH_2Cl_2 was added to a solution of **1a** (0.370 g, 0.411 mmol) in 40 mL of CH_2Cl_2. The mixture was heated to reflux and the reaction was monitored by TLC (CH_2Cl_2/hexane, 40/60) and follow the disappearence of **1a**. A green product progressively formed which did not migrate on the TLC plate and after 4 h formation of an other green, unidentified product, was observed which migrates immediately after the precursor. The reaction was stopped after 7 h. The solution was filtered and the solvent was removed under reduced pressure. Purification from toluene/pentane at –20 °C gave viscous **4a** (0.333 g, 0.289 mmol, 71%). IR (CH_2Cl_2): 2061 (sh), 2054 (s), 2029 (m), 2002 (vs), 1976 (m), 1830 (w), $\nu_{C\equiv O}$, 1646 (vs, $\nu_{C=O}$). ^{1}H NMR (300.13 MHz, $CDCl_3$) δ: 0.68 (m, 2H, $SiCH_2$), 1.69 (m, 2H, $CH_2C\mathit{H}_2CH_2$), 3.35 (m, 2H, NCH_2), 3.57 (s, 9H, CH_3), 6.36 (br, 1H, NH), 7.03-8.35 (m, 25H, Ph). $^{31}P\{^1H\}$ NMR (121.5 MHz, $CDCl_3$) δ: 39.8 (br, $w_{1/2}$ = 83 Hz).

Synthesis of $[Co_4(\mu\text{-}CO)_2(CO)_6(\mu\text{-}dppa)\{\mu_4\text{-}\eta^2\text{-}PhC_2C(O)NH(CH_2)_3Si(OMe)_3\}]$ (4b). By a similar procedure, the reaction of **2b** (0.157 g, 0.166 mmol) with $PhC{\equiv}CC(O)NH(CH_2)_3Si(OMe)_3$ (0.511 g, 1.660 mmol) in 25 ml of CH_2Cl_2 gave **4b** (0.132 g, 0.114 mmol, 69%). IR (CH_2Cl_2): 2054 (m), 2015 (s), 2000 (vs), 1970 (sh), 1832 (mbr), $\nu_{C\equiv O}$, 1646 (m, $\nu_{C=O}$). ^{1}H NMR (300.13 MHz, $CDCl_3$) δ: 0.42 (m, 2H, $SiCH_2$), 1.70 (m, 2H, $CH_2C\mathit{H}_2CH_2$), 3.11 (m, 2H, NCH_2), 3.46 (s, 9H, CH_3), 5.68 (br, NH), 6.53 (m, NH), 7.11-7.51 (m, 25H, Ph). $^{31}P\{^1H\}$ NMR (121.5 MHz, $CDCl_3$) δ: 91.1 (br, $w_{1/2}$ = 81 Hz), 103.5 (br, $w_{1/2}$ = 648 Hz).

Synthesis of $[Co_4(\mu\text{-}CO)_2(CO)_6(\mu\text{-}dppm)\{\mu_4\text{-}\eta^2\text{-}HC_2CH_2NHC(O)NH(CH_2)_3Si(OEt)_3\}]$ (5a). A solution of **1a** (0.134 g, 0.148 mmol) and

$HC{\equiv}CCH_2NHC(O)NH(CH_2)_3Si(OEt)_3$ (0.445 g, 1.470 mmol) was refluxed in 35 mL of CH_2Cl_2 for 7 h. Completion of the reaction was monitored by TLC (CH_2Cl_2/hexane, 40/60) to follow the disappearance of **1a**. The solvent was then removed under vacuum and the product was purified from toluene/pentane at –20 °C to afford green viscous **5a** (0.141 g, 0.123 mmol, 83%). IR (CH_2Cl_2): 2052 (s), 1993 (vs), 1966 (m), 1831 (w) $\nu_{C{\equiv}O}$; 1679 (vs, $\nu_{C=O}$). ^{1}H NMR (300.13 MHz, $CDCl_3$) δ: 0.62 (m, 2H, $SiCH_2$), 1.21 (m, 9H, CH_3), 1.60 (m, 2H, $CH_2CH_2CH_2$), 2.19 (br, 1H, $CH^ACH^BP_2$, part of an ABXY spin system), 3.16 (br, 3H, $HNCH_2CH_2$ and $CH^ACH^BP_2$, part of an ABXY spin system), 3.79 (m, 6H, OCH_2), 3.96 (m, 2H, HC_2CH_2N), 5.14 (m, 2H, NH), 6.91-7.85 (m, 20H, Ph), HC_2 masked by aryl protons. $^{31}P\{^1H\}$ NMR (121.5 MHz, $CDCl_3$) δ: 26.4 (br, $w_{1/2}$ = 83 Hz).

Synthesis of $[Co_4(\mu\text{-}CO)_2(CO)_6(\mu\text{-}dppa)\{\mu_4\text{-}\eta^2\text{-}HC_2CH_2NHC(O)NH(CH_2)_3Si(OEt)_3\}]$ (5b). By a similar procedure, refluxing a solution of **1b** (0.107 g, 0.118 mmol) with $HC{\equiv}CCH_2NHC(O)NH(CH_2)_3Si(OEt)_3$ (0.356 g, 1.184 mmol) in 30 mL of CH_2Cl_2 for 5 h gave **5b** (0.109 g, 0.095 mmol, 81%). IR (CH_2Cl_2): 2049 (vs), 1998 (vs), 1970 (sh), 1832 (m), $\nu_{C{\equiv}O}$; 1679 (vs, $\nu_{C=O}$). ^{1}H NMR (300.13 MHz, $CDCl_3$) δ: 0.62 (m, 2H, $SiCH_2$), 1.21 (m, 9H, CH_3), 1.42 (m, 2H, $CH_2CH_2CH_2$), 3.16 (m, 2H, $HNCH_2CH_2$), 3.82 (m, 6H, OCH_2), 3.95 (m, 2H, HC_2CH_2N), 4.83 (m, 2H, NH), 7.08-7.80 (m, 20H, Ph), H-C_2 and PNHP masked. $^{31}P\{^1H\}$ NMR (121.5 MHz, $CDCl_3$) δ: 78.3 (br, $w_{1/2}$ = 331 Hz), 89.0 (br, $w_{1/2}$ = 248 Hz).

Synthesis of $[Co_4(\mu\text{-}CO)_2(CO)_6(\mu\text{-}dppm)\{\mu_4\text{-}\eta^2\text{-}HC_2(CH_2)_2OC(O)NH(CH_2)_3Si(OEt)_3\}]$ (6a). A solution of **1a** (0.300 g, 0.333 mmol) and $HC{\equiv}C(CH_2)_2OC(O)NH(CH_2)_3Si(OEt)_3$ (1.05 g, 3.310 mmol) was refluxed in 40 mL of CH_2Cl_2 for 9 h. The solvent was removed under reduced pressure and the viscous green product was extracted with hexane. After keeping the extract for 3 days at –20 °C, the product

precipitated, the solvent was discarded and the residue was triturated with pentane to afford **6a** (0.354 g, 0.304 mmol, 92%). IR (CH_2Cl_2): 2048 (vs), 2001 (vs), 1975 (sh), 1831 (w), $\nu_{C\equiv O}$; 1720 (m, $\nu_{C=O}$). ^{1}H NMR (300.13 MHz, $CDCl_3$): δ 0.63 (m, 2H, $SiCH_2$), 1.22 (t, ^3J(HH) = 7.15 Hz, 9H, CH_3), 1.61 (m, 2H, $CH_2CH_2CH_2$), 2.50 (m, 1H, $CH^ACH^BP_2$, part of an ABXY spin system), 3.07 (m, 1H, $CH^ACH^BP_2$, part of an ABXY spin system), 3.14 (m, 4H, HC_2CH_2 and $HNCH_2$), 3.85 (m, 8H, OCH_2CH_2 and OCH_2CH_3), 4.74 (br, NH). ^{31}P{^{1}H} NMR (121.5 MHz, $CDCl_3$) δ: 29.8 (br, $w_{1/2}$ = 249 Hz).

Synthesis of $[Co_2(CO)_6\{\mu\text{-}\eta^2\text{-}PhC_2C(O)NH(CH_2)_3Si(OMe)_3\}]$ (7). A solution of $[Co_2(CO)_8]$ (0.320 g, 0.940 mmol) in 30 mL CH_2Cl_2 and $PhC\equiv CC(O)NH(CH_2)_3Si(OMe)_3$ **(L^1)** (0.298 g, 0.968 mmol) was stirred at room temperature for 50 min. Completion of the reaction was revealed from TLC by the disappearance of $[Co_2(CO)_8]$. The solvent was then removed under vacuum. Extraction with hexane afforded **7** as red crystals (0.380 g, 0.640 mmol, 68%). This product was also obtained, in lower yield (26%), by reaction of $\mathbf{L^1}$ with $[Co_4(CO)_{12}]$. IR (hexane): 2096 (m), 2064 (vs), 2032 (vs), 1977 (w), $\nu_{C\equiv O}$; 1660 (m, $\nu_{C=O}$). ^{1}H NMR (300.13 MHz, $CDCl_3$) δ: 0.70 (m, 2H, $SiCH_2$), 1.74 (m, 2H, $CH_2CH_2CH_2$), 3.44 (m, 2H, NCH_2), 3.56 (s, 9H, CH_3), 6.17 (br, 1H, NH), 7.33-7.79 (m, 5H, Ph). Anal. Calcd. for $C_{21}H_{21}Co_2NO_{10}Si$: C, 42.51; H, 3.57; N, 2.36, Found: C, 42.48; H, 3.51; N, 2.31.

Synthesis of $[Co_4(\mu\text{-}CO)_3(CO)_5(\mu\text{-}dppm)(\mu\text{-}dppaSi)]$ (8). $[Co_4(\mu\text{-}CO)_3(CO)_7(\mu\text{-}dppm)]$ (**1a**) (0.100 g, 0.111 mmol) and dppaSi (0.065 g, 0.111 mmol) in 30 mL of CH_2Cl_2 were mixed and stirred at room temperature. The reaction was stopped after ca. 3 h when all starting materials were consumed (TLC). Separation of the reaction mixture was performed by preparative TLC (CH_2Cl_2) giving three green bands. Immediate extraction with CH_2Cl_2 of the first and the third band afforded unidentified products and that of the second band $[Co_4(CO)_8(\mu\text{-}dppm)(\mu\text{-}dppaSi)]$ (**8**) (0.089 g, 0.062 mmol, 56%). Data for **8**: IR (CH_2Cl_2,

ν_{CO}): 2054 (m), 2005 (s), 1971 (vs), 1955 (sh), 1820 (w), 1791 (m), 1765 (m). ^{1}H NMR (300.13 MHz, $CDCl_3$) δ: -0.39 (m, 2H, $SiCH_2$), 0.67(m, 2H, $CH_2CH_2CH_2$), 0.94 (m, 9H, CH_3), 2.52 (br, 2H, PCH_2P), 3.43 (m, 8H, OCH_2 and NCH_2), 6.90-7.61 (m, 40H, Ph). $^{31}P\{^{1}H\}$ NMR (121.5 MHz, $CDCl_3$) δ: 28.1 (br, $w_{1/2}$ = 146 Hz), 100.5 (br, $w_{1/2}$ = 219 Hz). Anal. Calcd. for $C_{66}H_{63}Co_4NO_{11}P_4Si$: C, 55.28; H, 4.43; N, 0.98, Found: C, 54.64; H, 4.43; N, 0.95.

Reaction of $[Co_4(CO)_{12}]$ with $Me_3SiC{\equiv}CC{\equiv}CSiMe_3$. To a solution of $[Co_4(CO)_{12}]$ (0.153 g, 0.268 mmol) in 25 mL of hexane was added a solution of 1,4-bis(trimethylsilyl)butadiyne (0.522 g, 2.680 mmol) in 2 ml hexane. TLC with hexane as eluent indicated the formation of a blue product which transforms rapidly to a green one, and other secondary products. The reaction was stopped after 24 h stirring at room temperature. Chromatographic separation on SiO_2 column with hexane as eluent afforded green $[\{Co_2(CO)_6(\mu\text{-}\eta^2\text{-}Me_3SiC_2\text{-})\}_2]$ (**10**) (0.042 g, 0.055 mmol, 21%). IR (hexane, ν_{CO}): 2094 (m), 2076 (s), 2055 (vs), 2027 (vs), 1979 (w). ^{1}H NMR (300.13 MHz, $CDCl_3$) δ: 0.12 (s, $SiMe_3$). Anal. Calcd. for $C_{22}H_{18}Co_4O_{12}Si_2$: C, 34.48; H, 2.37. Found: C, 34.79; H, 1.93.

Reaction of 1a with $Me_3SiC{\equiv}CC{\equiv}CSiMe_3$. A solution of **1a** (0.235 g, 0.261 mmol) in 30 mL of CH_2Cl_2 and 1,4-bis(trimethylsilyl)butadiyne (0.453 g, 2.326 mmol) was heated at 55 °C for 3 days. The reaction was monitored by TLC which indicated the formation of two major products (red and green) and other secondary unidentified products. The solvent was removed and the mixture was separated by preparative TLC with hexane/CH_2Cl_2 (50/50) as eluent. The red band yielded $[Co_2(CO)_4(\mu\text{-dppm})(\mu\text{-}\eta^2\text{-}Me_3SiC_2C{\equiv}CSiMe_3)]$ (**13**) (0.045 g, 0.055 mmol, 21%) after recrystallization from hexane. IR (hexane, ν_{CO}): 2058 (w), 2030 (vs), 2008 (vs), 1982 (vs), 1960 (m). ^{1}H NMR (300.13 MHz, $CDCl_3$) δ: 0.23 (s, 9H, $SiMe_3$), 0.36 (s, 9H, $SiMe_3$), 3.33 (m, 1H, PCH^AH^BP, part of an ABX_2 spin system), 3.89 (m, 1H,

PCH^{A}*H*^{B}P, part of an ABX_2 spin system), 7.02-7.47 (m, 20H, Ph). $^{31}P\{^{1}H\}$ NMR (121.5 MHz, $CDCl_3$): δ 37.6 (br, $w_{1/2}$ = 133 Hz). Anal. Calcd. for $C_{39}H_{40}Co_2O_4P_2Si_2$: C, 57.92; H, 4.99. Found: C, 57.37; H, 4.65.

The green band gave [$Co_4(\mu\text{-}CO)_2(CO)_6(\mu\text{-dppm})(\mu_4\text{-}\eta^2\text{-}Me_3SiC_2C{\equiv}CSiMe_3)$] (**12**) (0.081 g, 0.078 mmol, 30%) by extraction with hexane. The product should be stored at –20 °C in the solid state. IR (hexane, ν_{CO}): 2050 (vs), 2005 (vs), 1994 (m), 1967 (w), 1843 (m), 1835 (m). ^{1}H NMR (300.13 MHz, $CDCl_3$) δ: -0.18 (s, 9H, ≡$CSiMe_3$), 0.33 (s, 9H, -C_2SiMe_3), 4.23 (m, 1H, PC*H*^{A}H^{B}P, part of an ABXY spin system), 5.00 (m, 1H, PCH^{A}*H*^{B}P, part of an ABXY spin system), 7.15-7.94 (m, 20H, Ph). $^{31}P\{^{1}H\}$ NMR (121.5 MHz, $CDCl_3$) δ: 25.0 (br, $w_{1/2}$ = 498 Hz). Anal. Calcd. for $C_{43}H_{40}Co_4O_8P_2Si_2$: C, 49.73; H, 3.88. Found: C, 50.12 ; H, 4.51.

Desilylation of 12. To a solution of **12** (0.060 g, 0.057 mmol) in 10 mL THF was added dropwise with stirring *n*-Bu_4NF (1.0 M in THF/5 wt% H_2O; 0.014 mmol, 0.014 ml). The mixture was stirred at room temperature for 8 h until TLC indicated complete consumption of the precursor. A minor, green fraction followed that of the desired product. The solvent was evaporated under vacuum and the product was extracted with CH_2Cl_2 and filtered through Celite. Separation by preparative TLC with hexane/CH_2Cl_2 (50/50) as eluent afforded [$Co_4(\mu\text{-}CO)_2(CO)_6(\mu\text{-dppm})(\mu_4\text{-}\eta^2\text{-}HC_2C{\equiv}CSiMe_3)$] (**16**) (0.028 g, 0.028 mmol, 50%). IR (hexane, ν_{CO}): 2057 (vs), 2022 (vs), 2016 (vs), 1988 (m), 1866 (m), 1838 (w). ^{1}H NMR (300.13 MHz, $CDCl_3$) δ: 0.15 (s, 9H, $SiMe_3$), 3.22 (m, 1H, PC*H*^{A}H^{B}P, part of an ABXY spin system), 3.95 (m, 1H, PCH^{A}*H*^{B}P, part of an ABXY spin system), 7.05-7.65 (m, 20H, Ph). $^{31}P\{^{1}H\}$ NMR (121.5 MHz, $CDCl_3$) δ: 30.7 br. Anal. Calcd. for $C_{40}H_{32}Co_4O_8P_2Si$: C, 49.71; H, 3.34. Found: C, 50.12; H, 3.55.

X-ray Structural Analyses of $[Co_4(\mu\text{-}CO)_3(CO)_7(\mu\text{-}dppm)]$ (1a), $[Co_4(\mu\text{-}CO)_2(CO)_6(\mu\text{-}dppm)(\mu_4\text{-}\eta^2\text{-}PhC_2H)]$ (2a), $[Co_4(\mu\text{-}CO)_2(CO)_6(\mu\text{-}dppa)(\mu_4\text{-}\eta^2\text{-}PhC_2H)]\bullet 0.5CH_2Cl_2$ (2'b$\bullet 0.5CH_2Cl_2$), $[Co_4(\mu\text{-}CO)_3(CO)_5(\mu\text{-}dppm)(\mu\text{-}dppaSi)]$ (8) and $[Co_4(\mu\text{-}CO)_2(CO)_6(\mu\text{-}dppm)(\mu_4\text{-}\eta^2\text{-}HC_2C{\equiv}CSiMe_3)]$ (16). Single crystals were mounted on a Nonius Kappa-CCD area detector diffractometer (MoKα, λ = 0.71073 Å). The complete conditions of data collection (Denzo software) and structure refinements are given below. The cell parameters were determined from reflections taken from one set of ten frames (1.0° steps in phi angle), each at 20 s exposure. The structures were solved using direct methods (SIR97) and refined against F^2 using the SHELXL97 software.[50,51] The absorption was corrected empirically with Sortav. All non-hydrogen atoms were refined anisotropically. Hydrogen atoms were generated according to stereo-chemistry and refined using a riding model in SHELXL97.

Acknowledgment. We are grateful to the CNRS, the Université Louis Pasteur Strasbourg and the Ministère de la Recherche (Paris) for financial support. This project was also supported by the Fonds International de Coopération Universitaire - FICU (AUPELF-UREF, Agence Universitaire de la Francophonie).

Supporting Information Available. Tables of atomic coordinates, thermal parameters, bond distances, and angles for **1a**, **2a**, **2'b**$\bullet 0.5CH_2Cl_2$, **8** and **16**, respectively. This material is available free of charge via the Internet at http://pubs.acs.org. This material has also been deposited in .cif format with the Cambridge Crystallographic Data Centre as Supplementary publication N° CCDC 214676 - 214680. Copies of the data can be obtained free of charge on application to CCDC, 12 Union Road, Cambridge CB2 1EZ, UK (fax: (+44)1223-336-033; e-mail: deposit@ccdc.cam.ac.uk).

References

* To whom correspondence should be addressed. E-mail: braunst@chimie.u-strasbg.fr

(1) (a) Simon, U. *Adv. Mater.* **1998**, *10*, 1487. (b) Schmid, G.; Chi, L. F. *Adv. Mater.* **1998**, *10*, 515. (c) Simon, U. in *Metal Clusters in Chemistry*; Braunstein, P.; Oro, L. A.; Raithby, P. R. (Eds.), Wiley-VCH, Weinheim, 1999, Vol. 3, p. 1342.

(2) (a) Braunstein, P.; Devenish, R.; Gallezot, P.; Heaton, B. T.; Humphreys, C. J.; Kervennal, J.; Mulley S.; Ries, M. *Angew. Chem. Int. Ed*. **1988**, *27*, 927. (b) Kawi, S. ; Gates, B. C. in *Clusters and Colloids. From Theory to Applications*; Schmid, G. (Ed), Wiley-VCH, Weinheim, 1994, Chap. 4, p. 298. (c) Lindner, E.; Schneller, T.; Auer, F.; Mayer, H. A. *Angew. Chem Int. Ed. Engl.* **1999**, *38*, 2154. (d) Sasaki, M.; Osada, M.; Higashimoto, N.; Yamamoto, T.; Fukuoka A.; Ichikawa, M. *J. Mol. Catal. A: Chemical*, **1999**, *141*, 223. (e) Hermans, S.; Raja, R.; Thomas, J. M.; Johnson, B. F. G.; Sankar, G.; Gleeson, D. *Angew. Chem Int. Ed. Engl.* **2001**, 40, 1211. (f) Thomas, J. M.; Johnson, B. F. G.; Raja, R.; Sankar, G.; Midgley, P. A. *Acc. Chem. Res.* **2003**, *36*, 20 and references cited.

(3) Braunstein, P.; Rosé, J. *Heterometallic Clusters in Catalysis*, in *Metal Clusters in Chemistry,* Braunstein, P.; Oro, L. A.; Raithby, P. R., Eds.; Wiley-VCH, Weinheim (Germany), **1999**, Vol. 2, pp. 616-677.

(4) Schweyer, F.; Braunstein, P.; Estournès, C.; Guille, J.; Kessler, H.; Paillaud, J.-L.; Rosé, J. *Chem. Commun.* **2000**, 1271.

(5) (a) Brunel, D.; Bellocq, N.; Sutra, P.; Cauvel, A.; Laspéras, M.; Moreau, P.; Di Renzo, F.; Galarneau, A.; Fajula, F. *Coord. Chem. Rev.* **1998**, *180*, 1085. (b) Behringer, K. D.; Blümel, J. *Inorg. Chem.* **1996**, *35*, 1814.

(6) (a) Mercier, L.; Pinnavaia, T. J. *Adv. Mater.* **1997**, *9*, 500. (b) Brunel, D. *Microporous Mesoporous Mater.* **1999**, *27*, 329. (c) Price, P. M.; Clark, J. H.; Macquarrie, D. J. *J. Chem. Soc., Dalton Trans.* **2000**, 101. (d) Carpenter, J. P.; Lukehart, C. M.; Milne,

S. B.; Stock, S. R.; Wittig,J. E.; Jones, B. D.; Glosser,R. ; Zhu, J. G. *J. Organomet. Chem.* **1998**, *557*, 121.

(7) Braunstein, P.; Kormann, H.-P.; Meyer-Zaika, W.; Pugin, R.; Schmid, G. *Chem. Eur. J*. **2000**, *6*, 4637.

(8) For $(Ph_2P)_2N(CH_2)_3Si(OEt)_3$, see: Bachert, I.; Braunstein, P.; Hasselbring, R. *New J. Chem.* **1996**, *20*, 993.

(9) Moreno, C.; Macazaga, M. J.; Marcos, M. L.; Gonzalez-Velasco, J.; Delgado, S. *J. Organomet. Chem.* **1993**, *452*, 185.

(10) Zhao, D.; Feng, J.; Huo, Q.; Melosh, N.; Fredrickson, G. H.; Chmelka, B. F.; Stucky, G. D. *Science* **1998**, *279*, 548.

(11) Schweyer-Tihay, F.; Braunstein, P.; Estournès, C.; Guille, J. L.; Lebeau, B.; Paillaud, J.–L.; Richard-Plouet, M.; Rosé, J. *Chem. Mater.* **2003**, *15*, 57.

(12) Braunstein, P.; Cauzzi, D.; Predieri, G.; Tiripicchio, A. *J. Chem. Soc., Chem. Commun.* **1995**, 229.

(13) See for example: (a) Sappa, E.; Tiripicchio, A.; Braunstein, P. *Chem. Rev.* **1983**, *83*, 203. (b) Allison, N. T.; Fritch, J. R.; Vollhardt, K. P. C.; Walborsky, E. C. *J. Am. Chem. Soc.* **1983**, *105*, 1384. (c) Raithby, P. R.; Rosales, M. J. *Adv. Inorg. Chem. Radiochem.* **1985**, *29*, 169.

(14) Choualeb, A.; Rosé, J.; Braunstein, P.; Welter, R. *Organometallics*, **2003***, 22*, 2688.

(15) (a) Chini, P.; Heaton, B. T. *Top. Curr. Chem*. **1977**, *71*, 1. (b) Went, M. J. *Adv. Organomet. Chem.* **1997**, *41*, 69-125. (c) Darensbourg, D. J.; Incorvia, M. J. *Inorg. Chem.* **1980***, 19,* 2585.

(16) Holland, G. F.; Ellis, D. E.; Trogler, W. C. *J. Am. Chem. Soc.* **1986**, *108*, 1884.

(17) Wang, J.-Q.; Shen, J. K.; Gao, Y.-C.; Shi, Q.-Z.; Basolo, F. *J. Organomet. Chem.* **1991**, *417*, 131.

(18) Sizun, C.; Kempgens, P.; Raya, J.; Elbayed, K.; Granger, P.; Rosé, J. *J. Organomet. Chem.* **2000**, *604*, 27.

(19) Dahl, L. F.; Smith, D. L. *J. Am. Chem. Soc.* **1962**, *84*, 2450.

(20) Dickson, R. S.; Tailby, G. R. *Aust. J. Chem*., **1970**, *23*, 229.

(21) Krüerke, U.; Hübel, W. *Chem. Ber.,* **1961**, *94*, 2829.

(22) See for example Kennedy, J. R.; Selz, P.; Rheingold, A. L.; Trogler, C. W.; Basolo, F. *J. Am. Chem. Soc.* **1989**, *111*, 3615.

(23) (a) Braunstein, P.; Knorr, M.; Stern, C. *Coord. Chem. Rev.* **1998**, *178-180*, 903. (b) Bachert, I.; Braunstein, P.; Guillon, E.; Massera, C.; Rosé, J.; DeCian, A.; Fischer, J. *J. Cluster Sci*. **1999**, *10*, 445. (c) Bachert, I.; Braunstein, P.; McCart, M. K.; Fabrizi de Biani, F.; Laschi, F.; Zanello, P.; Kickelbick, G.; Schubert, U. *J. Organomet. Chem.* **1999**, *573*, 47. (d) Bachert, I.; Bartussek, P.; Braunstein, P.; Guillon, E.; Rosé, J.; Kickelbick, G. *J. Organomet. Chem.* **1999**, *588*, 143. (e) Braunstein, P.; Durand, J.; Kickelbick, G.; Knorr, M.; Morise, X.; Pugin, R.; Tiripicchio, A.; Ugozzoli, F. *J. Chem. Soc. Dalton Trans*. **1999**, 4175.

(24) Dickson, R. S.; Tailby, G. R. *Aust. J. Chem*. **1969**, *22*, 1143.

(25) Costa, M.; Gervasio, G.; Marabello, D.; Sappa, E. *J. Organomet. Chem.* **2002**, *656*, 57.

(26) Bahsoun, A. A.; Osborn, J. A.; Voelker, G.; Bonnet, J. J.; Lavigne, G. *Organometallics* **1982**, *1*, 1114.

(27) Darensbourg, D. J.; Zalewski, D. J.; Delord, T. *Organometallics* **1984**, *3*, 1210.

(28) (a) Mirza, H. A.; Vittal, J. J.; Puddephatt, R. J.; Frampton, C. S.; Manojlovic-Muir, L.; Xia, W.; Hill, R. H. *Organometallics* **1993**, *12*, 2767. (b) Schmidbaur, H.; Reber, G.; Schier, A.; Wagner, F. E.; Müller, G. *Inorg. Chim. Acta* **1988**, *147*, 143. (c) Nöth, H.; Fluck, E. *Z. Naturforsch.* **1984**, *39b*, 744. (d) For a recent comparison of Pt(II) complexes with the

bridging ligands dppa and dppm, see: Jamali, S.; Rashidi, M; Jennings, M. C.; Puddephatt, R. J. *Dalton Trans*. **2003**, 2313.

(29) Aime, S.; Gobetto, R.; Osella, D.; Milone, L.; Hawkes, G. E.; Randall, E. W. *J. Magn. Reson.* **1988***, 65,* 308.

(30) (a) Huq, R.; Poë, A. *J. Organomet. Chem.* **1982**, *226*, 277. (b) Lisic, E. C.; Hanson, B. E. *Inorg. Chem.* **1986***, 25*, 812.

(31) Braunstein, P.; Rosé, J.; Bars, O. *J. Organomet. Chem.* **1983**, *252*, C101.

(32) Raithby, P. R. In *Transition Metal Clusters;* Johnson, B. F. G., Ed.; Wiley, New York*,* **1980**; Chapter 2.

(33) Osella, D.; Ravera, M.; Nervi, C.; Housecroft, C. E.; Raithby, P. R.; Zanello, P.; Laschi, F. *Organometallics* **1991**, *10*, 3253.

(34) Adams, H.; Guio, L. V. Y. Morris, M. J.; Wildgoose, F. A. *J. Organomet. Chem.* **2002**, *659*, 142 and references cited therein.

(35) Carré, F. H.; Cotton. F. A.; Frenz, B. A. *Inorg. Chem.* **1976***, 15,* 380.

(36) (a) Darensbourg, D. J.; Zalewski, D. J.; Rheingold, A. L.; Durney, R. L. *Inorg. Chem.* **1986***, 25,* 3281. (b) Darensbourg, D. J.; Incorvia, M. J. *Inorg. Chem.* **1981***, 20,* 1911.

(37) Crabtree, R. H.; Lavin, M. *Inorg. Chem*. **1986**, *25*, 805.

(38) Sonogashira, K. *J. Organomet. Chem.* **2002**, *653*, 46.

(39) Spectroscopic data for **9**: IR (hexane, ν_{CO}): 2028 (s), 2000 (vs), 1976 (vs), 1957 (w). ^{1}H NMR (300.13 MHz, $CDCl_3$) δ: 3.09 (m, 1H, PC*H*^{A}H^{B}P, part of an ABX_2 spin system), 3.58 (m, 1H, PCH^{A}*H*^{B}P, part of an ABX_2 spin system), 5.79 (t, 1H, ^{3}J(HP) = 7.5 Hz), 7.20-7.87 (m, 20H, Ph). ^{31}P{^{1}H} NMR (121.5 MHz, $CDCl_3$) δ: 44.0 (br, $w_{1/2}$ = 133 Hz). Anal. Calcd. for $C_{37}H_{28}Co_2O_4P_2$•1/5 hexane: C, 62.54; H, 4.23. Found: C, 62.55; H, 4.09.

(40) Snaith, T. J.; Low, P. J.; Rousseau, R.; Puschmann, H.; Howard, J. A. K. *J. Chem. Soc. Dalton Trans*. **2001**, 292.

(41) Aggarval, R. P.; Connelly, N. G.; Crespo, M. C.; Dunne, B. J.; Hopkins, P. M.; Orpen, A. G. *J. Chem. Soc. Dalton Trans*. **1992**, 655.

(42) Pannel, K. H.; Crawford, G. M. *J. Coord. Chem.,* **1973***, 2,* 251.

(43) Magnus. P.; Becker. D. P. *J. Chem. Soc. Chem. Commun.* **1985**, 640.

(44) Bruce, M. I.; Low, P. J.; Werth, A.; Skelton, B. W.; White, A. H. *J. Chem. Soc., Dalton Trans.* **1996**, 1551.

(45) Rubin, Y.; Knobler, C. B.; Diederich, F. *J. Am. Chem. Soc.* **1990**, *112*, 4966.

(46) Diederich, F.; Rubin, Y.; Chapman, O. L.; Goroff, N. S. *Helv Chim Acta,* **1994**, *77*, 1441.

(47) Choualeb, A.; Braunstein, P.; Rosé, J.; Welter, R., manuscript in preparation.

(48) Sommer, K. *Z. Anorg. Chem*. **1970**, *376*, 37

(49) Nöth, H.; Meinel, L. *Z. Anorg. Allg. Chem*. **1967**, *349*, 225

(50) Kappa CCD Operation Manual, Nonius B.V., Delft, The Netherlands, **1997**

(51) Sheldrick, G. M. SHELXL97, Program for the refinement of crystal structures, University of Gottingen, Germany, **1997**.

Table 1. Selected bond lengths (Å) and bond angles (°) for 1a (estimated standard deviations in parentheses)

Co(1)-Co(2)	2.4268(8)	Co(2)-C(5)	1.920(4)
Co(1)-Co(3)	2.4565(7)	Co(3)-Co(4)	2.528(1)
Co(1)-Co(4)	2.5014(7)	Co(3)-C(3)	1.957(4)
Co(1)-P(1)	2.190(1)	Co(3)-C(5)	1.945(4)
Co(1)-C(1)	1.759(5)	Co(3)-C(6)	1.789(5)
Co(1)-C(2)	1.932(5)	Co(3)-C(7)	1.779(5)
Co(1)-C(3)	1.929(4)	Co(4)-C(8)	1.809(5)
Co(2)-Co(3)	2.4540(8)	Co(4)-C(9)	1.830(6)
Co(2)-Co(4)	2.5348(8)	Co(4)-C(10)	1.791(5)
Co(2)-P(2)	2.194(1)	P(1)-C(23)	1.855(4)
Co(2)-C(2)	1.923(4)	P(2)-C(23)	1.843(4)
Co(2)-C(4)	1.767(5)		
Co(2)-Co(1)-Co(3)	60.33(2)	Co(2)-Co(4)-Co(3)	57.98(2)
Co(2)-Co(1)-Co(4)	61.89(2)	P(1)-C(23)-P(2)	114.5(2)
Co(2)-Co(1)-P(1)	99.71(4)	C(23)-P(1)-Co(1)	110.5(1)
Co(3)-Co(1)-Co(4)	61.32(3)	C(23)-P(2)-Co(2)	111.3(1)
Co(3)-Co(1)-P(1)	102.84(4)	Co(1)-C(1)-O(1)	177.0(4)
Co(4)-Co(1)-P(1)	159.56(4)	Co(1)-C(2)-O(2)	142.1(4)
Co(1)-Co(2)-Co(3)	60.43(2)	Co(2)-C(2)-O(2)	139.9(4)
Co(1)-Co(2)-Co(4)	60.50(2)	Co(1)-C(3)-O(3)	143.0(3)
Co(1)-Co(2)-P(2)	98.22(4)	Co(3)-C(3)-O(3)	138.5(3)
Co(3)-Co(2)-Co(4)	60.88(2)	Co(2)-C(4)-O(4)	179.2(4)
Co(3)-Co(2)-P(2)	104.17(4)	Co(2)-C(5)-O(5)	143.6(4)
Co(4)-Co(2)-P(2)	157.70(4)	Co(3)-C(5)-O(5)	137.5(4)
Co(1)-Co(3)-Co(2)	59.23(2)	Co(3)-C(6)-O(6)	179.2(4)
Co(1)-Co(3)-Co(4)	60.22(2)	Co(3)-C(7)-O(7)	177.9(4)
Co(2)-Co(3)-Co(4)	61.14(2)	Co(4)-C(8)-O(8)	178.1(5)
Co(1)-Co(4)-Co(2)	57.61(2)	Co(4)-C(9)-O(9)	179.1(5)
Co(1)-Co(4)-Co(3)	58.47(2)	Co(4)-C(10)-O(10)	178.4(5)

Table 2. Selected bond lengths (Å) and bond angles (°) for 2a (estimated standard deviations in parentheses)

Co(1)-Co(2)	2.410(1)	Co(3)-C(4)	1.791(4)
Co(1)-Co(3)	2.620(1)	Co(3)-C(5)	1.790(4)
Co(1)-Co(4)	2.411(1)	Co(3)-C(6)	1.967(4)
Co(1)-P(1)	2.218(1)	Co(3)-C(10)	2.007(3)
Co(1)-C(1)	1.782(4)	Co(4)-C(6)	1.895(4)
Co(1)-C(2)	1.965(3)	Co(4)-C(7)	1.763(4)
Co(1)-C(9)	1.988(3)	Co(4)-C(8)	1.756(4)
Co(2)-Co(3)	2.480(1)	Co(4)-C(9)	2.057(3)
Co(2)-P(2)	2.200(1)	Co(4)-C(10)	2.118(3)
Co(2)-C(2)	1.845(3)	P(1)-C(29)	1.856(4)
Co(2)-C(3)	1.746(4)	P(2)-C(29)	1.840(3)
Co(2)-C(9)	2.026(3)	C(9)-C(10)	1.405(4)
Co(2)-C(10)	2.091(3)	C(10)-C(11)	1.484(4)
Co(3)-Co(4)	2.455(1)		
Co(2)-Co(1)-Co(3)	58.90(3)	Co(1)-Co(4)-C(10)	75.91(9)
Co(2)-Co(1)-Co(4)	93.80(4)	Co(3)-Co(4)-C(9)	74.31(9)
Co(2)-Co(1)-P(1)	98.01(4)	Co(3)-Co(4)-C(10)	51.42(8)
Co(2)-Co(1)-C(9)	53.83(10)	C(9)-Co(4)-C(10)	39.3(1)
Co(3)-Co(1)-Co(4)	58.24(3)	P(1)-C(29)-P(2)	112.6(1)
Co(3)-Co(1)-P(1)	156.89(4)	Co(1)-P(1)-C(29)	108.0(1)
Co(3)-Co(1)-C(9)	71.6(1)	Co(2)-P(2)-C(29)	107.7(1)
Co(4)-Co(1)-P(1)	128.80(4)	Co(1)-C(9)-Co(2)	73.8(1)
Co(4)-Co(1)-C(9)	54.76(10)	Co(1)-C(9)-Co(4)	73.1(1)
P(1)-Co(1)-C(9)	94.68(10)	Co(1)-C(9)-C(10)	109.7(2)
Co(1)-Co(2)-Co(3)	64.78(4)	Co(2)-C(9)-Co(4)	119.1(2)
Co(1)-Co(2)-P(2)	99.32(5)	Co(2)-C(9)-C(10)	72.5(2)
Co(1)-Co(2)-C(9)	52.38(10)	Co(2)-C(10)-Co(3)	74.45(10)
Co(1)-Co(2)-C(10)	76.42(10)	Co(2)-C(10)-Co(4)	113.5(1)
Co(3)-Co(2)-P(2)	164.03(3)	Co(2)-C(10)-C(9)	67.6(2)
Co(3)-Co(2)-C(9)	74.25(10)	Co(3)-C(10)-Co(4)	73.0(1)
Co(3)-Co(2)-C(10)	51.23(8)	Co(4)-C(10)-C(9)	68.0(2)
P(2)-Co(2)-C(9)	95.13(10)	Co(1)-C(1)-O(1)	178.5(3)
P(2)-Co(2)-C(10)	126.17(9)	Co(1)-C(2)-O(2)	136.9(3)
C(9)-Co(2)-C(10)	39.86(12)	Co(2)-C(2)-O(2)	144.7(3)
Co(1)-Co(3)-Co(2)	56.32(3)	Co(2)-C(3)-O(3)	178.8(3)
Co(1)-Co(3)-Co(4)	56.61(2)	Co(3)-C(4)-O(4)	178.4(3)
Co(1)-Co(3)-C(10)	72.97(9)	Co(3)-C(5)-O(5)	175.8(4)
Co(2)-Co(3)-Co(4)	91.00(3)	Co(3)-C(6)-O(6)	138.6(3)
Co(2)-Co(3)-C(10)	54.31(9)	Co(4)-C(6)-O(6)	142.3(3)
Co(4)-Co(3)-C(10)	55.6(1)	Co(4)-C(7)-O(7)	175.8(4)
Co(1)-Co(4)-Co(3)	65.16(2)	Co(4)-C(8)-O(8)	171.6(4)
Co(1)-Co(4)-C(9)	52.11(9)		

Table 3. Selected bond lengths (Å) and bond angles (°) for 2'b•0.5CH_2Cl_2 (estimated standard deviations in parentheses)

Co(1)-Co(2)	2.456(1)	Co(3)-C(3)	2.055(3)
Co(1)-Co(3)	2.543(1)	Co(3)-C(4)	1.795(3)
Co(1)-Co(4)	2.419(1)	Co(3)-C(5)	1.800(3)
Co(1)-P(1)	2.172(1)	Co(3)-C(10)	2.009(3)
Co(1)-C(1)	1.785(3)	Co(4)-C(6)	1.759(3)
Co(1)-C(8)	1.914(3)	Co(4)-C(7)	1.776(3)
Co(1)-C(9)	1.983(3)	Co(4)-C(8)	1.935(3)
Co(2)-Co(3)	2.448(1)	Co(4)-C(9)	2.050(3)
Co(2)-P(2)	2.168(1)	Co(4)-C(10)	2.142(3)
Co(2)-C(2)	1.777(3)	P(1)-N	1.683(3)
Co(2)-C(3)	1.833(3)	P(2)-N	1.694(3)
Co(2)-C(9)	2.072(3)	C(9)-C(10)	1.409(4)
Co(2)-C(10)	2.050(3)	C(10)-C(11)	1.498(4)
Co(3)-Co(4)	2.456(1)		
Co(2)-Co(1)-Co(3)	58.61(3)	Co(3)-Co(4)-C(10)	51.27(8)
Co(2)-Co(1)-Co(4)	93.60(2)	C(9)-Co(4)-C(10)	39.2(1)
Co(2)-Co(1)-P(1)	101.73(3)	P(1)-N-P(2)	119.9(1)
Co(2)-Co(1)-C(9)	54.40(9)	C(17)-P(1)-C(23)	102.5(1)
Co(3)-Co(1)-Co(4)	59.28(2)	Co(1)-P(1)-N	104.5(1)
Co(3)-Co(1)-P(1)	159.14(3)	C(29)-P(1)-C(35)	104.8(1)
Co(3)-Co(1)-C(9)	72.89(9)	Co(2)-P(2)-N	114.6(1)
Co(4)-Co(1)-P(1)	120.41(3)	Co(1)-C(9)-Co(4)	73.7(1)
Co(4)-Co(1)-C(9)	54.44(9)	Co(1)-C(9)-Co(2)	74.5(1)
P(1)-Co(1)-C(9)	90.19(9)	Co(1)-C(9)-C(10)	108.6(2)
Co(1)-Co(2)-Co(3)	62.48(2)	Co(2)-C(9)-Co(4)	119.1(1)
Co(1)-Co(2)-P(2)	85.22(3)	Co(2)-C(9)-C(10)	69.2(2)
Co(1)-Co(2)-C(9)	5 1.10(8)	Co(4)-C(9)-C(10)	73.9(2)
Co(1)-Co(2)-C(10)	75.43(9)	Co(2)-C(10)-Co(3)	74.2(1)
Co(3)-Co(2)-P(2)	141.59(3)	Co(2)-C(10)-Co(4)	115.9(1)
Co(3)-Co(2)-C(9)	73.66(9)	Co(2)-C(10)-C(9)	70.8(2)
Co(3)-Co(2)-C(10)	52.15(8)	Co(3)-C(10)-Co(4)	72.5(1)
P(2)-Co(2)-C(9)	102.89(9)	Co(3)-C(10)-C(9)	104.4(2)
P(2)-Co(2)-C(10)	141.94(9)	Co(4)-C(10)-C(9)	66.9(2)
C(9)-Co(2)-C(10)	40.0(1)	C(9)-C(10)-C(11)	125.9(3)
Co(1)-Co(3)-Co(2)	58.90(2)	Co(1)-C(1)-O(1)	178.7(4)
Co(1)-Co(3)-Co(4)	57.84(2)	Co(2)-C(2)-O(2)	179.1(3)
Co(1)-Co(3)-C(10)	74.06(9)	Co(2)-C(3)-O(3)	149.4(3)
Co(2)-Co(3)-Co(4)	92.86(2)	Co(3)-C(3)-O(3)	132.7(3)
Co(2)-Co(3)-C(10)	53.67(8)	Co(3)-C(4)-O(4)	179.0(3)
Co(4)-Co(3)-C(10)	56.25(9)	Co(3)-C(5)-O(5)	175.6(4)
Co(1)-Co(4)-Co(3)	62.89(2)	Co(4)-C(6)-O(6)	173.4(4)
Co(1)-Co(4)-C(9)	51.89(8)	Co(4)-C(7)-O(7)	176.3(3)
Co(1)-Co(4)-C(10)	74.68(8)	Co(1)-C(8)-O(8)	144.3(3)
Co(3)-Co(4)-C(9)	73.84(9)	Co(4)-C(8)-O(8)	137.8(3)

Table 4. Selected bond lengths (Å) and bond angles (°) for 8 (estimated standard deviations in parentheses)

Co(1)-Co(2)	2.434(1)	Co(3)-Co(4)	2.535(1)
Co(1)-Co(3)	2.507(1)	Co(3)-P(3)	2.183(1)
Co(1)-Co(4)	2.490(1)	Co(3)-C(4)	1.981(4)
Co(1)-P(1)	2.184(1)	Co(3)-C(5)	1.757(5)
Co(1)-C(1)	1.773(5)	Co(3)-C(6)	1.941(4)
Co(1)-C(2)	1.921(4)	Co(4)-P(4)	2.188(1)
Co(1)-C(6)	1.936(4)	Co(4)-C(7)	1.775(5)
Co(2)-Co(3)	2.477(1)	Co(4)-C(8)	1.793(5)
Co(2)-Co(4)	2.543(1)	P(1)-C(21)	1.847(4)
Co(2)-P(2)	2.219(1)	P(2)-C(21)	1.847(4)
Co(2)-C(2)	1.920(4)	P(3)-N	1.706(4)
Co(2)-C(3)	1.763(4)	P(4)-N	1.697(4)
Co(2)-C(4)	1.897(5)		
Co(2)-Co(1)-Co(3)	60.18(2)	Co(2)-Co(4)-Co(3)	58.40(2)
Co(2)-Co(1)-Co(4)	62.20(2)	Co(2)-Co(4)-P(4)	111.56(4)
Co(2)-Co(1)-P(1)	98.41(4)	Co(3)-Co(4)-P(4)	94.04(4)
Co(3)-Co(1)-Co(4)	60.98(2)	P(1)-C(21)-P(2)	108.5(2)
Co(3)-Co(1)-P(1)	104.75(4)	C(21)-P(1)-Co(1)	110.1(1)
Co(4)-Co(1)-P(1)	159.51(4)	C(21)-P(2)-Co(2)	108.6(1)
Co(1)-Co(2)-Co(3)	61.37(2)	N-P(3)-Co(3)	116.5(1)
Co(1)-Co(2)-Co(4)	59.98(2)	N-P(4)-Co(4)	111.0(1)
Co(1)-Co(2)-P(2)	96.08(4)	P(3)-N-P(4)	114.9(2)
Co(3)-Co(2)-Co(4)	60.63(2)	Co(1)-C(1)-O(1)	178.8(4)
Co(3)-Co(2)-P(2)	109.01(4)	Co(1)-C(2)-O(2)	140.4(3)
Co(4)-Co(2)-P(2)	156.04(4)	Co(2)-C(2)-O(2)	140.9(3)
Co(1)-Co(3)-Co(2)	58.45(2)	Co(2)-C(3)-O(3)	178.9(4)
Co(1)-Co(3)-Co(4)	59.18(2)	Co(2)-C(4)-O(4)	141.2(4)
Co(1)-Co(3)-P(3)	133.11(4)	Co(3)-C(4)-O(4)	139.3(4)
Co(2)-Co(3)-Co(4)	60.97(2)	Co(3)-C(5)-O(5)	177.7(4)
Co(2)-Co(3)-P(3)	134.51(4)	Co(1)-C(6)-O(6)	139.8(3)
Co(4)-Co(3)-P(3)	87.34(4)	Co(3)-C(6)-O(6)	139.4(3)
Co(1)-Co(4)-Co(2)	57.82(2)	Co(4)-C(7)-O(7)	177.1(4)
Co(1)-Co(4)-Co(3)	59.84(2)	Co(4)-C(8)-O(8)	177.2(4)
Co(1)-Co(4)-P(4)	153.84(4)		

Table 5. Selected bond lengths (Å) and bond angles (°) for 16 (estimated standard deviations in parentheses)

Co(1)-Co(2)	2.406(1)	Co(3)-C(4)	1.809(4)
Co(1)-Co(3)	2.594(1)	Co(3)-C(5)	1.785(4)
Co(1)-Co(4)	2.442(1)	Co(3)-C(6)	1.963(4)
Co(1)-P(1)	2.219(1)	Co(3)-C(10)	1.988(3)
Co(1)-C(1)	1.776(4)	Co(4)-C(6)	1.888(3)
Co(1)-C(2)	2.015(4)	Co(4)-C(7)	1.780(4)
Co(1)-C(9)	1.973(3)	Co(4)-C(8)	1.760(4)
Co(2)-Co(3)	2.483(1)	Co(4)-C(9)	2.069(3)
Co(2)-P(2)	2.184(1)	Co(4)-C(10)	2.074(3)
Co(2)-C(2)	1.844(3)	P(1)-C(28)	1.847(3)
Co(2)-C(3)	1.751(4)	P(2)-C(28)	1.848(3)
Co(2)-C(9)	2.020(3)	C(9)-C(10)	1.413(5)
Co(2)-C(10)	2.071(3)	C(10)-C(11)	1.437(5)
Co(3)-Co(4)	2.441(1)	C(11)-C(12)	1.203(5)
Co(2)-Co(1)-Co(3)	59.41(3)	Co(1)-Co(4)-C(10)	74.75(9)
Co(2)-Co(1)-Co(4)	93.09(3)	Co(3)-Co(4)-C(9)	74.7(1)
Co(2)-Co(1)-P(1)	97.56(3)	Co(3)-Co(4)-C(10)	51.46(9)
Co(2)-Co(1)-C(9)	53.8(1)	C(9)-Co(4)-C(10)	39.9(1)
Co(3)-Co(1)-Co(4)	57.89(3)	P(1)-C(28)-P(2)	115.8(2)
Co(3)-Co(1)-P(1)	155.77(3)	Co(1)-P(1)-C(28)	108.3(1)
Co(3)-Co(1)-C(9)	72.7(1)	Co(2)-P(2)-C(28)	108.6(1)
Co(4)-Co(1)-P(1)	121.67(4)	Co(1)-C(9)-Co(2)	74.1(1)
Co(4)-Co(1)-C(9)	54.6(1)	Co(1)-C(9)-Co(4)	74.3(1)
P(1)-Co(1)-C(9)	87.9(1)	Co(1)-C(9)-C(10)	107.9(2)
Co(1)-Co(2)-Co(3)	64.05(2)	Co(2)-C(9)-Co(4)	118.8(2)
Co(1)-Co(2)-P(2)	101.04(3)	Co(2)-C(9)-C(10)	71.7(2)
Co(1)-Co(2)-C(9)	52.04(9)	Co(2)-C(10)-Co(3)	75.4(1)
Co(1)-Co(2)-C(10)	75.62(9)	Co(2)-C(10)-Co(4)	116.2(1)
Co(3)-Co(2)-P(2)	165.09(3)	Co(2)-C(10)-C(9)	67.9(2)
Co(3)-Co(2)-C(9)	74.5(1)	Co(3)-C(10)-Co(4)	73.8(1)
Co(3)-Co(2)-C(10)	50.8(1)	Co(4)-C(10)-C(9)	69.8(2)
P(2)-Co(2)-C(9)	96.4(1)	C(10)-C(11)-C(12)	176.8(4)
P(2)-Co(2)-C(10)	128.0(1)	Co(1)-C(1)-O(1)	178.5(4)
C(9)-Co(2)-C(10)	40.4(1)	Co(1)-C(2)-O(2)	136.4(3)
Co(1)-Co(3)-Co(2)	56.54(3)	Co(2)-C(2)-O(2)	146.5(3)
Co(1)-Co(3)-Co(4)	57.95(3)	Co(2)-C(3)-O(3)	178.2(4)
Co(1)-Co(3)-C(10)	72.6(1)	Co(3)-C(4)-O(4)	179.7(5)
Co(2)-Co(3)-Co(4)	91.27(2)	Co(3)-C(5)-O(5)	179.7(4)
Co(2)-Co(3)-C(10)	53.81(9)	Co(3)-C(6)-O(6)	138.1(3)
Co(4)-Co(3)-C(10)	54.71(9)	Co(4)-C(6)-O(6)	143.2(3)
Co(1)-Co(4)-Co(3)	64.16(2)	Co(4)-C(7)-O(7)	178.5(4)
Co(1)-Co(4)-C(9)	51.04(9)	Co(4)-C(8)-O(8)	171.7(4)

	1a	**2a**	**2'b•0.5CH_2Cl_2**	**8**	**16**
formula	$C_{35}H_{22}Co_4O_{10}P_2$	$C_{41}H_{28}Co_4O_8P_2$	$C_{40}H_{27}Co_4NO_8P_2$	$C_{66}H_{63}Co_4NO_{11}P_4Si$	$C_{40}H_{32}Co_4O_8P_2Si$
fw	900.19	946.29	989.75	1433.95	966.41
color	red	green	green	green	green
crystal system	triclinic	triclinic	monoclinic	triclinic	triclinic
a (Å)	10.2475(3)	11.139(5)	22.045(5)	11.6370(2)	10.807(5)
b (Å)	11.6675(4)	11.258(5)	17.711(5)	17.9680(3)	12.078(5)
c (Å)	16.3918(7)	17.036(5)	21.797(5)	18.6170(3)	17.196(5)
α, deg	74.4260(10)	83.81(2)	90.000(5)	70.6790(9)	79.490(5)
βdeg	89.2080(10)	77.82(2)	110.557(5)	77.3030(9)	74.334(5)
γdeg	72.497(2)	65.28(2)	90.000(5)	73.4500(7)	68.537(5)
V (Å3)	1795.70(11)	1896.5(13)	7968(3)	3487.19(10)	2002.5(14)
Z	2	2	4	2	2
D_{calc} (gcm^{-3})	1.665	1.657	1.652	1.349	1.603
wavelength (Å)	0.71069	0.71069	0.71069	0.71069	0.71069
μ (mm^{-1})	1.960	1.857	1.837	1.099	1.789
space group	*P*-1	*P*-1	*C* 2/c	*P*-1	*P*-1
temperature (K)	173(2)	173(2)	173(2)	173(2)	173(2)
Radiation	MoKα graphite monochromated				
Diffractometer	KappaCCD				
hkl limits	-14.14/-16.15/-20.23	0.14/1-12.14/-21.22	-32.30/0.26/0/32	-11.15/-21.23/0.24	-14.15/-16.16/0.20
F(000)	900	952	3976	1438	976
Theta limits (deg)	2.50-29.98	1.22-27.54	2.51-32.05	1.84- 27.46	2.2-30.0
Number of data meas	12946	8657	13817	15787	11653

Number of data ($I \rangle 2\sigma(I)$)	7210	6342	7360	12392	7930
R^a	0.1014	0.0388	0.0559	0.0696	0.0552
R_W^a	0.1181	0.1154	0.1224	0.2098	0.1409
GOF	1.172	1.039	0.819	1.074	0.89
Largest peak in final difference ($eÅ^{-3}$)	0.953	0.500	0.492	2.969	0.62

Captions to the Figures

Figure 1. View of the molecular structure of cluster **1a.** Only the ipso carbons of the phenyl groups are shown and the hydrogen atoms have been omitted for clarity.

Figure 2. View of the molecular structure of cluster **2a.** Only the ipso carbons of the phenyl groups of the phosphine ligand are shown and the hydrogen atoms have been omitted for clarity.

Figure 3. View of the molecular structure of the cluster **2'b** in **2'b•**$0.5CH_2Cl_2$**.** Only the ipso carbons of the phenyl groups of the phosphine ligand are shown, the solvent and hydrogen atoms have been omitted for clarity.

Figure 4. View of the molecular structure of cluster **8.** Only the ipso carbons of the phenyl groups are shown and the hydrogen atoms have been omitted for clarity.

Figure 5. View of the molecular structure of cluster **16.** Only the ipso carbons of the phenyl groups are shown and the hydrogen atoms have been omitted for clarity.

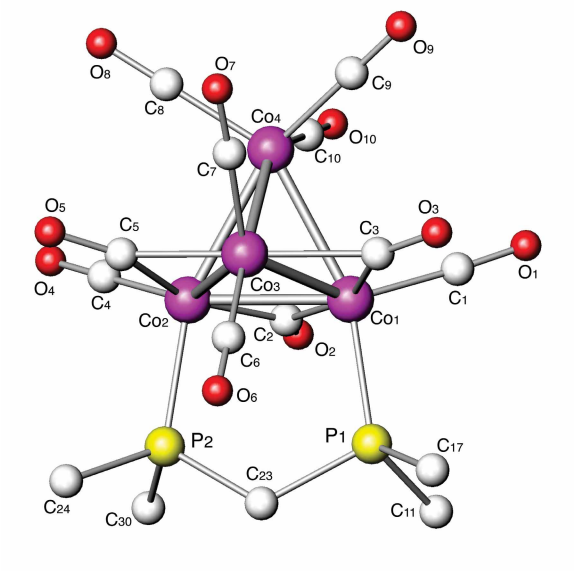

Figure 1. View of the molecular structure of cluster **1a.** Only the ipso carbons of the phenyl groups are shown and the hydrogen atoms on C(23) have been omitted for clarity.

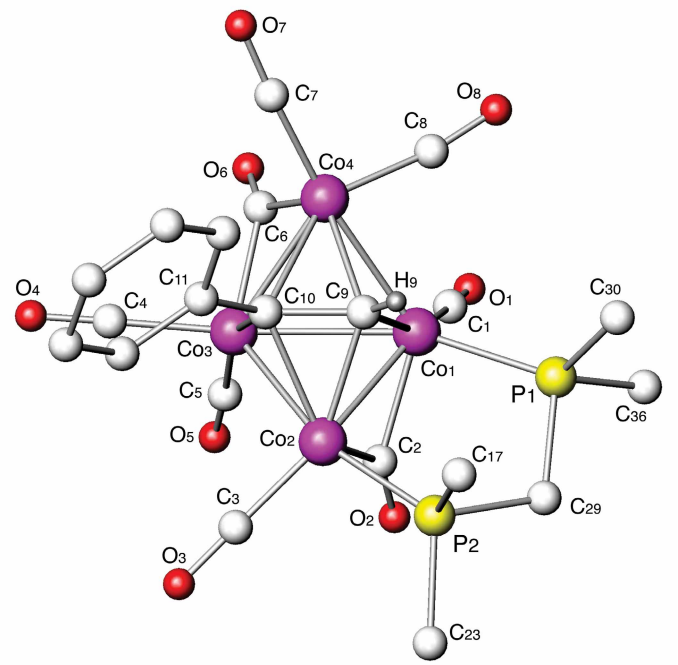

Figure 2. View of the molecular structure of cluster **2a.** Only the ipso carbons of the phenyl groups of the phosphine ligand are shown and the hydrogen atoms have been omitted for clarity.

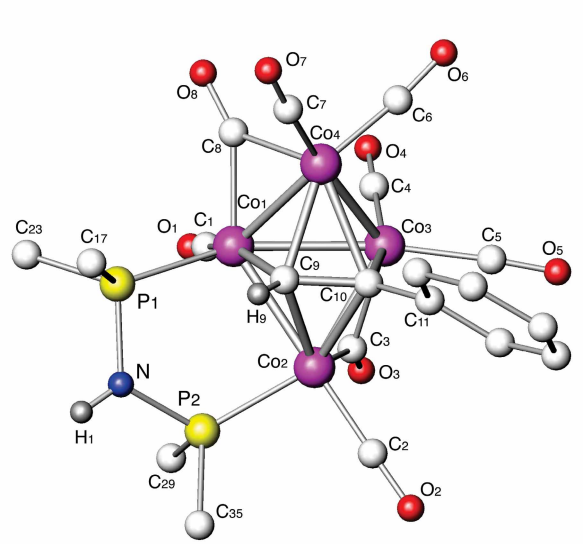

Figure 3. View of the molecular structure of the cluster **2'b** in **2'b**•0.5CH_2Cl_2. Only the ipso carbons of the phenyl groups of the phosphine ligand are shown, the solvent and hydrogen atoms have been omitted for clarity.

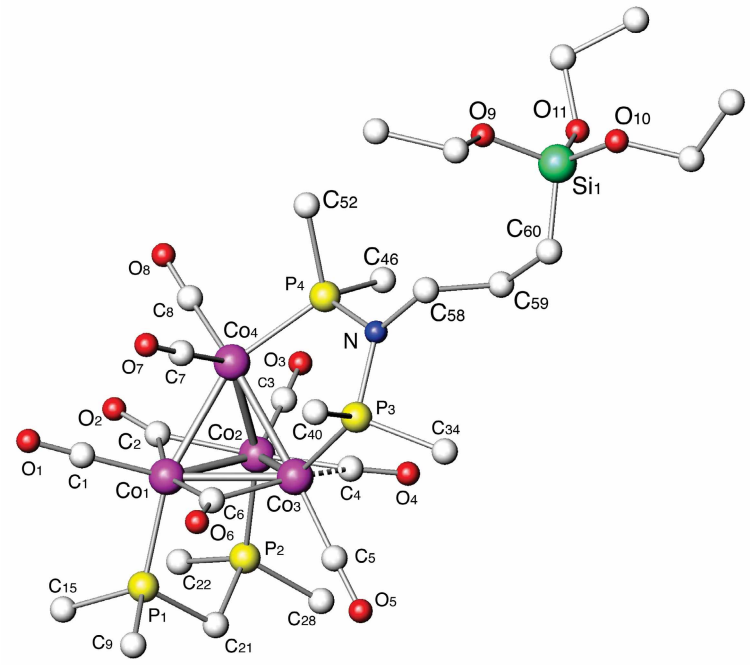

Figure 4. View of the molecular structure of cluster **8.** Only the ipso carbons of the phenyl groups are shown and the hydrogen atoms have been omitted for clarity.

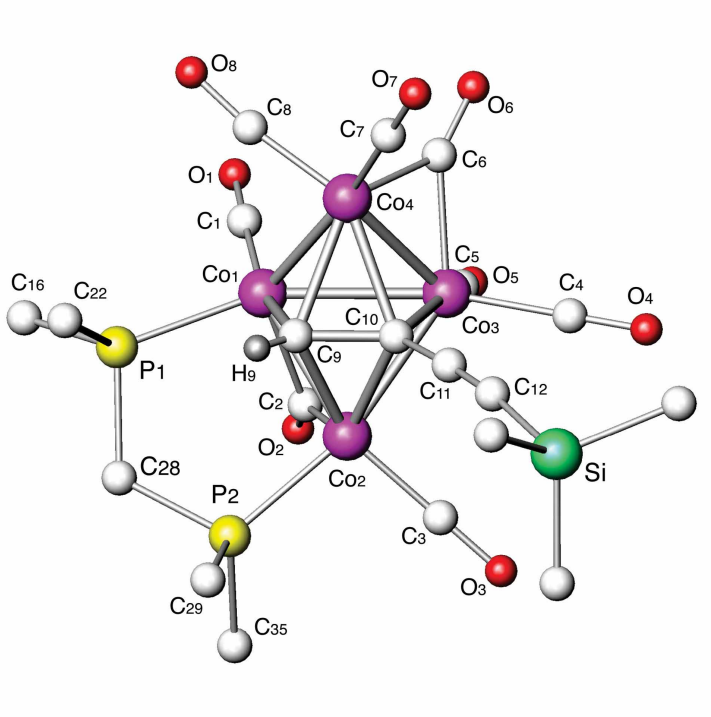

Figure 5. View of the molecular structure of cluster **16.** Only the ipso carbons of the phenyl groups are shown and the hydrogen atoms have been omitted for clarity.

Chapitre 2

Voies de synthèse de clusters ruthénium-cobalt et de complexes dinucléaires de cobalt à partir de nouveaux alcynes contenant les fonctions –SR ou –Si(OR)$_3$. Structures cristallines de [NEt$_4$][RuCo$_3$(CO)$_{10}${μ$_4$-η²-HC$_2$(CH$_2$)$_2$OC(O)NH(CH$_2$)$_3$Si(OEt)$_3$}] et [Co$_2$(CO)$_6${μ$_2$-η²-HC$_2$CH$_2$NHC(O)NH(CH$_2$)$_3$Si(OEt)$_3$}]

Ce chapitre est présenté sous la forme d'une publication parue dans *Organometallics* **2003**, *22*, 2688-2693.

Routes to Ruthenium−Cobalt Clusters and Dicobalt Complexes with New Alkoxysilyl- or Sulfur-Functionalized Alkynes. X-ray Structures of $[NEt_4][RuCo_3(CO)_{10}\{\mu_4\text{-}\eta^2\text{-}HC_2(CH_2)_2OC(O)NH(CH_2)_3Si(OEt)_3\}]$ and $[Co_2(CO)_6\{\mu_2\text{-}\eta^2\text{-}HC_2CH_2NHC(O)NH(CH_2)_3Si(OEt)_3\}]$

Aldjia Choualeb,[†] Jacky Rosé,[†] Pierre Braunstein,*[,†] and Richard Welter[‡]

Laboratoire de Chimie de Coordination (UMR 7513 CNRS), and Laboratoire DECMET (UMR 7513 CNRS), Université Louis Pasteur, 4 rue Blaise Pascal, F-67070 Strasbourg Cedex, France

Received November 22, 2002

Two general approaches are presented and compared to covalently link metal clusters to alkynes terminated with a trialkoxysilyl or a thioether group. They consist in the direct reaction of the functional alkyne with the cluster or in the functionalization of an alkyne already coordinated to the cluster. These are applied to the tetrahedral mixed-metal cluster $[NEt_4][RuCo_3(CO)_{12}]$ (NEt_4·**1**). Complexes with the new alkynes $HC{\equiv}C(CH_2)_2OC(O)NH(CH_2)_3Si(OEt)_3$ (**L**[1]), $HC{\equiv}CCH_2NHC(O)NH(CH_2)_3Si(OEt)_3$ (**L**[2]), and $HC{\equiv}CCH_2NHC(O)NHC_6H_4SMe$ (**L**[3]) have been characterized, and the crystal structures of $[NEt_4][RuCo_3(CO)_{10}\{\mu_4\text{-}\eta^2\text{-}HC_2(CH_2)_2OC(O)NH(CH_2)_3Si(OEt)_3\}]$ (NEt_4·**2a**) and $[Co_2(CO)_6\{\mu_2\text{-}\eta^2\text{-}HC_2CH_2NHC(O)NH(CH_2)_3Si(OEt)_3\}]$ (**9**) have been determined by X-ray diffraction.

Introduction

The current interest in stable functional metal clusters that could be subsequently covalently anchored onto surfaces or act as precursors to new cluster-derived nanomaterials has led us to consider the use of alkynes as a way to introduce the desired functionality, such as a $-Si(OR)_3$ group, owing to its ability to condense with surface OH groups of inorganic supports and to form sol−gel materials,[1] or a thiol or thioether for, for example, the formation of organized monolayers on gold surfaces.[2] Indeed, reactions of alkynes with carbonyl-metal clusters afford a considerable diversity of structural types and bond activation processes,[3] and the stability of the products is largely due to the formation of covalent metal−carbon bonds, usually involving a triangular or rectangular face of the metal polyhedron. If one considers the large family of tetrahedral metal clusters, the products generally obtained are of the butterfly type, with the organic fragment interacting with the metals in a μ_4-η^2-bonding mode.[3,4] Alternatively, these clusters may be viewed as having a *closo* structure in which the two carbon atoms originating from the alkyne are part of the skeleton. The stability of the metal−carbon σ bonds explains that subsequent reactions may occur by breaking of metal−metal bond(s) and partial cluster fragmentation rather than by splitting of the organic moiety.[5]

Covalent linking rather than dative bonding of a functional ligand to a metal cluster represents a significant advantage to avoid leaching phenomena and is also gaining increasing attention in heterogeneous catalysis.[6] Two strategies may be envisaged to link covalently a metal cluster to a functional alkyne: either by the reaction of a metal cluster with the desired functional alkyne (route A_2 in Scheme 1) or by the functionalization of an organic backbone already linked to the metal cluster (route B_2 in Scheme 1).

It is not obvious that both methods may be used indiscriminately, but if they can, a comparative study of their respective advantages/disadvantages should be particularly instructive. In all cases, the chemo- and regioselectivity of the reactions represent central issues to be investigated. A prerequisite in approach A is that the functional group -FG will not compete with the alkyne in the reaction with the cluster (A_2). Approach

* Corresponding author. E-mail: braunst@chimie.u-strasbg.fr.
† Laboratoire de Chimie de Coordination (UMR 7513 CNRS).
‡ Laboratoire DECMET (UMR 7513 CNRS).

(1) (a) Braunstein, P.; Cauzzi, D.; Predieri, G.; Tiripicchio, A. *J. Chem. Soc., Chem. Commun.* **1995**, 229−230. (b) Corriu, R. J. P.; Leclercq, D. *Angew. Chem., Int. Ed. Engl.* **1996**, *35*, 1420−1436. (c) Hüsing, N.; Schubert, U. *Angew. Chem., Int. Ed.* **1998**, *37*, 22−45. (d) Schweyer, F.; Braunstein, P.; Estournès, C.; Guille, J.; Kessler, H.; Paillaud, J.-L.; Rosé, J. *Chem. Commun.* **2000**, 1271−1272. (e) Bezombes, J. P.; Chuit, C.; Corriu, R. J. P.; Reyé, C. *J. Organomet. Chem.* **2002**, *643*−*644*, 453−460. (f) Boury, B.; Corriu, R. J. P. *Chem. Commun.* **2002**, 795−802.

(2) See for example: (a) Dhirani, A.; Zehner, R. W.; Hsung, R. P.; Guyot-Sionnest, P.; Sita, L. R. *J. Am. Chem. Soc.* **1996**, *118*, 3319−3320. (b) Hasan, M.; Bethell, D.; Brust, M. *J. Am. Chem. Soc.* **2002**, *124*, 1132−1133, and references therein.

(3) (a) Sappa, E.; Tiripicchio, A.; Braunstein, P. *Chem. Rev.* **1983**, *83*, 203−239. (b) Raithby, P.; Rosales, M. J. *Adv. Inorg. Chem. Radiochem.* **1985**, *29*, 169−247.

(4) (a) Chetcuti, M. J.; Fanwick, P. E.; Gordon, J. C. *Inorg. Chem.* **1991**, *30*, 4710−4717. (b) Waterman, S. M.; Humphrey, M. G.; Tolhurst, V.-A.; Bruce, M. I.; Low, P. J.; Hockless, D. C. R. *Organometallics* **1998**, *17*, 5789−5795. (c) Ferrand, V.; Süss-Fink, G.; Neels, A.; Stoeckli-Evans, H. *Eur. J. Inorg. Chem.* **1999**, 853−862. (d) Zhu, B.-H.; Zhang, W.-Q.; Zhao, Q.-Y.; Bian, Z.-G.; Hu, B.; Zhang, Y.-H.; Yin, Y.-Q.; Sun, J. *J. Organomet. Chem.* **2002**, *650*, 181−187.

(5) Braunstein, P.; Rosé, J.; Bars, O. *J. Organomet. Chem.* **1983**, *252*, C101−C105.

(6) Smith, G. V.; Notheisz, F. In *Heterogeneous Catalysis in Organic Chemistry*; Academic Press: San Diego, CA, 1999.

10.1021/om020965m CCC: $25.00
Publication on Web 05/23/2003

Scheme 1. General Approaches for the Incorporation of Functional Alkynes into Metal Clusters, *FG* = −Si(OR)$_3$ or −SR

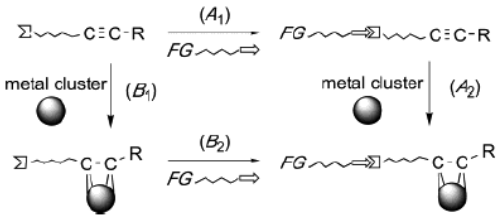

B offers the potential of using a larger diversity of organic substituents but requires that the first step (B_1), i.e., the binding of the alkyne to the cluster, occur with maximum selectivity and efficiency. It also requires that at least one intact organic function remain available for further transformation (B_2). It appeared to us that, to the best of our knowledge, strategy *B* has not been previously applied to cluster chemistry. We decided to explore and compare these two approaches, using the mixed-metal cluster $[RuCo_3(CO)_{12}]^-$ (**1**) as precursor (as NEt_4^+ salt throughout). This cluster is known to react with alkynes[5,7] and offers the advantage over the related $[Co_4(CO)_{12}]$ to allow a study of the metalloselectivity of the reaction.

Results and Discussion

The new alkyne **L^1** was prepared in high yield by condensation of 3-butyn-1-ol and 3-(triethoxysilyl)propylisocyanate in the presence of triethylamine (eq 1). It was characterized by ^{1}H, ^{13}C, and ^{29}Si NMR and IR spectroscopy (see Experimental Section).

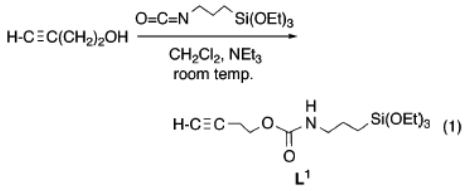

Reaction of **L^1** with **1** afforded cluster **2** by selective alkyne insertion into a Co–Co bond (eq 2). Its ^{1}H NMR

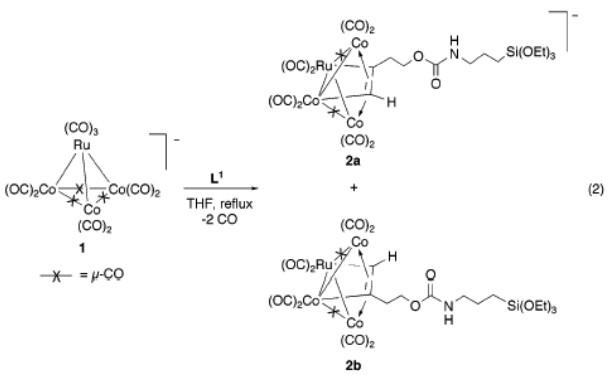

spectrum contains two singlets for the alkyne CH proton at δ 8.74 and 8.27, indicating that two isomers **2a**/**2b** have been formed, in a 3:2 ratio, which differ in the orientation of the alkyne with respect to the Co–Ru hinge but could not be separated by column chromatography. Formation of such isomers is not uncommon in mixed-metal clusters, but the stereoelectronic factors that govern their ratio are not yet clear.[8] On the basis of experiments carried out with related $RuCo_3$ clusters bearing the alkyne HC≡CMe(=CH$_2$),[9] we suggest that the more deshielded ^{1}H NMR signal should be assigned to the Co-bound CH proton. The cluster identified by X-ray diffraction, **2a**, has the CH group attached to Co (Figure 1). The main bonding parameters in this 60-electron cluster are given in the caption of Figure 1 and are comparable to those in related molecules.[3,5] The four metal atoms form a butterfly skeleton where the ruthenium atom occupies a hinge position. The alkyne is coordinated to the concave side such that the C–C bond is parallel to the hinge of the butterfly. It coordinates to all metal atoms in a μ_4-η^2-mode, leading to a distorted *closo* $RuCo_3C_2$ octahedral framework with 7 skeletal electron pairs. For comparison, we explored the pos-

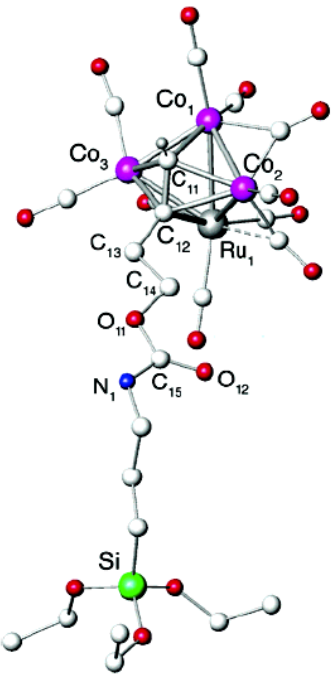

Figure 1. View of the molecular structure of the anionic cluster in NEt$_4$·**2a**. Hydrogen atoms have been omitted for clarity. Thermal ellipsoids are drawn at the 50% probability level. All hydrogen atoms have been placed mathematically except for H(11). Selected bond lengths (Å) and angles (deg): Ru(1)–Co(1) = 2.745(2), Ru(1)–Co(2) = 2.557(2), Ru(1)–Co(3) = 2.5240(19), Ru(1)–C(12) = 2.160(10), Co(1)–Co(2) = 2.464(2), Co(1)–Co(3) = 2.449(2), Co(1)–C(11) = 1.985(10), Co(2)···Co(3) = 3.560, Co(2)–C(11) = 2.091(10), Co(2)–C(12) = 2.048(9), Co(3)–C(11) = 2.073(11), Co(3)–C(12) = 2.170(10), C(11)–C(12) = 1.378; Co(2)–Ru(1)–Co(1) = 55.25(6), Co(3)–Ru(1)–Co(1) = 55.21(5), Co(2)–Co(1)–Ru(1) = 57.81(6), Co(3)–Co(1)–Ru(1) = 58.51(7), Co(1)–Co(3)–Ru(1) = 66.98(6). Dihedral angle between the wings = 117°. The carbonyl ligand C(8)O(8) conforms to the semibridging category of Crabtree–Lavin.[10]

(7) Braunstein, P.; Jiao, F. Y.; Rosé, J.; Granger, P.; Balegroune, F.; Bars, O. Grandjean, D. *J. Chem. Soc., Dalton Trans.* **1992**, 2543–2550.

(8) Fox, J. R.; Gladfelter, W. L.; Geoffroy, G. L.; Tavanaiepour, I.; Abdel-Mequid, S.; Day, V. W. *Inorg. Chem.* **1981**, *20*, 3230–3237.

(9) Choualeb, A.; Rosé, J.; Braunstein, P.; Welter, R., manuscript in preparation.

Scheme 2

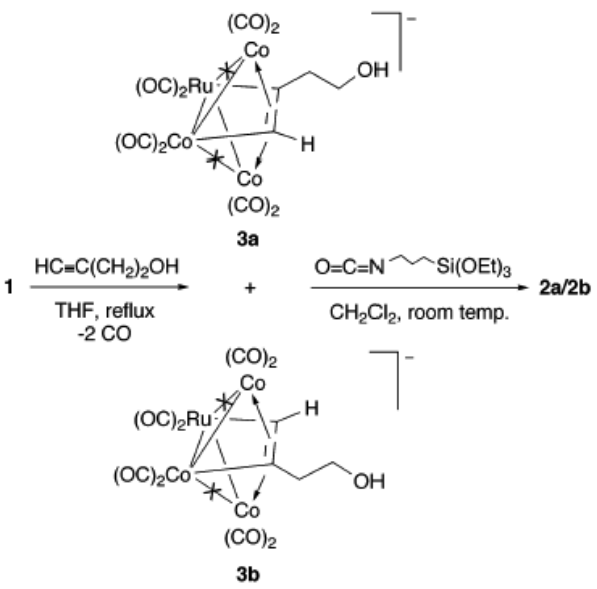

Scheme 3. Alternative Procedures for the Synthesis of 4

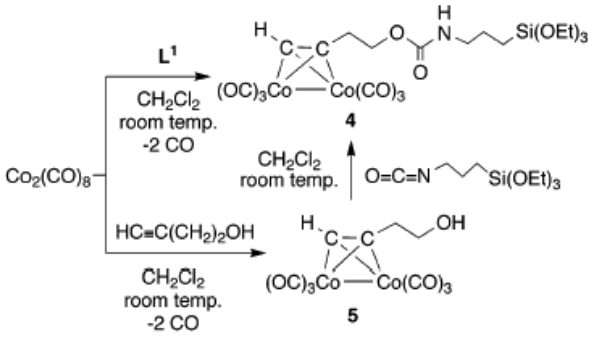

sibility of obtaining **2** following strategy *B* in Scheme 1 and thus first reacted **1** with 3-butyn-1-ol (Scheme 2). This afforded the new cluster $[RuCo_3(CO)_{10}(\mu_4\text{-}\eta^2\text{-}HC_2(CH_2)_2OH]^-$ (**3**), and again two ^{1}H NMR CH resonances were observed, at δ 8.74 and 8.25 in a 5:1 ratio, for isomers **3a**/**3b**.

These clusters were then reacted with 3-(triethoxysilyl)propylisocyanate (route B_2) to afford the corresponding isomeric clusters **2a** and **2b** in a 5:1 ratio (Scheme 2). Interestingly, the reaction proceeded without the need for additional triethylamine, in contrast to the synthesis of $\mathbf{L^1}$. Although addition of NEt_3 may increase the rate of condensation, it also leads to some decomposition of the precursor cluster. Owing to the ionic nature of these clusters, it is difficult to monitor the progress of the reaction by TLC. Furthermore, clusters **2** and **3** are both violet. IR spectroscopy indicates the formation of the product, which has a characteristic ν(C=O) absorption at 1720 cm^{-1}, but does not indicate if the reaction has reached completion. The reaction mixture was therefore stirred for 2 days at room temperature.

For comparison and in order to better characterize coordinated $\mathbf{L^1}$, the latter was reacted with $[Co_2(CO)_8]$, and complex **4** was obtained in high yield (Scheme 3). The latter was also obtained, in comparable yield, when strategy *B* was followed. First, $[Co_2(CO)_8]$ was reacted with 3-butyn-1-ol to give **5**, which was then reacted with 3-(triethoxysilyl)propylisocyanate to afford **4** (Scheme 3). Interestingly, **4** was obtained even in the absence of triethylamine, but the reaction is more rapid if the latter is used.

We then examined the behavior of alkynes carrying an amine instead of an alcohol function. The new alkynes $\mathbf{L^2}$ and $\mathbf{L^3}$ were prepared in quantitative yield by condensation of propargylamine with a functional isocyanate[11] (route A_1, eqs 3, 4) and reacted with **1**

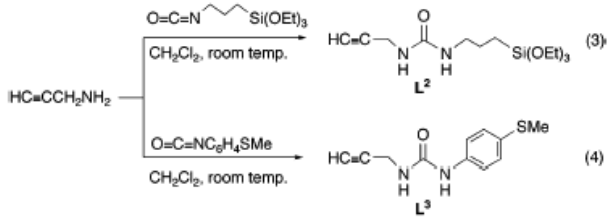

(route A_2). This afforded clusters **6a**/**6b** in a 5:1 ratio and **7a**/**7b** in 2:1 ratio, respectively (eqs 5, 6).

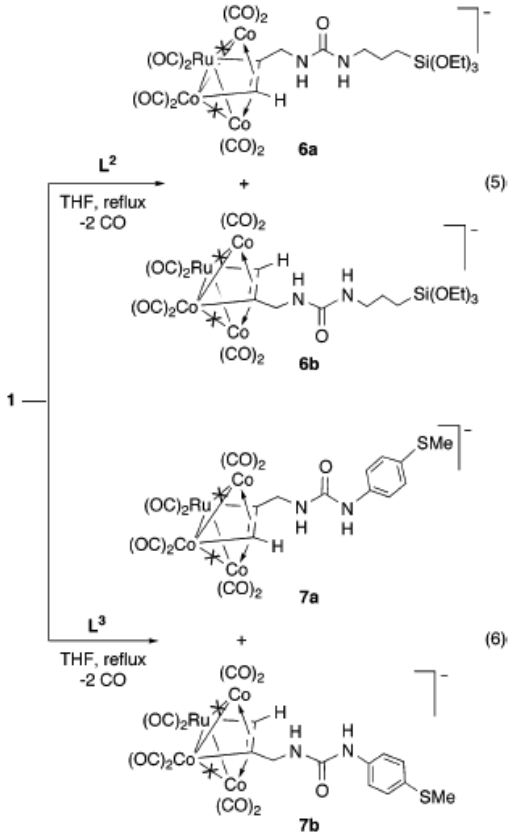

For comparison, we reacted **1** with propargylamine (Scheme 4). This afforded two isomeric clusters, **8a** and **8b**, in 88% yield (route B_1). These clusters were characterized by IR and ^{1}H NMR spectroscopy. The ^{1}H NMR spectrum of the isomeric mixture **8a**/**8b** contains two singlets at δ 8.72 and 8.41 in a 2:1 ratio, respectively, for the alkyne CH proton. These clusters were too unstable to be stored for a prolonged period of time and

(10) Crabtree, R. H.; Lavin, M. *Inorg. Chem.* **1986**, *25*, 805−812.
(11) Lindner, E.; Salesch, T.; Brugger, S.; Hoehn, F.; Wegner, P.; Mayer, H. A. *J. Organomet. Chem.* **2002**, *641*, 165−172.

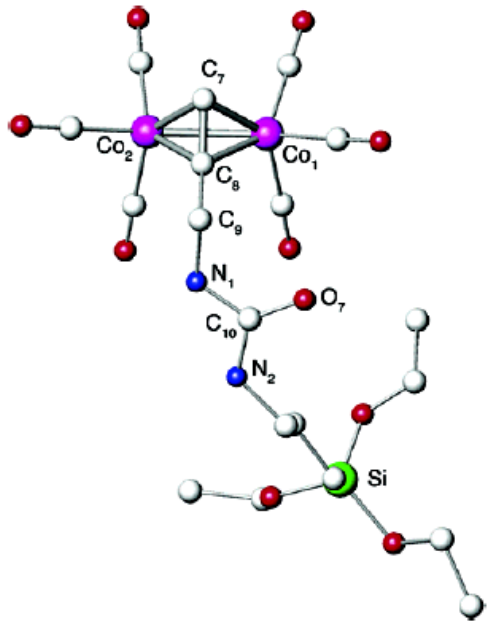

Figure 2. View of the molecular structure of **9** (hydrogen atoms omitted for clarity). Selected bond lengths (Å) and angles (deg): Co(1)–Co(2) = 2.474(1), Co(1)–C(7) = 1.956(6), Co(1)–C(8) = 1.970(6), Co(2)–C(7) = 1.949(6), Co(2)–C(8) = 1.963(6), C(7)–C(8) = 1.323(8); C(7)–Co(1)–C(8) = 39.4(2), C(7)–Co(2)–C(8) = 39.5(2), Co(1)–C(7)–Co(2) = 78.6(2), Co(1)–C(8)–Co(2) = 78.0(2).

Scheme 4

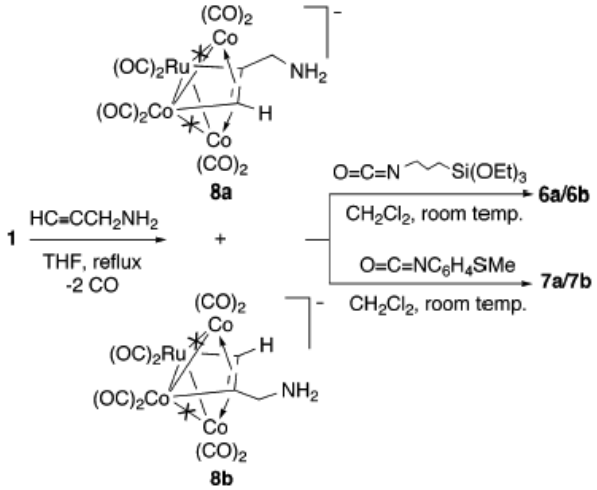

were reacted immediately with 3-(triethoxysilyl)propylisocyanate (route B_2). This afforded the corresponding isomeric clusters **6a** and **6b** in a 1:2 ratio (Scheme 4). Similarly, their reaction with 4-(methylthio)phenylisocyanate yielded **7a** and **7b**, in a 2:1 ratio. Method A gave a better yield of functional cluster compared to B owing to the limited stability of the intermediate clusters **8**.

Since single crystals of the functionalized cluster **6** or **7** could not be obtained, we reacted $\mathbf{L^2}$ and $\mathbf{L^3}$ with $[Co_2(CO)_8]$ in order to better characterize the new, coordinated alkynes and obtained **9** and **10**, respectively (eqs 7, 8). Interestingly, these two complexes could not be obtained according to method B since propargylamine reacts with $[Co_2(CO)_8]$ to give $[\{Co_2(CO)_6(\mu_2\text{-}\eta^2\text{-}$

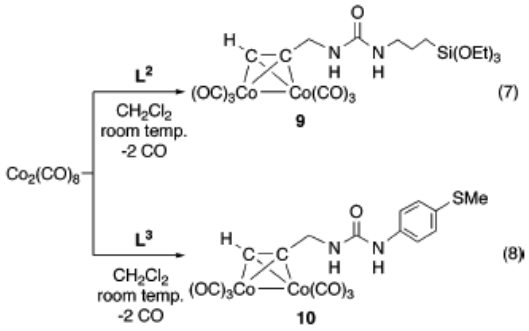

$HC{\equiv}CCH_2NH\}_2CO]$.[12] Complex **9** was characterized by X-ray diffraction (Figure 2) and shows the usual Co_2C_2 tetrahedral core.[13] The $-Si(OEt)_3$ group appears sterically unhindered, which is promising for further condensation reactions using the dicobalt or the cluster complexes, and such studies are in progress.

In conclusion, we have examined and compared two complementary approaches to covalently link dinuclear complexes and metal clusters to functional alkynes terminated with an alkoxysilyl or a thioether function. The strategies depicted in Scheme 1 should be rather general and since they are not necessarily interchangeable, they should be useful in providing different potential access to a given class of functional clusters. Their use as precursors in materials science is the subject of ongoing work.

Experimental Section

All reactions and manipulations were carried out under an inert atmosphere of purified nitrogen using standard Schlenk tube techniques. Solvents were dried and distilled under nitrogen before use: hexane, pentane, and tetrahydrofuran over sodium-benzophenone, dichloromethane over phosphorus pentoxide. Nitrogen (Air Liquide, R-grade) was passed through BASF R3-11 catalyst and molecular sieves columns to remove residual oxygen and water. Elemental C, H, N, and S analyses were performed by the Service de Microanalyses du CNRS (ULP Strasbourg). Infrared spectra were recorded on a Perkin-Elmer 1600 series FTIR spectrometer. The ^1H NMR spectra were recorded at 300.13 MHz, $^{13}C\{^1H\}$ NMR spectra at 75.48 or 100.62 MHz, and $^{29}Si\{^1H\}$ at 79.48 MHz on a Bruker AC300, AVANCE 300 or AVANCE 400 instrument. The ratios between the isomeric clusters **a** and **b** determined from the alkyne CH resonance may not always represent the situation at thermodynamic equilibrium.

Synthesis of $HC{\equiv}C(CH_2)_2OC(O)NH(CH_2)_3Si(OEt)_3$ (L^1). To a solution of 3-butyn-1-ol (19.75 mmol, 1.5 mL) and dry triethylamine (17.85 mmol, 2.35 mL) in 10 mL of CH_2Cl_2, cooled in an ice bath, was added dropwise a solution of 3-(triethoxysilyl)propylisocyanate (4.45 mL, 17.85 mmol) in 5 mL of CH_2Cl_2. After stirring overnight at room temperature, the resulting solution was filtered, and the excess of 3-butyn-1-ol and the solvent were evaporated under reduced pressure

(12) Hong, F.-E.; Tsai, Y.-T.; Chang, Y.-C.; Ko, B.-T. *Inorg. Chem.* **2001**, *40*, 5487–5488.

(13) (a) Schore, N. E. In *Comprehensive Organometallic Chemistry II*; Abel, E. W., Stone, F. G. A., Wilkinson, G., Eds.; Pergamon: Oxford, 1995; Vol. 7. (b) Schore, N. E. *Chem. Rev.* **1988**, *88*, 1081–1119. (c) Pauson, P. L. In *Organometallics in Organic Synthesis, Aspects of a Modern Interdisciplinary Field*; de Meijere, A., tom Dieck, H., Eds.; Springer: Berlin, 1988. (d) Housecroft, C. E.; Johnson, B. F. G.; Khan, M. S.; Lewis, J.; Raithby, P. R.; Robson, M. E.; Wilkinson, D. A., *J. Chem. Soc., Dalton Trans.* **1992**, 3171–3178. (e) Wong, W.-Y.; Lam, H.-Y.; Lee, S.-M. *J. Organomet. Chem.* **2000**, *595*, 70–80. (f) Went, M. J. *Adv. Organomet. Chem.* **1997**, *41*, 69–125.

to afford **L¹** as a colorless liquid (5.27 g, 16.60 mmol, 93%). IR (CH_2Cl_2, cm^{-1}): 3304 (s, $\nu_{\equiv CH}$), 2274 (vs, $\nu_{C\equiv C}$), 1720 (vs, $\nu_{C=O}$), and 1517 (vs, δ_{NH}). ^1H NMR ($CDCl_3$): δ 0.53 (m, 2H, $SiCH_2$), 1.12 (t, ^3J(HH) = 7 Hz, 9H, CH_3), 1.52 (m, 2H, $CH_2CH_2CH_2$), 1.92 (t, ^4J(HH) = 2.74 Hz, 1H, HC≡), 2.41 (dt, ^3J(HH) = 7 Hz, ^4J(HH) = 2.74 Hz, 2H, ≡CCH_2), 3.06 (m, 2H, NCH_2), 3.72 (q, ^3J(HH) = 7 Hz, 6H, OCH_2CH_3), 4.05 (t, ^3J(HH) = 7 Hz, 2H, OCH_2), 5.27 (br, NH). $^{13}C\{^1H\}$ NMR (100.62 MHz, $CDCl_3$): δ 7.46 (s, $SiCH_2$), 18.16 (s, OCH_2CH_3), 19.32 (s, $CH_2CH_2CH_2$), 23.13 (s, ≡CCH_2), 42.84 (s, NCH_2), 58.34 (s, OCH_2CH_3), 62.54 (s, OCH_2), 69.58 (s, HC≡C), 80.38 (s, HC≡*C*), 156.07 (s, C=O). $^{29}Si\{^1H\}$ NMR ($CDCl_3$): δ −45.93.

Synthesis of HC≡$CCH_2NHC(O)NH(CH_2)_3Si(OEt)_3$ (L²). A solution of 3-(triethoxysilyl)propylisocyanate (1.64 g, 1.66 mL, 6.65 mmol) in 5 mL of CH_2Cl_2 was added dropwise to a solution of propargylamine (7.32 mmol, 0.50 mL) in 15 mL of CH_2Cl_2, cooled in an ice bath. After stirring overnight at room temperature, the solvent was evaporated under vacuum and the product was quantitatively obtained as a pale yellow solid (2.00 g, 6.61 mmol). IR (KBr, cm^{-1}): 3332 (s, $\nu_{\equiv CH}$), 1624 (vs, $\nu_{C=O}$), and 1586 (vs, δ_{NH}). ^1H NMR ($CDCl_3$): δ 0.58 (m, 2H, $SiCH_2$), 1.11 (t, 9H, ^3J(HH) = 7 Hz, CH_3), 1.56 (quint, 2H, ^3J(HH) = 7 Hz, $CH_2CH_2CH_2$), 2.17 (t, ^4J(HH) = 2.5 Hz, 1H, ≡CH), 3.11 (q, ^3J(HH) = 7 Hz, 2H, NCH_2CH_2), 3.75 (q, ^3J(HH) = 7 Hz, 6H, OCH_2), 3.90 (dd, ^3J(HH) = 5.8 Hz, ^4J(HH) = 2.5 Hz, 2H, ≡CCH_2N), 5.48 (br t, ^3J(HH) = 5.8 Hz, 1H, CH_2-CH_2NH), 5.64 (br t, ^3J(HH) = 5.8 Hz, 1H, ≡CCH_2NH). $^{13}C\{^1H\}$ NMR (100.62 MHz, $CDCl_3$): δ 7.62 (s, $SiCH_2$), 18.10 (s, CH_3), 23.26 (s, $CH_2CH_2CH_2$), 29.92 (≡CCH_2N), 42.90 (s, NCH_2-CH_2), 58.61 (s, OCH_2), 70.79 (s, HC≡), 81.13 (s, HC≡*C*−), 158.3 (C=O). $^{29}Si\{^1H\}$ NMR (79.48 MHz, $CDCl_3$): δ −45.5. Anal. Calcd for $C_{13}H_{26}N_2O_4Si$: C, 51.63; H, 8.66; N, 9.26. Found: C, 50.95; H, 8.66; N, 9.24.

Synthesis of HC≡$CCH_2NHC(O)NHC_6H_4SMe$ (L³). A solution of 4-(methylthio)phenylisocyanate (0.93 mL, 6.65 mmol) in 15 mL of CH_2Cl_2 was added dropwise to a solution of propargylamine (0.50 mL, 7.32 mmol) in 15 mL of CH_2Cl_2 placed at 0 °C. The solution was stirred at room temperature overnight, and the product was obtained quantitatively as a white powder that is scarcely soluble in CH_2Cl_2 (1.46 g, 6.65 mmol). IR (KBr, cm^{-1}): 3320 (s, $\nu_{\equiv CH}$), 1629 (vs, $\nu_{C=O}$) and 1586 (vs, δ_{NH}). ^1H NMR (acetone-d_6): δ 2.40 (s, 3H, CH_3), 2.61 (t, ^4J(HH) = 2.55 Hz, 1H, ≡CH), 3.98 (dd, ^4J(HH) = 2.55 Hz, ^3J(HH) = 7 Hz, 2H, CH_2N), 6.04 (m, 1H, CH_2NH), 7.17 and 7.44 (AA′BB′ spin system, 4H, C_6H_4), 8.05 (br s, 1H, C_6H_4NH). $^{13}C\{^1H\}$ NMR (75.48 MHz, acetone-d_6): δ 16.06 (s, CH_3), 29.16 (s, ≡CCH_2N), 70.87 (s, HC≡), 81.0 (s, HC≡*C*−), 118.92 and 128.24 (2s, CH of C_6H_4), 131.0 and 138.0 (2s, C_{quater} of C_6H_4), 158.0 (s, C=O). Anal. Calcd for $C_{11}H_{12}N_2OS$: C, 59.98; H, 5.49; N, 12.72; S, 14.55. Found: C, 59.61; H, 5.41; N, 12.83; S, 14.53.

$[NEt_4][RuCo_3(CO)_{10}\{\mu_4\text{-}\eta^2\text{-}HC_2(CH_2)_2OC(O)NH(CH_2)_3Si(OEt)_3\}]$ (NEt_4·2). Procedure A: Reaction of $[NEt_4][RuCo_3(CO)_{12}]$ with $HC\equiv C(CH_2)_2OC(O)NH(CH_2)_3Si(OEt)_3$. A solution of NEt_4·**1** (0.174 g, 0.235 mmol) and **L¹** (0.092 g, 0.282 mmol) was refluxed in 40 mL of THF for 6 h. The solution was filtered and the solvent was removed under vacuum. Violet crystals of NEt_4·**2** (0.158 g, 0.157 mmol, 67%) were obtained by recrystallization of the product from CH_2Cl_2/pentane. IR (CH_2Cl_2, cm^{-1}): 2048 (mw), 2002 (vs), 1970 (sh), 1814 (m) $\nu_{C=O}$, 1720 (m, $\nu_{C=O}$). ^1H NMR ($CDCl_3$): δ 0.60 (m, 2H, $SiCH_2$), 1.21 (m, 12H, NCH_2CH_3), 1.33 (m, 9H, OCH_2CH_3), 1.54 (m, 2H, $CH_2CH_2CH_2$), 2.74 (m, 2H, HC_2CH_2), 3.20 (m, 10H, NCH_2CH_3 and $HNCH_2$), 3.90 (m, 8H, OCH_2CH_3 and CH_2CH_2O), 4.81 (br, NH), 8.27 (br s, 0.40H, HC_2 of one isomer), 8.74 (br s, 0.60H, HC_2 of the other isomer). Anal. Calcd for $C_{32}H_{47}Co_3N_2O_{15}RuSi$: C, 38.22; H, 4.71; N, 2.79. Found: C, 37.59; H, 4.55; N, 2.73.

Procedure B: Reaction of $[NEt_4][RuCo_3(CO)_{10}(\mu_4\text{-}\eta^2\text{-}HC_2(CH_2)_2OH)]$ (NEt_4·3) (see below) with $OCN(CH_2)_3Si(OEt)_3$. To a solution of NEt_4·**3** (0.100 g, 0.132 mmol) in 15 mL CH_2Cl_2 was added dropwise 3-(triethoxysilyl)propylisocyanate (0.148 mmol, 0.037 mL). The mixture was stirred at room temperature for 2 days. The solution was filtered through Celite and concentrated. Violet crystals of NEt_4·**2** (0.065 g, 0.065 mmol, 48%) were obtained after recrystallizing twice the product from CH_2Cl_2/pentane. When this procedure was followed, the ratio between isomers **2a** and **2b** was 5:1.

Synthesis of $[NEt_4][RuCo_3(CO)_{10}(\mu_4\text{-}\eta^2\text{-}HC_2(CH_2)_2OH)]$ (NEt_4·3). Using a procedure similar to that described for NEt_4·**2**, NEt_4·**1** (0.223 g, 0.301 mmol) and 3-butyn-1-ol (0.105 g, 1.50 mmol, 0.114 mL) were refluxed in 50 mL of THF for 5 h. After workup, NEt_4·**3** (0.200 g, 0.264 mmol, 87%) was obtained as dark violet crystals by recrystallization from CH_2Cl_2/hexane. IR (CH_2Cl_2, ν(CO), cm^{-1}): 2049 (m), 2003 (vs), 1970 (sh), 1819 (m). ^1H NMR ($CDCl_3$): δ 1.37 (m, 12H, CH_3), 1.51 (br, OH), 2.72 (m, 2H, HC_2CH_2), 3.26 (m, 8H, NCH_2), 3.44 (m, 2H, OCH_2), 8.25 (br s, 0.16H, HC_2 of one isomer), 8.74 (br s, 0.84H, HC_2 of the other isomer). Anal. Calcd for $C_{22}H_{26}Co_3NO_{11}Ru$·$1/2H_2O$: C, 33.75; H, 3.40; N, 1.75, Found: C, 33.57; H, 3.41; N, 1.75.

Synthesis of $[Co_2(CO)_6\{\mu_2\text{-}\eta^2\text{-}HC_2(CH_2)_2OC(O)NH(CH_2)_3Si(OEt)_3\}]$ (4). Procedure A: Reaction of $[Co_2(CO)_8]$ with L¹. A solution of $[Co_2(CO)_8]$ (0.387 g, 1.140 mmol) in 30 mL of CH_2Cl_2 and **L¹** (0.522 g, 1.60 mmol) was stirred at room temperature for 3 h. Completion of the reaction was revealed from TLC by the disappearance of $[Co_2(CO)_8]$. The solvent was then removed under vacuum. Extraction with hexane afforded red viscous compound **4** (0.626 g, 1.04 mmol, 91%). IR (hexane, cm^{-1}): 2098 (vs), 2063 (vs), 2029 (vs), 1979 (w), ν(C≡O) and 1740 (vs), ν(C=O). ^1H NMR (300.13 MHz, $CDCl_3$): δ 0.61 (m, 2H, $SiCH_2$), 1.21 (t, ^3J(HH) = 7.5 Hz, 9H, CH_3), 1.63 (m, 2H, $CH_2CH_2CH_2$), 3.16 (m, 4H, $HNCH_2CH_2$ and HC_2CH_2,), 3.81 (q, ^3J(HH) = 7.5 Hz, 6H, OCH_2CH_3), 4.12 (t, ^3J(HH) = 6.15 Hz, 2H, OCH_2CH_2), 4.89 (br, NH), 6.02 (s, 1H, H−C−Co). In benzene-d_6, the ^1H NMR signals for $HNCH_2CH_2$ and HC_2CH_2 were separated: 2.74 (HC_2CH_2), 3.16 ($HNCH_2CH_2$).

Procedure B: Reaction of $[Co_2(CO)_6\{\mu_2\text{-}\eta^2\text{-}HC_2(CH_2)_2OH\}]$ (5) (see below) with $OCN(CH_2)_3Si(OEt)_3$. Synthesis of $[Co_2(CO)_6\{\mu_2\text{-}\eta^2\text{-}HC_2(CH_2)_2OH\}]$ (5). A solution of $[Co_2(CO)_8]$ (0.325 g, 0.954 mmol) in 25 mL of CH_2Cl_2 and 3-butyn-1-ol (0.079 mL, 1.05 mmol) was stirred at room temperature for 2 h. Completion of the reaction was revealed from TLC by the disappearance of $[Co_2(CO)_8]$. The solvent was then removed under vacuum. Extraction with hexane afforded red viscous compound **5** (0.304 g, 0.854 mmol, 89%). IR (hexane, ν(CO), cm^{-1}): 2098 (vs), 2053 (vs), 2029 (vs), 1980 (w). ^1H NMR ($CDCl_3$): δ 1.58 (br, OH), 3.11 (t, ^3J(HH) = 6.5 Hz, 2H, HC_2CH_2), 3.90 (m, 2H, OCH_2), 6.02 (s, 1H, H−C−Co).

To a solution of **5** (0.092 g, 0.258 mmol) was then added dropwise 3-(triethoxysilyl)propylisocyanate (0.071 mL, 0.284 mmol). The solution was stirred at room temperature for 11 h. Completion of the reaction was revealed from TLC by the disappearance of **5** (eluent CH_2Cl_2). The solvent was removed under vacuum. Extraction with hexane afforded red viscous compound **4** (0.144 g, 0.240 mmol, 93%).

Synthesis of $[NEt_4][RuCo_3(CO)_{10}\{\mu_4\text{-}\eta^2\text{-}HC_2CH_2NHC(O)NH(CH_2)_3Si(OEt)_3\}]$ (NEt_4·6). Procedure A: Reaction of $[NEt_4][RuCo_3(CO)_{12}]$ with HC≡$CCH_2NHC(O)NH(CH_2)_3Si(OEt)_3$. A solution of NEt_4·**1** (0.253 g, 0.341 mmol) and **L²** (0.114 g, 0.377 mmol) was refluxed in 50 mL of THF for 6 h. The solution was filtered and the solvent was removed under reduced pressure. The product was recrystallized twice from CH_2Cl_2/pentane to afford a violet powder of NEt_4·**6** (0.277 g, 0.279 mmol, 82%). IR (CH_2Cl_2, ν(CO), cm^{-1}): 2050 (m), 2005 (vs), 1970 (s), 1820 (m), 1671 (m, C≡O). ^1H NMR ($CDCl_3$): δ 0.63 (m, 2H, $SiCH_2$), 1.22 (m, 21H, OCH_2CH_3 and NCH_2CH_3), 1.60 (m, 2H, $CH_2CH_2CH_2$), 3.13 (m, 2H, $HNCH_2CH_2$), 3.8 (m, 16H, OCH_2CH_3, NCH_2CH_3 and $HNCH_2C_2H$), 4.41 (m, 1H, NH), 4.64 (m, 1H, NH), 8.24 (br s, 0.16H, HC_2− of one isomer), 8.67 (br s, 0.84H, HC_2− of the second isomer). Anal. Calcd for $C_{31}H_{46}Co_3N_3O_{14}RuSi-2CH_2Cl_2$: C, 34.15; H, 4.34; N, 3.62. Found: C, 33.85; H, 4.43; N, 3.99.

Procedure B: Reaction of $[NEt_4][RuCo_3(CO)_{10}(\mu_4\text{-}\eta^2\text{-}HC_2CH_2NH_2)]$ with $OCN(CH_2)_3Si(OEt)_3$. To a solution of NEt_4·**8**, prepared by reaction of NEt_4·**1** (0.140 g, 0.188 mmol) with propargylamine (0.052 mL, 0.756 mmol) in 35 mL of CH_2Cl_2 at 0 °C, was added dropwise 0.053 mL (0.215 mmol) of 3-(triethoxysilyl)propylisocyanate. The solution was stirred at room temperature for 24 h, filtered, and concentrated, and the product was recrystallized from CH_2Cl_2/hexane to give NEt_4·**6** (0.069 g, 0.070 mmol, 37% based on NEt_4·**1**). When this procedure was followed, the ratio between isomers **6a** and **6b** was 1:2.

Synthesis of $[NEt_4][RuCo_3(CO)_{10}\{\mu_4\text{-}\eta^2\text{-}HC_2CH_2NHC(O)NHC_6H_4SMe\}]$ (NEt_4·7). Procedure A: Reaction of $[NEt_4][RuCo_3(CO)_{12}]$ with $HC{\equiv}CCH_2NHC(O)NHC_6H_4SMe$. A solution of NEt_4·**1** (0.146 g, 0.197 mmol) and $\mathbf{L^3}$ (0.173 g, 0.787 mmol) was refluxed in 35 mL of THF for 5 h. After filtration through Celite, evaporation to dryness, extraction of the product with CH_2Cl_2, and recrystallization from CH_2Cl_2/hexane afforded NEt_4·**7** (0.168 g, 0.185 mmol, 94%) as a violet powder. IR (CH_2Cl_2, ν(CO), cm^{-1}): 2051 (m), 2006 (vs), 1972 (s), 1820 (m), 1702 (m, $\nu_{C=O}$). ^1H NMR (acetone-d_6): δ 1.32 (m, 12H, CH_2CH_3), 2.39 (s, 3H, SCH_3), 3.34 (m, 8H, CH_2CH_3), 3.91 (s, 2H, CH_2NH), 5.45 (m, 1H, CH_2NH), 5.60 (m, 1H, C_6H_4NH), 7.16 and 7.42 (AA′BB′ spin system, 4H, C_6H_4), 8.08 (br s, 0.33H, HC_2– of one isomer), 8.75 (br s, 0.66H, HC_2– of the second isomer). Anal. Calcd for $C_{33}H_{32}Co_3N_3O_{11}RuS$: C, 41.44; H, 3.37; N, 4.39; S, 3.35. Found: C, 41.74; H, 3.84; N, 4.76; S, 3.84.

Procedure B: Reaction of $[NEt_4][RuCo_3(CO)_{10}(\mu_4\text{-}\eta^2\text{-}HC_2CH_2NH_2)]$ with $OCNC_6H_4SMe$. To a CH_2Cl_2 solution of NEt_4·**8** prepared by reaction of NEt_4·**1** (0.111 g, 0.150 mmol) with propargylamine (0.041 mL, 0.6 mmol) was added dropwise at 0 °C 0.15 mmol (0.021 mL) of $OCNC_6H_4SMe$. After stirring for 24 h at room temperature, the solution was filtered through Celite, concentrated, and recrystallized from CH_2Cl_2/hexane to give violet crystals of NEt_4·**7** (0.057 g, 0.063 mmol, 42% based on NEt_4·**1**).

Synthesis of $[NEt_4][RuCo_3(CO)_{10}(\mu_4\text{-}\eta^2\text{-}HC_2CH_2NH_2)]$ (NEt_4·8). Propargylamine (1.286 mmol, 0.088 mL) was added to a solution of $[NEt_4][RuCo_3(CO)_{12}]$ (0.238 g, 0.321 mmol) in 50 mL of THF. The mixture was heated under reflux for 5 h. After cooling, the solution was filtered and the solvent and the propargylamine in excess were evaporated under vacuum. Extraction with CH_2Cl_2 afforded NEt_4·**8** (0.210 g, 0.282 mmol, 88%). This cluster decomposes even under N_2 and should be used immediately. IR (CH_2Cl_2, ν(CO), cm^{-1}): 2048 (m), 2002 (vs), 1969 (s), 1889 (m, $Co(CO)_4^-$ resulting from decomposition), 1819 (m). ^1H NMR (CD_2Cl_2): δ 1.32 (m, 12H, CH_3), 1.67 (m, 2H, NH_2), 2.33 (m, 2H, CH_2NH_2), 3.20 (m, 8H, NCH_2CH_3), 8.41 (br s, 0.33H, HC_2) of one isomer), 8.72 (br s, 0.66H, HC_2 of the second isomer).

Synthesis of $[Co_2(CO)_6\{\mu_2\text{-}\eta^2\text{-}HC_2CH_2NHC(O)NH(CH_2)_3Si(OEt)_3\}]$ (9). A mixture of $[Co_2(CO)_8]$ (0.350 g, 1.028 mmol) and $\mathbf{L^2}$ (0.342 g, 1.131 mmol) in 35 mL of CH_2Cl_2 was allowed to react at room temperature for 2 h. A color change from brown to red was observed, and monitoring by TLC showed the disappearance of the starting complex. After filtration, the solvent was removed and the product was extracted with a mixture of hexane/CH_2Cl_2 (90:10) and placed at –20 °C to give red prismatic crystals (0.54 g, 0.918 mmol, 90%). IR (CH_2Cl_2, ν(CO), cm^{-1}): 2094 (vs), 2052 (vs), 2026 (vs), 1679 (m, $\nu_{C=O}$). ^1H NMR ($CDCl_3$): δ 0.62 (m, $SiCH_2$), 1.21 (t, ^3J(HH) = 7 Hz, 9H, CH_3), 1.61 (quint, ^3J(HH) = 7.4 Hz, 2H, $CH_2CH_2CH_2$), 3.16 (q, ^3J(HH) = 6.82 Hz, 2H, NCH_2CH_2), 3.82 (q, ^3J(HH) = 7 Hz, 6H, OCH_2), 4.54 (d, ^3J(HH) = 6 Hz, 2H, $\equiv CCH_2N$), 4.63 (br t, ^3J(HH) ≈ 6 Hz, 1H, NH), 4.76 (br t, ^3J(HH) ≈ 6 Hz, 1H, NH), 6.06 (s, 1H, HC–Co). Anal. Calcd for $C_{19}H_{26}Co_2N_2O_{10}Si$: C, 38.79; H,4.45; N, 4.76, Found: C, 38.49; H, 4.30; N,4.61.

Synthesis of $[Co_2(CO)_6\{\mu_2\text{-}\eta^2\text{-}HC_2CH_2NHC(O)NHC_6H_4SMe)\}]$ (10). The ligand $\mathbf{L^3}$ (0.152 g, 0.688 mmol) was reacted with $[Co_2(CO)_8]$ (0.190 g, 0.555 mmol) in 30 mL of CH_2Cl_2 at room temperature. After being stirred for 2 h, the solution was filtered through Celite and the solvent was removed under reduced pressure. The product was extracted with CH_2Cl_2/hexane (80:20), and the solution was concentrated and placed at –20 °C for 1 week to give orange microcrystals (0.177 g, 0.41 mmol, 65%). IR (CH_2Cl_2, ν(CO), cm^{-1}): 2095 (s), 2055 (vs), 2026 (vs), 1676 (m, $\nu_{C=O}$). ^1H NMR ($CDCl_3$): δ 2.45 (s, 3H, CH_3), 4.59 (d, ^3J(HH) = 6.26 Hz, 2H, CH_2N), 5.08 (br t, ^3J(HH) = 6.26 Hz, 1H, CH_2NH), 6.07 (s, 1H, HC–Co), 6.38 (br s, 1H, C_6H_4NH), 7.23 (m, 4H, C_6H_4). Anal. Calcd for $C_{17}H_{12}Co_2N_2O_7S$: C, 40.34; H, 2.39; N, 5.53; S, 6.33. Found: C, 40.41; H, 2.39; N, 5.47; S, 6.05.

X-ray Structural Analysis of $[NEt_4][RuCo_3(CO)_{10}(\mu_4\text{-}\eta^2\text{-}HC_2(CH_2)_2OC(O)NH(CH_2)_3Si(OEt)_3]$ (NEt_4·2) and $[Co_2(CO)_6\{\mu_2\text{-}\eta^2\text{-}HC_2CH_2NHC(O)NH(CH_2)_3Si(OEt)_3\}]$ (9). Single crystals were mounted on a Nonius Kappa-CCD area detector diffractometer (Mo Kα, λ = 0.71073 Å). The complete conditions of data collection (Denzo software) and structure refinements are given below. The cell parameters were determined from reflections taken from one set of 10 frames (1.0° steps in phi angle), each at 20 s exposure. The structures were solved using direct methods (SIR97) and refined against F^2 using the SHELXL97 software.[14,15] The absorption was corrected empirically [with Sortav]. All non-hydrogen atoms were refined anisotropically. Hydrogen atoms were generated according to stereochemistry and refined using a riding model in SHELXL97.

Crystal data and structure refinement details for NEt_4·**2**: $C_{32}H_{47}Co_3N_2O_{15}RuSi$, M = 1005.67, violet crystals, triclinic, space group $P\bar{1}$, a = 7.501(2) Å, b = 13.762(2) Å, c = 21.544(2) Å, α = 97.07(5)°, β = 93.91(5)°, γ = 97.82(5)°, V = 2178.4(7) Å^3, Z = 2, ρ_{calcd} = 1.533 g cm^{-3}, μ(Mo Kα) = 1.552 mm^{-1}. Intensity measurements were performed by ω–2θ scans in the range 5.18° < 2θ < 60.24° at 173 K; 81 459 independent reflections with 5324 having $I > 2\sigma(I)$, F^2 refinement, 446 parameters, R1 = 0.1156, wR2 = 0.1530 and GOF = 0.965. CCDC 204010.

Crystal data and structure refinement details for **9**: $C_{19}H_{26}Co_2N_2O_{10}Si$, M = 588.37 g mol^{-1}, red crystal, monoclinic, space groupe $P2_1/a$, a = 9.099(3) Å, b = 19.989(5) Å, c = 14.404(4) Å, β = 93.20(2)°, Z = 4, ρ_{calcd} = 1.494 g cm^{-3}, μ(Mo Kα) = 1.365 mm^{-1}; a total of 22 545 reflections. Intensity measurements were performed by ω–2θ scans in the range 2.46° < θ < 30.05° at 173 K; 7620 independent reflections with 2753 having $I > 2\sigma(I)$, F^2 refinement, 272 parameters, R1 = 0.010; wR2 = 0.020 and GOF = 1.145. Owing to the large thermal parameters of the atoms in the group –Si(OEt)$_3$ (thermal motion and/or disorder), the C–C and C–O distances have been fixed at values of 1.5 and 1.35 Å, respectively. CCDC 197184.

Additional material has also been deposited with the Cambridge Crystallographic Data Centre as Supplementary Publication Nos. CCDC-197184 & 204010. Copies of the data can be obtained free of charge on application to CCDC, 12 Union Road, Cambridge CB2 1EZ, UK (fax: (+44)1223-336-033; e-mail: deposit@ccdc.

Acknowledgment. We are grateful to the CNRS, the Université Louis Pasteur Strasbourg, and the Ministère de la Recherche (Paris) for financial support. This project was also supported by the Fonds International de Coopération Universitaire–FICU (AUPELF-UREF, Agence Universitaire de la Francophonie).

Supporting Information Available: Tables of atomic coordinates (S-1, S-5), thermal parameters (S-2, S-6), bond distances (S-3, S-7), and angles (S-4, S-8) for NEt_4·**2** and **9**, respectively. This material is available free of charge via the Internet at http://pubs.acs.org.

OM020965M

(14) *Kappa CCD Operation Manual*; Nonius B.V.: Delft, The Netherlands, 1997.

(15) Sheldrick, G. M. *SHELXL97*, Program for the refinement of crystal structures; University of Gottingen: Germany, 1997.

Chapitre 3

Les réactions des clusters tétraédriques $[MCo_3(CO)_{12}]^-$ (M = Ru, Fe) avec les alcynes et les dialcynes

Ce chapitre est présenté sous la forme d'une publication en cours d'impression dans *Inorg. Chem.*

Reactions of the Tetrahedral Clusters $[MCo_3(CO)_{12}]^-$ (M = Ru, Fe) with Mono- and Diynes

Aldjia Choualeb,[a] Pierre Braunstein,[*a] Jacky Rosé[a] and Richard Welter[b]

[a] *Laboratoire de Chimie de Coordination (UMR 7513 CNRS), Université Louis Pasteur, 4 rue Blaise Pascal, F-67070 Strasbourg Cedex, France*

[b] *Laboratoire DECMET (UMR 7513 CNRS), Université Louis Pasteur, 4 rue Blaise Pascal, F-67070 Strasbourg Cedex, France*

Abstract

The tetrahedral cluster $[RuCo_3(CO)_{12}]^-$ reacts with various alkynes, including the new PhC≡CC(O)NHCH$_2$C≡CH (**L^1**), to afford the butterfly clusters $[RuCo_3(CO)_{10}(\mu_4\text{-}\eta^2\text{-}RC_2R')]^-$ (**1,** R = R' = C(O)OMe; **2,** R = H, R' = Ph; **3**, R = H, R' = MeC=CH$_2$; **4**, R = H, R' = CH$_2$OCH$_2$C≡CH; **5**, R = H, R' = CH$_2$N(H)C(O)C≡CPh), in which the ruthenium atom occupies a hinge position and the alkyne is coordinated in a μ_4-η^2 fashion. Reaction of the anions **1**-**3** with $[Cu(NCMe)_4]BF_4$ led to selective loss of the 12e fragment $Co(CO)^-$ to form $[RuCo_2(CO)_9(\mu_3\text{-}\eta^2\text{-}RC_2R')]$ (**6,** R = R' = C(O)OMe; **7,** R = H, R' = Ph; **8**, R = H, R' = MeC=CH$_2$). In order to prepare functionalized $RuCo_3$ or $FeCo_3$ clusters that could be subsequently condensed with a silica matrix via the sol-gel method, we reacted $[MCo_3(CO)_{12}]^-$ (M = Ru, Fe) with the alkyne PhC≡CC(O)NH(CH$_2$)$_3$Si(OMe)$_3$ (**L^2**) and obtained the butterfly clusters $[MCo_3(CO)_{10}(\mu_4\text{-}\eta^2\text{-}PhC_2C(O)NH(CH_2)_3Si(OMe)_3)]^-$ **9** and

10, respectively. Air-stable $[RuCo_3(CO)_{10}(\mu_4\text{-}\eta^2\text{-}Me_3SiC_2C{\equiv}CSiMe_3)]^-$ (**11**) was obtained from 1,4-bis(trimethylsilyl)butadiyne and reacted with $[Cu(NCMe)_4]BF_4$ to give $[RuCo_2(CO)_9(\mu_3\text{-}\eta^2\text{-}HC_2C{\equiv}CSiMe_3)]$ (**12**), owing to partial ligand proto-desilylation, and not the expected $[RuCo_2(CO)_9(\mu_3\text{-}\eta^2\text{-}Me_3SiC_2C{\equiv}CSiMe_3)]$. Reaction of **11** with $[NO]BF_4$ afforded, in addition to **12**, $[RuCo_3(CO)_9(NO)(\mu_4\text{-}\eta^2\text{-}Me_3SiC_2C{\equiv}CSiMe_3)]$ (**13**) owing to selective CO substitution on a wing-tip cobalt atom with NO. The thermal reaction of **11** with $[AuCl(PPh_3)]$ led to replacement of a CO on Ru by the PPh_3 originating from $[AuCl(PPh_3)]$ and afforded $[RuCo_3(CO)_9(PPh_3)(\mu_4\text{-}\eta^2\text{-}Me_3SiC_2C{\equiv}CSiMe_3)]^-$ (**14**), also obtained directly by reaction of **11** with one equivalent of PPh_3. Proto-desilylation of **11** using TBAF/THF-H_2O afforded $[RuCo_3(CO)_{10}(\mu_4\text{-}\eta^2\text{-}Me_3SiC_2C{\equiv}CH)]^-$ (**15**) which, by Sonogashira coupling with 1,4 diiodobenzene, yielded the dicluster complex $[\{[RuCo_3(CO)_{10}(\mu_4\text{-}\eta^2\text{-}Me_3SiC_2C{\equiv}C)]\}_2C_6H_4]^{2-}$ (**16**). The crystal structures of NEt_4•**3a,** NEt_4•**4, 6,** NEt_4•**11,** NEt_4•**14** and $[N(n\text{-}Bu)_4]$•**15a** have been determined by X-ray diffraction. Preliminary results indicate the potential of silica-tethered alkyne mixed-metal clusters, obtained by the sol-gel method, as precursors to bimetallic particles.

Introduction

We are currently interested in the selective incorporation of functional alkynes into metal carbonyl clusters in order to obtain low oxidation state molecular precursors to surface-anchored metal clusters that could lead to nanomaterials of controlled properties.[1,2] A covalent linkage between the metal cluster and the required functionality should enable a better control of the anchoring process and prevent the metal leaching often associated with the presence of dative bonds between the ligand and the metal(s). Although the reactions of simpler alkynes with carbonyl clusters have long been investigated, the factors governing their selectivity are not fully understood.[3] Various isomeric structures can be envisaged for the reaction products and ways to chemically differentiate in the precursor cluster the various metal-metal bonds, which are reactive sites, include the use of bridging ligands, as recently explored with $[Co_4(CO)_{10}(\mu\text{-dppy})]$ (dppy = $Ph_2PCH_2PPh_2$ (dppm), $Ph_2PNHPPh_2$ (dppa) or $(Ph_2P)_2N(CH_2)_3Si(OEt)_3$ (dppaSi)).[4] An extension of these studies to related isoelectronic mixed-metal systems was felt particularly desirable [5] and we report here on the reactions of the tetrahedral clusters $[MCo_3(CO)_{12}]^-$ (M = Ru, Fe) with functional alkynes and compare the results with those obtained with $[Co_4(CO)_{12}]$ and its derivatives. Some of the resulting alkyne clusters were reacted with electrophilic reagents, such as $[Cu(NCMe)_4]BF_4$ or $[NO]BF_4$, to give neutral derivatives with higher solubility.

Furthermore, clusters linked through π-delocalized backbones have come under considerable scrutiny, owing to expectations that new structural, redox and conductivity properties may result. The vast majority of such studies have involved the linking of identical homometallic cores.[6-14] and since only few examples of heterometallic clusters linked by unsaturated bridges have been reported,[15-17] we have used diynes to realize such a connection between $RuCo_3$ clusters.

Results and Discussion

The reaction between $[RuCo_3(CO)_{12}]^-$ and excess MeO(O)CC≡CC(O)OMe (dmad) in refluxing THF afforded the butterfly cluster **1** resulting from insertion of the alkyne into a Co-Co bond. A similar structure has been previously reported with PhC≡CPh.[18]

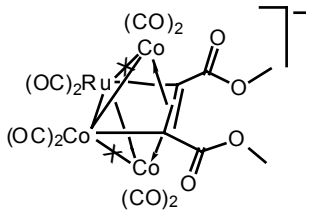

1

When unsymmetrical alkynes of the type HC≡CR were reacted with $[RuCo_3(CO)_{12}]^-$, two isomers **a** and **b** were often obtained (Scheme 1) which differ in the orientation of the alkyne with respect to the Co-Ru vector. Surprisingly, no reaction was observed when R = $-CH_2Cl$, or $-(CH_2)_3C{\equiv}CH$ nor with PhC≡CC(O)Cl.

Scheme 1: Reaction of the Cluster $[RuCo_3(CO)_{12}]^-$ with Terminal Alkynes

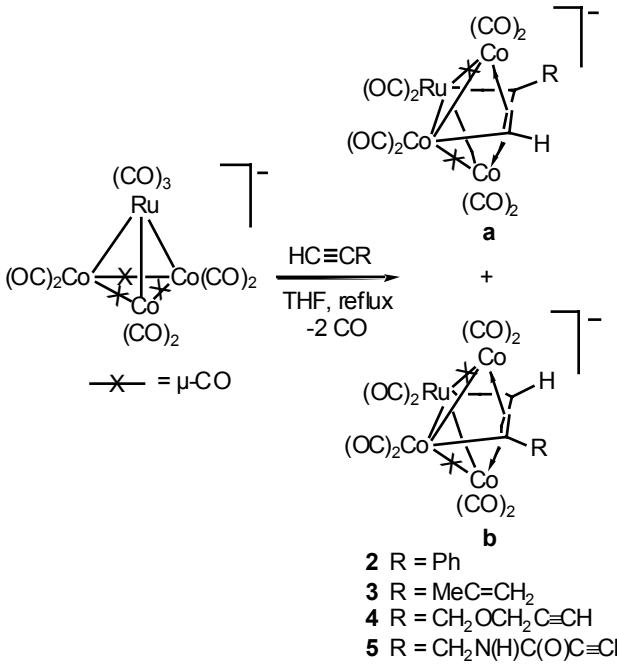

2 R = Ph
3 R = $MeC{=}CH_2$
4 R = $CH_2OCH_2C{\equiv}CH$
5 R = $CH_2N(H)C(O)C{\equiv}CPh$

All reactions proceeded either in refluxing THF or acetone for a few hours and were monitored by IR spectroscopy while the color of the solution changed from red to violet.

Recrystallization afforded clusters of the type $[RuCo_3(CO)_{10}(\mu_4\text{-}\eta^2\text{-}HC_2R)]^-$ (R = Ph (**2**), $MeC{=}CH_2$ (**3**), $CH_2OCH_2C{\equiv}CH$ (**4**), $CH_2N(H)C(O)C{\equiv}CPh$ (**5**)) in excellent yields (73-95%). The products have been characterized by IR and ^1H NMR spectroscopic methods, elemental analysis, and, in the case of **3** and **4**, by X-ray diffraction.

The new diyne ligand $PhC{\equiv}CC(O)NHCH_2C{\equiv}CH$ (**L**^{1}), which contains internal and terminal carbon-carbon triple bonds, was prepared in two steps by the method outlined in eq 1 which involved treatment of 3-phenylpropiolic acid with thionyl chloride, followed by the addition of propargylamine. The ligand was characterized by ^1H, ^{13}C NMR, IR spectroscopy and elemental analysis.

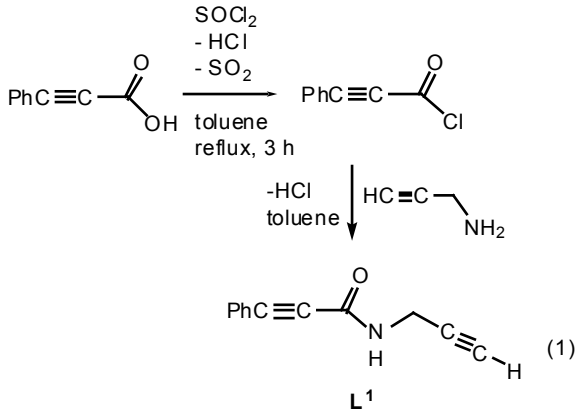

(1)

The reactivity of internal alkynes is lower than that of terminal alkynes which in turn are less reactive than acetylene.[19] Thus, as expected, the diyne **L**^{1} reacted with $[RuCo_3(CO)_{12}]^-$ selectively through its C≡CH triple bond. This was established by ^1H NMR spectroscopy of **5** (see Scheme 1 and below).

The IR spectra of clusters **2-5** display a similar pattern in spite of the diversity of alkynes used. Strong terminal carbonyl absorption bands are found between 2059-1970 cm^{-1} while the bridging carbonyls absorb between 1833-1817 cm^{-1}. In the IR spectra of NEt_4•**1** and NEt_4•**5**, an additional absorption band at 1712 or 1646 cm^{-1} is characteristic of the ester or amide carbonyl, respectively. The ^1H NMR spectra of clusters NEt_4•**1**-NEt_4•**5** show, in addition to the signals for the NEt_4^+ cation, typical resonances for the hydrogen atoms of the

alkyne-derived ligand. The hydrogen atoms in the CH^AH^B=C(CH_3) moiety of **3** are chemically different and present an ABX_3 spin system, like in the free alkyne, but the resolution of the signals did not allow extraction of the coupling constants. The singlets around δ 8.10-8.84 in the ^{1}H NMR spectra of NEt_4•**2**-NEt_4•**5** are assigned to the acetylenic protons. Their downfield shift is typical of hydrogen atoms bound to carbons interacting in a σ or π manner with metals.[3e,5] In addition, two singlets in this range are observed in the case of the anionc clusters **2** and **3**, which correspond to the formation of two isomers **a** and **b**, respectively (Scheme 1). These could not be separated by column chromatography. However, crystals of NEt_4•**3** with two different morphologies were obtained, which correspond to the two isomers **3a** and **3b**. ^{1}H NMR experiments carried out on two manually separated samples show that the more deshielded ^{1}H NMR signal should be assigned to the Co-bound CH proton. The isomer identified by X-ray diffraction was **3a** and crystals of **3b** were not suitable for X-ray diffraction. Clusters NEt_4•**2a,b** were also isolated from the reaction of $[RuCo_3(CO)_{12}]^-$ with PhC≡CC(O)OH owing to decarboxylation of this alkyne under reflux. For NEt_4•**4** and NEt_4•**5**, only one isomer was observed and the cluster identified by X-ray diffraction, NEt_4•**4a**, has the CH group attached to Co, not to Ru, whereas for NEt_4•**5**, we cannot state which isomer was formed.

Molecular structures of NEt_4•**3a and** NEt_4•**4.** Selected bond distances and angles are listed in Tables 1 and 2 and views of the molecular structures are shown in Figures 1 and 2, respectively. These clusters possess a $RuCo_3$ butterfly core with the ruthenium atom in a hinge position. In contrast, the cobalt atom occupies a wingtip position in the related cluster $[Ru_3Co(CO)_{11}(\mu_4\text{-}\eta^2\text{-}PhC_2Ph)]^-$.[20] In other mixed-metal anionic clusters with butterfly core structures, such as $[Ru_3M(CO)_{10}Cp(\mu_4\text{-}\eta^2\text{-}CH_3C_2CH_3)]^-$ (M = W, Mo), the metal atom M always occupies a hinge position,[21] as found in **1-5**. The alkyne ligand bridges all four

metals in a μ_4-η^2 fashion, lying parallel to the Ru-Co(1) bond. This arrangement completes an octahedral core structure consisting of the four metals and the two acetylenic carbon atoms. With an electron count of 60e, clusters **1-5** appear electron deficient, since an M_4 butterfly cluster obeying the EAN rule would require 62 electrons. However, considering **1-5** as octahedral $RuCo_3C_2$ clusters, their electron count is consistent with Wade's rules which predict a *closo* structure.[22] The non-bonding distances between the cobalt atoms Co(2) and Co(3) in **3** and **4** are 3.53 and 3.55 Å and the dihedral angles between the butterfly wings are 115.3° and 120.4°, respectively. The acetylenic protons have been located in both cases.

Bond lengths within the metal framework are typical of butterfly structures involving these metals. The Ru(1)-Co(1) distance is the longest of the Ru-Co distances, a general feature for metal-metal distances involving the metals in the hinge. There are two different, almost identical molecules, **A** and **B**, in the asymmetric unit of NEt_4•**3a**. The carbonyl ligands C(3)O(3), C(4)O(4), C(6)O(6) and C(8)O(8) in molecule **3aA** conform to the semibridging category of Crabtree-Lavin and the other carbonyls are terminal, whereas in **4**, C(3)O(3) and C(6)O(6) are bridging between Co(1), Co(3) and Ru(1), Co(2), respectively while C(8)O(8) is semibridging between Ru(1) and Co(3).[23] Owing to disorder or high thermal agitation, the NEt_4 group in molecule **3B** has been idealized and the distances N-C and C-C have been fixed at 1.53 and 1.58 Å, respectively.

Synthesis of the neutral trinuclear clusters 6-8 from the anionic clusters 1-3. In contrast to $[RuCo_3(CO)_{12}]^-$, the anionic clusters **1-3** did not lead to cluster expansion upon reaction with $[Cu(NCMe)_4]BF_4$ but rather to selective fragmentation with loss of the 12e fragment $Co(CO)^-$ to give the trinuclear alkyne-clusters **6-8**, as established by an X-ray diffraction study of **6**.[18,24]

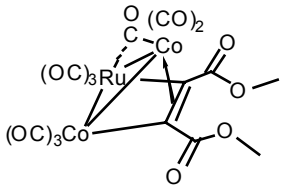

6

In contrast to **6** where the alkyne substituents are identical, two isomers of clusters **7** and **8** were obtained which differ by the orientation of the alkyne (Scheme 2). The infrared spectrum of **6** contains, in addition to the terminal and bridging carbonyl absorption bands, an absorption at 1720 cm^{-1} characteristic of the ester function. The ^1H NMR spectrum of **6** reveals two singlets for the chemically different methyl groups of the dmad ligand. In the case of **7** and **8**, the ^1H NMR spectra contain two singlets for the acetylenic hydrogen at 7.97, 9.59 and 7.83, 9.36 ppm, respectively. These singlets suggest the presence of isomers **a** and **b** (Scheme 2). For the $MeC{=}CH_2$ moiety in **8**, two resonances are observed for the methyl group (two isomers), and four resonances for the olefinic hydrogen atoms (ABX_3 spin system). These two isomers could not be separated.

Scheme 2

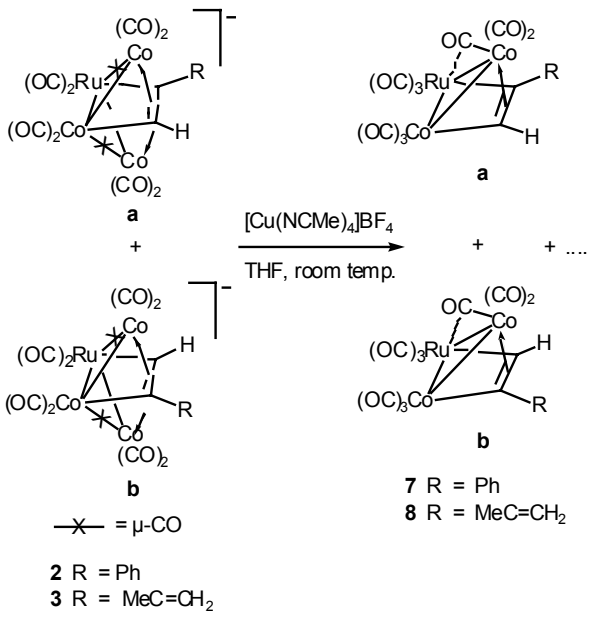

In each of the compounds **1-8** an organic function remains available which could be used for the subsequent functionalization of the coordinated ligands. Unfortunately, attempts

to hydrosilylate the C=C or a C=O double bond of **3** and **6**, respectively, with $HSi(OMe)_3$[25] or $HSiCl_3$[26] in the presence of H_2PtCl_6 or [Rh(diphos)(NBD)]BF_4, as catalysts, have not yet been successful.

Molecular structure of [$RuCo_2(CO)_9\{\mu_3$-η^2-MeOC(O)C_2C(O)OMe}] (6). Crystals suitable for X-ray structure analysis were obtained by recrystallization from hexane at –30 °C. A view of the molecular structure is depicted in Figure 3. Selected bond lengths and angles are presented in Table 3. The ruthenium and cobalt atoms form a triangle in which all the metal-metal distances are different but within the range of typical Ru-Co and Co-Co single bonds. The carbonyl C(6)O(6) is the only one to be semibridging, namely between Ru and Co(2): Co(2)-C(6)= 1.815(7) Å, Co(2)-C(6)-O(6) = 154.5(6)°, Ru···C(6) = 2.386(7) Å. The alkyne ligand is coordinated in a classical μ_3-η^2 fashion over the metal triangle, as observed in [$RuCo_2(CO)_9(\mu_3$-η^2-PhC_2Ph][18] and [$Ru_2Ir(CO)_9(\mu_3$-η^2-$PhC_2Ph]^-$.[27] The C(10)-C(11) bond is almost parallel to the Ru-Co(1) edge [C(10)-Co(1)-Ru-C(11) = 0.1(3)°]. Interestingly, in the related [$FeCo_2(CO)_9(\mu_3$-η^2-EtC_2Et] cluster, the alkyne is also bonded in a μ_3-η^2 mode but in contrast to **6** it is parallel to the Co-Co vector.[28] The alkyne carbon-carbon bond length of 1.372(8) Å compares with that in [$RuCo_2(CO)_9(\mu_3$-η^2-PhC_2Ph)] (1.370(3) Å)[18] and in [$Ru_2Ir(CO)_9(\mu_3$-η^2-$PhC_2Ph)]^-$ (1.363(11) Å).[27] Cluster **6** has the expected electron count of 48e for trinuclear clusters which obey the EAN rule. It also corresponds to a 7 skeletal electron pairs *nido*-octahedral cluster (square-based pyramid) constituted by the metals and C(10) and C(11).[22]

Reactions of the Tetrahedral $RuCo_3$ and $FeCo_3$ Clusters with Alkoxysilyl-Functionalized Alkynes. With the aim of incorporating a functional alkyne in a $RuCo_3$ or $FeCo_3$ cluster that could be subsequently condensed in a silica matrix via the sol-gel method,

we reacted clusters $[RuCo_3(CO)_{12}]^-$ and $[FeCo_3(CO)_{12}]^-$ with the recently prepared alkyne $PhC{\equiv}CC(O)NH(CH_2)_3Si(OMe)_3$ (**L²**).[4] This afforded the anionic clusters **9** and **10**, respectively, which were identified by their IR, NMR spectra and elemental analysis.

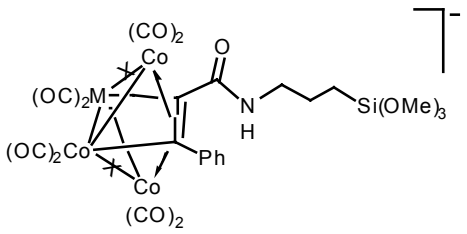

9a M = Ru
10a M = Fe

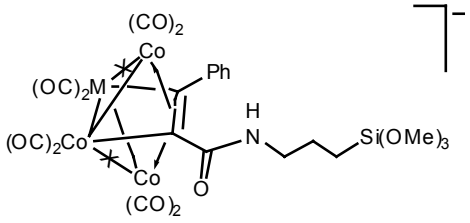

9b M = Ru
10b M = Fe

Their ^1H NMR spectra are similar and show two sets of signals in a 1:1 ratio, which correspond to the formation of two isomers which could not be separated but are reasonably assumed to correspond to the two possible orientations of the alkyne with respect to the Co-M edge, as indicated with **9a,b** and **10a,b**. The structure of these compounds was deduced from their spectroscopic properties and by analogy with the structurally characterized clusters **3** and **4** and the analogous cluster $[FeCo_3(CO)_{10}(\mu_4\text{-}\eta^2\text{-}PhC_2Ph)]^-$.[29] The IR spectra of **9** and **10** contain, besides the terminal and bridged carbonyl absorption bands, an absorption band at 1612 and 1637 cm^{-1}, respectively, which is characteristic of the amide carbonyl. We are currently evaluating these $Si(OMe)_3$-containing clusters as precursors to sol-gel materials.

Reaction of $RuCo_3$ clusters with a protected diyne. Reaction of $[NEt_4][RuCo_3(CO)_{12}]$ with 1,4-bi*s*(trimethylsilyl)butadiyne afforded in good yield the

expected butterfly, air-stable cluster $[NEt_4][RuCo_3(CO)_{10}(\mu_4\text{-}\eta^2\text{-}Me_3SiC_2C{\equiv}CSiMe_3)]$ (NEt_4•**11**) in two isomeric forms **11a** and **11b**, in a 2:3 ratio.

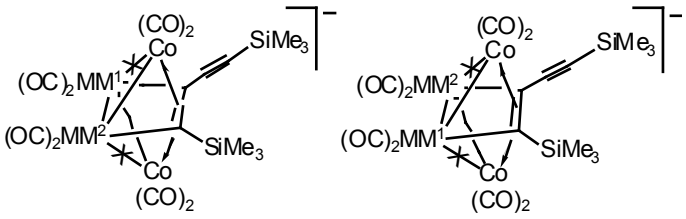

The identity of 11 was deduced from analytical and spectroscopic data and confirmed by a single-crystal X-ray diffraction study. The cluster contains an uncomplexed C≡C triple bond, but no IR absorption was found in the ν(C≡C) region. The ^{1}H NMR spectrum contained four resonances at δ 0.035, 0.094, 0.108 and 0.240 for the two $SiMe_3$ goups of the two isomers. The molecular structure of 11, shown in Figure 4, is similar to that of 3 and 4. The non-bonding Co(2)···Co(3) distance is 3.54(1) Å and the dihedral angle between the butterfly wings is 114.9(2)°. The refinement of the X-ray data led to consider the positions MM1 and MM2 as disordered, with occupancy factors of Ru: 0.43, Co: 0.57 and Ru: 0.57, Co: 0.43, respectively. The Co(2)-C(4), Co(2)-C(6), Co(3)-C(3) and Co(3)-C(8) distances of 1.87(1), 1.77(1), 1.79(1) and 1.88(1) Å, respectively, are considerably shorter than the MM2-C(4), MM1-C(6), MM2-C(3) and MM1-C(8) distances of 2.08(1), 2.48(1), 2.31(1) and 2.03(1), respectively, which suggests that C(3)O(3), C(4)O(4), C(6)O(6) and C(8)O(8) occupy semibridging positions. The six remaining carbonyl ligands are terminal.

Complexation of $[Co_2(CO)_8]$ or $[Pt(C_2H_4)(PPh_3)_2]$ to the free C(13)≡C(14) triple bond of **11** could not be achieved, probably for steric reasons.

Reaction of NEt_4•11 with $[Cu(NCMe)_4]BF_4$. This reaction yielded a red product, as observed with clusters **1-3** which afforded the triangular clusters **6-8,** respectively. We observed by ^{1}H NMR two $SiMe_3$ resonances at δ 0.15 and 0.19 in addition to two singlets at

δ 8.02 and 9.48, characteristic of the hydrogen atoms bound to carbon atoms interacting in a σ or π manner with metal centers. This suggests again the presence of two isomers of the cluster $[RuCo_2(CO)_9(\mu_3\text{-}\eta^2\text{-}HC_2C{\equiv}CSiMe_3)]$ (**12**) and not of the expected cluster $[RuCo_2(CO)_9(\mu_3\text{-}\eta^2\text{-}Me_3SiC_2C{\equiv}CSiMe_3)]$. By analogy with previous assignments on related clusters, the more deshielded ^1H NMR signal should be assigned to the Co-bound CH proton. The unexpected deprotection of the $SiMe_3$ group could be due to the presence of fluoride originating from $[Cu(NCMe)_4]BF_4$. Proto-desilylation occurred at the Co-C-$SiMe_3$ group rather than at the alkynyl carbon as might have been expected by analogy to $[Co_2(CO)_4(\mu\text{-dppm})(\mu\text{-}\eta^2\text{-}Me_3SiC_2C{\equiv}CSiMe_3)]$.[30] This was also observed in the case of the deprotection of $[Co_4(\mu\text{-}CO)_2(CO)_6(\mu\text{-dppm})(\mu_4\text{-}\eta^2\text{-}Me_3SiC_2C{\equiv}CSiMe_3)]$ with TBAF/THF-H_2O which afforded $[Co_4(\mu\text{-}CO)_2(CO)_6(\mu\text{-dppm})(\mu_4\text{-}\eta^2\text{-}HC_2C{\equiv}CSiMe_3)]$ instead of the expected $[Co_4(\mu\text{-}CO)_2(CO)_6(\mu\text{-dppm})(\mu_4\text{-}\eta^2\text{-}Me_3SiC_2C{\equiv}CH)]$.[4] Cluster **12** was characterized by the usual methods, details of which are given in the experimental section. The low yield (22%) and difficulties in crystallizing the product precluded full characterization. However, the IR spectrum is very similar to those of the related clusters **6-8**. The ν(C≡C) absorption for the uncoordinated C≡C triple bond was not observed whereas it appears at 2108 cm^{-1} for the cluster $[Ru_3(\mu\text{-}CO)(CO)_9(\mu_3\text{-}\eta^2\text{-}Me_3SiC_2C{\equiv}CSiMe_3)]$.[31] The FAB mass spectrum shows the presence of the parent ion, and by the stepwise loss of carbonyl ligands.

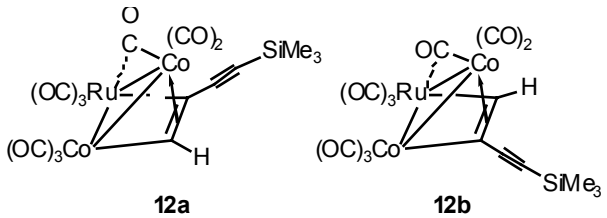

Reaction of NEt_4•11 with $[NO]BF_4$. Cluster NEt_4•**11** reacts with $[NO]BF_4$ to afford the new neutral cluster $[RuCo_3(CO)_9(NO)(\mu_4\text{-}\eta^2\text{-}Me_3SiC_2C{\equiv}CSiMe_3)]$ (**13**) by selective substitution of a carbonyl ligand on a wing-tip cobalt atom with a nitrosyl group. The

identity of **13** was deduced by comparaison with the known cluster $[RuCo_3(CO)_9(NO)(\mu_4\text{-}\eta^2\text{-PhC}\equiv\text{CPh})]$ synthesized by reaction of $[RuCo_3(CO)_{10}(\mu_4\text{-}\eta^2\text{-PhC}\equiv\text{CPh})]^-$ with $[NO]BF_4$ or by reaction of $[RuCo_3(CO)_{11}(NO)]$ with diphenylacetylene.[32] The nitrosyl group gives rise to an absorption band at 1805 cm^{-1}. The ^1H NMR spectrum contains two different signals for the two -$SiMe_3$ groups, which suggests the presence of only one isomer, in contrast to the situation in the precursor complex. However, we do not know which isomer was formed. The FAB mass spectrum contains a parent ion and shows stepwise loss of carbonyl groups.

The formation of **13** was accompanied by that of the partially deprotected cluster **12**. Similar decrease in nuclearity affording $[RuCo_2(CO)_9(\mu_3\text{-}\eta^2\text{-PhC}\equiv\text{CPh})]$ occurred during the reaction of $[RuCo_3(CO)_{10}(\mu_4\text{-}\eta^2\text{-PhC}\equiv\text{CPh})]^-$ with $[NO]BF_4$.[32] Deprotection leading to **12** is also due to the presence of fluoride ions originating from $[NO]BF_4$ and it is surprising that under similar conditions, the remaining **13** was not deprotected.

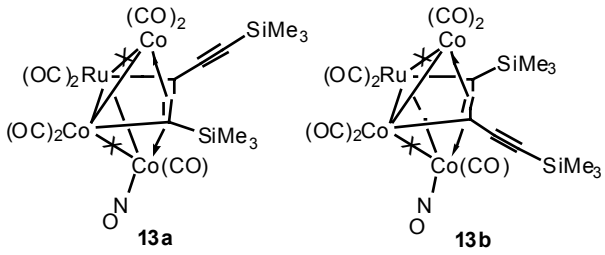

One of the objectives of the reactions of NEt_4•**11** with $[Cu(NCMe)_4]BF_4$ and $[NO]BF_4$ was the obtention of neutral clusters, which are often more soluble and easier to purify, but unfortunately, the yield was low in both cases.

Reaction of NEt_4•11 with $[AuCl(PPh_3)]$ and PPh_3. With the object of introducing the $AuPPh_3$ fragment in the cluster and examining its site of attachment, we reacted the cluster NEt_4•**11** with $[AuCl(PPh_3)]$ in toluene. Such reactions are generally favored by the addition of $TlPF_6$ which activates the gold-chlorine bond but when this reagent was used,

unidentified neutral products were obtained in addition to decomposition (TLC). When NEt_4•**11** was heated with [AuCl(PPh_3)] in toluene at reflux without addition of $TlPF_6$, the gold-phosphorus bond was broken and the phosphine liberated substituted selectively a carbonyl ligand on the ruthenium atom to afford [NEt_4][$RuCo_3(CO)_9(PPh_3)(\mu_4$-$\eta^2$-$Me_3SiC_2C{\equiv}CSiMe_3)$] ($NEt_4$•**14**). This cluster was also obtained directly, and in higher yield, by reaction of NEt_4•**11** with one equivalent of PPh_3 in refluxing toluene. None of these reactions was observed in THF. The cluster has the same color (violet) and an IR spectrum similar to that of the related clusters $[RuCo_3(CO)_{10}(\mu_4$-η^2-alkyne$)]^-$. As observed in **13**, the ^{1}H NMR spectrum of **14** contains only two different signals for the two -$SiMe_3$ groups, which suggests the presence of only one isomer. It was identified by X-ray diffraction and the molecular structure of **14** is similar to those of **3**, **4** and **11**. A view of the molecule is shown in Figure 5 and selected bond distances and angles are given in Table 5. The non-bonding Co(2)···Co(3) distance is 3.51(1) Å and the dihedral angle between the butterfly wings is 114°. The carbonyl C(8)O(8) is bridging between Ru and Co(3) whereas C(5)O(5) is semibridging between Ru and Co(2). The Ru-P distance of 2.345(1) is comparable to literature values.[33]

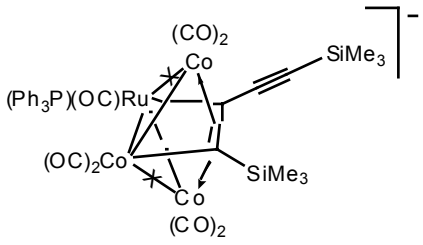

14

Proto-desilylation of 11. Under standard desilylation conditions,[34] NEt_4•**11** was treated with a catalytic amount of [*n*-Bu_4N]F (TBAF) in wet THF. In addition to the deprotection at the alkynyl group, the NEt_4^+ cation was partially exchanged for $N(n\text{-}Bu)_4^+$. We thus obtained a mixture of the clusters [NEt_4][$RuCo_3(CO)_{10}(\mu_4$-η^2-$Me_3SiC_2C{\equiv}CH)$] (NEt_4•**15**) and [$N(n\text{-}Bu)_4$][$RuCo_3(CO)_{10}(\mu_4$-η^2-$Me_3SiC_2C{\equiv}CH)$] [$N(n\text{-}Bu)_4$•**15**] (Scheme 3).

We have succeeded in separating N(*n*-Bu)$_4$•**15** from the mixture by recrystallization and crystals suitable for X-ray diffraction were obtained. The remaining of the product was a paste which contained a mixture of the two clusters. The ^{1}H NMR spectrum of the isolated N(*n*-Bu)$_4$•**15** contains, beside the Bu signals, two resonances at δ 0.12 and 0.25 for the non-deprotected -SiMe$_3$ group corresponding to the two isomers, and obviously two resonances at δ 3.41 and 3.51 for the HC≡ proton. The disappearence of the signals at δ 0.035 and 0.094 in **11a** confirms their assignment to the C≡CSiMe$_3$ protons. Full deprotection leading to a butadiyne complex was not observed. Whereas proto-desilylation occurred here at the anticipated site, it took place at the cluster core-bound alkyne carbon in the case of the neutral, isoelectronic Co$_4$ system.[4]

Scheme 3

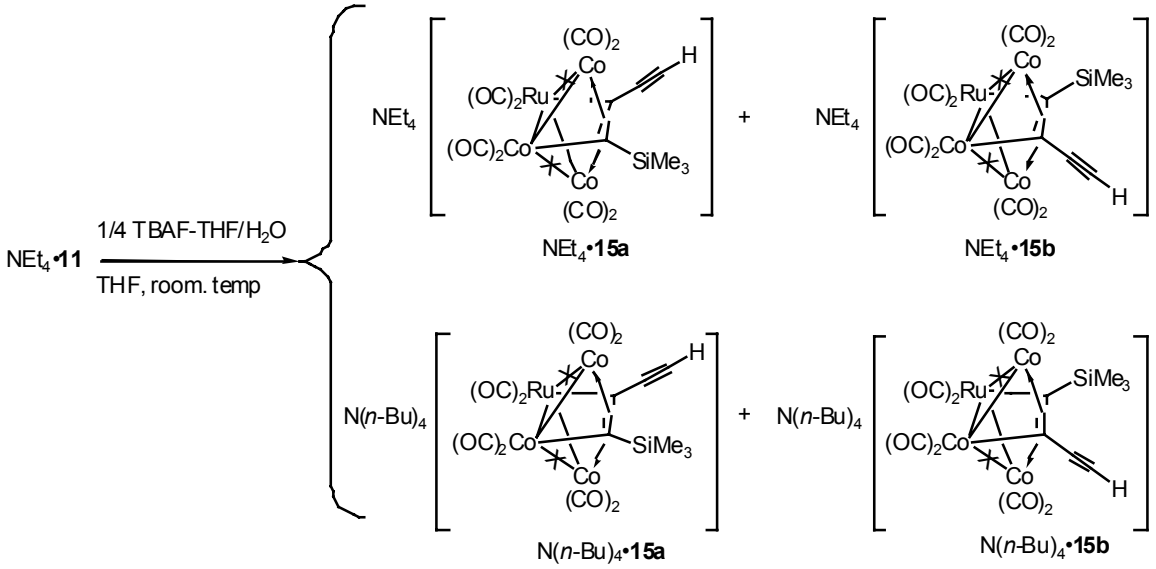

The molecular structure of N(*n*-Bu)$_4$•**15a** was established by X-ray diffraction (Figure 6) and selected bond distances and angles are given in Table 6. The structure is similar to that of **11** and two different, almost identical molecules, **A** and **B**, are present in the asymmetric unit. The C(4)O(4), and C(8)O(8) carbonyl ligands in **15aA** are bridging between Co(1), Co(2) and Ru(1), Co(3), respectively. The Co(1)-C(3) and Ru(1)-C(6) distances of 2.549(9)

and 2.199(8) Å, respectively, are considerably longer than the Co(3)-C(3) and Co(2)-C(6) distances of 1.781(8) Å and 1.818(8), respectively, which suggests that C(3)O(3) and C(6)O(6) occupy a bent semibridging position.[22] The remaining carbonyls are terminal. The non-bonding Co(2)···Co(3) and Co(5)···Co(6) distances in the molecules **A** and **B** are both 3.53(1) Å and the dihedral angles between the butterfly wings are of 113.4 and 116.4°, respectively.

To avoid the cation exchange in NEt_4•**11** for $N(n\text{-}Bu)_4^+$, we first prepared the cluster $[PPN][RuCo_3(CO)_{10}(\mu_4\text{-}\eta^2\text{-}Me_3SiC_2C{\equiv}CSiMe_3)]$ (PPN•**11)** by cation metathesis since subsequent replacement of PPN^+ with $N(n\text{-}Bu)_4^+$ should not occur during the desilylation step. As expected, PPN•**11** was obtained in two isomeric forms and treatment with TBAF afforded $[PPN][RuCo_3(CO)_{10}(\mu_4\text{-}\eta^2\text{-}Me_3SiC_2C{\equiv}CH)]$ (PPN•**15**) in high yield and also in two isomeric forms (eq. 2). This cluster was readily characterized by its spectroscopic properties, which included resonances in the ^1H NMR spectrum for the HC≡ proton at δ 3.23 and 3.44.

$$NEt_4\text{•}\mathbf{11} \xrightarrow[\text{THF, 60 °C, 2 h}]{\text{[PPN]Cl}} \text{PPN•}\mathbf{11} \xrightarrow[\text{THF, room. temp}]{\text{1/4 TBAF-THF/}H_2O} \text{PPN•}\mathbf{15} \quad (2)$$

Coupling of the Diyne-Cluster to Form a Linked "Dicluster" Compound through π-Delocalized Organic Frameworks. As shown in eq. 3, the synthesis of the dianion **16** could be achieved through the Pd(II)/Cu(I) catalytic Sonogashira coupling reaction of cluster $[RuCo_3(CO)_{10}(\mu_4\text{-}\eta^2\text{-}Me_3SiC_2C{\equiv}CH)]^-$ (**15**) with 1,4 diiodobenzene.[35] The benzene ring represents a suitable spacer for a π-conjugated system linking cluster molecules. Since it was difficult to separate NEt_4•**15** from $N(n\text{-}Bu)_4$•**15**, we have used the mixture for the coupling reaction. The reaction was performed in THF/NEt_3 at 50 °C for 18 h and the color of the solution changed from violet to brown. Extraction with hexane removed a yellow,

copper iodide complex (see below) and purification of the remaining product with toluene/pentane afforded **16**. The solution IR spectrum of this latter exhibits the characteristic ν(CO) pattern seen for e.g. **15**. In the ^{1}H NMR spectrum we observe the disappearance of the HC≡ signals present in **15**, and negative ion electrospray mass spectrometry (CH_2Cl_2 solution) showed the highest mass molecular weight ions at *m/z* 717.5 (*Z* = 2) corresponding to the doubly charged, coupled clusters, with fragments resulting from loss of CO groups. When PPN•**15** was used, the yellow product could be characterized by X-ray diffraction to be the centrosymmetric dimer $[PPN]_2[Cu_2(\mu\text{-}I)_2I_2]$ ($[PPN]_2$•**17**). These data are not reported here since complexes containing $[Cu_2I_4]^{2-}$ associated with large cations $[NR_4]^+$, $[PR_4]^+$ or $[AsR_4]^+$ (R = alkyl or phenyl) have already been described in the literature.[36]

Unfortunately, the oxidative coupling of **15**, using standard Eglinton-Glaser conditions[37] ($Cu(OAc)_2$, pyridine, 25 °C), failed.

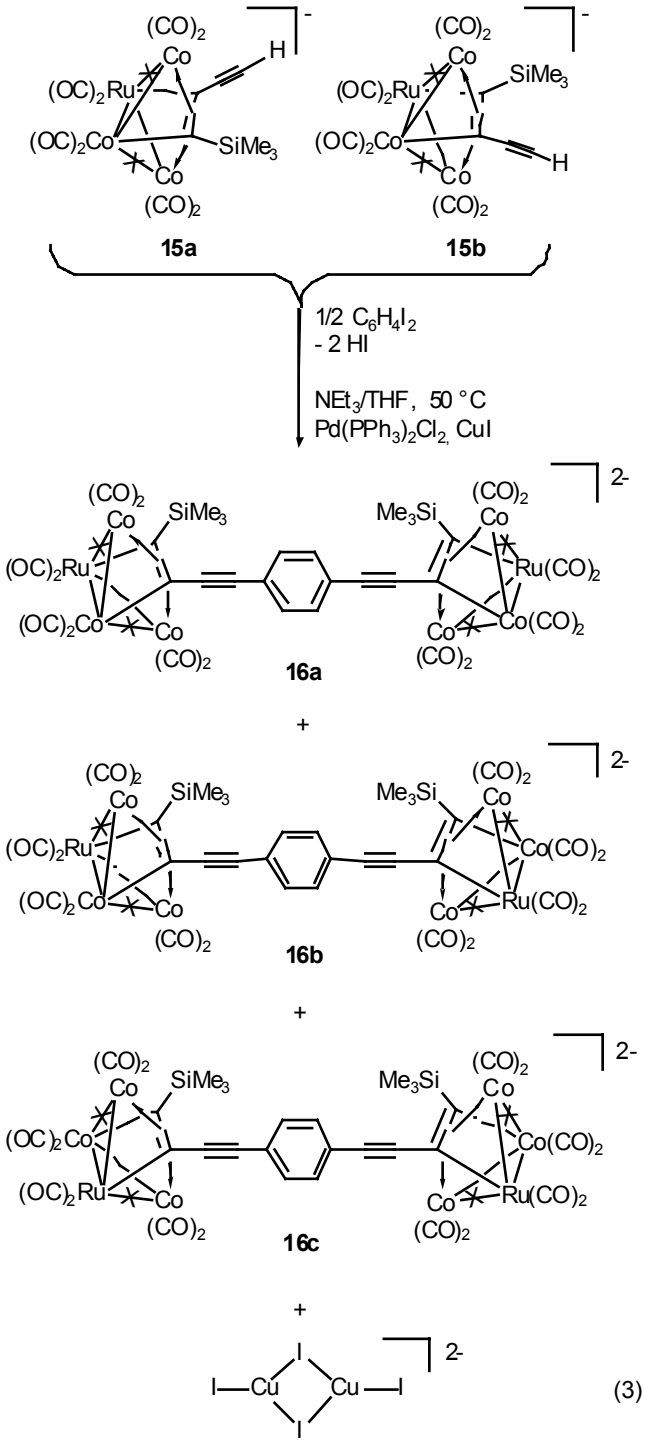

Formation of Bimetallic Particles by the Sol-Gel Method. As indicated in the Introduction, we considered the use of alkynes containing a -Si(OR)$_3$ group as a way to covalently anchor metal carbonyl clusters onto surfaces and form new cluster-derived nanomaterials. Two complementary approaches are conceivable: first attach the –Si(OR)$_3$ end of the ligand to the inorganic matrix (Scheme 4, A_1) and then react its alkyne function with the

molecular cluster (Scheme 4, A_2), or first prepare the alkyne cluster (Scheme 4, B_1) and react its -Si(OR)$_3$ group with the host matrix to generate the covalent linkage (Scheme 4, B_2).[2]

Scheme 4. Complementary strategies based on functional alkyne ligands for the covalent grafting of metal clusters, followed by thermal treatment to generate nanoparticles.

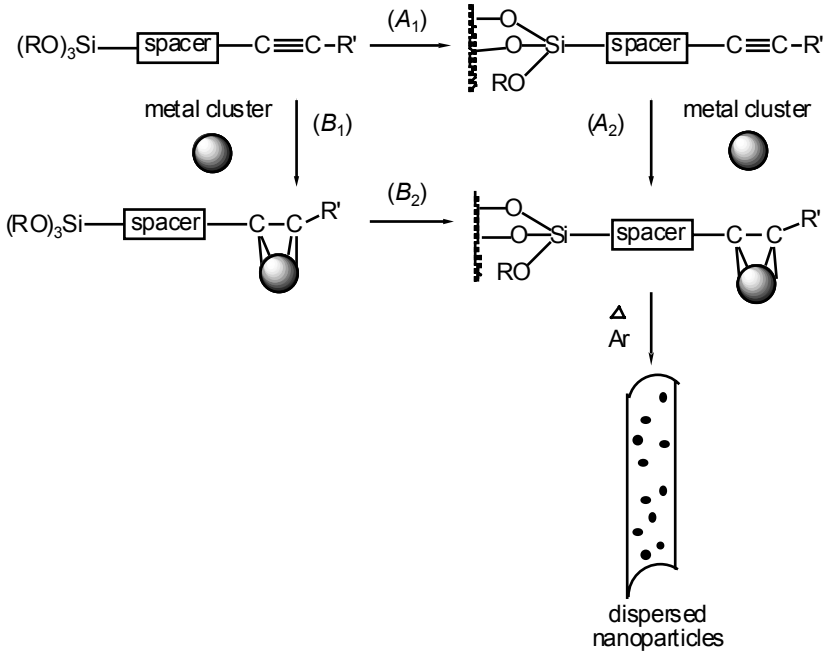

In a preliminary study, we have used the newly reported[5] trialkoxysilyl alkyne HC≡C(CH$_2$)$_2$OC(O)NH(CH$_2$)$_3$Si(OEt)$_3$ to prepare a xerogel according to Scheme 4, A_1. It was characterized by ^{29}Si CP-MAS NMR spectroscopy and shown to remain highly porous, 657 m^2/g (determined by nitrogen adsorption isotherms), despite the grafting of the functional alkyne, with a mean pore diameter of 11 nm. Anchoring of [RuCo$_3$(CO)$_{12}$]$^-$ was done by reaction of the cluster in THF with the functionalized xerogel. Thermal decomposition was followed in situ in a magnetic thermobalance[1a] and led to spherical particles of 2.2-5.5 nm in diameter (TEM). X-ray diffraction showed the presence of a hexagonal phase of a RuCo$_3$ alloy. Magnetic measurements show that these particles display ferromagnetic behavior.[38] Further studies are in progress to explore the scope of this sol-gel method applied to mixed-metal clusters for the preparation of bimetallic nanoparticles.

Conclusion

In this work we have described the synthesis and characterization of a series of new alkyne clusters of the type $[RuCo_3(CO)_{10}(\mu_4\text{-}\eta^2\text{-}RC_2R')]^-$ (**1-5**) obtained in excellent yields by reaction of the tetrahedral cluster $[RuCo_3(CO)_{12}]^-$ with MeOC(O)C≡C(O)OMe, PhC≡CH**,** HC≡C(Me)C=CH_2, HC≡CCH_2OCH_2C≡CH and the new alkyne HC≡CCH_2N(H)C(O)C≡CPh, respectively. All the alkynes were linked to the cluster in a μ_4-η^2 fashion. Reactions of the anionic clusters **1-3** with $[Cu(NCMe)_4]BF_4$ led to their selective fragmentation to the trinuclear neutral clusters **6-8**. The coordinated alkynes in clusters **1**, **3-5** and **7-8** offer the potential of further derivatization. The functionalization of clusters $[RuCo_3(CO)_{12}]^-$ and $[FeCo_3(CO)_{12}]^-$ was also performed directly by reaction with PhC≡CC(O)NH$(CH_2)_3$Si$(OMe)_3$, which is of interest for future condensation with a silica matrix via the sol-gel method. Indeed, preliminary results indicate the potential of porous gels, obtained from HC≡C$(CH_2)_2$OC(O)NH$(CH_2)_3$Si$(OEt)_3$, for tethering alkyne mixed-metal clusters which can be used as precursors to bimetallic particles. Reaction of 1,4-bis(trimethylsilyl)butadiyne with $[RuCo_3(CO)_{12}]^-$ afforded the air-stable cluster **11** whose reaction with $[Cu(NCMe)_4]BF_4$ led, in addition to fragmentation, to the unexpected proto-desilylation of the core-bound $SiMe_3$ group due to the presence of fluoride ions. The thermal reaction of **11** with [AuCl(PPh_3)] or PPh_3 led to selective substitution of a carbonyl ligand on the ruthenium atom by triphenylphosphine. Although CO ligands on cobalt are more labile than on ruthenium, the latter center is more electron-deficient and will form stronger bonds with the phosphine. Proto-desilylation of **11** using TBAF/THF-H_2O occurred at the expected site to yield $[RuCo_3(CO)_{10}(\mu_4\text{-}\eta^2\text{-}Me_3SiC_2C{\equiv}CH)]^-$. A Sonogashira coupling reaction between cluster $[RuCo_3(CO)_{10}(\mu_4\text{-}\eta^2\text{-}Me_3SiC_2C{\equiv}CH)]^-$ (**15**) and 1,4-diiodobenzene afforded an isomeric mixture of the diclusters $[\{RuCo_3(CO)_{10}(\mu_4\text{-}\eta^2\text{-}Me_3SiC_2C{\equiv}C)\}_2C_6H_4]^{2-}$ (**16**), the properties of which will be the subject of future work.

Experimental Section

All the reactions and manipulations were carried out under an inert atmosphere of purified nitrogen using standard Schlenk tube techniques. Solvents were dried and distilled under nitrogen before use: toluene over sodium, tetrahydrofuran, hexane and pentane over sodium-benzophenone, dichloromethane over phosphorus pentoxide. Nitrogen (Air liquide, R-grade) was passed through BASF R3-11 catalyst and molecular sieves columns to remove residual oxygen and water. The ligand $PhC{\equiv}CC(O)NH(CH_2)_3Si(OMe)_3$[4] and the clusters $[NEt_4][RuCo_3(CO)_{12}]$[24c] and $[NEt_4][FeCo_3(CO)_{12}]$[39] were prepared according to literature methods. Elemental C, H and N analyses were performed by the Service de microanalyses du CNRS (ULP Strasbourg). Infrared spectra (cm^{-1}) were recorded on a IFS-66 FTIR Bruker or a Perkin Elmer 1600 series FTIR spectrometers. The ^1H NMR spectra were recorded at 200.13, 300.13, 400.13 or 500.13 MHz on a Bruker AC200, AC300, AVANCE 300, AVANCE 400 or AVANCE 500 instruments.

Synthesis of the ligand $PhC{\equiv}CC(O)NHCH_2C{\equiv}CH$ (L^1). A solution of propargylamine (0.783 mL, 11.42 mmol) in 20 mL of toluene was added dropwise to a toluene solution of 3-phenylpropynoyl chloride, obtained by reaction of 3-phenylpropiolic acid (0.459 g, 3.425 mmol) with thionyl chloride (0.300 mL, 4.110 mmol). After the addition was complete, the mixture was stirred at room temperature for 1 h and then poored into 60 mL of cold water. The mixture was filtered and the solid was discarded. The layers were separated and the organic fraction was dried over $MgSO_4$ and then evaporated to afford $\mathbf{L^1}$ (0.496 g, 2.710 mmol, 79% (based on 3-phenylpropiolic acid) as a yellow solid. IR ($CHCl_3$): 3439 (m, ν_{NH}), 3307 (s, $\nu_{{\equiv}CH}$), 2223 (vs, $\nu_{C{\equiv}C}$), 1654 (vs, $\nu_{C=O}$), 1506 (vs, δ_{NH}). ^1H NMR (300.13 MHz, $CDCl_3$): δ 2.28 (t, ^4J(HH) = 2.6 Hz, 1H, HC≡), 4.15 (dd, ^3J(HH) = 5.4

Hz, ^4J(HH) = 2.6 Hz, 2 H, CH_2N), 6.22 (br, NH), 7.25-7.53 (m, 5H, Ph). $^{13}C\{^1H\}$ NMR (100.62 MHz, $CDCl_3$) δ: 29.62 (s, NCH_2), 72.27 (s, H*C*≡C), 78.61 (s, HC≡*C*), 82.42 (s, PhC≡*C*), 85.74 (s, Ph*C*≡C), 120.0, 127.1, 128.3, 128.6, 130.3 (5 s, C_6H_5), 132.6 (s, C_{ipso} of C_6H_5), 153.0 (s, C=O). Anal. Calcd. for $C_{12}H_9NO$: C, 78.67; H, 4.95; N, 7.65. Found: C, 78.82; H, 5.12; N, 7.78.

Synthesis of [NEt$_4$][RuCo$_3$(CO)$_{10}$\{μ_4-η^2-MeOC(O)C$_2$C(O)OMe\}] (NEt$_4$•1). To a solution of [NEt_4][$RuCo_3(CO)_{12}$] (0.550 g, 0.739 mmol) in 50 mL of THF was added dimethylacetylene dicarboxylate (dmad) (0.460 mL, 3.736 mmol). The mixture was heated to reflux and the progress of the reaction was monitored by IR spectroscopy. After ca. 7 h the reaction was complete. Recrystallization of the residue from CH_2Cl_2/hexane yielded violet crystals of NEt_4•**1** (0.450 g, 0.542 mmol, 73%). IR (CH_2Cl_2): 2059 (m), 2015 (vs), 1988 (s, sh), 1833 (m), $\nu_{C\equiv O}$, 1712 (m, $\nu_{C=O}$). ^1H NMR (200.13 MHz, $CDCl_3$): δ 1.28 (m, 12 H, CH_2CH_3), 3.20 (m, 8 H, CH_2), 3.50 (s, 3 H, OCH_3), 3.57 (s, 3 H, OCH_3). Anal. Calcd. for $C_{24}H_{26}Co_3NO_{14}Ru$: C, 34.72; H, 3.16; N, 1.69. Found: C, 34.84; H, 3.23; N, 1.76.

Synthesis of [NEt$_4$][RuCo$_3$(CO)$_{10}$(μ_4-η^2-HC$_2$Ph)] (NEt$_4$•2). Similary to the synthesis of NEt_4•**1**, the reaction of [NEt_4][$RuCo_3(CO)_{12}$] (0.740 g, 0.994 mmol) in 50 mL of THF with phenylacetylene (0.556 mL, 5.064 mmol) was monitored by IR which indicated the completion of the reaction after ca. 7 h. After filtration, the solvent was removed under vacuum. The residue was washed with hexane and recrystallized from CH_2Cl_2/hexane to yield violet crystals of NEt_4•**2** (0.576 g, 0.729 mmol, 73%). IR (CH_2Cl_2, ν_{CO}): 2049 (m), 2005 (vs), 1975 (sh), 1820 (m). ^1H NMR (200.13 MHz, $CDCl_3$): δ 1.27 (m, 12 H, CH_3), 3.11 (m, 8 H, CH_2), 6.80-7.26 (m, 5 H, Ph), 8.36 (br s, 0.25 H, HC_2- of one isomer), 8.84 (br

s, 0.75 H, HC_2- of the other isomer). Anal. Calcd. for $C_{26}H_{26}Co_3NO_{10}Ru$: C, 39.51; H, 3.32; N, 1.77. Found: C, 39.67; H, 3.25; N, 1.61.

Synthesis of [NEt_4][$RuCo_3(CO)_{10}(\mu_4$-η^2-$HC_2(Me)C{=}CH_2$] (NEt_4•3). By a similar procedure to that detailed for NEt_4•**1**, the reaction of [NEt_4][$RuCo_3(CO)_{12}$] (0.670 g, 0.900 mmol) in 50 mL of THF with 2-methyl-1-buten-3-yne (0.407 mL, 4.277 mmol) at reflux for 5 h afforded, after workup, cluster NEt_4•**3** (0.539 g, 0.715 mmol, 80%) as violet crystals, which were further washed with hexane. IR (CH_2Cl_2, ν_{CO}): 2048 (m), 2003 (vs), 1973 (s), 1817 (m). The two isomers were separated manually under the microscope and their NMR spectra recorded. Isomer NEt_4•**3a** gives rise to large, parallelipipedic crystals whereas NEt_4•**3b** crystallized as thin plates. ^{1}H NMR for NEt_4•**3a** (300.13 MHz, $CDCl_3$): δ 1.37 (m, 12H, CH_2CH_3), 1.75 (m, 3H, $CH^AH^B{=}C(CH_3)$, X_3 part of an ABX_3 spin system), 3.24 (m, 8H, CH_2CH_3), 4.40 (m, 1H, $CH^AH^B{=}C(CH_3)$, A part of an ABX_3 spin system), 4.54 (m, 1H, $CH^AH^B{=}C(CH_3)$, B part of an ABX_3 spin system), 8.72 (br s, 1H, HC_2). ^{1}H NMR for NEt_4•**3b** (300.13 MHz, $CDCl_3$): δ 1.37 (m, 12H, CH_2CH_3), 1.82 (m, 3H, $CH^AH^B{=}C(CH_3)$, X_3 part of an ABX_3 spin system), 3.25 (m, 8H, CH_2CH_3), 4.55 (m, 1H, $CH^AH^B{=}C(CH_3)$, A part of an ABX_3 spin system), 4.92 (m, 1H, $CH^AH^B{=}C(CH_3)$, B part of an ABX_3 spin system), 8.17 (br s, 1 H, HC_2). Anal. Calcd. for $C_{23}H_{26}Co_3NO_{10}Ru$: C, 36.62; H, 3.47; N, 1.86. Found: C, 36.45; H, 3.29; N, 1.75.

Synthesis of [NEt_4][$RuCo_3(CO)_{10}(\mu_4$-η^2-$HC_2CH_2OCH_2C{\equiv}CH)$] ($NEt_4$•4). A solution of [$NEt_4$][$RuCo_3(CO)_{12}$] (0.275 g, 0.369 mmol) and propargyl ether (0.042 mL, 0.408 mmol) was refluxed in 50 mL of THF for 5 h. The solution was filtered and evaporated under vacuum. Violet crystals of NEt_4•**4** (0.266 g, 0.340 mmol, 92%) were obtained by recrystallization of the product from CH_2Cl_2/hexane. IR (CH_2Cl_2, ν_{CO}): 2049

(m), 2003 (vs), 1970 (s), 1819 (m). ^{1}H NMR (300.13 MHz, $CDCl_3$): δ 1.38 (m, 12 H, CH_2CH_3), 2.30 (br s, 1 H, ≡CH), 3.60 (m, 8 H, CH_2CH_3), 3.93 (s, 2 H, OCH_2), 4.09 (s, 2 H, OCH_2), 8.76 (br s, 1 H, -C_2H). Anal. Calcd. for $C_{24}H_{26}Co_3NO_{11}Ru$: C, 36.85; H, 3.35; N, 1.79. Found: C, 36.98; H, 3.41; N, 1.83.

Synthesis of [NEt$_4$][RuCo$_3$(CO)$_{10}$(μ_4-η^2-HC$_2$C(O)NHCH$_2$C≡CPh] (NEt$_4$•5). By a similar procedure to that described for NEt$_4$•**1**, the cluster NEt$_4$•**5** (0.278g, 0.320 mmol, 95%) was obtained by reaction of [NEt$_4$][RuCo$_3$(CO)$_{12}$] (0.250 g, 0.336 mmol) with PhC≡CC(O)NHCH$_2$C≡CH (**L^1**) (0.062 g, 0.339 mmol) in 50 mL refluxing THF for 5 h, and recrystallization from CH_2Cl_2/hexane. IR (CH_2Cl_2): 2051 (m), 2007 (vs), 1972 (s), 1820 (m) $\nu_{C\equiv O}$, 1646 (w, $\nu_{C=O}$). ^{1}H NMR (300.13 MHz, $CDCl_3$): δ 1.36 (m, 12H, CH_2CH_3), 3.25 (m, 8H, CH_2CH_3), 3.95 (m, 2H, HNCH_2), 5.65 (br, NH), 7.26-7.53 (m, 5H, Ph), 8.70 (br s, 1H, -C_2H). Anal. Calcd. for $C_{30}H_{29}Co_3N_2O_{11}Ru$: C, 41.35; H, 3.35; N, 3.21. Found: C, 41.48; H, 3.17; N, 3.08.

Synthesis of [RuCo$_2$(CO)$_9$(μ_3-η^2-MeOC(O)C$_2$C(O)OMe] (6). Solid [Cu(NCMe)$_4$]BF_4 (0.227 g, 0.724 mmol) was added to a solution of NEt$_4$•**1** (0.300 g, 0.361 mmol) in 50 mL THF. After the mixture was stirred for 2.5 h at room temperature, a second equivalent of [Cu(NCMe)$_4$]BF_4 was added. The reaction occurs with a change of color from violet to red and it was stopped after *ca*. 5 h. The reaction mixture was then filtered and the solvent was evaporated under vacuum. Extraction of the residue with hexane afforded the neutral cluster **6** (0.119 g, 0.195 mmol, 54%). IR (hexane): 2108 (m), 2075 (vs), 2058 (sh), 2042 (vs), 2016 (sh), 1911 (w), $\nu_{C\equiv O}$, 1721 (m, $\nu_{C=O}$). ^{1}H NMR (300.13 MHz, $CDCl_3$): δ 3.78 (s, 3H, OCH_3), 3.79 (s, 3H, OCH_3). Anal. Calcd. for $C_{15}H_6Co_2O_{13}Ru$: C, 29.38; H, 0.99. Found: C, 29.59; H, 1.15.

Synthesis of [$RuCo_2(CO)_9(\mu_3$-η^2-$HC_2Ph)$] (7). Cluster **7** (0.047 g, 0.082 mmol, 34%) was obtained as red crystals by a similar procedure and workup to **6** by addition of $[Cu(NCMe)_4]BF_4$ (0.074 g, 0.237 mmol) to a solution of NEt_4•**2** (0.187 g, 0.237 mmol) in 30 mL THF. IR (hexane, ν_{CO}): 2098 (s), 2062 (vs), 2047 (vs), 2036 (vs), 2012 (s), 1900 (m, br). ^{1}H NMR (300.13 MHz, $CDCl_3$): δ 7.10-7.45 (m, 5H, Ph), 7.97 (br s, 0.5 H, CH of one isomer), 9.59 (br s, 0.5 H, CH of the other isomer). Anal. Calcd. for $C_{17}H_6Co_2O_9Ru$: C, 35.62; H, 1.06. Found: C, 35.84; H, 1.19.

Synthesis of [$RuCo_2(CO)_9(\mu_3$-η^2-$HC_2(Me)C{=}CH_2)$] (8). By a similar procedure to that leading to **6** or **7**, cluster **8** (0.099 g, 0.186 mmol, 38%) was obtained by reaction of NEt_4•**3** (0.364 g, 0.483 mmol) in 35 mL of THF with $[Cu(NCMe)_4]BF_4$ (0.304 g, 0.966 mmol). IR (hexane, ν_{CO}): 2098 (m), 2061 (vs), 2046 (vs), 2034 (vs), 2022 (s), 2010 (s), 1902 (br,w)· ^{1}H NMR (300.13 MHz, $CDCl_3$): δ 1.98 (m, 1.5H, $CH^AH^B{=}C(CH_3)$, X_3 part of an ABX_3 spin system of the first isomer), 2.19 (m, 1.5H, $CH^AH^B{=}C(CH_3)$, X_3 part of an ABX_3 spin system of the second isomer), 4.78 (m, 0.5H, $CH^AH^B{=}C(CH_3)$, A part of an ABX_3 spin system of the first isomer), 4.81 (m, 0.5H, $CH^AH^B{=}C(CH_3)$, B part of an ABX_3 spin system of the first isomer), 4.84 (m, 0.5H, $CH^AH^B{=}C(CH_3)$, A part of an ABX_3 spin system of the second isomer), 4.98 (m, 0.5H, $CH^AH^B{=}C(CH_3)$, B part of an ABX_3 spin system of the second isomer), 7.83 (br s, 0.5H, HC_2 of the second isomer), 9.36 (br s, 0.5H, HC_2 of the first isomer). Anal. Calcd. for $C_{14}H_6Co_2O_9Ru$: C, 31.31; H, 1.13; Found: C, 31.46; H, 1.25.

Synthesis of [NEt_4][$RuCo_3(CO)_{10}(\mu_4$-η^2-$PhC_2C(O)NH(CH_2)_3Si(OMe)_3$] ($NEt_4$•9). A slight excess of $PhC{\equiv}CC(O)NH(CH_2)_3Si(OMe)_3$ (**L^2**) (0.122 g, 0.397 mmol) was reacted with $[NEt_4][RuCo_3(CO)_{12}]$ (0.212 g, 0.284 mmol) in 50 mL refluxing THF for 6 h. Treatment of the solution by the procedures detailed above for related clusters and

purification by repeated reprecipitations of the product from CH_2Cl_2/pentane and then CH_2Cl_2/hexane afforded NEt_4•**9** (0.240 g, 0.241 mmol, 85%) as a violet powder. IR (CH_2Cl_2): 2052 (m), 2011 (vs), 1976 (s), 1826 (m), $\nu_{C\equiv O}$, 1650 (m, $\nu_{C=O}$). ^{1}H NMR (300.13 MHz, CD_2Cl_2): δ 0.34 (m, 1H, $SiCH_2$ of one isomer), 0.49 (m, 1H, $SiCH_2$ of the other isomer), 1.19 (m, 13H, $CH_2CH_2CH_2$ of one isomer and NCH_2CH_3), 1.45 (m, 1H, $CH_2CH_2CH_2$ of the other isomer), 2.86 (m, 1H, NCH_2, of one isomer), 3.10 (m, 9H, NCH_2 of the other isomer and NCH_2CH_3), 3.47 (s, 4.5H, $Si(OMe)_3$ of one isomer), 3.50 (s, 4.5H, $Si(OMe)_3$ of the other isomer), 5.30 (br, NH of one isomer), 5.85 (br, NH of the other isomer), 7.03-7.11 (m, 5H, Ph). Anal. Calcd. for $C_{33}H_{41}Co_3N_2O_{14}RuSi$•1/3$C_6H_{14}$: C, 41.05; H, 4.49; N, 2.73. Found: C, 40.83; H, 3.91; N, 2.91.

Synthesis of $[NEt_4][FeCo_3(CO)_{10}(\mu_4\text{-}\eta^2\text{-}PhC_2C(O)NH(CH_2)_3Si(OMe)_3]$ (NEt_4•10). A four-fold excess of $PhC{\equiv}CC(O)NH(CH_2)_3Si(OMe)_3$ (**L^2**) (0.443 g, 1.44 mmol) was reacted with $[NEt_4][FeCo_3(CO)_{12}]$ (0.250 g, 0.357 mmol) in 50 mL refluxing THF for 4 h. The intense violet-black product was isolated by a procedure similar to that for NEt_4•**2**. Purification by repeated reprecipitation from CH_2Cl_2/pentane and then CH_2Cl_2/hexane at –20 °C afforded NEt_4•**10** (0.280 g, 0.295 mmol, 83%). IR (CH_2Cl_2): 2051 (m), 2003 (vs), 1996 (sh), 1932 (m,sh), 1813 (m,br), $\nu_{C\equiv O}$, 1650 (m, $\nu_{C=O}$). ^{1}H NMR (400.13 MHz, $CDCl_3$): δ 0.40 (m, 1H, $SiCH_2$ of one isomer), 0.50 (m, 1H, $SiCH_2$ of the other isomer), 1.13 (t, ^3J(HH) = 7.1 Hz, 12H, CH_2CH_3), 1.30 (m, 2H, $CH_2CH_2CH_2$), 2.97 (m, 1H, NCH_2 of one isomer), 3.11 (m, 1H, NCH_2 of the other isomer), 3.44 (q, ^3J(HH) = 7.1 Hz, 8H, CH_2CH_3), 3.48 (s, 4.5H, $Si(OMe)_3$ of one isomer), 3.50 (s, 4.5H, $Si(OMe)_3$) of the other isomer), 5.64 (br, NH of one isomer), 6.20 (br, NH of the other isomer), 6.74-7.85 (m, 5H, Ph). Anal. Calcd. for $C_{33}H_{41}Co_3FeN_2O_{14}Si$•1/2$C_6H_{14}$: C, 43.52; H, 4.87; N, 2.82, Found, C, 43.27; H, 4.39; N, 3.36.

Synthesis of [NEt_4][$RuCo_3(CO)_{10}(\mu_4$-η^2-$Me_3SiC_2C{\equiv}CSiMe_3)$] ($NEt_4$•11). To a solution of [$NEt_4$][$RuCo_3(CO)_{12}$] (0.206 g, 0.276 mmol) in 30 mL THF was added 1,4-bis(trimethylsilyl)butadiyne (0.059 g, 0.303 mmol). After refluxing for 7 h, the solution was evaporated under reduced pressure and the resulting solid was washed with hexane to remove excess alkyne. The resulting solid was extracted with CH_2Cl_2, the solution was filtered, concentrated and and addition of hexane afforded violet, air-stable crystals of NEt_4•**11** (0.166 g, 0.188 mmol, 68%). IR (CH_2Cl_2, ν_{CO}): 2047 (m), 2004 (vs), 1973 (s), 1820 (m). ^{1}H NMR (500.13 MHz, $CDCl_3$): δ 0.035 (s, 5.4H, ≡$CSiMe_3$ of the first isomer), 0.094 (s, 3.6H, ≡$CSiMe_3$ of the second isomer), 0.108 (s, 3.6H, -C_2SiMe_3 of second isomer), 0.24 (s, 5.4H, -C_2SiMe_3 of the first isomer), 1.39 (m, 12H, CH_2CH_3), 3.27 (m, 8H, CH_2CH_3). Anal. Calcd. for $C_{28}H_{38}Co_3NO_{10}RuSi_2$: C, 38.10; H, 4.34; N, 1.59. Found: C, 37.81; H, 4.39; N, 1.57.

Synthesis of [$RuCo_2(CO)_9(\mu_3$-η^2-$HC_2C{\equiv}CSiMe_3)$] (12). The red cluster **12** (0.017 g, 0.029 mmol, 22%) was obtained similarly to **6-8** by reaction of NEt_4•**11** (0.118 g, 0.134 mmol) with [$Cu(NCMe)_4$]BF_4 (0.084 g, 0.268 mmol) in 25 mL of THF at room temperature. Surprisingly, partial desilylation of the ligand occurred (see text). IR (hexane, ν_{CO}): 2100 (m), 2066 (vs), 2055 (vs), 2037 (vs), 2011 (m,w), 1903 (w). ^{1}H NMR (300.13 MHz, $CDCl_3$): δ 0.15 (s, 4.5H, $SiMe_3$ of one isomer), 0.19 (s, 4.5H, $SiMe_3$ of the other isomer), 8.02 (br s, 0.5H, -C_2H of one isomer), 9.48 (br s, 0.5H, -C_2H of the other isomer). FAB$^+$/MS: *m/z* 594 (M^+), 566 (M - CO)$^+$, 538 (M^+ - 2 CO)$^+$, 510 (M – 3 CO)$^+$, 482 (M – 4 CO)$^+$, 454 (M – 5 CO)$^+$, 426 (M – 6 CO)$^+$, 398 (M – 7 CO)$^+$. Satisfactory elemental analyses could not be obtained.

Synthesis of [$RuCo_3(CO)_9(NO)(\mu_4$-η^2-$Me_3SiC_2C{\equiv}CSiMe_3)$] (13). Solid $[NO]BF_4$ (0.057 g, 0.490 mmol) was added to a suspension of NEt_4•**11** (0.226 g, 0.256 mmol) in 25 mL CH_2Cl_2. After being stirred for 40 min at room temperature, the reaction was stopped and the solution was filtered and concentrated under reduced pressure. Separation by preparative TLC (SiO_2) using hexane as eluent afforded two bands. The first red band contains **12** (0.016 g, 0.028 mmol, 11%) described above and the brown band contains **13** (0.040 g, 0.053 mmol, 21%) with the following data: IR (hexane): 2084 (m), 2055 (vs), 2045 (s), 2037 (s), 2022 (m), 2005 (m), 1915 (s), 1888 (m), 1874 (m), $\nu_{C\equiv O}$, 1805 (m, ν_{NO}). ^1H NMR (300.13 MHz, $CDCl_3$): δ 0.09 (s, 9H, $SiMe_3$), 0.35 (s, 9H, $SiMe_3$). FAB^+/MS: *m/z* 755 (M^+), 727 (M - CO)$^+$, 699 (M – 2 CO)$^+$, 671 (M – 3 CO)$^+$, 643 (M – 4 CO)$^+$, 615 (M – 5 CO)$^+$, 587 (M – 6 CO)$^+$, 531 (M – 8 CO)$^+$, 503 (M – 9 CO)$^+$. Satisfactory elemental analyses could not be obtained.

Synthesis of [NEt_4][$RuCo_3(CO)_9(PPh_3)(\mu_4$-$\eta^2$-$Me_3SiC_2C{\equiv}CSiMe_3)$] ($NEt_4$•14). Cluster NEt_4•**11** (0.161 g, 0.182 mmol) and $[AuCl(PPh_3)]$ (0.090 g, 0.182 mmol) were refluxed in 40 mL of toluene for 3 h. The dark-brown solution was filtered, evaporated and the solid was recrystallized from CH_2Cl_2/pentane to yield violet crystals of NEt_4•**14** (0.081 g, 0.073 mmol, 41%). This product was also obtained, in a better yield (55%), by reaction of NEt_4•**11** with one equivalent of PPh_3 in refluxing toluene. IR (CH_2Cl_2, ν_{CO}): 2060 (w), 2021 (s), 1969 (vs), 1948 (sh), 1798 (m). ^1H NMR (300.13 MHz, acetone-d_6): δ -0.47 (s, 9H, ≡$CSiMe_3$), 0.35 (s, 9H, -C_2SiMe_3), 1.33 (m, 12H, CH_2CH_3), 3.43 (m, 8H, CH_2CH_3), 7.57-7.95 (m, 15H, Ph). $^{31}P\{^1H\}$ NMR (acetone-d_6) δ: 44.0 (s, $w_{1/2}$ = 50 Hz). Anal. Calcd. for $C_{45}H_{53}Co_3NO_9PRuSi_2$: C, 48.39; H, 4.78; N, 1.25. Found: C, 48.58; H, 4.96; N, 1.39.

Proto-desilylation of [NEt$_4$][RuCo$_3$(CO)$_{10}$(μ_4-η^2-Me$_3$SiC$_2$C≡CSiMe$_3$)] (NEt$_4$•11). To a solution of NEt$_4$•**11** (0.274 g, 0.311 mmol) in 10 mL of THF was added dropwise N(*n*-Bu)$_4$F (1.0 M in THF/5 wt% H_2O; 0.077 mL, 0.077 mmol) with stirring. After 45 min, the solvent was evaporated to dryness and the product was extracted from CH_2Cl_2 and the solution was filtered, concentrated and addition of hexane afforded after 10 days violet crystals of [N(*n*-Bu)$_4$)][RuCo$_3$(CO)$_{10}$(μ_4-η^2-Me$_3$SiC$_2$C≡CH)] ([N(*n*-Bu)$_4$]•**15**) (0.051 g, 0.055 mmol, 18%) and a paste containing mixture of [NEt$_4$][RuCo$_3$(CO)$_{10}$(μ_4-η^2-Me$_3$SiC$_2$C≡CH)] (NEt$_4$•**15**) and N(*n*-Bu)$_4$•**15** (0.179 g). Data for N(*n*-Bu)$_4$•**15**: IR ($CDCl_3$, ν_{CO}): 2048 (m), 2005 (vs), 1972 (s), 1818 (m). ^{1}H NMR (300.13 MHz, $CDCl_3$): δ 0.12 (s, 3H, -C$_2$SiMe$_3$ of the first isomer), 0.25 (s, 6H, -C$_2$SiMe$_3$ of the second isomer), 1.04 (m, 12H, CH$_2$C*H*$_3$), 1.42 (m, 8H, C*H*$_2$CH$_3$), 1.59 (m, 8H, CH$_2$C*H*$_2$CH$_2$), 3.25 (m, 8H, NCH$_2$), 3.41 (s, 0.66H, C-H of the second isomer), 3.51 (s, 0.34H, C-H of the first isomer).

Synthesis and proto-desilylation of [PPN][RuCo$_3$(CO)$_{10}$(μ_4-η^2-Me$_3$SiC$_2$C≡CSiMe$_3$)] (PPN•11). A solution of NEt$_4$•**11** (0.218 g, 0.247 mmol) and solid PPNCl (0.156 g, 0.272 mmol) in 20 mL of THF was heated at 60 °C for 2 h. The solution was cooled to –20 °C then filtered and the solvent was evaporated. Purification from toluene/pentane afforded violet PPN•**11** (0.303 g, 0.234 mmol, 95%), characterized by its ^{1}H NMR spectrum. ^{1}H NMR (300.13 MHz, $CDCl_3$): δ 0.012 (s, 5.4H, ≡CSiMe$_3$ of the first isomer), 0.097 (s, 3.6H, ≡CSiMe$_3$ of the second isomer), 0.118 (s, 3.6H, -C$_2$SiMe$_3$ of the second isomer), 0.23 (s, 5.4H, -C$_2$SiMe$_3$ of the first isomer), 7.17-7.82 (m, 30H, Ph)

To a Schlenk flask containing PPN•**11** (0.210 g, 0.162 mmol) and THF (14 mL) was added dropwise with stirring N(*n*-Bu)$_4$F (1.0 M in THF/5 wt% H_2O; 0.032 mL, 0.032 mmol). After 45 min, the solvent was evaporated to dryness and the product was extracted with toluene and the solution was filtered. Recrystallization from toluene/pentane gave

violet [PPN][$RuCo_3(CO)_{10}(\mu_4$-η^2-$Me_3SiC_2C{\equiv}CH)$] (PPN•**15**) (0.169 g, 0.139 mmol, 86%). IR (CH_2Cl_2, ν_{CO}): 2047 (m), 2005 (vs), 1973 (s), 1821 (m). ^{1}H NMR (300.13 MHz, $CDCl_3$): δ 0.11 (s, 3.6H, -C_2SiMe_3 of the first isomer), 0.24 (s, 5.4 H, -C_2SiMe_3 of the second isomer), 3.23 (s, 0.4H, C-H of the second isomer), 3.44 (s, 0.6H, C-H of the first isomer), 7.16-7.87 (m, 30H, Ph). Anal. Calcd. for $C_{53}H_{40}Co_3NO_{10}P_2RuSi$: C, 52.23; H, 3.31; N, 1.15. Found: C, 52.48; H, 3.48; N, 1.39.

Coupling reaction of [NEt_4/N(*n*-Bu)$_4$]•15 with $C_6H_4I_2$. To the mixture of [NEt_4]•**15** and [N(*n*-Bu)$_4$]•**15** (0.065 g), obtained by desilylation of [NEt_4]•**11** (see above), dissolved in THF/dry triethylamine 2/10 mL, was added a mixture of catalytic amounts of [$PdCl_2(PPh_3)_2$] and CuI. After stirring for 5 min, pure 1,4-diodobenzene (0.012 g, 0.035 mmol) was added and the mixture was heated at 50 °C for 18 h and the color of the solution changed from violet to brown. The solution was filtered, evaporated to dryness under vacuum and extraction of the solid with hexane afforded yellow [NEt_4/(*n*-Bu)$_4$N]$_2$[$Cu_2(\mu$-$I)_2I_2$] (0.01 g). Purification of the remaining solid from CH_2Cl_2/hexane at –20 °C afforded the coupled product [NEt_4/N(*n*-Bu)$_4$]$_2$[{$RuCo_3(CO)_{10}(\mu_4$-η^2-$Me_3SiC_2C{\equiv}C$-)}$_2C_6H_4$] ([NEt_4/N(*n*-Bu)$_4$]$_2$•**16**) (0.052 g). IR (CH_2Cl_2, ν_{CO}): 2047 (m), 2004 (vs), 1972 (s), 1820 (m). ES/MS *m/z* of the dianion **16**$^{2-}$: 717.5 $(M)^{2-}$, 703.5 $(M - CO)^{2-}$, 689.5 $(M - 2\ CO)^{2-}$, 675.5 $(M - 3\ CO)^{2-}$, 661.5 $(M - 4\ CO)^{2-}$, 647.5 $(M - 5\ CO)^{2-}$, 633.5 $(M - 6\ CO)^{2-}$, 619.5 $(M - 7\ CO)^{2-}$, 605.5 $(M - 8\ CO)^{2-}$, 591.5 $(M - 9\ CO)^{2-}$, 577.5 $(M - 10\ CO)^{2-}$, 563.5 $(M - 11\ CO)^{2-}$, 549.5 $(M - 12\ CO)^{2-}$, 535.5 $(M - 13\ CO)^{2-}$, 521.5 $(M - 14\ CO)^{2-}$, 507.5 $(M - 15\ CO)^{2-}$. The ^{1}H NMR spectrum (300 and 500 MHz) contained numerous poorly resolved signals corresponding to the expected mixture of isomers and associated with the NEt_4^+ and N(*n*-Bu)$_4^+$ cations.

X-ray Structural Analyses of [NEt_4][$RuCo_3(CO)_{10}(\mu_4\text{-}\eta^2\text{-}HC_2(Me)C{=}CH_2$] ($NEt_4$•3a), [$NEt_4$][$RuCo_3(CO)_{10}(\mu_4\text{-}\eta^2\text{-}HC_2CH_2OCH_2C{\equiv}CH)$] ($NEt_4$•4), [$RuCo_2(CO)_9(\mu_3\text{-}\eta^2\text{-}MeOC(O)C_2C(O)OMe$] (6), [$NEt_4$][$RuCo_3(CO)_{10}(\mu_4\text{-}\eta^2\text{-}Me_3SiC_2C{\equiv}CSiMe_3)$] ($NEt_4$•11), [$NEt_4$][$RuCo_3(CO)_9(PPh_3)(\mu_4\text{-}\eta^2\text{-}Me_3SiC_2C{\equiv}CSiMe_3)$] ($NEt_4$•14) and [*n*-$Bu_4N$][$RuCo_3(CO)_{10}(\mu_4\text{-}\eta^2\text{-}Me_3SiC_2C{\equiv}CH)$] ([$N(n\text{-}Bu)_4$]•15a). A summary of the crystal and refinement data for NEt_4•**3a,** NEt_4•**4, 6,** NEt_4•**11,** NEt_4•**14** and [$N(n\text{-}Bu)_4$]•**15a,** is given in Table 7. Single crystals were mounted on a Nonius Kappa-CCD area detector diffractometer (MoKα, λ = 0.71073 Å). The complete conditions of data collection (Denzo software) and structure refinements are given in Table 7. The cell parameters were determined from reflections taken from one set of ten frames (1.0° steps in phi angle), each at 20 s exposure. The structures were solved using direct methods (SIR97) and refined against F^2 using the SHELXL97 software.[40,41] The absorption was corrected empirically with Sortav. All non-hydrogen atoms were refined anisotropically. Hydrogen atoms were generated according to stereo-chemistry and refined using a riding model in SHELXL97.

Acknowledgment. We thank Dr. C. Estournès (IPCMS Strasbourg) for the TEM and magnetic studies and helpful discussions. We are grateful to the CNRS, the Université Louis Pasteur Strasbourg and the Ministère de la Recherche (Paris) (ACI Nanostructures 2001) for financial support. This project was also supported by the Fonds International de Coopération Universitaire - FICU (AUPELF-UREF, Agence Universitaire de la Francophonie) and by the International Research Training Group 532 "Physical Methods for the Structural Investigation of New Materials" (DFG Bonn, CNRS, Ministère de la Recherche, Paris).

Supporting Information Available. Tables of atomic coordinates, thermal parameters, bond distances, and angles for NEt_4•**3a**, NEt_4•**4**, **6,** NEt_4•**11**, NEt_4•**14** and [N(*n*-Bu)$_4$]•**15**, respectively. This material is available free of charge via the Internet at http://pubs.acs.org. This material has also been deposited in .cif format with the Cambridge Crystallographic Data Centre as Supplementary publication N° CCDC-218645-218650. Copies of the data can be obtained free of charge on application to CCDC, 12 Union Road, Cambridge CB2 1EZ, UK (fax: (+44)1223-336-033; e-mail: deposit@ccdc.cam.ac.uk).

References

(1) (a) Schweyer, F.; Braunstein, P.; Estournès, C.; Guille, J.; Kessler, H.; Paillaud, J.-L.; Rosé, J. *Chem. Commun.* **2000**, 1271-1272; (b) Schweyer-Tihay, F.; Braunstein, P.; Estournès, C.; Guille, J. L.; Lebeau, B.; Paillaud, J.–L.; Richard-Plouet, M.; Rosé, J. *Chem. Mater.* **2003**, *15*, 57-62.

(2) Braunstein, P.; Kormann, H. -P.; Meyer-Zaika, W.; Pugin, R.; Schmid, G. *Chem. Eur. J.* **2000**, *6*, 4637-4646.

(3) See for example: (a) Sappa, E.; Tiripicchio, A.; Braunstein, P. *Chem. Rev.* **1983**, *83*, 203-239; (b) Raithby, P. R.; Rosales, M. J. *Adv. Inorg. Chem. Radiochem.* **1985**, *29*, 169-247; (c) Chetcuti, M. J.; Fanwick, P. E.; Gordon, J. C. *Inorg. Chem.* **1991**, *30*, 4710-4717; (d) Waterman, S. M.; Humphrey, M. G.; Tolhurst, V.-A.; Bruce, M. I.; Low, P. J.; Hockless, D. C. R. *Organometallics* **1998**, *17*, 5789-5795; (e) Zhu, B.-H.; Zhang, W.-Q.; Zhao, Q.-Y.; Bian, Z.-G.; Hu, B.; Zhang, Y.-H.; Yin, Y.-Q.; Sun, J. *J. Organomet. Chem.* **2002**, *650*, 181-187.

(4) Choualeb, A.; Braunstein, P.; Rosé, J.; Bouaoud, S. E.; Welter, R. *Organometallics,* in press.

(5) Choualeb, A.; Rosé, J.; Braunstein, P.; Welter, R. *Organometallics* **2003***, 22,* 2688-2693.

(6) Bruce, M. I.; Smith, M. E.; Zaitseva, N. N.; Skelton, B. W.; White, A. H. *J. Organomet. Chem.* **2003**, *670*, 170-177.

(7) Worth, G. H.; Robinson, B. H.; Simpson, J. *Organometallics* **1992**, *11*, 3863-3874.

(8) Wong, W.-Y.; Cheung, S.-H.; Lee, S.-M.; Leung, S.-Y. *J. Organomet. Chem.* **2000**, *596*, 36-45.

(9) Osella, D.; Gambino, O.; Nevi, C.; Ravera, M.; Bertolino, D. *Inorg. Chim. Acta* **1993**, *206*, 155-161.

(10) Fritch, J. R.; Vollhardt, K. P. C. *Angew. Chem., Int. Ed. Engl.* **1980**, *19*, 559-561.

(11) Dellaca, R. J.; Penfold, B. R.; Robinson, B. H.; Robinson, W. T.; Spencer, J. L. *Inorg. Chem*. **1970**, *9*, 2204-2211.

(12) Dellaca, R. J.; Penfold, B. R. *Inorg. Chem*. **1971**, *10*, 1269-1275.

(13) Bruce, M. I.; Williams, M. L.; Patrick, J. M.; White, A. H. *J. Chem. Soc., Dalton Trans*. **1985**, 1229-1234.

(14) Adams, C. J.; Bruce, M. I.; Horn, E.; Skelton, B. W.; Tiekink, E. R. T.; White, A. H. *J. Chem. Soc., Dalton Trans*. **1993**, 3299-3312.

(15) Lucas, N. T.; Notaras, E. G. A.; Cifuentes, M. P.; Humphrey, M. G. *Organometallics* **2003**, *22*, 284-301.

(16) Imhof, D.; Burckhardt, U.; Dahmen, K.-H.; Joho, F.; Nesper, R. *Inorg. Chem*. **1997**, *36*, 1813-1820.

(17) Bruce, M. I.; Halet, J.-F.; Kahlal, S.; Low, P. J.; Skelton, B. W.; White, A. H. *J. Organomet. Chem*. **1999**, *578*, 155-168.

(18) Braunstein, P.; Rosé, J.; Bars, O. *J. Organomet. Chem.* **1983**, *252*, C101-C105.

(19) Lucas, N. T.; Humphrey, M. G.; Healy, P. C.; Williams, M. L. *J. Organomet. Chem*. **1997**, *545-546*, 519-530.

(20) Benali-Baitich, O.; Daran, J. -C.; Jeannin, Y. *J. Organomet. Chem*. **1988**, *344*, 393-400.

(21) Cazanoue, M.; Lugan, N.; Bonnet, J.-J.; Mathieu, R. *Organometallics* **1988,** *7*, 2480-2486.

(22) Wade, K, *Adv. Inorg. Chem. Radiochem*. **1976**, *18*, 1.

(23) Crabtree, R. H.; Lavin, M. *Inorg. Chem*. **1986**, *25*, 805-812.

(24) (a) Braunstein, P.; Rosé, J.; Dedieu, A.; Dusausoy, Y.; Mangeot, J.-P.; Tiripicchio, A.; Tiripicchio-Camellini, M, *J. Chem. Soc., Dalton Trans.* **1986**, 225-234; (b) Braunstein, P.;

Rosé, J.; Tiripicchio, A.; Tiripicchio-Camellini, M, *J. Chem. Soc., Dalton Trans.,* **1992**, 911-920. (c) Braunstein, P.; Rosé, J, *Inorg. Synth.,* **1989**, *26,* 356-360.

(25) Lindner, E.; Enderle, A.; Baumann, A. *J. Organomet. Chem*. **1998**, *558*, 235-237.

(26) Lindner, E.; Salesch, T. *J. Organomet. Chem*. **2001**, *628*, 151-154.

(27) Ferrand, V.; Süss-Fink, G.; Neels, A.; Stoeckli-Evans, H. *Eur. J. Inorg. Chem.* **1999**, 853-862.

(28) Aime, S.; Milone, L.; Osella, D.; Tiripicchio, A.; Manotti-Lanfredi, A. M. *Inorg. Chem*. **1982**, *21*, 501-505.

(29) Cooke, C. G.; Mays, M. J. *J. Organomet. Chem*. **1974**, *74*, 449-455.

(30) Rubin, Y.; Knobler, C. B.; Diederich, F. *J. Am. Chem. Soc.* **1990**, *112*, 4966-4968.

(31) Bruce, M. I.; Low, P. J.; Werth, A.; Skelton, B. W.; White, A. H. *J. Chem. Soc., Dalton Trans.* **1996**, 1551-1566.

(32) Braunstein, P.; Jiao, F. Y.; Rosé, J.; Granger, P.; Balegroune, F.; Bars, O.; Grandjean, D. *J. Chem. Soc., Dalton Trans.* **1992**, 2543-2550.

(33) Bouherour, S.; Braunstein, P.; Rosé, J.; Toupet, L. *Organometallics* **1999,** *18,* 4908-4915.

(34) (a) Dembinski, R.; Bartik, T.; Bartik, B.; Jaeger, M.; Gladysz, J. A. *J. Am. Chem. Soc.* **2000**, *122*, 810-822; (b) Mohr, W.; Peters, T. B.; Bohling, J. C.; Hampel, F.; Arif, A. M.; Gladysz, J. A. *C. R. Chimie* **2002**, *5*, 111-118; (c) Dembinski, R.; Lis, T.; Szafert, S.; Mayne, C. L.; Bartik, T.; Gladysz, J. A. *J. Organomet. Chem*. **1999**, *578*, 229-246.

(35) Sonogashira, K. *J. Organomet. Chem.* **2002**, *653*, 46-49.

(36) (a) Su, C.-Y.; Cai, Y.-P.; Chen, C.-L.; Lissner, F.; Kang, B.-S.; Kaim, W. *Angew. Chem. Int. Ed.* **2002**, *41*, 3371-3375; (b) Pfitzner, A.; Schmitz, D. *Z. anorg. allg. Chem.* **1997,** *623,* 1555-1560 and references cited.

(37) Behr, O. M.; Eglinton, G.; Raphael, R. A. *J. Chem. Soc.* **1960***,* 3614-3625.

(38) Choualeb, A., PhD Thesis, Université Louis Pasteur, Strasbourg (France), Sept. 2003.

(39) Chini, P.; Colli, L.; Peraldo, M, *Gazz. Chim. Ital.,* **1960**, *90,* 1005-1020.

(40) Kappa CCD Operation Manual, Nonius B.V., Delft, The Netherlands, **1997**.

(41) Sheldrick, G. M. SHELXL97, Program for the refinement of crystal structures, University of Gottingen, Germany, **1997**.

Table 1. Selected bond [Å] and bond angles [°] for **3** with estimated standard deviations in parentheses.

Molecule A

Ru(1)-Co(1)	2.751(1)	Co(2)-C(4)	1.78(1)
Ru(1)-Co(2)	2.541(2)	Co(2)-C(5)	1.74(1)
Ru(1)-Co(3)	2.545(2)	Co(2)-C(6)	1.84(1)
Ru(1)-C(6)	2.17(1)	Co(2)-C(11)	2.067(8)
Ru(1)-C(8)	2.17(1)	Co(2)-C(12)	2.121(9)
Ru(1)-C(9)	1.87(1)	Co(3)-C(3)	1.78(1)
Ru(1)-C(10)	1.88(1)	Co(3)-C(7)	1.74(1)
Ru(1)-C(12)	2.216(9)	Co(3)-C(8)	1.83(1)
Co(1)-Co(2)	2.462(2)	Co(3)-C(11)	2.070(8)
Co(1)-Co(3)	2.464(2)	Co(3)-C(12)	2.070(8)
Co(1)-C(1)	1.78(1)	C(11)-C12	1.39(1)
Co(1)-C(2)	1.74(1)	C(12)-C(13)	1.49(1)
Co(1)-C(3)	2.35(1)	C(13)-C(14)	1.52(2)
Co(1)-C(4)	2.32(1)	C(13)-C(15)	1.30(1)
Co(1)-C(11)	1.97(9)		

C(12)-Ru(1)-Co(2)	52.4(2)	O(3)-C(3)-Co(1)	126.9(9)
C(12)-Ru(1)-Co(3)	51.0(2)	O(3)-C(3)-Co(3)	161.0(1)
Co(2)-Ru(1)-Co(3)	87.95(4)	O(4)-C(4)-Co(1)	128.3(9)
C(12)-Ru(1)-Co(1)	68.2(2)	O(4)-C(4)-Co(2)	159.0(1)
Co(2)-Ru(1)-Co(1)	55.28(4)	O(5)-C(5)-Co(2)	178.6(11)
Co(3)-Ru(1)-Co(1)	55.29(4)	O(6)-C(6)-Co(2)	145.9(9)
C(11)-Co(1)-Co(2)	54.3(2)	O(6)-C(6)-Ru(1)	135.6(8)
C(11)-Co(1)-Co(3)	54.3(2)	O(7)-C(7)-Co(3)	175.0(13)
Co(2)-Co(1)-Co(3)	91.59(6)	O(8)-C(8)-Co(3)	144.6(9)
C(11)-Co(1)-Ru(1)	73.8(2)	O(8)-C(8)-Ru(1)	136.9(8)
Co(2)-Co(1)-Ru(1)	58.03(4)	O(9)-C(9)-Ru(1)	179.0(1)
Co(3)-Co(1)-Ru(1)	58.10(4)	O(10)-C(10)-Ru(1)	178.4(9)
C(11)-Co(2)-C(12)	38.8(3)	C(12)-C(11)-Co(1)	113.2(6)
C(11)-Co(2)-Co(1)	50.5(3)	C(12)-C(11)-Co(2)	72.7(5)
C(12)-Co(2)-Co(1)	75.6(2)	Co(1)-C(11)-Co(2)	75.2(3)
C(11)-Co(2)-Ru(1)	77.3(2)	C(12)-C(11)-Co(3)	70.4(5)
C(12)-Co(2)-Ru(1)	55.9(2)	Co(1)-C(11)-Co(3)	75.2(3)
Co(1)-Co(2)-Ru(1)	66.69(4)	Co(2)-C(11)-Co(3)	117.2(4)
C(11)-Co(3)-C(12)	39.3(3)	C(11)-C(12)-C(13)	125.4(8)
C(11)-Co(3)-Co(1)	50.5(3)	C(11)-C(12)-Co(3)	70.4(5)
C(12)-Co(3)-Co(1)	76.4(3)	C(11)-C(12)-Co(2)	68.5(5)
C(11)-Co(3)-Ru(1)	77.1(2)	C(13)-C(12)-Co(2)	119.7(6)
C(12)-Co(3)-Ru(1)	56.3(3)	Co(3)-C(12)-Co(2)	114.8(4)
Co(1)-Co(3)-Ru(1)	66.61(4)	C(11)-C(12)-Ru(1)	104.8(6)
O(1)-C(1)-Co(1)	177.8(10)	Co(3)-C(12)-Ru(1)	72.8(3)
O(2)-C(2)-Co(1)	177.1(12)	Co(2)-C(12)-Ru(1)	71.7(3)

Table 1 (continued).

Molecule B

Ru(2)-Co(4)	2.724(2)	Co(5)-C(27)	1.81(1)
Ru(2)-Co(5)	2.573(2)	Co(5)-C(28)	1.72(1)
Ru(2)-Co(6)	2.542(1)	Co(5)-C(29)	1.93(1)
Ru(2)-C(29)	2.11(1)	Co(5)-C(34)	2.081(9)
Ru(2)-C(31)	2.28(1)	Co(5)-C(35)	2.056(8)
Ru(2)-C(32)	1.85(1)	Co(6)-C(26)	1.83(1)
Ru(2)-C(33)	1.90(1)	Co(6)-C(30)	1.75(1)
Ru(2)-C(35)	2.174(8)	Co(6)-C(31)	1.79(1)
Co(4)-Co(5)	2.487(2)	Co(6)-C(34)	2.071(9)
Co(4)-Co(6)	2.433(2)	Co(6)-C(35)	2.121(8)
Co(4)-C(24)	1.80(1)	C(34)-C(35)	1.45(1)
Co(4)-C(25)	1.78(1)	C(35)-C(36)	1.48(1)
Co(4)-C(26)	2.02(1)	C(36)-C(37)	1.44(1)
Co(4)-C(34)	1.947(8)	C(36)-C(38)	1.32(1)

C(35)-Ru(2)-Co(6)	52.7(2)	O(26)-C(26)-Co(4)	133.6(8)
C(35)-Ru(2)-Co(5)	50.5(2)	O(26)-C(26)-Co(6)	148.4(9)
Co(6)-Ru(2)-Co(5)	87.63(5)	O(27)-C(27)-Co(5)	174.8(12)
C(35)-Ru(2)-Co(4)	68.7(2)	O(28)-C(28)-Co(5)	172.7(10)
Co(6)-Ru(2)-Co(4)	54.90(4)	O(29)-C(29)-Co(5)	140.0(9)
Co(5)-Ru(2)-Co(4)	55.92(5)	O(29)-C(29)-Ru(2)	141.2(9)
C(34)-Co(6)-C(35)	40.6(3)	O(30)-C(30)-Co(6)	176.1(11)
C(34)-Co(6)-Co(4)	50.4(2)	O(31)-C(31)-Co(6)	150.9(9)
C(35)-Co(6)-Co(4)	75.6(2)	O(31)-C(31)-Ru(2)	132.8(8)
C(34)-Co(6)-Ru(2)	78.0(2)	O(32)-C(32)-Ru(2)	173.9(11)
C(35)-Co(6)-Ru(2)	54.7(2)	O(33)-C(33)-Ru(2)	179.0(11)
Co(4)-Co(6)-Ru(2)	66.36(5)	C(35)-C(34)-Co(6)	71.5(5)
C(34)-Co(4)-Co(6)	55.1(3)	C(35)-C(34)-Co(4)	110.0(5)
C(34)-Co(4)-Co(5)	54.3(3)	Co(4)-C(34)-Co(6)	74.5(3)
Co(6)-Co(4)-Co(5)	92.06(6)	C(35)-C(34)-Co(5)	68.5(5)
C(34)-Co(4)-Ru(2)	75.5(2)	Co(4)-C(34)-Co(5)	76.2(3)
Co(6)-Co(4)-Ru(2)	58.74(4)	Co(6)-C(34)-Co(5)	117.1(3)
Co(5)-Co(4)-Ru(2)	58.96(4)	C(34)-C(35)-C(36)	123.5(8)
C(35)-Co(5)-C3(4)	41.2(3)	C(34)-C(35)-Co(5)	70.3(5)
C(35)-Co(5)-Co(4)	75.5(3) .	C(34)-C(35)-Co(6)	67.9(5)
C(34)-Co(5)-Co(4)	49.5(2)	Co(5)-C(35)-Co(6)	116.0(4)
C(35)-Co(5)-Ru(2)	54.7(2)	C(34)-C(35)-Ru(2)	105.7(5)
C(34)-Co(5)-Ru(2)	77.1(2)	C(36)-C(35)-Ru(2)	130.5(7)
Co(4)-Co(5)-Ru(2)	65.12(5)	Co(5)-C(35)-Ru(2)	74.9(3)
O(24)-C(24)-Co(4)	176.8(10)	Co(6)-C(35)-Ru(2)	72.6(3)
O(25)-C(25)-Co(4)	178.3(13)		

Table 2. Selected bond [Å] and bond angles [°] for **4** with estimated standard deviations in parentheses.

Ru(1)-Co(1)	2.754(1)	Co(2)-C(4)	1.745(3)
Ru(1)-Co(2)	2.570(1)	Co(2)-C(5)	1.793(3)
Ru(1)-Co(3)	2.531(1)	Co(2)-C(6)	1.889(3)
Ru(1)-C(6)	2.100(3)	Co(2)-C(11)	2.073(2)
Ru(1)-C(8)	2.221(3)	Co(2)-C(12)	2.046(2)
Ru(1)-C(9)	1.909(3)	Co(3)-C(3)	1.817(3)
Ru(1)-C(10)	1.880(3)	Co(3)-C(7)	1.755(3)
Ru(1)-C(12)	2.171(3)	Co(3)-C(8)	1.824(3)
Co(1)-Co(2)	2.4935(9)	Co(3)-C(11)	2.098(2)
Co(1)-Co(3)	2.435(1)	Co(3)-C(12)	2.134(2)
Co(1)-C(1)	1.788(3)	C(11)-C12	1.404(3)
Co(1)-C(2)	1.788(3)	C(12)-C(13)	1.501(3)
Co(1)-C(3)	2.052(3)	C(14)-C(15)	1.468(4)
Co(1)-C(11)	1.961(3)	C(15)-C(16)	1.174(5)
C(12)-Ru(1)-Co(2)	50.28(5)	O(3)-C(3)-Co(3)	149.0(2)
C(12)-Ru(1)-Co(3)	53.32(6)	O(4)-C(4)-Co(2)	174.0(3)
Co(2)-Ru(1)-Co(3)	88.33(1)	O(5)-C(5)-Co(2)	177.5(3)
C(12)-Ru(1)-Co(1)	67.75(6)	O(6)-C(6)-Co(2)	140.0(2)
Co(2)-Ru(1)-Co(1)	55.73(1)	O(6)-C(6)-Ru(1)	139.9(2)
Co(3)-Ru(1)-Co(1)	54.66(2)	O(7)-C(7)-Co(3)	178.8(3)
C(11)-Co(1)-Co(2)	53.87(7)	O(8)-C(8)-Co(3)	149.3(2)
C(11)-Co(1)-Co(3)	55.77(6)	O(8)-C(8)-Ru(1)	133.8(2)
Co(2)-Co(1)-Co(3)	92.30(4)	O(9)-C(9)-Ru(1)	179.0(3)
C(11)-Co(1)-Ru(1)	74.23(7)	O(10)-C(10)-Ru(1)	179.2(2)
Co(2)-Co(1)-Ru(1)	58.39(3)	C(12)-C(11)-Co(1)	110.8(2)
Co(3)-Co(1)-Ru(1)	58.01(1)	C(12)-C(11)-Co(2)	69.0(1)
C(11)-Co(2)-C(12)	39.86(9)	Co(1)-C(11)-Co(2)	76.32(8)
C(11)-Co(2)-Co(1)	49.82(7)	C(12)-C(11)-Co(3)	72.0(1)
C(12)-Co(2)-Co(1)	75.03(7)	Co(1)-C(11)-Co(3)	73.63(7)
C(11)-Co(2)-Ru(1)	76.93(6)	Co(2)-C(11)-Co(3)	116.9(1)
C(12)-Co(2)-Ru(1)	54.70(6)	C(11)-C(12)-C(13)	123.1(2)
Co(1)-Co(2)-Ru(1)	65.88(3)	C(11)-C(12)-Co(3)	69.2(1)
C(11)-Co(3)-C(12)	38.74(9)	C(13)-C(12)-Co(3)	118.9(2)
C(11)-Co(3)-Co(1)	50.59(6)	C(11)-C(12)-Co(2)	71.1(1)
C(12)-Co(3)-Co(1)	74.87(6)	C(13)-C(12)-Co(2)	124.1(2)
C(11)-Co(3)-Ru(1)	77.39(6)	Co(3)-C(12)-Co(2)	116.4(1)
C(12)-Co(3)-Ru(1)	54.66(6)	C(11)-C(12)-Ru(1)	107.2(2)
Co(1)-Co(3)-Ru(1)	67.33(1)	C(13)-C(12)-Ru(1)	129.3(2)
O(1)-C(1)-Co(1)	179.3(3)	Co(3)-C(12)-Ru(1)	72.02(7)
O(2)-C(2)-Co(1)	179.5(3)	Co(2)-C(12)-Ru(1)	75.02(8)
O(3)-C(3)-Co(1)	133.2(2)		

Table 3. Selected bond [Å] and bond angles [°] for **6** with estimated standard deviations in parentheses.

Co(1)-Co(2)	2.495(1)	Co(2)-C(10)	2.040(5)
Co(1)-C(1)	1.828(7)	Co(2)-C(11)	2.039(6)
Co(1)-C(2)	1.842(7)	Ru-C(6)	2.386(7)
Co(1)-C(3)	1.828(7)	Ru-C(7)	1.971(7)
Co(1)-C(10)	1.942(6)	Ru-C(8)	1.906(7)
Co(1)-Ru	2.726(1)	Ru-C(9)	1.921(7)
Co(2)-Ru	2.585(1)	Ru-C(11)	2.084(6)
Co(2)-C(4)	1.809(8)	C(10)-C(11)	1.372(8)
Co(2)-C(5)	1.766(8)	C(11)-C(12)	1.502(9)
Co(2)-C(6)	1.815(7)	C(14)-C(10)	1.492(8)
Co2-Co(1)-Ru	59.16(3)	O(6)-C(6)-Ru	130.7(5)
Co(2)-Co1-C(10)	53.0(2)	O(7)-C(7)-Ru	177.8(6)
Ru-Co(1)-C(10)	73.2(2)	O(8)-C(8)-Ru	179.2(6)
Co(1)-Co(2)-Ru	64.88(3)	O(9)-C(9)-Ru	175.2(6)
C(10)-Co(2)-Co(1)	49.5(2)	C(11)-C(10)-C14	124.1(6)
C(11)-Co(2)-Co(1)	73.1(2)	C(11)-C(10)-Co(1)	109.5(4)
C(10)-Co(2)-Ru	75.2(2)	C(14)-C(10)-Co1	125.7(4)
C(11)-Co(2)-Ru	51.9(2)	C(11)-C(10)-Co(2)	70.3(3)
Co(2)-Ru-Co(1)	55.95(3)	C(14)-C(10)-Co(2)	125.6(4)
C(11)-Ru-Co(1)	67.5(2)	Co(1)-C(10)-Co(2)	77.5(2)
C(11)-Ru-Co(2)	50.4(2)	C(10)-C(11)-C(12)	124.0(5)
O(1)-C(1)-Co(1)	178.9(7)	C(10)-C(11)-Co(2)	70.4(4)
O(2)-C(2)-Co(1)	176.6(7)	C(12)-C(11)-Co(2)	127.8(4)
O(3)-C(3)-Co1	175.9(6)	C(10)-C(11)-Ru	109.7(4)
O(4)-C(4)-Co(2)	179.0(8)	C(12)-C(11)-Ru	125.3(4)
O(5)-C(5)-Co(2)	176.6(6)	Co(2)-C(11)-Ru	77.6(2)
O(6)-C(6)-Co(2)	154.5(6)		

Table 4. Selected bond [Å] and bond angles [°] for **11** with estimated standard deviations in parentheses.

MM1–Co(2)	2.484(2)	Co(2)–C(4)	1.87(1)
MM1–Co(3)	2.512(2)	Co(2)-C(5)	1.70(2)
MM1–C(6)	2.48(1)	Co(2)-C(6)	1.77(1)
MM1–C(8)	2.03(1)	Co(2)–C(11)	2.129(9)
MM1–C(9)	1.83(1)	Co(2)–C(12)	2.065(9)
MM1–C(10)	1.81(1)	Co(3)–C(3)	1.79(1)
MM1–C(11)	2.11(1)	Co(3)–C(7)	1.77(1)
MM2–Co(2)	2.545(2)	Co(3)–C(8)	1.88(1)
MM2–Co(3)	2.487(2)	Co(3)–C(11)	2.069(9)
MM2-C(1)	1.856(9)	Co(3)–C(12)	2.101(9)
MM2-C(2)	1.81(1)	C(11)–C(12)	1.41(1)
MM2-C(3)	2.31(1)	C(12)–C(13)	1.45(1)
MM2-C(4)	2.08(1)	C(13)–C(14)	1.20(1)
MM2-C(12)	2.09(1)		
Co(2)-MM1-Co(3)	90.34(5)	Co(3)–C(7)–O(7)	177.0(1)
Co(2)-MM1-C(11)	54.5(2)	MM1-C(8)-O(8)	138.7(9)
Co(3)-MM1-C11	52.3(2)	Co(3)-C(8)-O(8)	141.5(9)
Co(2)-MM2-Co(3)	89.52(5)	MM1–C(9)–O(9)	174.3(9)
Co(2)-MM2-C(12)	51.8(3)	MM1-C(10)-O10	178.8(1)
Co(3)-MM2-C(12)	53.8(2)	MM1-C(11)-Co(2)	71.8(3)
MM1–Co(2)-C(11)	53.7(3)	MM1–C(11)–Co(3)	74.0(3)
MM1-Co(2)-C(12)	76.8(3)	MM1-C(11)-C(12)	106.4(6)
MM2-Co(2)-C(11)	76.0(2)	Co(2)–C(11)–Co(3)	115.1(4)
MM2-Co(2)-C(12)	52.7(3)	Co(2)-C(11)-C(12)	67.9(5)
C(11)–Co(2)-C(12)	39.2(3)	Co(3)-C(11)–C(12)	71.5(5)
MM1-Co(3)-C(11)	53.7(3)	MM2-C(12)-Co(2)	75.5(3)
MM1-Co(3)-C(12)	75.6(3)	MM2-C(12)–Co(3)	72.8(3)
MM2-Co(3)-C(11)	78.4(2)	MM2-C(12)-C(11)	110.3(7)
MM2-Co(3)-C(12)	53.4(3)	MM2–C(12)–C(13)	121.0(7)
C(11)-Co(3)-C(12)	39.4(3)	Co2-C(12)-Co(3)	116.5(4)
MM2-C(1)-O(1)	175.6(9)	Co(2)-C(12)-MM2	75.5(3)
MM2-C(2)-O(2)	177.0(1)	Co(2)-C(12)-C(11)	72.9(5)
MM2-C3–O(3)	128.7(8)	Co(2)-C(12)-C(13)	118.4(6)
Co(3)-C(3)-O(3)	157.2(9)	Co(3)-C(12)-MM2	72.8(3)
MM2-C(4)-O(4)	138.3(9)	Co(3)–C(12)-C(11)	69.0(5)
Co(2)–C(4)–O(4)	141.7(10)	Co(3)-C(12)-C(13)	125.0(6)
Co(2)-C(5)-O(5)	178.5(16)	C(11)-C(12)-C(13)	128.7(9)
MM1–C(6)–O(6)	128.8(8)	C(12)-C(13)-C(14)	174.0(1)
Co(2)-C(6)-O(6)	161.9(10)		

Table 5. Selected bond [Å] and bond angles [°] for **14** with estimated standard deviations in parentheses.

Ru - Co(2)	2.5106(7)	Co(1) - C(10)	2.016(4)
Ru - Co(3)	2.5880(7)	Co(2)...Co(3)	3.51(1)
Ru - P	2.345(1)	Co(2) - C(3)	1.837(4)
Ru - C(5)	2.191(4)	Co(2) - C(4)	1.747(4)
Ru - C(8)	2.026(4)	Co(2) - C(5)	1.838(4)
Ru - C(9)	1.872(4)	Co(2) - C(10)	2.081(4)
Ru - C(11)	2.222(4)	Co(2) - C(11)	2.114(4)
Co(1) - Co(2)	2.4408(8)	Co(3) - C(6)	1.765(4)
Co(1) - Co(3)	2.4697(8)	Co(3) - C(7)	1.753(5)
Co(1) - C(1)	1.777(5)	Co(3) - C(8)	1.951(4)
Co(1) - C(2)	1.775(4)	Co(3) - C(10)	2.113(4)
Co(1) - C(3)	2.055(4)	Co(3) - C(11)	2.031(4)
Co(1)-Ru-C(11)	67.7(1)	Co(1) - C(1) - O(1)	170.8(4)
Co(2)-Ru-Co(1)	55.21(2)	Co(1) - C(2) - O(2)	176.3(4)
Co(2) - Ru - Co(3)	87.05(2)	Co(1) - C(3) - O(3)	133.3(3)
Co(2) - Ru - C(11)	52.6(1)	Co(2) - C(3) - O(3)	149.3(3)
Co(3) - Ru - C(11)	49.2(1)	Co(2) - C(4) - O(4)	177.6(4)
Co(3)-Ru-Co(1)	55.17(2)	Ru - C(5) - O(5)	136.4(3)
Co(2)-Co(1)-C(10)	54.7(1)	Co(2) - C(5) - O(5)	147.0(3)
Co(2)-Co(1)-Co(3)	105.5(2)	Co(3) - C(6) - O(6)	177.3(4)
Co(2)-Co(1)-Ru	57.65(2)	Co(3) - C(7) - O(7)	172.1(5)
Co(3)-Co(1)-Ru	59.32(2)	Ru - C(8) - O(8)	145.1(3)
Co(3)-Co(1)-C(10)	55.1(1)	Co(3) - C(8) - O(8)	133.6(3)
Ru -Co(1)-C(10)	76.2(1)	Ru - C(9) - O(9)	175.0(3)
Co(1)-Co(2)-C(10)	52.2(1)	Co(1)-C(10)-Co(2)	73.1(1)
Co(1)-Co(2)-C(11)	75.4(1)	Co(1)-C(10)-Co(3)	73.4(1)
Ru-Co(2)-C(10)	80.6(1)	Co(1)-C(10)-C(11)	107.6(3)
Ru-Co(2)-C(11)	56.6(1)	Co(2)-C(10)-Co(3)	113.7(2)
Ru-Co(2)-Co(1)	67.14(2)	Co(2)-C(10)-C(11)	71.4(2)
C(10)-Co(2)-C(11)	39.6(2)	Co(3)-C(10)-C(11)	66.9(2)
Ru-Co(3)-Co(1)	65.52(2)	Ru - C(11) - Co(2)	70.7(1)
Ru-Co(3)-C(10)	78.2(1)	Ru - C(11) - Co(3)	74.8(1)
Ru-Co(3)-C(11)	55.9(1)	Ru - C(11) - C(10)	108.2(3)
Co(1)-Co(3)-C(10)	51.8(1)	Co(2)-C(11)-Co(3)	115.8(2)
Co(1)-Co(3)-C(11)	76.1(1)	Co(2)-C(11)-C(10)	69.0(2)
C(10)-Co(3)-C(11)	40.0(2)	Co(3)-C(11)-C(10)	73.1(2)

Table 6. Selected bond [Å] and bond angles [°] for n-Bu_4N•**15a** with estimated standard deviations in parentheses.

Molecule A

Ru(1)-Co(1)	2.738(1)	Co(1)-C(11)	2.051(6)
Ru(1)-Co(2)	2.519(1)	Co(2)-C(4)	1.835(8)
Ru(1)-Co(3)	2.552(1)	Co(2)-C(5)	1.759(8)
Ru(1)-C(6)	2.199(8)	Co(2)-C(6)	1.818(8)
Ru(1)-C(8)	2.093(8)	Co(2)-C(11)	2.105(8)
Ru(1)-C(9)	1.884(8)	Co(2)-C(12)	2.104(7)
Ru(1)-C(10)	1.89(1)	Co(3)-C(3)	1.781(8)
Ru(1)-C(12)	2.138(7)	Co(3)-C(7)	1.791(8)
Co(1)-Co(2)	2.445(1)	Co(3)-C(8)	1.886(8)
Co(1)-Co(3)	2.474(1)	Co(3)-C(11)	2.116(7)
Co(1)-C(1)	1.808(8)	Co(3)-C(12)	2.059(7)
Co(1)-C(2)	1.77(1)	C(11)-C12)	1.43(1)
Co(1)-C(3)	2.549(9)	C(12)-C(13)	1.44(1)
Co(1)-C(4)	2.069(7)	C(13)-C(14)	1.17(1)
C(12)-Ru(1)-Co(2)	52.96(2)	O(3)-C(3)-Co(1)	125.9(7)
C(12)-Ru(1)-Co(3)	51.2(2)	O(3)-C(3)-Co(3)	167.1(8)
Co(2)-Ru(1)-Co(3)	88.26(3)	O(4)-C(4)-Co(1)	134.0(6)
C(12)-Ru(1)-Co(1)	66.87(2)	O(4)-C(4)-Co(2)	148.6(7)
Co(2)-Ru(1)-Co(1)	55.24(3)	O(5)-C(5)-Co(2)	178.3(7)
Co(3)-Ru(1)-Co(1)	55.65(3)	O(6)-C(6)-Co(2)	148.2(6)
C(11)-Co(1)-Co(2)	55.0(2)	O(6)-C(6)-Ru(1)	134.6(6)
C(11)-Co(1)-Co(3)	54.78(2)	O(7)-C(7)-Co(3)	176.6(7)
Co(2)-Co(1)-Co(3)	91.74(4)	O(8)-C(8)-Co(3)	141.3(7)
C(11)-Co(1)-Ru(1)	75.0(2)	O(8)-C(8)-Ru(1)	138.8(7)
Co(2)-Co(1)-Ru(1)	57.803(3)	O(9)-C(9)-Ru(1)	176.3(8)
Co(3)-Co(1)-Ru(1)	58.37(3)	O(10)-C(10)-Ru(1)	178.9(7)
C(11)-Co(2)-C(12)	39.9(3)	C(12)-C(11)-Co(1)	105.6(5)
C(11)-Co(2)-Co(1)	52.9(2)	C(12)-C(11)-Co(2)	70.0(4)
C(12)-Co(2)-Co(1)	75.6(2)	Co(1)-C(11)-Co(2)	72.1(2)
C(11)-Co(2)-Ru(1)	79.2(2)	C(12)-C(11)-Co(3)	67.8(4)
C(12)-Co(2)-Ru(1)	54.2(2)	Co(1)-C(11)-Co(3)	72.8(2)
Co(1)-Co(2)-Ru(1)	66.92(3)	Co(2)-C(11)-Co(3)	113.6(3)
C(11)-Co(3)-C(12)	39.9(3)	C(11)-C(12)-Co(3)	72.0(4)
C(11)-Co(3)-Co(1)	52.4(2)	C(11)-C(12)-Co(2)	70.1(4)
C(12)-Co(3)-Co(1)	75.7(2)	Co(3)-C(12)-Co(2)	116.0(3)
C(11)-Co(3)-Ru(1)	78.2(2)	C(11)-C(12)-Ru(1)	110.6(4)
C(12)-Co(3)-Ru(1)	54.0(2)	Co(3)-C(12)-Ru(1)	74.9(2)
Co(1)-Co(3)-Ru(1)	65.99(3)	Co(2)-C(12)-Ru(1)	72.9(2)
O(1)-C(1)-Co(1)	174.7(9)	C(12)-C(13)-C(14)	175.0(9)
O(2)-C(2)-Co(1)	178.7(8)		

Table 6 (continued)

Molecule B

Ru(2)-Co(4)	2.765(1)	Co(4)-C(28)	2.064(7)
Ru(2)-Co(5)	2.54(1)	Co(5)-C(20)	1.796(8)
Ru(2)-Co(6)	2.528(1)	Co(5)-C(21)	1.757(9)
Ru(2)-C(24)	2.146(7)	Co(5)-C(27)	1.858(8)
Ru(2)-C(25)	1.874(9)	Co(5)-C(28)	2.121(7)
Ru(2)-C(26)	1.889(8)	Co(5)-C(29)	2.084(7)
Ru(2)-C(27)	2.124(9)	Co(6)-C(22)	1.808(8)
Ru(2)-C(29)	2.149(7)	Co(6)-C(23)	1.759(9)
Co(4)-Co(5)	2.47(1)	Co(6)-C(24)	1.837(8)
Co(4)-Co(6)	2.459(2)	Co(6)-C(28)	2.117(8)
Co(4)-C(18)	1.79(1)	Co(6)-C(29)	2.080(7)
Co(4)-C(19)	1.79(1)	C(28)-C(29)	1.41(1)
Co(4)-C(20)	2.279(9)	C(29)-C(30)	1.45(1)
Co(4)-C(22)	2.235(9)	C(30)-C(31)	1.20(1)

C(29)-Ru(2)-Co(6)	52.0(2)	O(11)-C(18)-Co(4)	174.6(9)
C(29)-Ru(2)-Co(5)	52.0(2)	O(12)-C(19)-Co(4)	179.1(8)
Co(6)-Ru(2)-Co(5)	88.33(4)	O(13)-C(20)-Co(4)	129.9(7)
C(29)-Ru(2)-Co(4)	68.2(2)	O(15)-C(22)-Co(6)	155.7(7)
Co(6)-Ru(2)-Co(4)	55.13(3)	O(16)-C(23)-Co(6)	179.7(7)
Co(5)-Ru(2)-Co(4)	55.23(3)	O(17)-C(24)-Co(6)	145.2(6)
C(28)-Co(6)-C(29)	39.3(3)	O(13)-C(20)-Co(5)	156.7(8)
C(28)-Co(4)-Co(5)	54.9(2)	O(14)-C(21)-Co(5)	173.7(8)
Co(6)-Co(4)-Co(5)	91.58(4)	O(17)-C(24)-Ru(2)	136.2(6)
C(28)-Co(4)-Ru(2)	74.4(2)	O(18)-C(25)-Ru(2)	177.8(7)
Co(6)-Co(4)-Ru(2)	57.53(3)	O(19)-C(26)-Ru(2)	177.7(6)
Co(5)-Co(4)-Ru(2)	57.72(3)	O(20)-C(27)-Ru(2)	136.8(6)
C(28)-Co(4)-Co(6)	55.0(2)	C(29)-C(28)-Co(4)	105.8(5)
C(29)-Co(5)-C(28)	39.2(3)	Co(4)-C(28)-Co(6)	112.8(3)
C(29)-Co(5)-Co(4)	75.4(2) .	C(29)-C(28)-Co(5)	69.0(4)
C(28)-Co(5)-Co(4)	52.8(2)	Co(4)-C(28)-Co(5)	72.2(2)
C(29)-Co(5)-Ru(2)	54.3(2)	Co(6)-C(28)-Co(5)	112.8(3)
C(28)-Co(5)-Ru(2)	78.8(2)	C(28)-C(29)-Co(5)	71.8(4)
Co(4)-Co(5)-Ru(2)	67.05(4)	C(28)-C(29)-Co(6)	71.8(4)
C(28)-Co(6)-Co(4)	53.0(2)	Co(5)-C(29)-Co(6)	116.0(3)
C(29)-Co(6)-Co(4)	75.7(2)	C(28)-C(29)-Ru(2)	111.6(5)
C(28)-Co(6)-Ru(2)	79.1(2)	Co(5)-C(29)-Ru(2)	73.7(2)
C(29)-Co(6)-Ru(2)	54.56(2)	Co(6)-C(29)-Ru(2)	116.0(3)
Co(4)-Co(6)-Ru(2)	67.34(4)	C(29)-C(30)-C(31)	174.4(8)

	NEt_4•**3**	NEt_4•**4**	**6**	NEt_4•**11**	NEt_4•**14**	N(*n*-Bu_4)•**15a**
empirical formula	$C_{23}H_{26}Co_3NO_{10}Ru$	$C_{24}H_{26}Co_3NO_{11}Ru$	$C_{15}H_6Co_2O_{13}Ru$	$C_{28}H_{38}Co_3NO_{10}RuSi_2$	$C_{45}H_{53}Co_3NO_9PRuSi_2$	$C_{33}H_{46}Co_3NO_{10}RuSi$
molecular weight	754.31	782.32	613.13	882.63	1116.89	922.66
colour	violet	violet	red	violet	violet	violet
cryst system	monoclinic	monoclinic	triclinic	orthorhombic	orthorhombic	triclinic
space group	*P* 21	$P2_1/c$	*P*-1	$P2_12_12_1$	$P2_12_12_1$	*P*-1
α (Å)	12.037(4)	9.766(5)	8.809(1)	9.886(5)	12.531(2)	10.534(1)
β (Å)	18.318(5)	11.686(5)	8.958(1)	11.468(5)	13.382(2)	14.500(1)
γ(Å)	13.362(4)	25.695(5)	13.857(1)	32.221(5)	29.276(3)	26.686(1)
α(deg)	90.00	90.00	93.529(5)	90.00	90.00	87.389(5)
β(deg)	100.958(8)	95.038(5)	106.739(5)	90.00	90.00	87.001(5)
γ(deg)	90.00	90.00	101.978(5)	90.00	90.00	86.167(5)
V (Å^3)	2892.6(15)	2921(2)	1015.72(18)	3653(3)	4909.3(12)	4057.8(5)
Z	4	4	2	4	4	4
D_{calc} (g•cm^{-3})	1.732	1.779	2.005	1.605	1.5111(4)	1.510
wavelength (Å)	0.71069	0.71069	0.71069	0.71069	0.71069	0.71069
μ (mm^{-1})	2.253	2.237	2.414	1.859	1.431	1.649
temp (K)	173(2)	173(2)	173(2)	173(2)	173(2)	293(2)
hkl limiting indices	-15/15,-21/23,-17/17	-14/14,0/17,0/38	-12/10; -12/12;-18/19	0/13,-0/16,-45/45	0/16, 0/17, -37/37	-12/13,-18/17,-34/34
F(000)	1504	1560	596	1784	2280	1880
Theta limits (deg)	2.71-27.46	0.99-32.02	2.97-30.12	2.4-30.0	2.33-27.47	2.29-27.46
Number of data meas	12018	10119	5580	10356	10871	17153
Number of data (I›2σ(I))	6888	6256	3595	6183	8984	9646
R	0.0543	0.0333	0.1232	0.0834	0.0368	0.0815
Rw	0.1279	0.0697	0.1083	0.1551	0.0770	0.1499
GOF	0.965	0.714	1.12	1.09	0.860	1.030
Largest peak in final difference (e•Å^{-3})	1.066	0.46	1.32	0.71	0.453	1.016

Captions to the Figures

Figure 1. View of the molecular structure of the anionic cluster in **3a**. Hydrogen atoms have been omitted for clarity.

Figure 2. View of the molecular structure of the anionic cluster in **4**. Hydrogen atoms have been omitted for clarity.

Figure 3. View of the molecular structure of the cluster **6**. Hydrogen atoms have been omitted for clarity.

Figure 4. View of the molecular structure of the cluster **11**. Hydrogen atoms have been omitted for clarity.

Figure 5. View of the molecular structure of the cluster **14**. Only the ipso carbons of the phenyl groups at phosphorus are shown and the hydrogen atoms have been omitted for clarity.

Figure 6. View of the molecular structure of the cluster **15a**. Hydrogen atoms have been omitted for clarity.

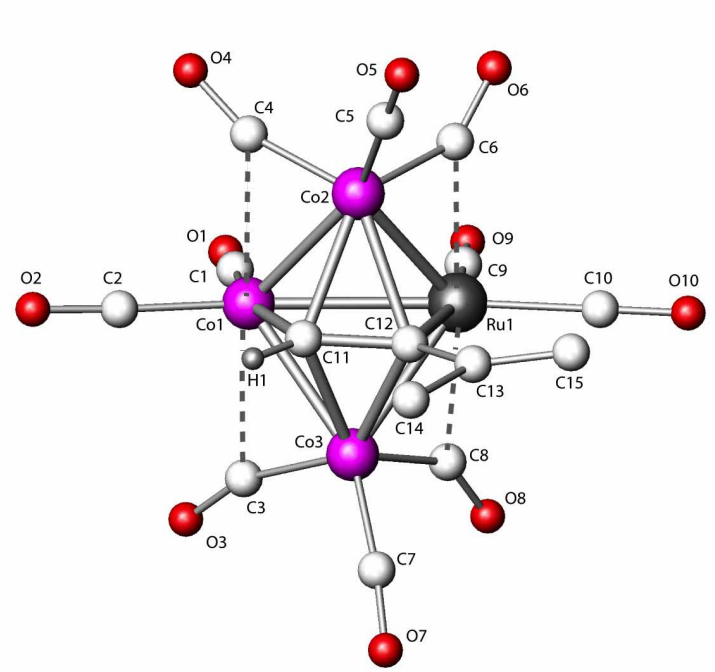

Figure 1. View of the molecular structure of the anionic cluster in **3**. Hydrogen atoms have been omitted for clarity.

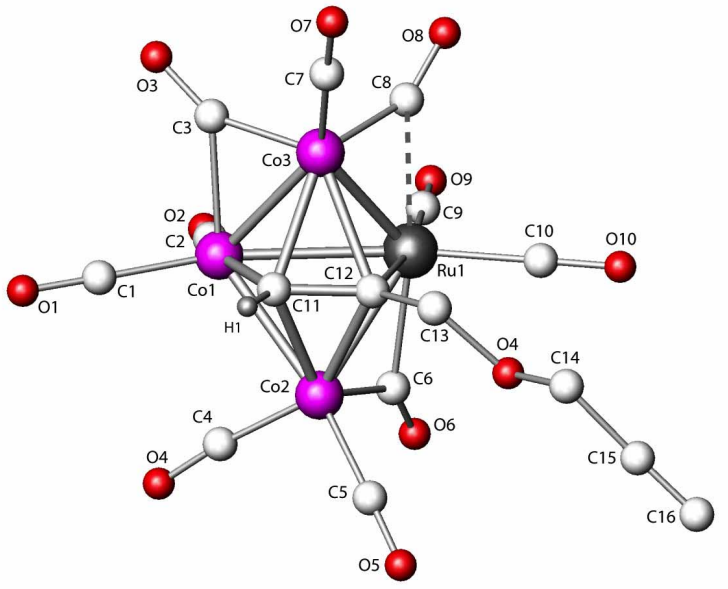

Figure 2. View of the molecular structure of the anionic cluster in **4**. Hydrogen atoms have been omitted for clarity.

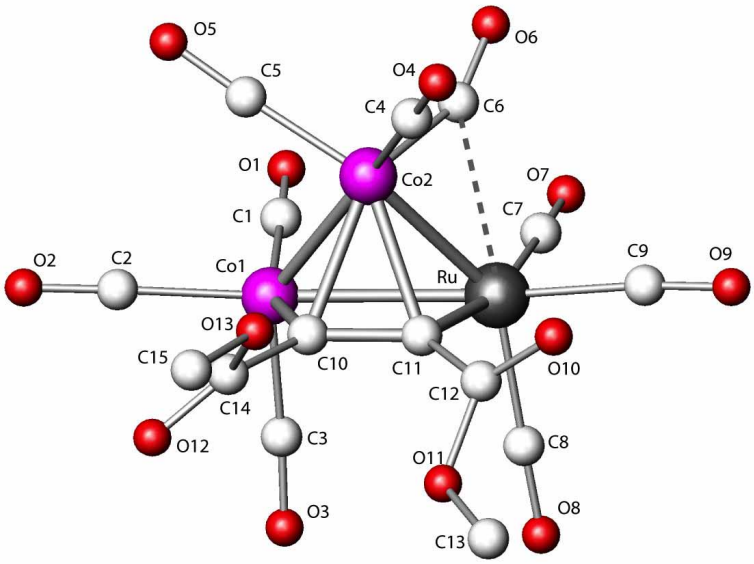

Figure 3. View of the molecular structure of the cluster **6**. Hydrogen atoms have been omitted for clarity.

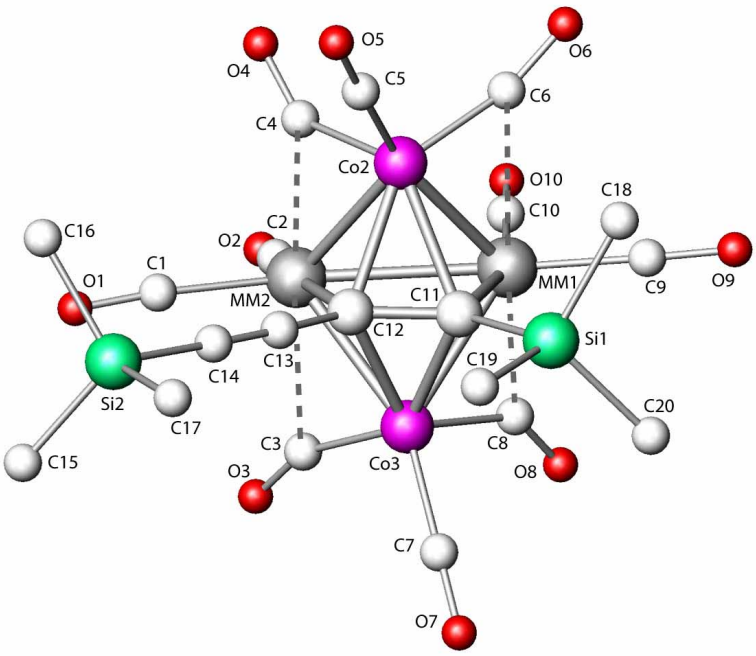

Figure 4. View of the molecular structure of the cluster **11**. Hydrogen atoms have been omitted for clarity.

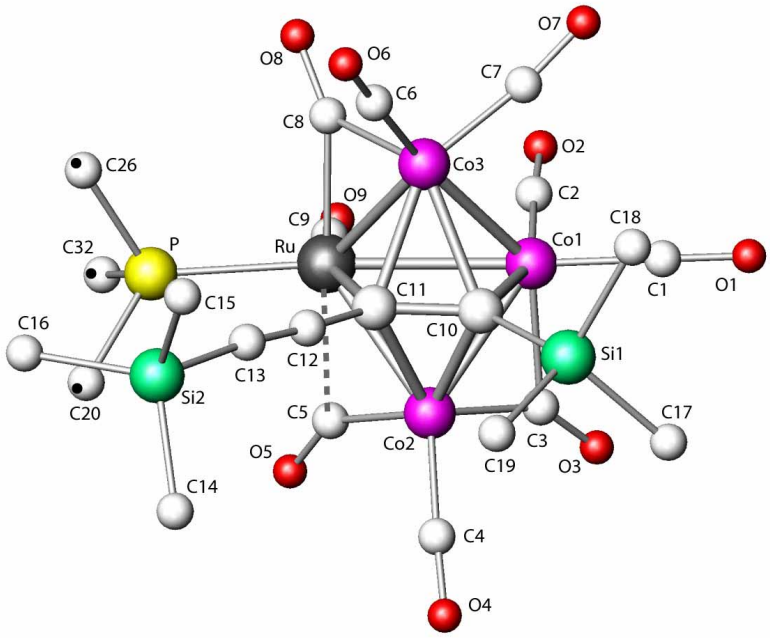

Figure 5. View of the molecular structure of the cluster **14**. Only the ipso carbons of the phenyl groups at phosphorus are shown and the hydrogen atoms have been omitted for clarity.

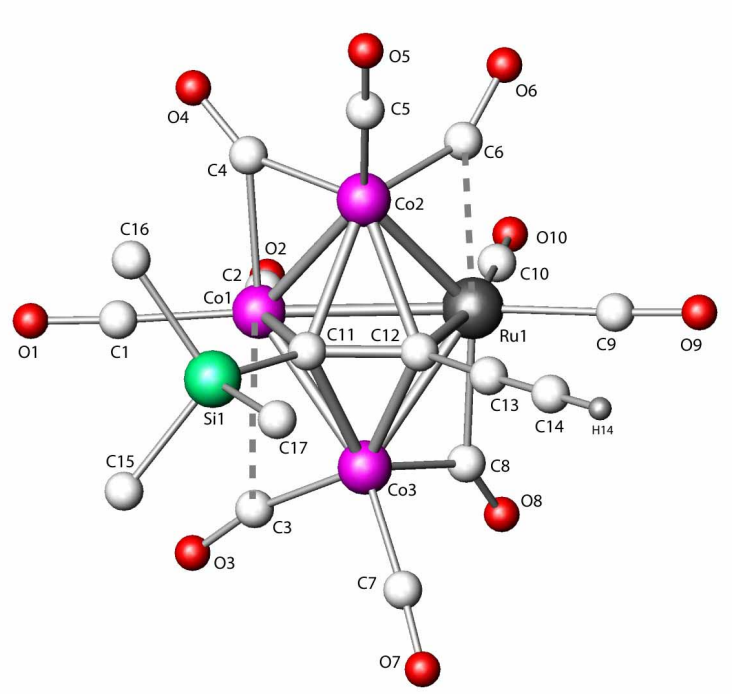

Figure 6. View of the molecular structure of the cluster 15a. Hydrogen atoms have been omitted for clarity.

Chapitre 4

Formation de Matériaux Magnétiques par Greffage de Clusters dans des Matrices de Silice Poreuses

4.1. Introduction

Si de nombreuses voies de synthèse sont mises en oeuvre dans certains laboratoires, réaction à l'état solide, réaction d'échange, synthèse hydrothermale, coprécipitation, etc..., les voies sol-gel sont apparues comme d'excellentes méthodes d'élaboration de matrices contenant des nanoparticules à propriétés chimiques (catalyse) ou physiques (optiques, électroniques ou magnétiques) originales.

Le processus sol-gel implique l'élaboration des réseaux inorganiques par la formation d'une suspension colloïdale (sol) à partir d'un mélange liquide de précurseurs alcoxydes, donc homogène à l'échelle moléculaire, et de la condensation du sol pour former un réseau solide tridimentionnel bicontinu (gel), emprisonnant la phase liquide.[1] Après séchage, le solide homogène obtenu -**xérogel**- est poreux et amorphe. Les alcoxydes métalliques sont les plus utilisés parce qu'ils réagissent facilement avec l'eau et ceux qui sont les plus largement répandus sont les alcoxysilanes, tels que le tétraméthoxysilane (TMOS) et le tétraéthoxysilane (TEOS). Cependant, d'autres alcoxydes, tels que des aluminates, des titanates, et des borates, sont également employés dans le processus sol-gel.

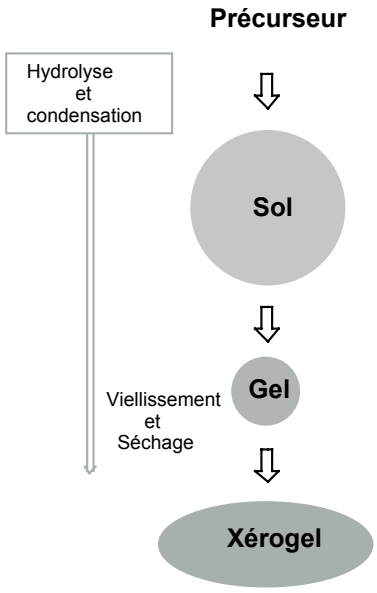

Figure 1. Description schématique des étapes principales pour l'élaboration d'un xérogel par le procédé sol-gel.

Trois réactions sont généralement employées pour décrire le processus sol-gel (eq 1-3).

Hydrolyse:

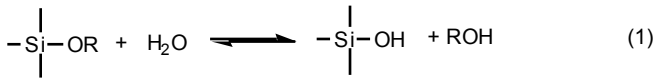

Condensation:

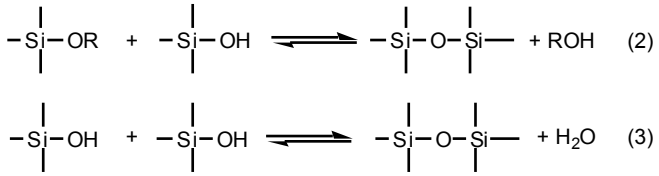

L'eau et les alcoxydes ne sont pas miscibles, et donc l'addition d'un solvant mutuel tel qu'un alcool est nécessaire. On devrait souligner, cependant, que l'addition des solvants peut favoriser des réactions d'estérification et de dépolymérisation selon l'inverse des équations (1-3).[2,3] Bien que l'hydrolyse puisse se faire sans addition d'un catalyseur externe, elle est plus rapide en présence d'un catalyseur. Pour cela, des acides minéraux (HCl, HNO_3) ou bases (KOH) sont généralement utilisés.

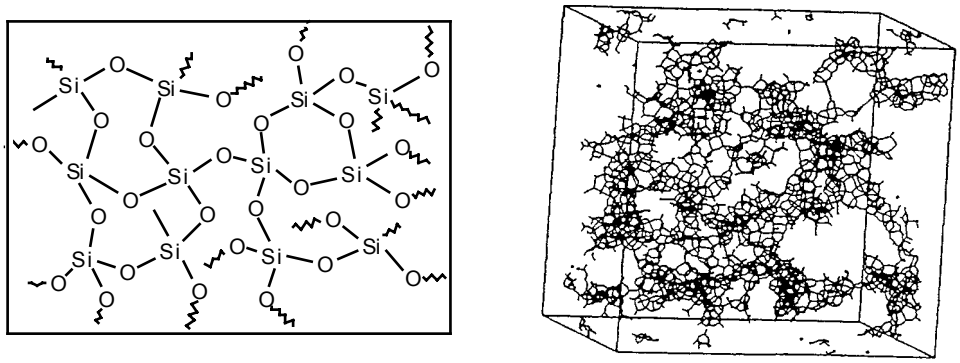

Figure 2. Descriptions schématiques d'un gel de silice.

Cependant, les caractéristiques et les propriétés d'un réseau inorganique de sol-gel particulier sont liées à un certain nombre de facteurs, tels que le pH, la température et la durée de la réaction, les concentrations des réactifs, la nature et la concentration du catalyseur, la température de vieillissement et le temps de séchage.[3,4] Ainsi, en maîtrisant ces facteurs, il est possible de changer la structure et les propriétés du réseau.[3]

Les xérogels présentent une très grande distribution en taille de pores, pouvant aller des micropores aux macropores, ce qui offre la possibilité d'ancrer des molécules de tailles

variées. La température d'élaboration des xérogels est compatible avec le domaine de stabilité des espèces moléculaires, en particulier avec celui des composés organiques et organométalliques. La richesse de la chimie moléculaire a permis de préparer de nombreux matériaux par simple insertion de molécules ou d'agrégats dans les xérogels transparents. De nombreuses applications ont été proposées pour ces solides, en particulier dans le domaine de l'otique (capteurs, lasers, mémoires optiques, optique non linéaire).[5-7]

Ces dernières années, de nouveaux matériaux organo-minéraux ont été préparés à température ambiante, en modifiant la procédure de synthèse et en utilisant des précurseurs de formules $RSi(OR)_3$, où R est un groupe organique stable au cours de la polymérisation, tels que le méthyltriéthoxysilane (MTEOS) ou le le vinyltriéthoxysilane (VTEOS), ou en utilisant des alcoxydes fonctionnalisés de formules $F\text{-}R\text{-}Si(OR)_3$ où F est une fonction chimique, par exemple un groupe amine ou isocyanate, et R un groupe alkyle. Ces précurseurs permettent un greffage par liaison covalente de molécules organiques ou biologiques dans la matrice.[8] Un des avantages apporté par ce type de greffage est l'augmentation très importante de la concentration en espèces moléculaires par rapport aux systèmes simplement dissous dans le gel. Braunstein et *al*. ont exploité cette méthode de synthèse *in-situ* pour élaborer des systèmes Fe, Mo, W et Fe-Mo[**9**] ainsi que pour ancrer des clusters de cobalt[10] à l'aide d'un ligand assembleur, la diphosphine fonctionnelle $(Ph_2P)_2N(CH_2)_3Si(OEt)_3$ (dppaSi) utilisée comme fonction chimique coordinante, pour l'élaboration de nanoparticules magnétiques. En effet, selon la taille et la composition des nanoparticules magnétiques, on peut atteindre des propriétés magnétiques différentes, et trouver ainsi des applications pratiques. Elles sont utilisées pour l'enregistrement magnétique, par exemple celui des cassettes audio et vidéo, des disquettes, ou encore dans le domaine de l'imagerie médicale.[11] Dans le but de poursuivre de telles études et de comparer les résultats provenant d'approches différentes mais complémentaires, nous avons pensé utiliser les alcynes au lieu des phosphines. Cela fut réalisé en collaboration avec l'Institut de Physique et Chimie des Matériaux de Strasbourg.

La compréhension de notre travail et de son exposé nécessite un rappel de notions essentielles du magnétisme.

4. 2. Aspect général sur les phénomènes magnétiques.[12]

Tout corps, particule isolée, molécule, association macromoléculaire, quelques soient les conditions physiques en particulier de température et de pression, manifeste des propriétés magnétiques, c'est à dire présente une certaine réaction lorsqu'il est plongé dans un champ magnétique.

Susceptibilité magnétique

Un corps quelconque, qu'il s'agisse d'un gaz, d'un liquide, d'un solide, ou d'une solution, s'il est placé dans un champ magnétique $\vec{H}$ acquiert une certaine aimantation M,

$$\vec{M} = \chi \vec{H}$$

χ est la susceptibilité magnétique.

Considérons une masse *m* d'une substance de susceptibilité χ placée dans un champ magnétique d'intensité uniforme $\vec{H}$. Elle acquiert une certaine aimantation, mais elle n'est soumise à aucune force: elle ne se déplace pas dans le champ spontanément.

Supposons que cette même substance soit placée en un point *A* d'un champ magnétique non uniforme. Au point *A,* le champ est $\vec{H}$. Le long de la ligne de force passant par *A*, le gradient de champ est $\partial \vec{H} / \partial \chi$. La substance est alors soumise à une force de grandeur:

$$\vec{F} = m \chi \frac{\partial \vec{H}}{\partial \chi}$$

Les méthodes de détermination de la susceptibilité magnétique sont basées sur cette formule.

Classification des corps d'après leur susceptibilité magnétique.

Une classification sommaire est basée sur la valeur de χ et ses variations en fonction des différents facteurs physiques, en particulier de la température:

A)- Les composés diamagnétiques. Ces substances sont caractérisées par une susceptibilité magnétique χ négative, petite, de l'ordre de 10^{-6}/ g, indépendante du champ $\vec{H}$ et indépendante de la température. Placée dans un champ magnétique non uniforme, une substance diamagnétique est soumise à une force $\vec{F}$ qui est négative; elle s'éloigne des zones

de champ fort pour gagner les zones de champ faible. Le fait qu'un corps soit diamagnétique implique l'absence d'électron célibataire.

B)- Les composés paramagnétiques. Ces substances sont caractérisées par une susceptibilité magnétique χ positive, dont la grandeur est de l'ordre de 10^{-6} à 10^{-4}/g, et par le fait qu'elle est indépendante du champ $\vec{H}$. Placée dans un champ magnétique non uniforme, une substance paramagnétique est soumise à une force $\vec{F}$ positive; elle est attirée vers les zones de champ fort.

Phénomènes magnétiques dans l'état solide.

Les matériaux magnétiques sont constitués de réseaux d'atomes porteurs de moment magnétique. Une classification sommaire des solides a été proposée:

1- La somme des moments des particules constitutives est nulle: le corps est **diamagnétique**.

2- Un certain nombre de particules constitutives possèdent un moment non nul. Il y aura deux possibilités:

a- Des interactions nulles ou faibles: il n'y aura pas d'ordre magnétique entre les moments, ce qui conduira au **paramagnétisme** variable. Lorsqu' un champ est appliqué l'aimantation résultante est proportionnelle à ce champ et χ varie avec la température selon la loie de Curie, $\chi = C/T$ où C est la constante de Curie. Lorsque le champ est coupé, l'agitation thermique désordonne à nouveau les moments et l'aimantation disparaît (Figure 3).

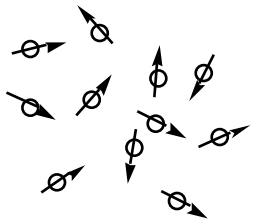

M = 0

Figure 3. Arrangement des moments dans le cas d'un matériau paramagnétique.

b- Des interactions fortes: il existera un ordre magnétique entre les moments. En effet, les interactions magnétiques "l'emportent" sur l'agitation thermique et il en résulte une mise en ordre des moments magnétiques en l'absence de champ extérieur appliqué; on parle de *magnétisme coopératif*. Trois cas peuvent se présenter suivant les particularités de la structure: le **ferromagnétisme**, l'**antiferromagnétisme**, ou le **ferrimagnétisme**.

L'apparition d'une de ces formes de magnétisme est directement dépendante de facteurs qui déterminent l'amplitude des interactions d'échanges à savoir:

a) La structure électronique du porteur de moment: les particules magnétogènes possèdent des électrons célibataires -non couplés-.

b) Le mécanisme de liaison: liaison délocalisée (métallique, ionique) ou localisée (covalente) et l'on trouve une participation fréquente de la liaison métallique, de la liaison covalente et de la liaison ionique.

c) La structure cristalline qui va imposer le mode d'interaction entre porteurs de moment magnétique. Ces interactions ont pour origine des couplages électroniques entre atomes voisins.

Le ferromagnétisme

Les matériaux ferromagnétiques sont des corps solides qui, comme le fer, le nickel, le cobalt, sont caractérisés par une susceptibilité magnétique positive très grande, dépendant de la température, du champ H, des traitements thermiques et mécaniques et possèdent un cycle d'hystérésis (voir plus loin). Dans ces matériaux, les moments s'orientent tous dans le même sens en-dessous d'une certaine température nommée température de Curie T_c (Figure 4). Une aimantation nommée *aimantation rémanente* M_r est conservée lorsque le champ est coupé. Pour annuler cette aimantation M_r, il faut appliquer un champ opposé de valeur H_c, appelé *champ coercitif*.

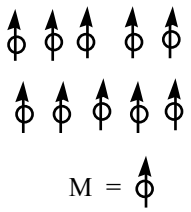

Figure 4. Arrangement des spins dans le cas d'un matériau ferromagnétique.

Pour une température au-dessus de T_c, l'aimantation spontanée disparaît et le matériau retrouve un comportement paramagnétique. La susceptibilité magnétique, dans ce cas, est donnée par la relation de *Curie-Weiss*:

$$\chi = \frac{C}{T - T_c}$$

L'antiferromagnétisme

Il peut être représenté simplement comme la superposition de deux sous réseaux ferromagnétiques possédant des orientations opposées (mais de même valeur absolue) dûes aux interactions d'échange négatives. Cela représente l'orientation antiparallèle des moments entre eux (Figure 5).

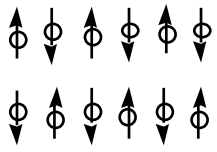

M = 0

Figure 5. Arrangement des spins dans le cas d'un matériau antiferromagnétique.

L'aimantation d'un matériau antiferromagnétique est nulle, et sa susceptibilité magnétique suit la relation:

$$\chi = \frac{C}{T + \Theta}$$

où Θ représente une température fictive, négative et dépendant de la force du champ moléculaire. La susceptibilité présente un maximum à une température nommée température de Néel T_N.

Le ferrimagnétisme

Il peut être représenté comme la superposition de deux sous réseaux ferromagnétiques possédant des orientations opposées mais qui n'ont pas la même valeur absolue. L'aimantation est non nulle, et le comportement du matériau se rapproche de celui d'un matériau ferromangnétique (Figure 6).

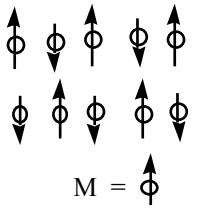

Figure 6. Arrangement des spins dans le cas d'un matériau ferrimagnétique.

Processus d'aimantation d'un composé ferromagnétique, cycle d'hystérésis

Lorsque l'on mesure l'aimantation en fonction du champ croissant et décroissant d'un matériau ferromagnétique, on constate l'apparition d'un cycle d'hystérésis (Figure 7). En effet, il représente la réponse d'un matériau à un champ magnétique appliqué.

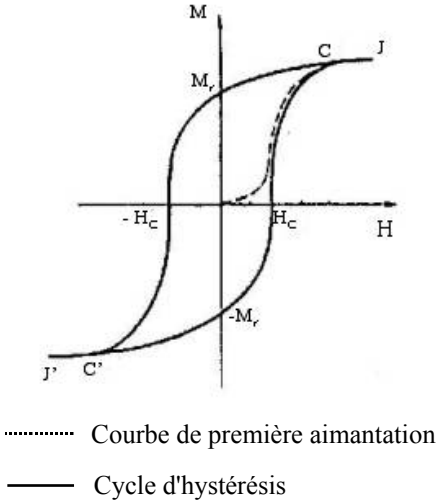

Figure 7. Courbe de première aimantation et cycle d'hystérésis d'un ferromagnétique

Si, la saturation étant atteinte, le champ se met à décroître, la partie *JC* réversible est décrite, puis le tracé quitte la courbe de première aimantation au point *C* et, pour un champ nul, il subsiste une certaine aimantation *rémanente* M_r. Si après s'être annulé, le champ change de sens, le point représentant l'aimantation du ferromagnétique va décrire une courbe M_r - H_c au cours de laquelle l'aimantation va baisser du fait des retournements à l'intérieur des domaines. Au point – H_c , dont l'abscisse correspond au champ *coercitif*, l'aimantation globale spontanée est nulle. Si le champ continue à croître dans le même sens, les retournements continuent à se produire: quand le point *C′* est atteint, tous les moments des différents domaines sont parallèles. Si, au-delà du point *C′*, le champ continue à croître, le ferromagnétique s'approche de la saturation (point *J′*) qui n'est obtenue que dans les champs très élevés. Si, à partir de *J′*, le champ décroît, une nouvelle portion de courbe est décrite, qui est l'homologue de la portion JM_r. Au-delà de $-M_r$ est décrite une courbe - M_rH_c homologue de M_r - H_c et au-delà de H_c, le champ continuant à croître, la partie H_cC rejoint alors la courbe de première aimantation. Les deux grandeurs, l'aimantation rémanente et le champ coercitif, expliquent le cycle d'hystérésis qui est représentatif des matériaux ferromagnétiques.

Le greffage dans les matrices peut se faire de deux manières différentes (Schéma 1):

-le ligand fonctionnalisé est greffé en premier lieu à la matrice puis le cluster est incorporé au gel [voie (a)].

- le cluster est fixé au ligand fonctionnalisé et l'ensemble est greffé à la matrice [voie (b)].

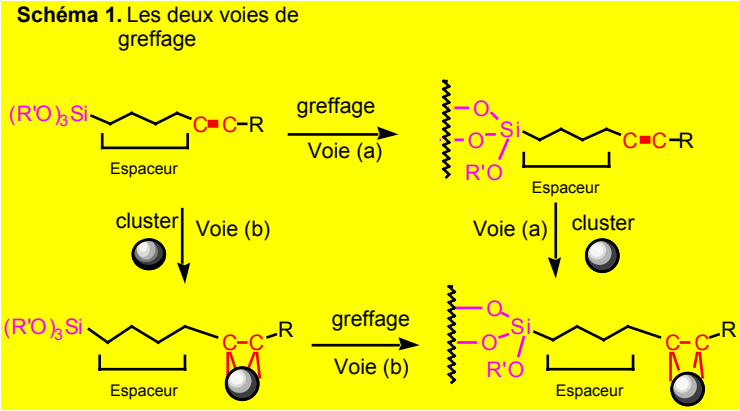

4. 3. Greffage selon la voie (a):

Nous avons utilisé les alcynes $HC{\equiv}C(CH_2)_2OC(O)NH(CH_2)_3Si(OEt)_3$ (**L**^{1}) et $HC{\equiv}CCH_2NHC(O)NH(CH_2)_3Si(OEt)_3$ (**L**^{2}) avec les deux clusters $[RuCo_3(CO)_{12}]^-$ **(1)** et $[Co_4(CO)_{10}(dppm)]$ **(2)** comme précurseurs.

4. 3. 1. Synthèse des xérogels de silice fonctionnalisés.

Nous avons réalisé des synthèses *in situ*, les alcynes étant incorporés lors du procédé sol-gel. La synthèse a été réalisée à l'air avec des solvants distillés, en utilisant la méthode décrite pour la dppaSi.[10] La composition molaire du xérogel est la suivante : 1 TEOS : 4 ETOH : 0,45 HNO_3 : 4,5 H_2O : 1$HCONH_2$: 0,05 alcyne (voir partie expérimentale). L'alcool assure l'homogénéité du mélange car les alcoxydes et l'eau ne sont pas miscibles, l'acide joue le rôle d'un catalyseur pour augmenter la cinétique de l'hydrolyse et le formamide est un agent chimique de contrôle de séchage qui permet de jouer sur les tensions dues à l'évaporation, lors du séchage du gel, et éviter les fissurations. Dans le cas de l'alcyne **L**^{2} l'utilisation d'une petite quantité de THF (environ 0,5 g) était nécessaire car sans THF le mélange se solidifie légèrement pendant l'étape de condensation.

On appelle le gel formé par l'alcyne **L**^{1} xérogel 1 et le gel formé par l'alcyne **L**^{2} xérogel 2-0,5 THF.

4. 3. 2. Caractérisation des xérogels fonctionnalisés formés.

4. 3. 2. a. RMN CP-MAS

Une étude de RMN du ^{29}Si a été réalisée par rotation à l'angle magique découplé (CP-MAS) sur les xérogels fonctionnalisés obtenus. La Figure 8 présente les différents sites Si qui ont des déplacements chimiques différents selon qu'ils sont plus ou moins condensés.[13]

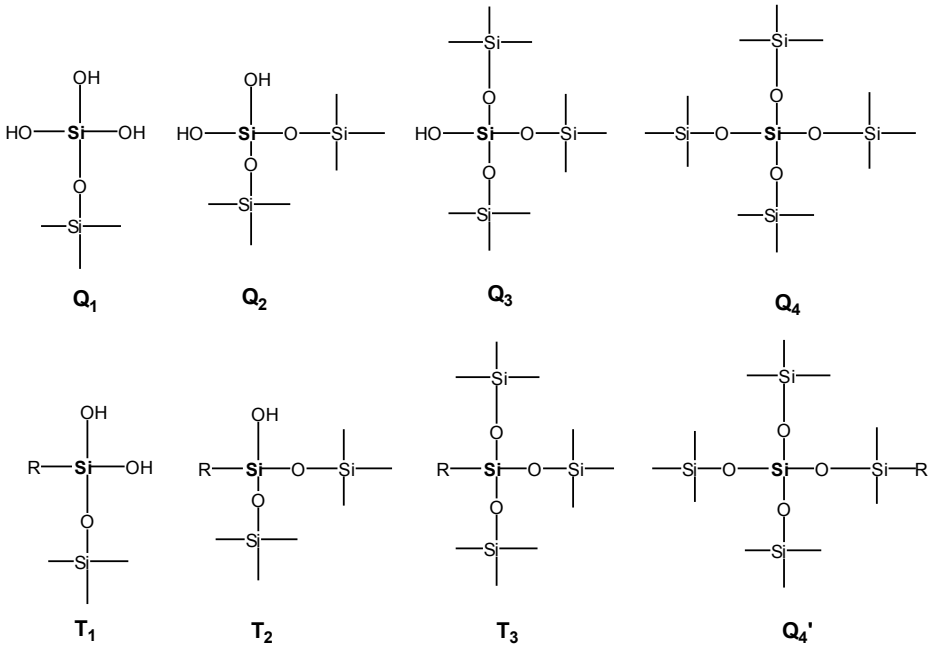

Figure 8. Les différents types de sites Si.

Les sites Q correspondent à des siloxanes de surface (Q_1-Q_3) ou de coeur (Q_4) et apparaissent à des déplacements chimiques entre –115 et –90 ppm, tandis que les sites T correspondent à des siloxanes attachés à un radical organique et apparaissent à des déplacements chimiques de l'ordre de –70 à –50 ppm. Les sites Q'4 sont des siloxanes de coeur en contact direct avec un silicium de type T. Les Figures 9 et 10 montrent les spectres RMN CP-MAS du ^{29}Si du xérogel 1 et du xérogel 2-0,5 THF, respectivement et le tableau 1 résume les valeurs des déplacements chimiques des différents sites de silicium dans les deux xérogels.

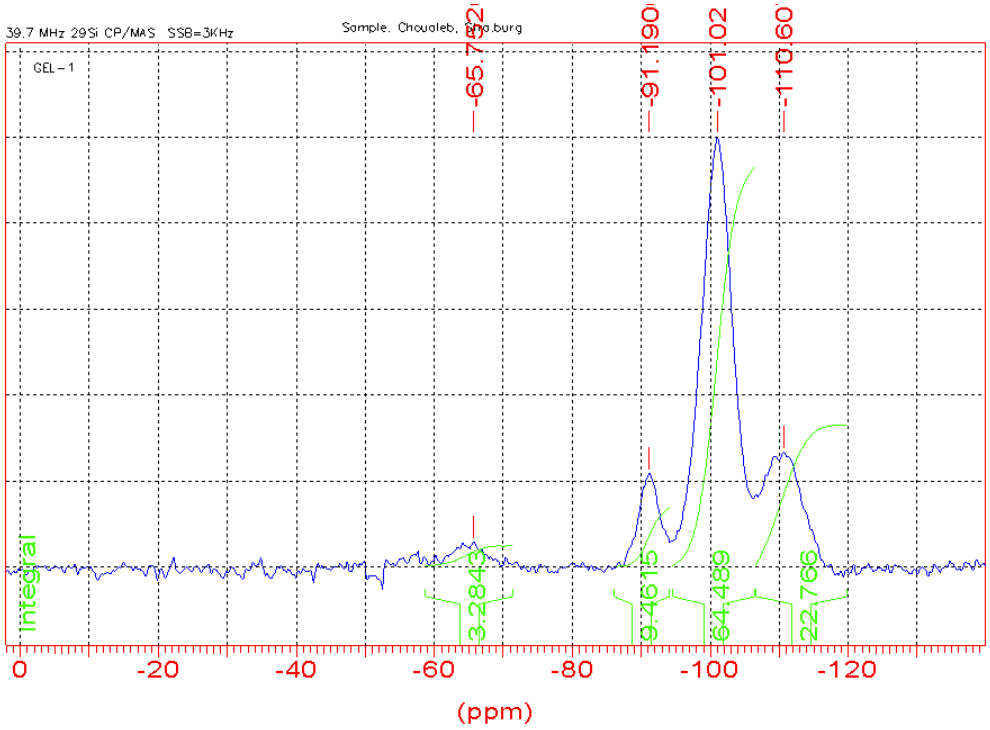

Figure 9. Spectre RMN CP-MAS du ^{29}Si du xérogel 1.

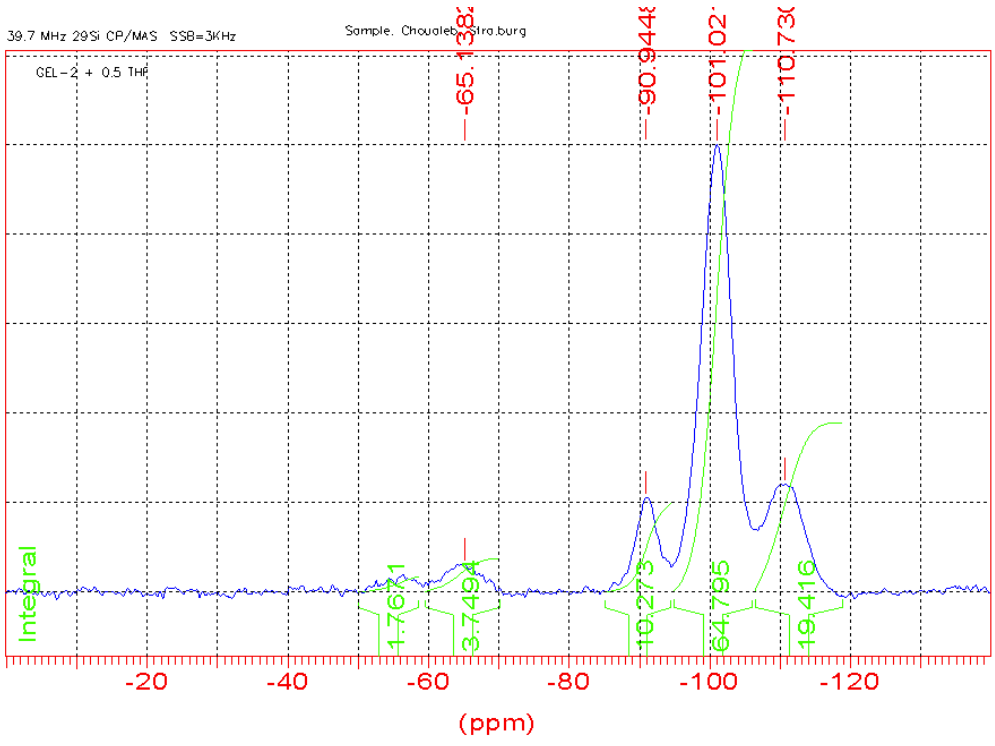

Figure 10. Spectre RMN CP-MAS du ^{29}Si du xérogel 2-0,5 THF.

Tableau 1. Déplacements chimiques des différents sites de silicium dans les deux xérogel.

	Q_4	Q_3	Q_2	T
Xérogel 1	-110	-101	-91	-66
Xérogel 2-0,5 THF	-110	-101	-91	-65

4. 3. 2. b. Porosité.

Les mesures de porosité ont été réalisées sur des gels préalablement dégazés à 100 °C pendant 1 h, par isothermes d'adsorption d'azote. La mesure de surface spécifique fait intervenir la théorie de Brunauer, Emmet et Teller (BET)[14] et la taille des pores a été déterminée par la théorie Barret, Joyner et Halenda (BJH)[15] afin de déterminer la distribution des mésopores. Le tableau 2 résume les résultats des mesures de surfaces spécifiques et des diamètres de pores des deux xérogels.

Tableau 2. Porosité des matrices.

	Surfaces spécifique ($m^2.g^{-1}$)	Diamètre des pores (nm)
Xérogel classique	800	2,0
Xérogel 1	657	11
Xérogel 2-0,5 THF	386	11

Dans le cas du xérogel 1, la surface spécifique est très élevée, elle est plus faible dans le cas du xérogel 2-0,5 THF mais tout de même élevée. La forme de l'isotherme d'adsorption du xérogel 1 indique la présence de micropores (surface spécifique de 99 m^2/g, volume 0.045 cm^3/g). Par contre le xérogel 2-0,5 THF ne contient pas de micropores mais des macropores. On note que les micropores possèdent une taille inférieure à 2,5 nm, les mésopores ont des tailles comprises entre 2,5 et 50 nm alors que les macropores ont des tailles supérieures à 50 nm.[16] La distribution des mésopores est centrée sur 11 nm dans les deux xérogels, ce qui est suffisant pour accueillir les cluster $[RuCo_3(CO)_{12}]^-$ et $[Co_4(CO)_{10}(dppm)]$. On note que la théorie BJH ne s'applique pas aux micropores. Comparé à des xérogels fonctionnalisés par la phosphine dppaSi (surface spécifique = 320 $m^2.g^{-1}$),[10] les xérogels fonctionnalisés par les alcynes étudiés sont plus poreux.

4. 4. Ancrage des clusters dans les xérogels fonctionnalisés. Dans ce travail nous avons ancré le cluster $[RuCo_3(CO)_{12}]^-$ **(1)** seulement dans le xérogel 1 alors que le cluster $[Co_4(\mu\text{-}CO)_3(CO)_7(\mu\text{-dppm})]$ **(2)** l'a été dans les deux xérogels.

Le xérogel fonctionnalisé, broyé, séché à 50 °C pendant 24 h, est immergé dans une solution saturée du cluster dans THF (à peu près 0,115 mol.l^{-1} pour le cluster **1** et 0,043 mol.l^{-1} pour **2**). Pour éviter de bloquer l'entrée des pores par une condensation trop rapide, l'agitation est maintenue pendant 1 jour à température ambiante. La suspension est alors portée à 90 °C pour **1** et à 75 °C pour **2**, durant 24 heures, puis filtrée. La poudre est lavée plusieurs fois avec du THF chaud afin d'oter le cluster qui ne serait pas fixé et le $[Co_4(CO)_8(\mu\text{-dppm})_2]$ formé dans le cas du cluster **2**. On appelle matériau 1 le matériau obtenu par la réaction du xérogel 1 avec le cluster **1** et matériau 2 et matériau 3 les matériaux formés par la réaction des xérogel 1 et 0,5 THF avec le cluster **2**, respectivement.

4. 5. Caractérisation des matériaux.

4. 5. 1. Spectroscopie infra-rouge. Les spectres des matériaux obtenus, dans KBr, ne correspondent pas aux clusters $[RuCo_3(CO)_{10}\{\mu_4\text{-}\eta^2\text{-}HC_2(CH_2)_2OC(O)NH(CH_2)_3Si(OEt)_3\}]^-$ **(3)**, $[Co_4(\mu\text{-}CO)_2(CO)_6(\mu\text{-dppm})\{\mu_4\text{-}\eta^2\text{-}HC_2(CH_2)_2OC(O)NH(CH_2)_3Si(OEt)_3\}]$ **(4)** et $[Co_4(\mu\text{-}CO)_2(CO)_6(\mu\text{-dppa})\{\mu_4\text{-}\eta^2\text{-}HC_2CH_2NHC(O)NH(CH_2)_3Si(OEt)_3\}]$ **(5)** greffés, attendus (Figure 11). Le tableau 3 résume les fréquences de vibrations IR des clusters **3**, **4**, **5** et celles des matériaux obtenus, dans le domaine des carbonyles (2200-1600 cm^{-1}).

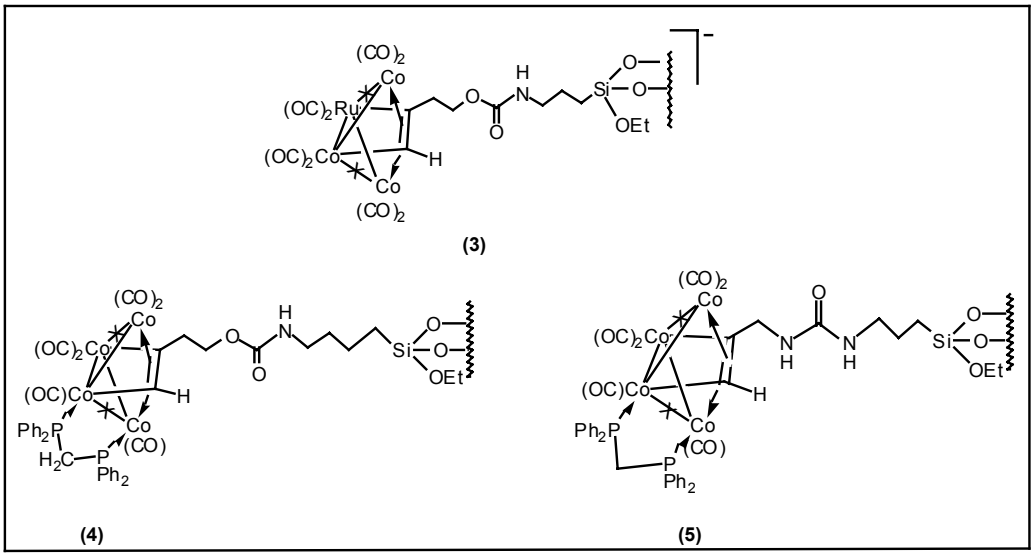

Figure 11. Les clusters greffés attendus par réaction des xérogels 1 et 2-0,5 THF avec les clusters **1** et **2**.

Tableau 3. Fréquences de vibrations IR [ν(CO)] des clusters **3**, **4**, **5** et des marériaux 1, 2 et 3.

	IR, ν(CO, cm^{-1}), [a] CH_2Cl_2, [b] KBr
Cluster **3**	[a] 2048 (mw), 2002 (vs), 1970 (sh), 1814 (m) $\nu_{C\equiv O}$, 1720 (m, $\nu_{C=O}$)
Matériau **1**	[b] 2051 (vs), 1971 (vs) $\nu_{C\equiv O}$, 1684 (m, $\nu_{C=O}$))
Cluster **4**	[a] 2048 (vs), 2001 (vs), 1975 (sh), 1831 (w), $\nu_{C\equiv O}$; 1720 (m, $\nu_{C=O}$) [b] 2040 (vs), 2005 (vs), 1986 (vs), 1971 (vs), 1831 (w), $\nu_{C\equiv O}$; 1720 (m, $\nu_{C=O}$)
Matériau **2**	[b] 1686 (vs, $\nu_{C=O}$)
Cluster **5**	[b] 2052 (s), 1993 (vs), 1966 (m), 1831 (w) $\nu_{C\equiv O}$; 1679 (vs, $\nu_{C=O}$)
Matériau **3**	[b] 1685 (vs, $\nu_{C=O}$)

Les bandes de vibration à 2051 et 1971 cm^{-1} dans le matériau 1 correspondent à des carbonyles terminaux et celle à 1684 cm^{-1} correspond à la fonction amide. Aucune bande dans le domaine des carbonyles pontant n'a été observée. On constate que le cluster s'est fragmenté après sa formation. Dans le cas des matériaux 2 et 3 aucune bande dans le domaine des carbonyles n'a été observée à part le carbonyle de la fonction amide qui appartient au ligand greffé. Cela veut dire que le cluster a perdu touts ses ligands après sa formation. La Figure 12 montre le spectre infra-rouge du matériau 2.

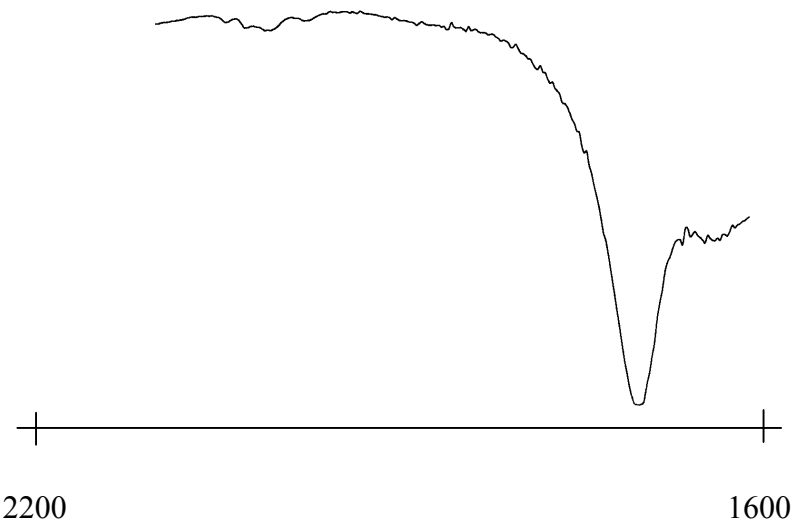

Figure 12. Spectre infra-rouge du matériau 2

4. 6. Mesures magnétiques.

Mesures magnétiques in-situ à la balance magnétique: Ce dispositif associe une balance de Faraday à une enceinte permettant de travailler sous différents atmosphères (vide, air, argon, H_2 ou N_2-H_2 95-5 %). Un champ constant de 0,58 Tesla est appliqué, tandis que la température de l'échantillon est imposée par un système de régulation thermique. L'échantillon, placé dans un porte-échantillon en quartz, est porté de la température ambiante à 1000 °C, à une vitesse de 200 °C/h.

Le Schéma sur la Figure 13 représente l'évolution attendue au cours du traitement thermique qui doit provoquer la décomposition du cluster, puis la formation de particules, dont la taille augmente avec la température.

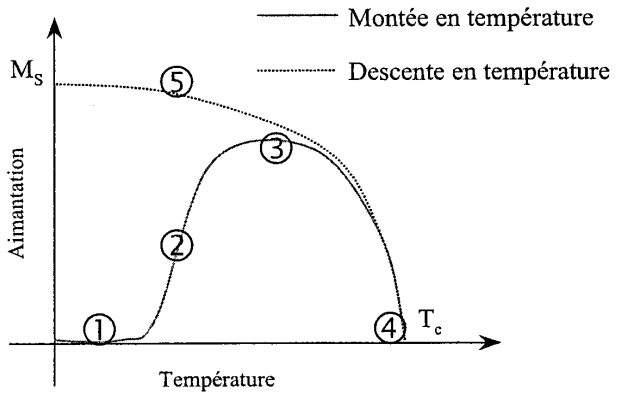

Figure 13. L'évolution attendu au cours du traitement thermique.

En théorie l'aimantation à température ambiante est presque nulle car même si les atomes du cobalt dans le cluster sont à un degré d'oxydation proche de zéro, ils sont trop dispersés et éloignés les uns des autres pour donner lieu à un phénomène de magnétisme coopératif (zone (1)). Au cours du traitement thermique, et à mesure que le cluster se dégrade, les atomes métalliques se regroupent pour former des particules. Une augmentation importante de l'aimantation doit apparaître une fois que la taille des particules est suffisante pour qu'un ordre magnétique apparaisse au sein de chacune (zone (2)). Toutefois, l'alignement des moments magnétiques des différents particules est en compétition avec l'agitation thermique qui fait diminuer l'ordre magnétique et à mesure que la température augmente, l'aimantation se stabilise (zone (3). Lorsque la température augmente encore, l'agitation thermique devient le phénomène prépondérant, l'aimantation décroît jusqu'au point de Curie pour lequel elle redevient proche de zéro (zone (4).

A ce stade de l'étude il est important de préciser les températures de Curie du cobalt métallique et de l'alliage Co_3Ru qui sont respectivement de 1400 et 643 K et les aimantations à saturation sont respectivement de 162 emu/g (Am^2/kg) et 64.5emu/g.[17]

Au cours de la descente en température on doit observer l'évolution classique d'un matériau ferromagnétique (zone (5)).

Cas du cluster $[RuCo_3(CO)_{12}]^-$.

La Figure 14 montre l'évolution de l'aimantation observée en cours du traitement thermique du matériau 1.

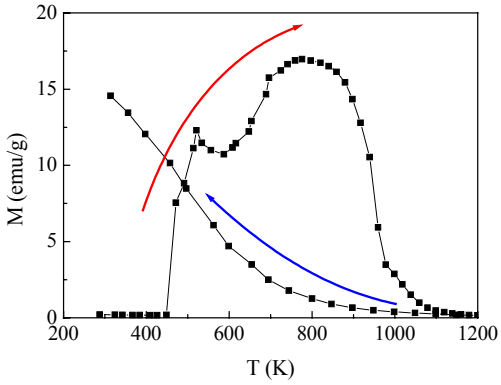

Figure 14. Aimantation M en fonction de la température du matériau 1.

Lors de la montée en température on observe l'apparition d'une réponse magnétique à partir de 450 K. Le signal augmente jusqu'à 520 K puis il rediminue jusqu'à 600 K pour augmenter de nouveau jusqu'à 780 K qui est la maximum de la courbe. Le changement de pente observé à 520 K s'explique par le fait que les particules de cobalt formées de structure hcp et présentant un comportement ferromagnétique se transforment en cobalt de structure cfc présentant un comportement superparamagnétique à cette température. Ce type de comportement a été observé dans des systèmes similaires. [17,18]

Au delà de cette température, si un alliage de type $RuCo_3$ se formait, l'aimantation devrait continuer à diminuer jusqu'à sa température de Curie (643 K). Or nous observons une augmentation de l'aimantation jusqu'à une température de 780 K. Ce phénomène est vraisemblablement dû à la formation d'une phase très riche en cobalt.

A partir de 780 K, l'agitation thermique l'emportant sur l'alignement des moments, le signal diminue de nouveau jusqu'à 980 K où on observe encore une fois un changement de pente qui est dû la présence simultanée de deux phases d'alliage Ru/Co de composition différente.

Lors de la descente en température, l'aimantation augmente à nouveau, mais contrairement à ce qu'on attendait (Figure 14 , zone 5), l'aimantation est plus faible que lors de la montée en température, ce qui peut s'expliquer par un processus irréversible qui à eu lieu à haute température et qui est associé à un changement de composition de l'alliage Ru/Co.[17]
L'allure de notre courbe est identique à celles obtenues par imprégnation du cluster **1** dans des matrices de silice ou des matrices organisées MCM-41,[18] par contre la réponse magnétique a eu lieu à température inférieure dans notre cas.

La Figure 15 présente les mesures d'aimantation en fonction du champ (T = 295 K) effectuées sur l'échantillon avant et après traitement thermique, à la balance thermo-magnétique.

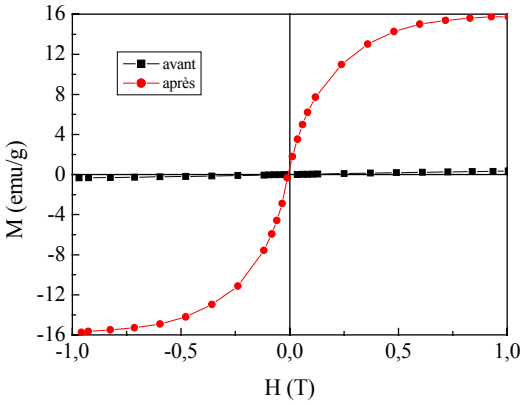

Figure 15. Cycle d'hystérésis du matériau 1.

Avant traitement thermique on peut noter une variation linéaire en fonction du champ magnétique appliqué; la faible susceptibilité magnétique observée (χ = M/H) est caractéristique d'un comportement paramagnétique lié au cluster non décomposé. Après le traitement thermique un cycle d'hystérésis caractéristique d'un matériaux ferromagnétique est observé.

Cas du [$Co_4(CO)_{10}$(dppm)]. Le comportement est très différent dans le cas des matériaux 2 et 3. Les mesures magnétiques in-situ à la balance thermo-magnétique montrent que les matériaux présentent une réponse magnétique à température ambiante avant tout traitement thermique (Figure 16). Le signal décroît légèrement jusqu' environ 800 K puis il augmente. Cette augmentation est due à la réduction d'une partie du produit qui s'est oxydée pendant le stockage ou lors de la pesée. Lors de la descente en température on observe un comportement classique.

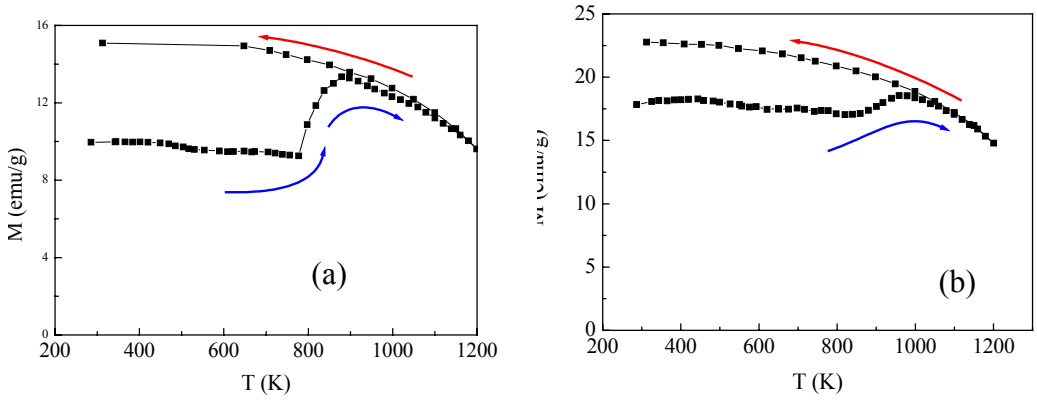

Figure 16. Aimantation en fonction de la température, des matériaux 2 (Fig a) et 3 (Fig b), sous un mélange de N_2 à 5% de H_2.

Des mesures d'aimantation à température ambiante en fonction du champ appliqué, réalisées sur les matériaux frais (sans traitement thermique) montrent des cycles d'hystérésis caractéristiques de matériaux ferromagnétiques.

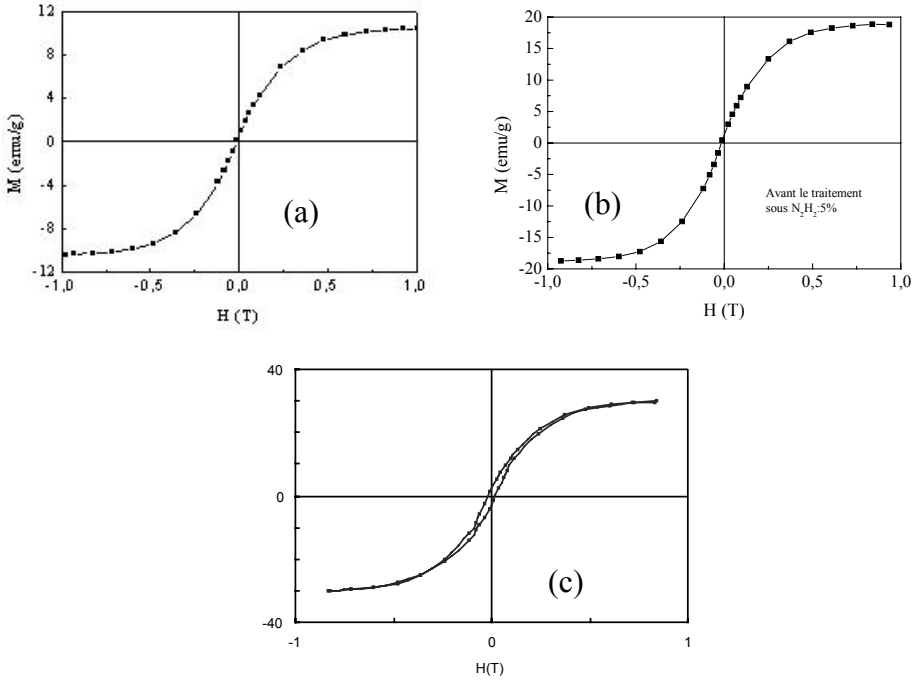

Figure 17. Cycles d'hystérésis des matériaux 2 et 3 (a) (b), respectivement, avant le traitement thermique, matériau 2 plus concentré en cobalt (c).

Si l'on estime que tout le cobalt dans les échantillons est réduit, les aimantations à saturation sont de 30,07 et 18,74 emu/g pour les matériaux 2 et 3, respectivement, et qu'il faut rapporter

à la quantité du cobalt dans les échantillons. Sachant que l'aimantation du cobalt métallique est de 162 emu/g on peut estimer qu'on a 18,56 et 11,56 % en masse de cobalt, respectivement. Il est intéressant de noter que l'ancrage du cluster $[Co_4(CO)_{10}(\mu\text{-dppa})]$ dans le xérogel fonctionnalisé par la diphosphine $(Ph_2P)_2N(CH_2)_3Si(OEt)_3$ (dppaSi) conduit à la formation de nanoparticules de type Co_2P qui sont paramagnétiques.[10] Ce résultat est donc en faveur d'une utilisation des alcynes fonctionnels en remplacement des phosphines.

4. 7. Diffraction des rayons X.

Des mesures de diffraction des rayons X réalisées sur un échantillon du matériau 1 ayant subi un traitement thermique à la balance thermo-magnétique montrent, après indexation, la présence d'une phase hexagonale (Figure 18 a). Les paramètres de maille, de a = 2,54 Å et c = 4,08 Å ne correspondent ni au cobalt hexagonal pur (a = 2,5031 Å et c = 4,06 Å)[19] ni au ruthénium hexagonal (a = 2,7058 Å et c = 4,2819 Å).[20] Comme les valeurs observées sont plus proches de celles du cobalt pur on peut conclure qu'il s'agit des particules d'un alliage Ru-Co de structure hexagonale plus riche en cobalt.

Dans le cas des matériaux 2 et 3, nous avons réalisé des mesures avant traitement thermique qui montrent la présence du cobalt métallique sous forme d'un mélange de phases hcp, cfc et epsilon avec des tailles de particules différentes (Figure 18 b,c). L'identification de ce mélange a été déduite par comparaison avec des données de la littérature.[21] Le diffractogramme du matériau 3, traité thermiquement, montre une phase cubique à faces centrée (cfc), qui est la phase la plus stable thermodynamiquement (Figure 18 d).

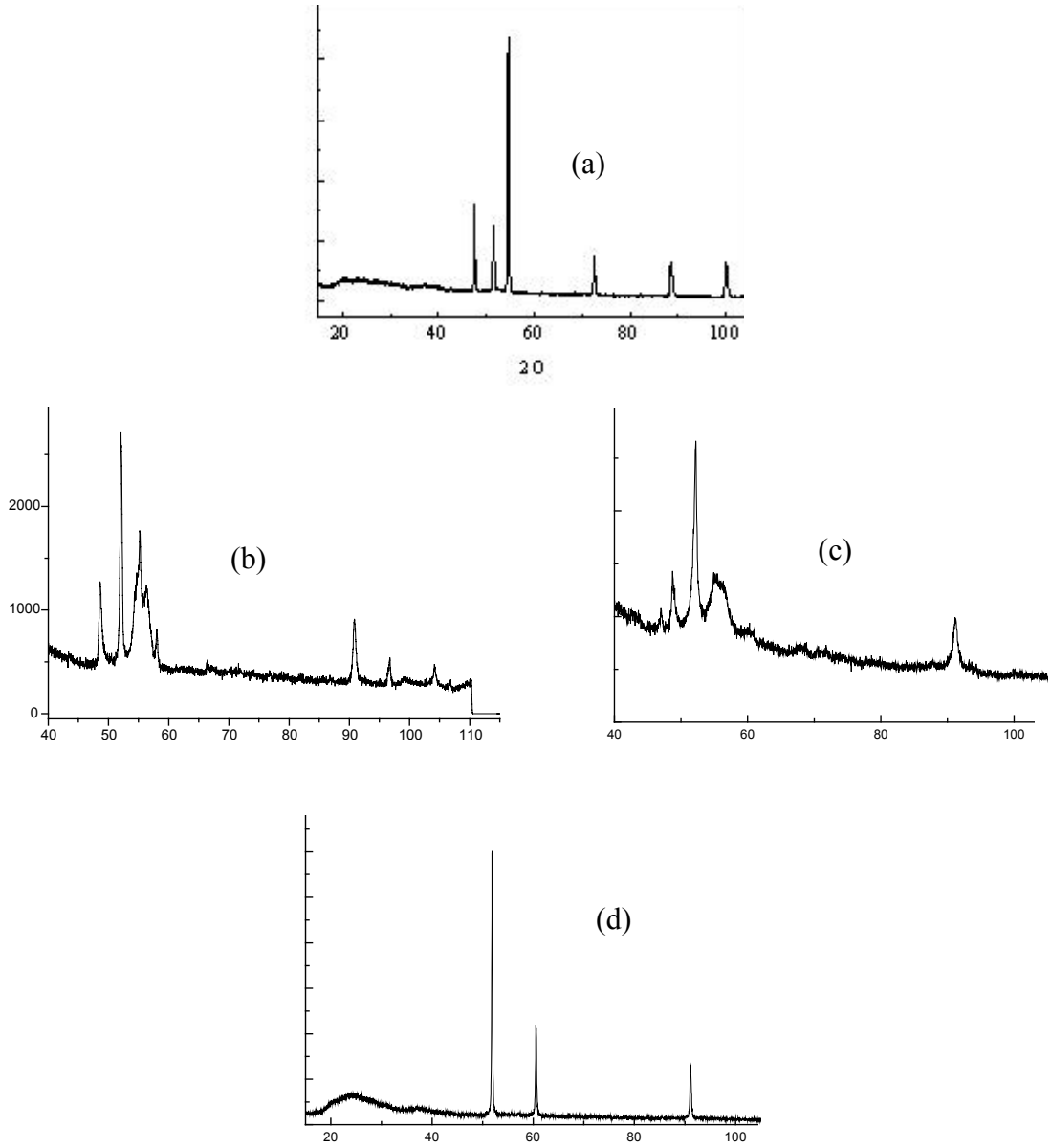

Figure 18. Diagrammes de diffraction des matériaux: matériau 1 après mesure à la balance thermo-magnétique(a), matériau 2 avant traitement thermique (b), matériau 3 avant traitement thermique (c), matériau 3 après traitement thermique (d).

4. 8. Microscopie électronique à transmission (MET).

Cas du $[RuCo_3(CO)_{12}]^-$ (matériau 1).

La figure 19 présente des clichés de diffraction sur un échantillon du matériau 1 (après les mesures magnétiques à la balance thermo-magnétique). On observe des particules de tailles différentes allant de 2,2 à 5,5 nm de formes sphériques et qui ne sont pas dispersées uniformément dans le matériau. Ceci est dû au fait que les pores, dans le xérogel, ne sont pas de tailles uniformes.

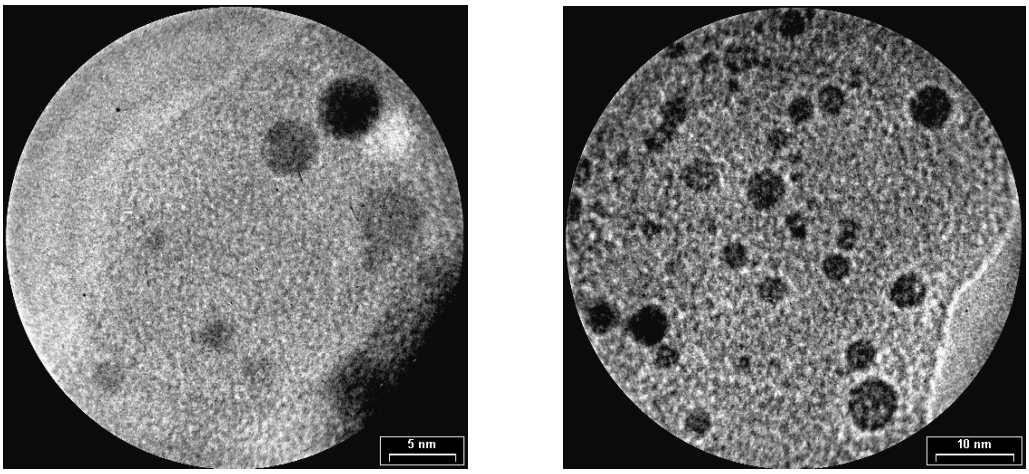

Figure 19. Micrographie au MET du matériau 1 après mesure à la balance thermo-magnétique.

Cas du $[Co_4(CO)_{10}(dppm)]$ (matériaux 2 et 3).

Des observations ont été effectuées sur les deux matériaux avant traitement thermique.

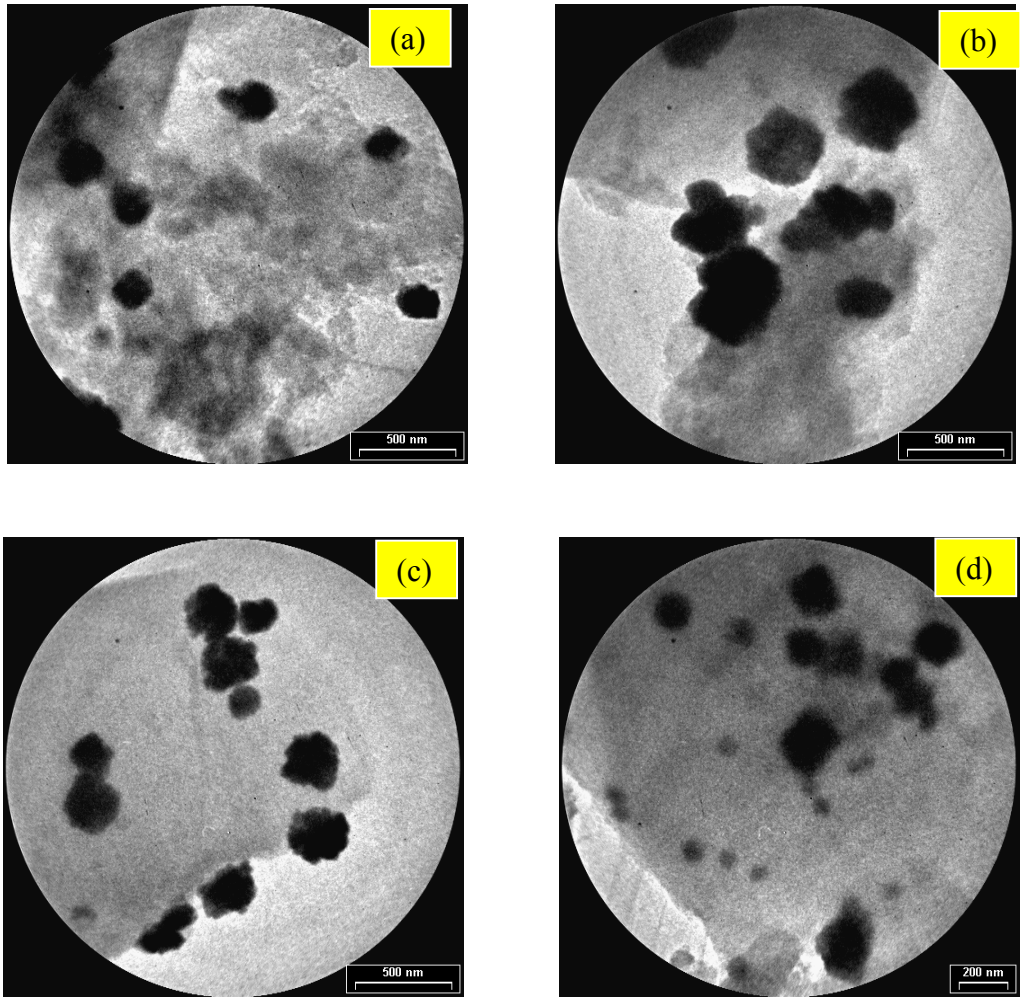

Figure 20. Photographie au MET du matériau 2 (a,b) et 3 (c,d) avant traitement thermique.

Les grosses particules (diamètre > 150 nm) semblent se trouver à la surface de la matrice plutôt que dans les pores. En effet, la taille de ces particules est plus grande que celle des pores. Les clichés de diffraction électronique réalisés sur la surface des particules laissent à penser qu'elles correspondent à des agrégats de particules de tailles plus petites (diamètre de l'ordre de 30 nm). Certaines de ces petites particules sont encore visibles notamment sur la micrographie (d) reportées à la figure 20.

Greffage selon la voie (b): nous avons testé seulement le cluster **4**. La condensation de ce dernier se fait de la même façon que les alcynes libres, mais sous atmosphère inerte. L'utilisation du THF était nécessaire, la composition molaire est donc: 1 TEOS : 4 ETOH : 0,45 HNO_3 : 4,5 H_2O : 1 $HCONH_2$: 0,05 alcyne: 6 THF (voir partie expérimentale).
La spectroscopie IR montre la présence des carbonyles du cluster.

Mesure magnétique du matériau

Les mesures magnétiques effectuées à la balance thermo-magnétique pour un champ appliqué de 0.58 Tesla et sous N_2H_2 :5%, montrent un signal faible (paramagnétique) jusqu'à 900 K (Figure 21). Le signal augmente fortement aux delà de 900 K signifiant l'apparition d'une phase magnétique à partir de cette température. Le cobalt initialement présent sous forme d'oxyde se réduit à cette température. Cependant, la présence de l'ensemble de cobalt sous forme d'oxyde reste inexpliquée.

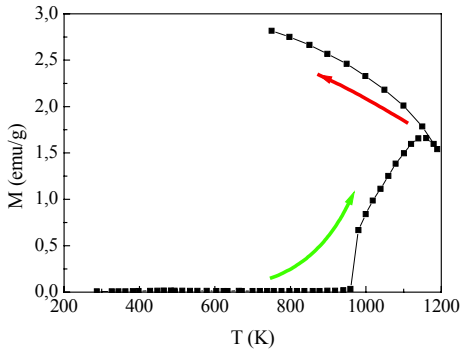

Figure 21. Aimantation M en fonction de la température.

Conclusion:

Le greffage dans les matrices par fixation des alcynes suivi par l'ancrage des clusters précurseurs $[RuCo_3(CO)_{12}]^-$ **(1)** ou $[Co_4(CO)_{10}(\mu\text{-dppm})]$ **(2)** est plus intéressant que la co-condensation directe de ces clusters fonctionnalisés par les alcynes. Les xérogels fonctionnalisés formés sont très poreux avec des tailles de pores grandes. L'ancrage des clusters est facile car il se fait par une simple réaction de ces clusters avec les alcynes préalablement greffés dans les matrices inorganiques. Les mesures magnétiques, à la balance thermo-magnétique, des matériaux obtenus, montrent qu'ils possèdent un comportement ferromagnétique. Il est à noter que le comportement du cluster **2**, en présence des xérogels fonctionnalisés est original vu qu'il conduit directement à des particules métalliques lors de la réaction d'ancrage.

Partie expérimentale

Synthèse de xérogels fonctionnalisés.

Les xérogels sont synthétisés de la même manière en utilisant l'alcyne $\mathbf{L^1}$ pour le xérogel 1 et l'alcyne $\mathbf{L^2}$ pour le xérogel 2-0,5 THF.

A l'alcyne (0,365 g, 1,15 mmol), dans un récipient, est ajouté un mélange de TEOS (4,78 g, 23 mmol) et d'éthanol (4,23 g, 92 mmol); l'agitation est maintenue une minute. On mélange de l'eau acidifiée par HNO_3 (0.1 M) (1,86 g, 92 mmol) avec le formamide (1,04 g, 23 mmol) dans un second récipient. Ce mélange est ajouté rapidement au mélange TEOS-éthanol-alcyne, et l'agitation est maintenue durant 1 heure. Le récipient est placé à l'étuve à 40 °C pour un vieillissement de 5 jours, la solution s'est transformé en un gel qui prend la couleur de l'alcyne. Le gel est séché sous flux d'azote pendant 2 jours puis sous vide à 40 °C pendant 1 jour pour obtenir le xérogel.

Ancrage des cluster dans le xérogels fonctionnalisés

Ancrage du cluster $[RuCo_3(CO)_{12}]^-$ (1) et $[Co_4(\mu\text{-}CO)_3(CO)_7(\mu\text{-}dppm)]$ (2) dans les xérogels. Le xérogel est broyé, séché à 50 °C pendant 24 heures, puis immergé dans une solution saturée du cluster dans THF. L'agitation est maintenue pendant 1 jour, à température ambiante. La suspension est alors portée à reflux durant 24 heures (à 90 °C dans le cas du cluster **1** et à 75 °C pour le cluser **2**), puis filtrée sur un frité, et la poudre lavée plusieurs fois avec du THF. Le matériau est séché sous flux d'azote pendant une nuit, puis sous vide.

Cocondensation du cluster $[Co_4(\mu\text{-}CO)_2(CO)_6(\mu\text{-}dppm)\{\mu_4\text{-}\eta^2\text{-}HC_2(CH_2)_2OC(O)NH(CH_2)_3Si(OEt)_3\}]$ (4). Le cluster **4** (0,107g, 0,092 mmol), est dissout dans 0,8 ml de THF (11 mmol) puis un mélange de TEOS (0,407 ml, 1,84 mmol) et d'éthanol (0,430 ml, 7,36 mmol) y sont ajoutés. Après une agitation pendant une minute, un mélange d'eau acidifiée par HNO_3 0.1 M, (0,148 ml, 7,36 mmol) avec le formamide (0,081 ml, 1,84 mmol) sont ajoutés rapidement à la solution du cluster. L'agitation est maintenue durant 1 heure, puis le Schlenk est placé à l'étuve à 40 °C pour un vieillissement de 15 heures. Le matériau est séché sous flux d'azote pendant deux jours puis sous vide pendant 1 jour, puis lavé au THF.

Appareillage

Les spectres Infra-rouge ont été réalisés sur un spectromètre Perkin Elmer 1600 series FTIR. Les spectres de RMN Cp MAS du ^{29}Si ont été effectués à 200 MHz sur un spectromètre Bruker MSL200S à un champ de 4,7 T. Les mesures de porosité ont été réalisées, sur un porosimètre Micrométrics ASAP 2010.

Références:

(1) (a) Lev, O. et al. *Analytical Chemistry*. **1995**, *67(1),* 22 A-30 A; (b) Sanchez, C.; Ribot, F. *New J. Chem.,* **1994**, *18*, 1007-1047; (c) Larry, L.; West, J. K. *Chem. Rev*, **1990**, *90*, 33-68.

(2) K.D. Keefer, in: *Silicon Based Polymer Science*: A Comprehensive Resource; eds. J.M. Zeigler and F.W.G. Fearon, ACS Advances in Chemistry Ser. No. 224, (American Chemical Society: Washington, DC, **1990**) pp. 227-240.

(3) Brinker, C.J. *J. Non-Crystalline Solids*. **1988**, *100*, 31-50.

(4) M. Prassas and L.L. Hench, in: *Ultrastructure Processing of Ceramics, Glasses, and Composites*; eds. L.L Hench and D.R. Ulrich, (John Wiley & Sons: New York, **1984**) pp. 100-125.

(5) Avnir, D.; Braun, S.; Ottolenghi, M. **1992** In *Supramolecular Architecture ACS 499.*

(6) Schmidt, H. *J. Non-Cryst. Solids,* **1985,** *73* (1-3), 681.

(7) Beghi, M.; Chiurlo, P.; Cogliati, G.; Costa, L.; Palladino, M.; Pirini, M. F, *Eur. Mater. Res. Soc. Monogr.;* **1992,** *5,* 213.

(8) (a) Collino R.*,* Therasse, J.; Binder, P.; Chaput, F.; Boilot, J.-P.; Lévy, Y., *Journal of Sol-Gel Science and Technology*, **1994**, *2*, 823; (b) Schubert, U, *Chem. Mater.* **2001,** *13*, 3487-3494; (c) Caruso, R. A.; Antonietti, M, *Chem. Mater.* **2001,** *13*, 3272-3282; (d) Pomogailo, A. D, *Russ. Chem. Rev.* **2000,** *69,* 53-80.

(9) Braunstein, P.; Cauzzi, D.; Predieri, G.; Tiripicchio, A. *J. Chem. Soc., Chem. Commun.* **1995**, 229-230.

(10) Schweyer-Tihay, F.; Braunstein, P.; Estournès, C.; Guille, J. L.; Lebeau, B.; Paillaud, J.–L.; Richard-Plouet, M.; Rosé, J. *Chem. Mater.* **2003**, *15*, 57-62.

(11) Kodama, R. H, *J. Magn. Mater.,* **1999,** 200, 359.

(12) Cyrot, M.; Décorps, M.; Dieny, B, *Magnétisme Tome I Fondement,* **1999**; Grenoble Presses universitaires de Grenoble.

(13) Lindner, E.; Schneller, T.; Auer, F.; Mayer, H. M. *Angew. Chem. Int. Ed.,* **1999**, *38,* 2154.

(14) Brunauer, S.; Emmet, P. H.; Teller, E, *J. Am. Chem. Soc,* **1938**, *60,* 309.

(15) Barrett, E. P.; Joyner, L. G.; Halenda, P. P. *J. Am. Chem. Soc,* **1951**, *73,* 373.

(16) Sing, K. S. W.; Everett, D. H.; Haul, R. A. W.; Moscou, L.; Pierotti, J.; Rouquerol, J.; Siemieniewska, T, *Pure Appl. Chem.,* **1985**, *57,* 603.

(17) Schweyer-Tihay, F.; Thèse de Doctorat de l'Université Louis Pasteur- Strasbourg, **2002**.

(18) Schweyer, F.; Braunstein, P.; Estournès, C.; Guille, J.; Kessler, H.; Paillaud, J.-L.; Rosé, J. *Chem. Commun.* **2000**, 1271-1272.

(19) Fiche JCPDS n° 05-0727, International Center for Diffraction Data.

(20) Fiche JCPDS n° 06-0663, International Center for Diffraction Data.

(21) Puntes, V. F.; Zanchet, D.; Erdonmez, C. K.; Alivisatos, A. P, *J. Am. Chem. Soc,* **2002**, *124,* 12874-12880.

Conclusion générale

Parmi les diverses stratégies pour ancrer des clusters moléculaires de manière covalente dans des matrices inorganiques, nous avons choisi d'utiliser des ligands alcynes possédant un groupe $-Si(OR)_3$ qui pourra être ensuite condensé avec $Si(OEt)_4$. De la même façon on utilise des alcynes possédant un groupe –SR pourra être fixé à une surface d'or.

Nous avons utilisé le cluster $[Co_4(CO)_{12}]$ après l'avoir stabilisé par les disphosphines bidentates dppm, dppa et la diphosphine fonctionnalisée dppaSi. En effet, la combinaison de l'effet de basicité des diphosphines et leur nature pontante a permis de stabiliser le coeur Co_4 des clusters ainsi formés.

La réaction de $[Co_4(CO)_{12}]$ avec un équiv. d'une diphosphine, dppm, dppa ou dppaSi, conduit à la formation des clusters tétraédriques **1a-c**, où le ligand diphosphine ponte deux atomes de cobalt de la base du tétraèdre (eq.1) et occupe des positions axiales. Ces clusters réagissent avec les alcynes pour conduire, avec de bons rendements, aux clusters *papillons* stabilisés **2a-c**. Nous présentons dans l'eq. (1) les résultats obtenus avec le phenylacétylène.

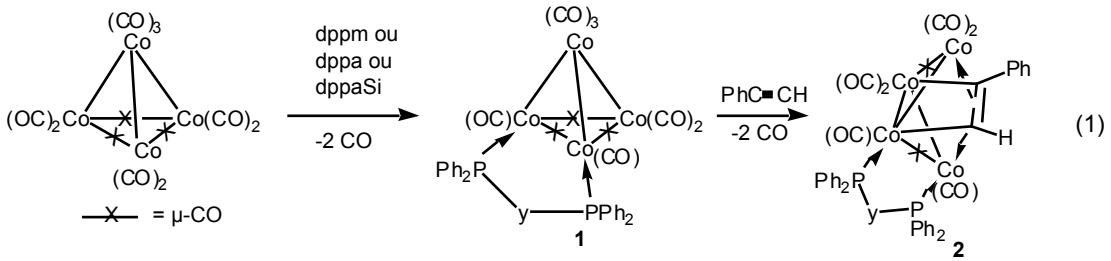

(1)

La fonction $-Si(OR)_3$ a été incorporée dans les clusters stabilisés **1a-c** grâce à l'utilisation des nouveaux alcynes $HC{\equiv}C(CH_2)_2OC(O)NH(CH_2)_3Si(OEt)_3$ **(L^1)**, $HC{\equiv}CCH_2NHC(O)NH(CH_2)_3Si(OEt)_3$ **(L^2)** et $PhC{\equiv}CC(O)NH(CH_2)_3Si(OMe)_3$ **(L^3)**, qui furent obtenus avec des rendements quantitatifs. Ceci a conduit aux clusters *papillons* fonctionnalisés correspondants. La réaction des clusters **1a-c** avec l'alcyne est facile et elle peut être suivie aisément par CCM du fait de la disparition du précurseur qui est d'une couleur rouge-brune et l'apparition du produit d'arrivée qui est vert. Cependant, la réaction nécessite un excès d'alcyne ce qui pose un problème de purification des clusters *papillons* résultant des alcynes fonctionnalisés mentionnés précédemment, vu que la purification par séparation sur colonne de chromatographie n'est pas possible dans ces cas. La RMN ^{31}P des clusters $[Co_4(\mu\text{-}CO)_2(CO)_6(\mu\text{-dppy})(\mu_4\text{-}\eta^2\text{-alcyne})]$ montre un seul pic dans le cas du ligand dppm qui se dédouble à basse température tandis qu' on observe deux pics bien séparés dans le cas de la dppa. Ces observations n'ont pas été expliquées à ce jour.

Le cluster hétéropolymétallique anionique, $[NEt_4][RuCo_3(CO)_{12}]$, isoélectronique de $[Co_4(CO)_{12}]$, réagit avec les alcynes par une insertion sélective de l'alcyne dans une liaison Co-Co pour conduire au cluster *papillon* dont la charnière est constituée par la liaison Co-Ru. Il est à noter que souvent deux isomères sont formés quand l'alcyne est dissymétrique (eq. 2).

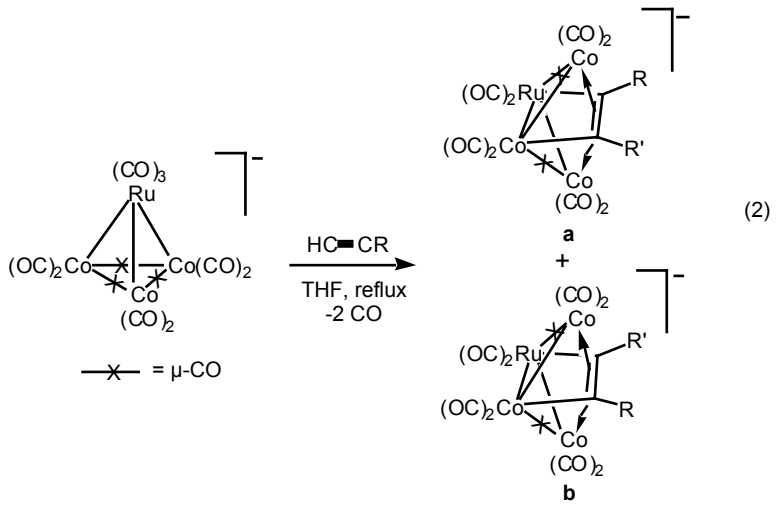

(2)

Il est possible d'incorporer des alcynes fonctionnels dans l'entité $RuCo_3$ selon deux stratégies (Schéma 1):

- par réaction du cluster métallique avec l'alcyne préalablement fonctionnalisé (stratégie *A*)

- par la fonctionnalisation de l'alcyne déjà coordiné au cluster (stratégie *B*).

Schéma 1. Deux approches pour l'incorporation d'alcynes fonctionnels dans des clusters

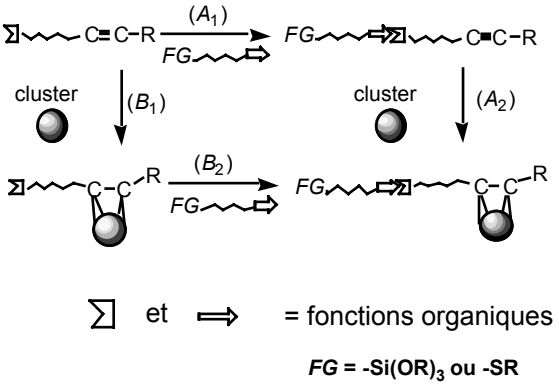

Nous avons examiné et comparé ces deux approches pour l'incorporation de fonctions –$Si(OR)_3$ ou –SR, . A notre connaissance, la stratégie *B* n'avait jamais été appliquée à la chimie des clusters. Nous avons ainsi synthétisé les clusters $[RuCo_3(CO)_{10}\{\mu_4\text{-}\eta^2\text{-}HC_2(CH_2)_2OC(O)NH(CH_2)_3Si(OEt)_3\}]^-$ **(2)**, $[RuCo_3(CO)_{10}\{\mu_4\text{-}\eta^2\text{-}$

$HC_2CH_2NHC(O)NH(CH_2)_3Si(OEt)_3\}]^-$ **(3)** et $[RuCo_3(CO)_{10}\{\mu_4\text{-}\eta^2\text{-}HC_2CH_2NHC(O)NHC_6H_4SMe\}]^-$ **(4)** selon ces deux stratégies. Cependant, il n'est pas possible d'obtenir le cluster $[RuCo_3(CO)_{10}(\mu_4\text{-}\eta^2\text{-}PhC_2C(O)NH(CH_2)_3Si(OMe)_3)]^-$ **(5)**, préparé par réaction de $[RuCo_3(CO)_{12}]^-$ avec $\mathbf{L^3}$, selon la stratégie *B*. En effet, $[RuCo_3(CO)_{12}]^-$ ne réagit pas avec l'alcyne fonctionnalisable PhC≡CC(O)Cl qui est le précurseur pour la synthèse de l'alcyne $\mathbf{L^3}$ par condensation avec l'amine fonctionnelle $H_2N(CH_2)_3Si(OEt)_3$.

Nous avons étendu cette approche à d'autres alcynes fonctionnels tels que MeO(O)CC≡CC(O)OMe, $HC{\equiv}CC(Me){=}CH_2$, $HC{\equiv}CCH_2OCH_2C{\equiv}CH$ et le nouveau ligand $PhC{\equiv}CC(O)NHCH_2C{\equiv}CH$ ($\mathbf{L^4}$). Ces alcynes sont incorporés au cluster $[RuCo_3(CO)_{12}]^-$ également par insertion de la triple liaison dans une liaison Co-Co pour donner les clusters *papillon* correspondants. Dans chaque composé obtenu, il subsiste une fonction pendante qui est C=O dans le premier cas, C=C dans le deuxième et C≡C dans le troisième et quatrième cas, dont la réactivité pourrait ultérieurement être mise à profit pour fonctionnaliser ces ligands liés au cluster (ex. hydrosilylation, ...).

Nous nous sommes également intéressés à la formation de chaînes insaturées C_X liant des clusters moléculaires, [Cluster] - C_X - [Cluster]. L'intérêt de connecter des clusters métalliques par des chaînes carbonées insaturées et conjuguées provient des propriétés structurales originales ainsi que des propriétés rédox et de conductivité que l'on peut en attendre. Ceci nous a conduits à l'utilisation de diynes, dont nous avons étudié la réactivité avec les clusters Co/Co ou Ru/Co.

Ainsi, la réaction du cluster $[Co_4(CO)_{10}(\mu\text{-dppm})]$ **(1a)** avec le diyne conjugué, 1,4-*bis* (trimethylsilyl)butadiyne, est très lente et conduit à la formation du produit $[Co_4(CO)_8(\mu\text{-dppm})(\mu_4\text{-}\eta^2\text{-}Me_3SiC_2C{\equiv}CSiMe_3)]$ **(6)**. La déprotection du ligand par désilylation de **6** est également lente et donne le cluster $[Co_4(CO)_8(\mu\text{-dppm})(\mu_4\text{-}\eta^2\text{-}HC_2C{\equiv}CSiMe_3)]$ **(7)** qui est très sensible à l'air (eq. 3) alors que nous attendions la désilylation de l'alcyne non lié au cluster qui est stériquement plus accessible. La réaction de couplage entre eux n'est de ce fait pas possible.

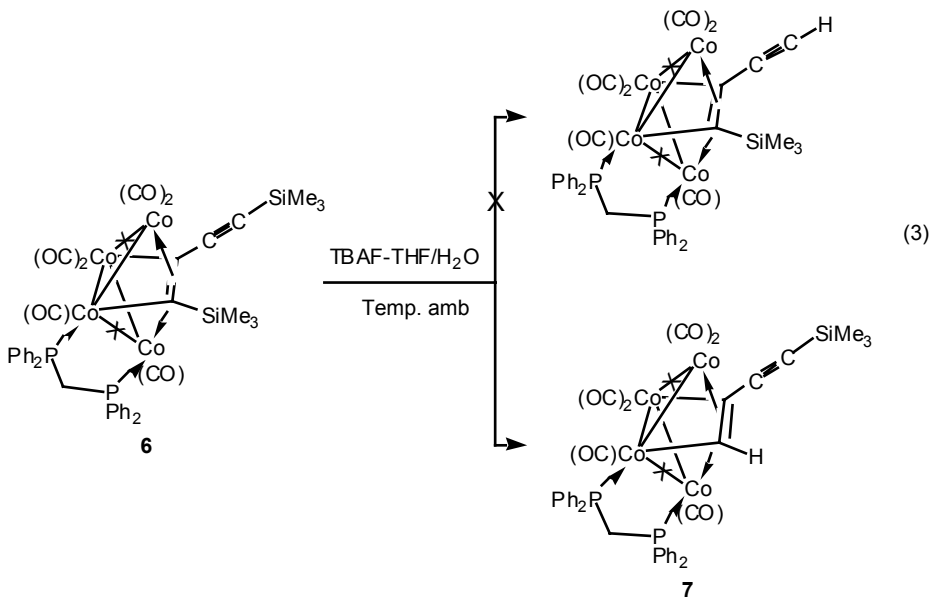

(3)

La réaction de $[RuCo_3(CO)_{12}]^-$ avec le 1,4-*bis* (trimethylsilyl)butadiyne conduit à la formation du cluster stable $[RuCo_3(CO)_{10}(\mu_4\text{-}\eta^2\text{-}Me_3SiC_2C{\equiv}CSiMe_3)]^-$ **(8)**. Contrairement au cas du cluster **6**, la réaction de déprotection de **8** conduit rapidement au cluster attendu $[RuCo_3(CO)_{10}(\mu_4\text{-}\eta^2\text{-}Me_3SiC_2C{\equiv}CH)]^-$ **(9)**. Deux unités du cluster **9** ont pu être liées par une réaction de couplage avec le 1,4 diodobenzène dans les conditions de Sonogashira et nous avons obtenu le cluster $[\{[RuCo_3(CO)_{10}(\mu_4\text{-}\eta^2\text{-}Me_3SiC_2C{\equiv}C)]\}_2C_6H_4]^{2-}$ **(10)**.

Les résultats différents obtenus dans le cas du $[Co_4(CO)_{10}(\mu\text{-dppm})]$ et de $[RuCo_3(CO)_{12}]^-$ prouvent encore que l'introduction d'un métal de nature différente dans le coeur du cluster en modifie sa réactivité.

La réaction du cluster **8** avec $[Cu(NCMe)_4]BF_4$ conduit à la formation du cluster $[RuCo_2(CO)_9(\mu_3\text{-}\eta^2\text{-}HC_2C{\equiv}CSiMe_3)]$ **(11)**, en partie désilylé, au lieu de $[RuCo_2(CO)_9(\mu_3\text{-}\eta^2\text{-}Me_3SiC_2C{\equiv}CSiMe_3)]$ **(12)**. Le cluster **11** a été également obtenu par la réaction du cluster 8 avec $[NO]BF_4$ en plus de $[RuCo_3(CO)_9(NO)(\mu_4\text{-}\eta^2\text{-}Me_3SiC_2C{\equiv}CSiMe_3)]$ **(13)**. Etant donné que la désilylation du cluster anionique **8** par le TBAF a eu lieu au niveau du carbone acétylénique et que, à l'inverse, la désilylation du cluster neutre **6** a eu lieu au niveau du carbone lié au coeur métallique, on peut supposer que le cluster **11** s'est formé après le cluster **12** par désilylation partielle de ce dernier par le fluorure provenant de $[Cu(NCMe)_4]BF_4$ ou $[NO]BF_4$. Il est intéressant de noter que la déprotection se fait au niveau acétylénique dans le cas d'un cluster chargé et au niveau du carbone attaché au coeur métallique quand le cluster est neutre. Il est par contre prématuré d'en tirer une conclusion générale.

Un autre volet de ce travail a consisté en la synthèse de nanoparticules magnétiques, dispersées dans des matrices de silice poreuses, ceci par greffage par le procédé sol-gel, d'alcynes et cluster alcynes, contenant la fonction alcoxysilyle, précédement décrits .
Le greffage peut se faire de deux manières différentes :

-l'alcyne fonctionnalisé est greffé en premier lieu à la matrice puis le cluster est incorporé au gel [voie (*A*)].

- le cluster est fixé à l'alcyne fonctionnalisé et l'ensemble est greffé à la matrice [voie (*B*)].

Après un premier essai à partir du cluster $[Co_4(CO)_8(\mu\text{-dppm})\{\mu_4\text{-}\eta^2\text{-}HC_2CH_2CH_2OC(O)NH(CH_2)_3Si(OEt)_3\}]$ la voie (*A*) s'est imposée. Ainsi, nous avons préparé des xérogels par incorporation *in situ* des alcynes $\mathbf{L^1}$ et $\mathbf{L^2}$ par le procédé sol-gel. L'ancrage des clusters $[RuCo_3(CO)_{12}]^-$ et $[Co_4(CO)_{10}(\mu\text{-dppm})]$ dans les xérogels fonctionnalisés conduit à des résultats différents. En effet, dans le cas du $[RuCo_3(CO)_{12}]^-$ on obtient un matériau ferromagnétique après traitement thermique, alors que dans le cas de $[Co_4(CO)_{10}(\mu\text{-dppm})]$ on obtient, sans traitement thermique, des matériaux ferromagnétiques. Dans ce dernier cas l'étude par diffraction des rayons X des matériaux montre qu'il s'agit du cobalt métallique en mélange de phases (hcp, cfc et epsilon), par ailleurs la microscopie électronique montre la formation de grosses particules de cobalt métalliques taille > 150 nm).

Cette étude nous a permis, en plus de la synthèse et la caractérisation des nouveaux alcynes et cluster alcynes fonctionnalisés, d'explorer le potentiel des méthodes sol-gel appliquées, pour la première fois, aux clusters mixtes.

Perspectives

Parmi les perspectives ouverts par ce travail, nous citerons:

- La fixation des clusters contenant la fonction -SR sur une surface d'or afin d'étudier l'émergence de propriétés collectives dues à l'organisation des clusters sur une telle surface.
- L'extention de la fonctionnalisation par des fonctions $–Si(OR)_3$ et -SR à d'autres combinaisons métalliques.
- L'étude de l'activité catalytique des matériaux inorganiques contenant des nanoparticules.